A FIRST PRINCIPLES INVESTIGATION OF THE ADSORPTION AND REACTIONS OF POLYFUNCTIONALIZED MOLECULES ON OXIDES AND METALS.

Giuliano Carchini

Dipòsit Legal: T 1601-2015

UNIVERSITAT ROVIRA I VIRGILI
DEPARTAMENT DE QUÍMICA FÍSICA I INORGÀNICA
Campus Sescelades
Marcel·lí Domingo, s/n
43007 Tarragona
Tel. +34 977 55 81 37
Fax +34 977 55 95 63
www.quimica.urv.es

ICIQ
Institut Català d'Investigació Química

I STATE that the present study, entitled "A First Principles Investigation of the Adsorption and Reactions of Polyfunctionalized Molecules on Oxides and Metals", presented by Giuliano Carchini for the award of the degree of Doctor, has been carried out under my supervision at the Institute of Chemical research of Catalonia.

Tarragona, November de 2014

Doctoral Thesis Supervisor

Prof. Núria López

Giuliano Carchini

A First Principles investigation of the Adsorption and Reactions of Polyfunctionalized Molecules on Oxides and Metals

Ph.D. Thesis supervised by Prof. Núria López

Tarragona
January 2015

Acknowledgements

This thesis represents the completion of four years of work which would have been impossible without the help of many people. Here I want to thank as many as possible, being aware that every person I've met has contribuited (not always pleasantly) to this moment.

Mamma e Papà, per il loro ininterrotto affetto e supporto e la infinita pazienza. Ringrazio mia madre per avermi dato la determinazione e il coraggio di seguire l'istinto. Ringrazio mio padre per la mia parte razionale e la passione per la scienza.

Mio fratello Junio per avermi guidato nelle scelte con la sua saggezza.

Mi directora de tesis, Núria López como jefa y persona. Como jefa, ha conseguido apasionarme en este trabajo con su entusiasmo y ahora sé que es lo que quiero hacer en mi vida. Como persona siempre ha estado disponible y comprensiva en mis malos momentos.

Mi querida Lucia por su presencia en este ultimo año. Siempre tendrás un lugar especiál en mi corazón. Sé que la distancia no logrará separarnos.

Le mie amiche Roberta e Serena, con il loro continuo supporto e affetto. Nonostante la distanza è stato come avervi qui ogni giorno.

My collegues in prof. López group Luca Bellarosa, Neyvis Almoras, Marcos Rellán, Guillem Revilla, Rodrigo García-Muelas, Miquel Garcia, Sergey Pogodin, Marçal Capdevila, Qiang Li

and Michael Higham (welcome!). Also, the "computer guys" Martin Gumbau and Moisés Álvarez, and the unstoppable secretary Núria Vendrell.

The ones that have left (but I'm confident I'll meet again in the future): Gerard Novell-Leruth (and its fundamental guide in the first years), Max García, Piotr Błoński and my bro Omotayo Salawu (I love you man!).

My life in the office (and outside) wouldn't have been the same without the other guys from the theoretician lab. The present ones: Nuno Bandeira, Stefano Serapian (new entry but he has already gained a special place), Dolores Melgar, Xavier Sanz, Joan Gonzáles, Maria Besora, Oier Lakuntza, Victor Fernández, Ignacio Funes, Rositha Kuniyil and Adiran De Aguirre. The former ones (but still in my thoughs): Fernando Castro (el man), Abel Locati, Alex Hamilton (I hope you are great, wherever you are now), Sameera (and his dark side), Adriá Gil, Cristina Pubill, Chunhui Liu.

Some special people from ICIQ (but by no means limited to it), present and past: Sofia Arnal, Chris Whiteoak, Maria José Hueso, Pablo Garrido and Victor Laserna, Antonio Bazzo and Mattia Silvi.

Algunas de las personas especiales que conocí en Tarragona: Nohora, Yanine, Luciana y Vincenzo, Susana, la gente de la isla (Magda, Yaneth, Ruth, Ramón), Norma, Pedro y Arturo (la primera cara que ví aquí).

Questa lista non sarebbe completa senza includere i sempioncini e la loro freschezza: Valeria, Silvia, Ambra, Chris, Luca e Chiara, Valentina e Alessiuccio (Bobini), Mery, PietroPaolo (aka Pippo), il buon Franco, Sanex (el desaparecido), Eleonora e Fabio, Claudia e Luigi, Elisabetta e Riccardo, Ale e Simy.

Un ringraziamento speciale va agli amici di una vita Alberto, Adriano e Marcello.

Infine voglio ringraziare Gloria per avermi confermato ancora una volta quanto la vita possa essere piacevolmente im-

prevedibile. Il suo entusiasmo contagioso mi ha aiutato ad uscire dal guscio e a ritrovare il sorriso.

Contents

Chapter 1

Introduction

1.1 Importance of catalysis

A catalytic process proceeds faster than the non-catalytic reaction, up to several orders of magnitude. Since many processes are too slow for practical applications, the modern chemical industry could not exist without catalysis; more than 90% of its products are made through a catalytic way. The catalyst can affect the reactants in different ways, usually weakening their intramolecular bonds, but also disposing them close to each others and with the correct arrangement. Once the product is formed, it will detach from the catalyst, leaving it unaltered and ready for another cycle. A good catalyst is therefore quite challenging to obtain, since the bond with the reactants must be strong enough to make them react but not too much that they will be stuck on it. A weak interaction is also needed with the product, for it must leave the surface easily. It has to be noted that the overall change in free energy is the same in both the catalytic and the non-catalytic reaction. Thus, if a reaction is thermodynamically unfavorable, a catalyst cannot change this situation, for it modifies the kinetics but not the thermodynamics. Both the catalytic and non-catalytic processes are shown

in Figure 1.1.

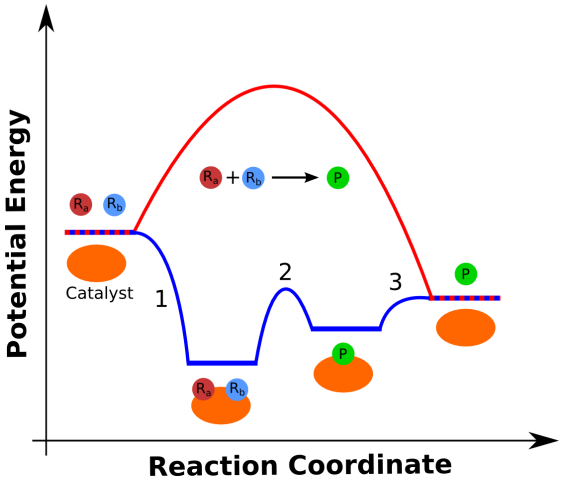

Figure 1.1: Representation of the catalytic (blue) and non-catalytic (red) ways for the process $R_a + R_b \rightarrow P$. The catalytic way is more complex and comprehend at least three steps: 1) Adsorption, 2) Reaction and 3) Separation. The two paths show the same difference in free energy but the catalytic way is energetically more convenient.

It is common practice to divide the catalysis into three types: bio-, homogeneous and heterogeneous catalysis. The boundary between them is somewhat blurred, since some systems can belong to more than one group. Biocatalysis is confined to living systems and comprehends enzymes, probably the most specific and efficient catalysts. The other two types refer to the phases of catalyst, reactants and products. If they are in the same phase (usually gas or liquid), we are in the domain of homogeneous catalysis; otherwise we talk about heterogeneous catalysis. In this case, liquid or gas reactants operate on a solid catalyst.

Perhaps the most noted process in homogeneous catalysis is the transformation of ozone (O_3) to molecular oxygen cat-

alyzed by chlorine atoms; the investigation of this process was essential in the prediction of ozone depletion. Also known for its environmental impact is the heterogeneous oxidation of CO to CO_2 on the surface of noble metals such as platinum, palladium and rhodium, which takes part in the automotive exhausts. Industrially, it is worth to stress the employment of TiO_2 as electrode in the photo-decomposition of water into H_2 and O_2;[1] despite still not commercially competitive, it inspired successive investigations in the field.

The entire investigation carried out in this thesis will focus on heterogeneous catalysis. As solids are usually impenetrable (unless they are porous), catalytic reactions occur at the surface. In this case, the catalytic active material (which is usually expensive) is applied in small quantity over a cheap support. Employed supports include TiO_2[2–5] and α-Al_2O_3,[6] which have been investigated in the next chapters. It has to be noted that the interaction between support and active phase can have strong influence in the final catalytic effect.

The first step in any catalytic reaction on solids involves the adsorption of the reactants on the surface. As described in the next section, the process itself can be very complex to model.

1.2 The process of adsorption

Adsorption is the result of an attractive interaction between an atom/molecule and a surface, strong enough to overcome the effect of thermal motion. When this interaction is essentially the result of van der Waals forces, it is called *Physisorption*. The resulting bonds are characterized by vdW energies below ~ 0.50 eV for small compounds. *Chemisorption* on the other hand takes place when there is an overlap between the molecular orbitals of the adsorbate and the ones of the substrate, which yields the formation of strong chemical bonds. The effect of vdW forces is not limited to the energy but it also affects

the molecular titling angle and it is responsible of distortions and possible isomerizations. It has to be noted that chemisorption is often an activated process, and there is a weakening of intramolecular bonds that can lead to the dissociation for the adsorbed species. Both processes are sketched in Figure 1.2.

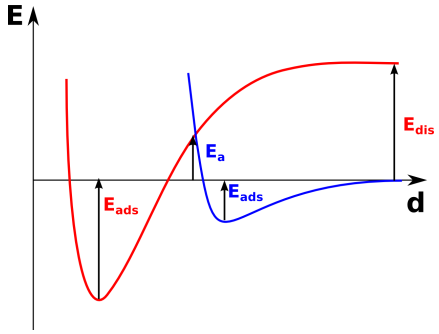

Figure 1.2: Sketch of the energies in the adsorption process. In red we have the chemisorption and in blue the physisorption. The chemisorption often need to overcome a barrier (E_a); A dissociation of the interatomic bond with energy E_{dis} can result afterwards.

Experimentally, there are a number of techniques that provide reliable information concerning adsorption energetics and geometries, such as Low Energy Electron Diffraction (LEED), microcalorimetry measurements,[7–10] and most important, Temperature Programmed Desorption (TPD). It has to be noted that most of these methods refer to a statistical ensemble of adsorbed molecules, therefore a comparison with with theoretical calculations is not straightforward. For this reason, it is of primary importance to represent the experimental structure and coverage in the simulations as close as possible. Special attention must be paid in the interpretation of experimental adsorbate geometry, binding (adsorption) energy and electronic properties. The situation is further complicated by steps, kinks, and defects which are always present in a real surface indepen-

dently of the care taken in the preparation of the sample. These are competitors site for the adsorption and can greatly affect the properties of the system adsorbate-substrate.

1.3 The interface at the adsorption site

The interface between substrate and adsorbate combines the characteristics of two distinct materials, *i.e.* the electrical conductivity of the surface with the tunable properties of the molecules.[11] This dual nature can be exploited in the so-called hybrid inorganic/organic systems (HIOS). Important applications include light-emitting diodes, single-molecule junctions, molecular sensors and switches and photovoltaics.[12–16] Another example of such hybrids is found in the employment of oxides like SnO_2 as gas sensors.[17,18] These materials have naturally high bulk electrical resistivity but the adsorption of certain molecules can produce changes in surface conductivity large enough to be measured. Finally, HIOS based on oxides are important in high-T_c superconductors (based on Cu oxide),[19] to understand the effect of environmental degradation.

Density Functional Theory (DFT) is the most promising approach to study complex systems, since it can be applied to both molecules and solids comprising thousands of atom. Unfortunately, at the interface vdW forces are almost the only interaction present in physisorption and a fundamental component in chemisorption. These are due to the correlation between electrons and they are long range in nature. Standard DFT implementations describe the electron correlation in a local (LDA) or semi-local (GGA) way, therefore van der Waals forces are neglected. Several workaround to this problem have been developed in the years, and it is still an open field of investigation. A detailed description of these methods is reported in

the following chapter. This is a fundamental problem regardless of the type of surface. Except for the last chapter, where we analyze metal surfaces, all the systems investigated comprehend metal oxide surfaces. As described in the next Section, the study of metal oxides present many underlying difficulties.

1.4 Challenges in metal oxides

Setting up theoretical models for metal oxides is far more complex compared to metals. First, even a simple structure such as corundum (α-Al_2O_3) has a ten-atom primitive unit cell. Also, there is a complex combination of chemical and physical properties. Especially transition metals display a range of possible oxidation states and hence a series of oxides with different compositions; these can be either stoichiometric or characterized by non-integer ratios between the oxygen and the metal. This means that even bulk samples of many oxides may be difficult to obtain with reproducible composition and properties. They often have high defect concentrations which may dominate the physical properties of even the purest available materials. As expected such difficulties will be greatly exacerbated at surfaces and can contribute to the problems in surface preparation. Another consequence is the wide range of chemical interactions possible with chemisorbed molecules. Finally, the electronic structure is also much more complex than that of metals and semiconductors. In fact, the bulk electronic structure of the late 3d-transition-metals oxides lies somewhere between itinerant and localized, and neither of these two descriptions is entirely appropriate. All these factors stress the intrinsic difficulties in setting reliable theoretical models.

Retrieving experimental data for comparison can be also troublesome. As an example, many of the most interesting metal oxides are very good electrical insulators. α-Al_2O_3 is of tremendous importance in the industry[20] but it is a wide-

bandgap insulators that cannot made conducting by doping or reduction. Many of the most powerful techniques involve the emission or absorption of charged particles and therefore cannot be employed if the material has a negligible bulk conductivity. Another problem emerges in the surface preparation. In fact the preparation of nearly perfect surface of any compound is difficult and the establishment of geometric order on the surface is not sufficient, since the stoichiometry can be different compared to the bulk. The most promising technique consists in cleavage in UltraHigh Vacuum (UHV) which yields well ordered surfaces having nearly the composition of the bulk. Still an analysis with Scanning Tunnelling Microscopy (STM), capable of depicting a surface at atomic level, shows that surfaces prepared this way are still far from being perfectly stoichiometric. The previous points stress the importance of characterize the stoichiometry and the geometric structure as completely as possible before meaningful interpretations of the data can be made. Even so, extremely caution need to be taken in the comparison with theoretical models.

1.5 Scope of the thesis

This thesis is structured in the following way. In Chapter 2, a description of the theoretical basis employed is presented. The following three chapters are focused on the study of titanium oxide, TiO_2. In Chapter 3, the phenomena of doping has been investigated for this compound and also for other three rutiles. In particular, the migration of impurities and the growth of overlayers have been addressed. In the first part of Chapter 4 the adsorption of a series of small alcohols of increasing complexity on TiO_2 has been investigated. Dependence on the length of the chain and the number of hydroxyls with the adsorption energies have been analyzed. Also we have considered defective surfaces and the competition between different

adsorption sites. A mechanism for the dehydration of polyalcohols on titania has been proposed in the second part. The last two chapters focus on different topics. Chapter 5 analyzes the behaviour of rare-earth oxides in aqueous environment. In particular, an explanation for their strong hydrophobicity has been presented along with a way to tune such property. Finally in Chapter 6, a simple and cheap methodology to compute accurate van der Waals coefficients for metals has been illustrated. The procedure is completely first principles and is applicable to both pristine and defective surfaces. The parameters have been employed in the calculation of the adsorption energy of benzene and yielded results in good agreement with experimental data.

Chapter 2

Theoretical Background

In this chapter, the methodologies employed throughout the rest of the work are described. First, a general description of the Density Functional Theory is reported. Particular attention has been focused on the choice of the exchange functional and the implementation of dispersion forces. Afterwards, it follows the implementation of DFT on solid systems. Finally, some important techniques are explained: the theoretical and practical aspects of the search of a transition state, followed by the method employed to extract adsorption energies from TPD experiments.

2.1 Ground state energy

Given a generic system described by the wave function (WF) Ψ, it is possible to evaluate its energy by solving the time-independent Schrödinger equation:

$$\widehat{H}\Psi = E\Psi \tag{2.1}$$

where $\widehat{H}$ is the Hamiltonian operator

$$\widehat{H} = -\frac{h^2}{2m}\nabla^2 + \widehat{V} \tag{2.2}$$

Due to the fact that the nuclei are much more massive than the electrons, we can separate their motion with a negligible loss in accuracy. This is known as the Born-Oppenheimer approximation (BO) and it is of fundamental importance in computational chemistry. It follows that the total wave function is now the plain sum of the electronic and the nuclear one

$$\Psi = \Psi_e + \Psi_n \tag{2.3}$$

It is therefore possible to define a new equation for the Ψ_e:

$$\begin{aligned}\widehat{H}_e\Psi_e &= \left[\widehat{T}_e + \widehat{V}_{ext} + \widehat{U}\right] = \\ &= \left[\sum_i^N -\frac{h^2}{2m}\nabla_i^2 - \sum_i^N V(\boldsymbol{r_i}, \boldsymbol{R}) + \sum_{i<j}^N U(\boldsymbol{r_i}, \boldsymbol{r_j})\right]\Psi_e = \\ &= E_e\Psi_e \end{aligned} \tag{2.4}$$

where the first term is the electronic kinetic energy ($\widehat{T}_e$), followed by the external potential ($\widehat{V}_{ext}$) and the electron-electron interaction ($\widehat{U}$). The electronic energy eigenvalue E_e depends on the positions of the nuclei ($\boldsymbol{R}$); varying these in small steps and repeatedly solving Equation 2.4, one obtains E_e as a function of $\boldsymbol{R}$.

This is know as the potential energy surface (PES) and it is employed as external potential in the nuclear time-independent Schrödinger equation

$$[T_n + E_e(\boldsymbol{R})]\Psi_n = E\Psi_n \tag{2.5}$$

which finally yields the total energy of the ground state.

Even with this improvement, an analytical solution exists only for few simple cases, for the motion of a single electron

is affected by the others as expressed by the interaction term $U(\boldsymbol{r_i}, \boldsymbol{r_j})$; more complex systems require a numerical treatment.

The simplest of these is the Hartree-Fock (HF) method. It is based on the assumption that that the many-body WF can be approximated by a single Slater determinant of independent spin-orbitals, one for each electron. Employing the variational method, one can then derive a set of coupled equations for the spin orbitals; once we have solved them, we obtain the total WF and the energy of the system. Unfortunately, the result of a standard HF calculations yields quite inaccurate results. This is due to the poor description of the WF as a single determinant which neglect almost completely the interaction between the single electrons. This effect is called electronic correlation and it can be divided in two components:

- Static correlation arises when there are small energy gaps between the ground state and other states, *e.g.* in the potential energy curve of a diatomic molecule until bond breaking.

- Dynamical correlation refers to the effect of the instantaneous electron repulsion, mainly between opposite-spin electrons.

The HF method includes a small portion of the electronic correlation, as it obeys antisymmetry, so two electrons of the same spin have a zero probability of being in the same location at the same time. Still the results are unsatisfactory and extensions to this method are required. These are collectively called post Hartree-Fock and can be quite different in the formulation. For the static correlation, we have to include a few, but very important determinants, while the dynamical effect is rectified including a large number of determinants with very small weight.

All these methods can reach noticeable accuracy but they are also very expensive. They are usually employed when very

good accuracy is needed, such as in benchmark for cheaper approaches. HF and its extensions imply the correct Hamiltonian operator while approximating the WF to solve the Scrödinger equation. Another approach consists in simplifying $\widehat{H}$. This approximation is the basis of the Density Functional Theory (DFT). This method cannot reach the accuracy of post Hartree-Fock expansions but it is far cheaper and it yields satisfying results for most cases.

2.2 The Density Functional Theory

DFT, bases its premises on the use of electronic density to evaluate the ground state energy. This is formulated into two theorems by Hohenberg and Kohn[21] which read:

- the ground state properties of a many-electron system are uniquely determined by its electron density
- it exists an energy functional for the system and it is minimized by the correct ground state electron density.

As a first step, a series of functions ϕ_i (the basis set) are chosen for the representation of the real WF. Among others we can use a linear combination of plane waves; the condition is that they have to reproduce the density $n(\boldsymbol{r})$ of the original system:

$$n(\boldsymbol{r}) \stackrel{def}{=} n_{eff}(\boldsymbol{r}) = \sum_{i=1}^{N} |\phi_i(\boldsymbol{r})|^2 \tag{2.6}$$

the functions defined this way are used to solve the so-called Kohn-Sham (KS) equations

$$\left[-\frac{1}{2}\nabla^2 + V_{eff}(\boldsymbol{r})\right] \phi_i(\boldsymbol{r}) = \epsilon_i \phi_i(\boldsymbol{r}) \tag{2.7}$$

with V_{eff} being the effective potential in which the electrons move

$$V_{eff}(\boldsymbol{r}) = V_{ext}(\boldsymbol{r}) + \int \frac{n(\boldsymbol{r'})}{|r - r'|} dr' + V_{xc}[n(\boldsymbol{r})] \tag{2.8}$$

where V_{ext} is the external potential generated by the nuclei, the second term represents the electron-electron Coulomb repulsion (Hartree term) and the last (V_{xc}) is known as the exchange-correlation potential. The exact definition of the latter is unknown and an approximation is due before proceeding with the KS equations. Therefore the whole sequence is treated self consistently:

- an initial guess is chosen the density $n(\boldsymbol{r})$
- an approximation for V_{xc} is selected and $n(\boldsymbol{r})$ is used to evaluate it and V_{eff} solving Equation 2.8
- the KS equations 2.7 are solved and the energies ϵ_i and the ϕ_i are retrieved.
- the obtained ϕ_i are used to compute a new density $n(\boldsymbol{r})$ through Equation 2.6
- the whole cycle is repeated until the energy difference between two steps is smaller than a defined threshold.

2.2.1 The Correlation-exchange Potential: Hierarchy of the V_{xc}

Along with the basis set, V_{xc} is responsible for the accuracy, while the numerical algorithms affect the efficiency. The hierarchy of available exchange-correlation functionals was described by John Perdew in "the Jacobs ladder of DFT"[22] where each

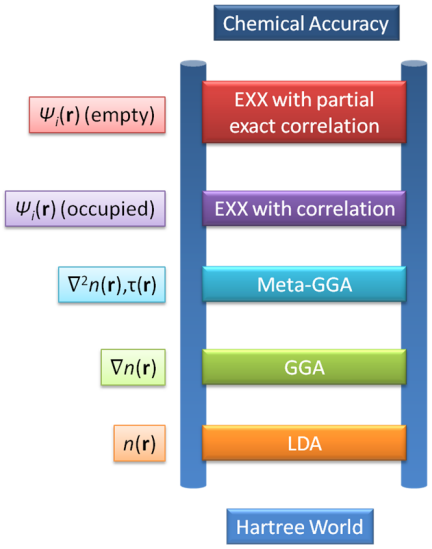

Figure 2.1: Hierarchy of the different V_{xc} leading to increasing accuracy.

rung yields more accuracy but it is also more computational expensive (see Figure 2.1).

The simplest part of the ladder is the local density approximation (LDA),[23] where the exchange-correlation energy (E_{xc}) is that of a homogeneous electron gas of the same density, $n(\boldsymbol{r})$.

$$E_{xc}^{LDA}[n(\boldsymbol{r})] = \int \epsilon_{xc}^{hom}[n] n(\boldsymbol{r}) d^3\boldsymbol{r} \tag{2.9}$$

The correlation part of E_{xc} is parametrized from quantum Monte-Carlo simulations.[24] A spin polarized version of LDA is also available, named Local-Spin Density Approximation (LSDA)[25] and allows difference between the spatial parts of $n_\uparrow$ and $n_\downarrow$. It is needed for atoms and molecules with unpaired electrons and for magnetic condensed materials:

$$E_{xc}^{LSDA}[n_\uparrow, n_\downarrow] = \int \epsilon_{xc}^{hom}[n_\uparrow, n_\downarrow] n(\boldsymbol{r}) d^3\boldsymbol{r} \tag{2.10}$$

LDA is adapt for many bulk[26] and surface systems but it usually leads to over-binding.[27]

The second rung is formed by the generalized gradient approximation (GGA) methods.[28,29] In this case, E_{xc} depends both on the electron density $n(\boldsymbol{r})$ and its local gradient, $\nabla n(\boldsymbol{r})$.

$$E_{xc}^{GGA}[n(\boldsymbol{r})] = \int \epsilon_{xc}[n, \nabla n(\boldsymbol{r})] n(\boldsymbol{r}) d^3\boldsymbol{r} \tag{2.11}$$

As well as in LDA, it is possible to treat spin-polarized systems; E_{xc} becomes

$$E_{xc}[n_\uparrow, n_\downarrow] = \int \epsilon_{xc}[n_\uparrow, n_\downarrow, \nabla n_\uparrow, \nabla n_\downarrow] n(\boldsymbol{r}) d^3\boldsymbol{r} \tag{2.12}$$

The GGAs solves some of the shortcomings of LDA, but tends to underestimate bond energies;[30] nevertheless, it is accurate enough for many chemical reactions.[31] Among the different methods in this group, PW91[32] and PBE[33] have been the standard in reactivity during the last decade. Unfortunately GGAs have two serious drawbacks. First, they do not account for van der Waals (vdW) interactions resulting from dynamical correlations between fluctuating charge distributions.[34] On the other hand, there is a non-zero interaction of a single electron with its own density, known as self-interaction error (SIE). SIE is the cause of many of the failures of approximate functionals, such as excessively narrow band gaps,[35,36] wrong dissociation energies for molecules,[37] and incorrect description of systems with localized f electrons.[38] Some of them can be fixed by introducing a strong intra-atomic interaction in a screened manner. This is known as the DFT+U[39] method, where U is the parameter which control the added electronic repulsion. The main concern is that this depends on the particular observable to be calculated, in contradiction with the universality claimed for the functional.

Meta-GGA includes higher-order terms of the gradient of the local kinetic energy density, $\nabla^2 n(\boldsymbol{r})$, and constitutes the third rung on the DFT ladder.[40] Unfortunately, such methods lack consistency as they do not systematically improve the properties compared to GGA. Examples of this behaviour have been reported, such as the adsorption of small molecules on metal surfaces[34] and the hydrogenation of benzene on Ni(111).[41]

The next step in the ladder corresponds to hybrid functional, that mix exact exchange (E_{XX}), as in HF) while the correlation is kept at the standard DFT level. The most popular hybrid in chemistry has been for more than one decade the B3LYP functional,[42,43] providing high accuracy for almost all properties of molecules, but failing when applied to solids, because the correlation part is incorrect in the homogeneous electron gas limit.[44,45] Hybrid functionals specific for this problem have been developed, such as PBE0[46] and HSE03,[47] which show better estimates for lattice parameters and bulk moduli of solids, and for the band gaps in semiconductors and insulators.[44,45] In general, these hybrid functionals properly describe both insulating antiferromagnetic rare-earth and transition metal oxides which are not correct with GGAs.[48,49]

The best way to treat correlation effects is represented by the Random Phase Approximation (RPA). It is one of the oldest non-perturbative methods for computing the ground-state correlation energy, being developed between 1951 and 1953 by Bohm and Pines.[50–52] The basic idea is to reduce the many-electron problem for the uniform electron gas to a much simpler coupled harmonic oscillator for long range plasma oscillations (plus a short-ranged correction). Its application to DFT is much more recent, thanks to Langreth and Perdew, which showed that RPA arises as a natural approximation when the Adiabatic Connection framework[25,53,54] is combined with the fluctuation-dissipation theorem. Strictly speaking it is not a new definition of the Exchange-Correlation functional, so it is

not present in Figure 2.1; in fact a standard DFT calculation is needed as a starting point for the method. The downside is that it is very expensive which strongly limits its use as benchmark. RPA was also the basis for the development of the first van der Waals density functionals,[55] employed by Dobson for the seamless treatment of long-range dispersion interactions.[56,57] Only in 2001, RPA using a KS reference was first applied to molecules.[58]

2.3 Application to solids

Practical aspects of DFT implementation can deeply vary based on the system. In the following sections the necessary details required in the case of solids will be described. The first aspect to consider is the basis set used for the expansion of the WF. This is followed by the description of the pseudopotential model, a cheap way to treat the large number of electrons. Finally the supercell approach is explained; it is used to deal when the periodicity is broken along one or more directions.

2.3.1 Basis set

Solid systems are characterized by a periodic potential. We can exploit this character to choose the basis set for the expansion of the WF. This was formulated by Bloch in his theorem:[59] given a particle in a periodic potential, its WF, $\psi_i(\boldsymbol{r})$, can be expressed as the product of an exponential, $e^{i\boldsymbol{kr}}$, and a periodic function, $U_n(\boldsymbol{r})$, which has the same periodicity of the potential. Therefore, we have

$$\psi_i(\boldsymbol{r}) = e^{i\boldsymbol{kr}} U_n(\boldsymbol{r}) \tag{2.13}$$

The periodic part can be further expanded in a discrete set of plane waves (PW) whose vectors are the reciprocal lattice vectors $\boldsymbol{G}$ of the crystal,

$$U_n(\boldsymbol{r}) = \sum_{\boldsymbol{G}} c_{n,\boldsymbol{G}} e^{i\boldsymbol{G}\boldsymbol{r}} \tag{2.14}$$

and the $\boldsymbol{G}$ vectors are defined by $\boldsymbol{G}l = 2\pi m$ for all the l lattice vectors of the crystal. m can take only integer values.

Finally, the electronic wave function can be rewritten as

$$\psi_i(\boldsymbol{r}) = \sum_{\boldsymbol{G}} c_{n,\boldsymbol{k}+\boldsymbol{G}} e^{i(\boldsymbol{k}+\boldsymbol{G})\boldsymbol{r}} \tag{2.15}$$

where $\boldsymbol{k}$ is the wave vector. Using plane waves with periodic boundary conditions we get rid of the infinite number of wave functions but end up having an infinite number of $\boldsymbol{G}$ vectors. However, the coefficients $c_{n,\boldsymbol{k}}$ for the PW with small kinetic energy are much greater than those with a large one. Therefore, their number can be safely truncated with negligible loss of accuracy. We still have to deal with infinite wave vectors $\boldsymbol{k}$; fortunately wave vectors with close values are very similar, therefore only a discrete set of $\boldsymbol{k}$ points is needed for the complete description of the system. We can further reduce the number of these points exploiting the high symmetry of the system; these define a smaller region of the most important points which are needed to effectively describe the WF of the system, called *Brillouin zone*.

2.3.2 Pseudo-Potentials

In a solid we usually have to deal with a huge number of electrons. Moreover, the valence electronic WF varies rapidly in the core region and are characterized by the presence of nodes; the correct description would need a very large number of PW. However, we are only interested in the explicit description of the valence electrons, for these are the ones that take part in the chemical process and bonds. The pseudo-potential (PPS) approximation[60] exploits this by removing the core electrons

and replacing the strong ionic potential by a weaker pseudo-potential in the core region. This situation is illustrated in Figure 2.2. This greatly reduces the computational effort as we only have to explicitly consider the valence electrons; moreover their WF are much simpler close to the nuclei so they need a few PW for a correct representation. These new functions are called *pseudo-wave functions*.

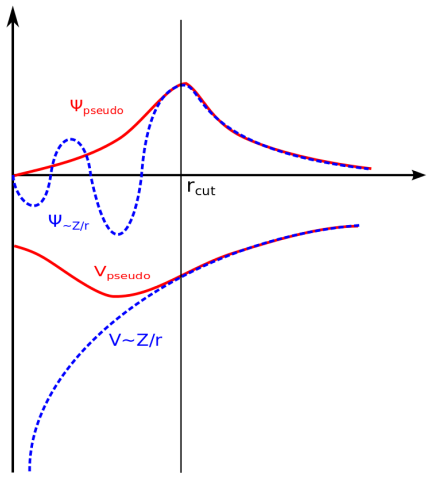

Figure 2.2: Representation of the Pseudo-Potential and the corresponding Pseudo-wave function. The strong ionic potential (in blue) is substituted by a weaker PPS (V_{pseudo}, in red). This approximation modified the Ψ in the core region; the resulting Ψ_{pseudo} is smoother and easier to reproduce.

2.3.3 Supercell approach

The use of the PW basis set requires to have the same periodicity in all the directions. Apart from few cases, we usually deal with systems non-fully periodic in one or more directions. The most common example is represented by surfaces, where the periodicity is broken along the z direction. We can easily

overcome this limit considering also the vacuum region as part of the same repeating unit (slab); the latter has to be chosen big enough to avoid interactions between the periodic images. This can easily be extended to the cases of adsorbates or defects as long as we can enlarge the unit cell, but also increasing the computational cost. In Figure 2.3 it is shown an example of the supercell approach applied to a surface.

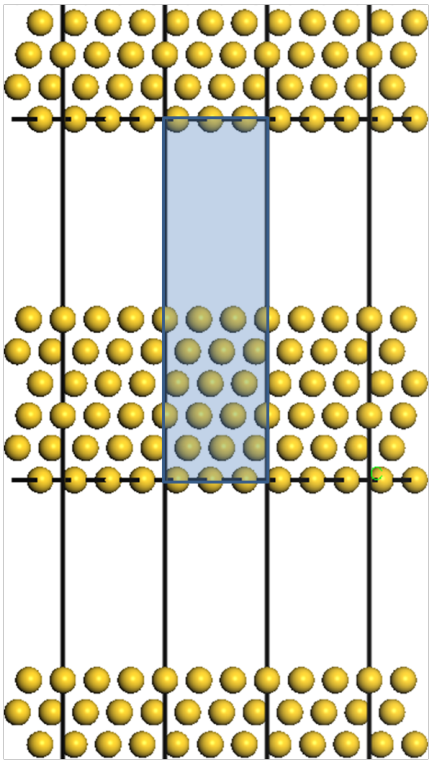

Figure 2.3: Application of the supercell approach for a metal surface (slab).

2.3.4 Van der Waals Interactions

As previously stated, a serious shortcoming of the standard DFT based methods is that they do not account for van der Waals interactions. In fact, calculations fail to reproduce the binding energies of the weakly interacting systems, e.g. organic molecules on metal surfaces.[61] Different extensions have been developed to solve this problem.[62–70] We can classify them based on the rigor of the treatment, which goes opposite to the computational effort.

The simplest approach considers the dispersion contribution as an additive term to the DFT energy. The most famous example of this group is the Grimme vdW-D2 method.[71] It is based on the London formula[72] for the pairwise interaction between two atoms, which leads to a sum over $\frac{C_6}{R^6}$. The coefficients C_6 are derived from atomic properties, therefore they yield an over-binding when applied to metals, due to their screening which is completely neglected.[73] The natural evolution of this method, the vdW-D3), includes the next terms (C_8 and C_{10}) in the expansion.[74] In this version, a range of precalculated coefficients for various elements is available, as a function of different reference states and number of neighbors. Despite these improvements the water-metal interaction is still largely overestimated.[73]

Based on the same principle, the group of Tkatchenko and Scheffler have developed a series of related methods. The first of them is known as DFT-vdW.[75] In this approach, the C_6 coefficients and R are determined non-empirically from the electron density; also, to obtain environment dependency, effective atomic volumes are used. However, it was not clear if the scaling of the properties would yield accurate results for more complex systems, such as metal surfaces. A possible remedy is to determine a metal surface C_6 coefficient taking into account the collective response (screening) of the substrate electrons, employing the Lifshitz-Zaremba-Kohn (LZK) theory;[76]

this method is known as DFT-vdW^{surf}.[77]

Alternatively, different functionals including dispersion have been constructed. Lundqvist *et al.*[55,78–81] proposed a non-local correlation functional that accounts for dispersion interactions approximately (vdW-DF). The results were found to depend on the particular combination between the exchange and the nonlocal correlation functionals (see e.g. Hamada *et al.*[82]).

Finally, the most rigorous approach is offered by the Random Phase Approximation (RPA) The method has been described in Section 2.2.1; it is capable of correctly describing both the correlation effect between the electrons and it includes the vdW energy seamlessly and accurately; unfortunately, it implies a tremendous computational effort, therefore its use is limited to benchmarks.

2.4 Estimate of Adsorption Energies from TPD experiments

Despite the already stated concerns, experimental data are fundamental to evaluate the theoretical models. In relation to this work, a special role is constituted by adsorption energies. It is possible to extract such information from Temperature Programmed Desorption (TPD) Experiments. Basically, the system (surface + adsorbate) is placed in Ultra-High Vacuum (UHV) and it is heated at a constant rate β (usually around 3 K/s) and the partial pressure of atoms and molecules evolving from the sample are measured, *e.g.* by mass spectrometry. When at a given temperature, a certain substance exit from the chamber, it generates a peak which is recorded (T_{max}). From this value and the heating rate β, it is possible to compute the adsorption energy for the species.

In this work, we have actuated the following procedure: An initial guess for the adsorption energy (E^I_{ads}) is obtained

through the Arrhenius formula

$$E_{ads}^{I} = -\left[RT_{max}\ln\left(\frac{k_r}{v}\right)\right] \tag{2.16}$$

where for the reaction constant k_r is used a default value of $1s^{-1}$ and for the prefactor v a default value of $1x10^{13}s^{-1}$. The result is introduced in the equation from Redhead,[83] to calculate a more refined value for the energy in a self consistent way (E_{ads}^{F}), till convergence is reached:

$$E_{ads}^{F} = RT_{max}\left[\ln\frac{vT_{max}}{\beta} - \ln\frac{E_{ads}^{I}}{RT_{max}}\right] \tag{2.17}$$

It must be stressed that the default value for the prefactor v has been demonstrated to be often grossly inaccurate. Campbell and Sellers[84] developed a procedure to improve the parameter, including the entropy effect

$$v = \left(\frac{k_b T_{max}}{h}\right)\exp\left\{\frac{0.30S_g^0}{R} + 3.3 + \right.$$
$$\left. - \frac{1}{3}\left\{18.6 + \ln\left[\left(\frac{m}{m_{Ar}}\right)^{3/2}\left(\frac{T_{max}}{298K}\right)^{5/2}\right]\right\}\right\} \tag{2.18}$$

2.5 Search for the Transition State

As stated in the Introduction, the study of adsorption processes and the evaluation of the related energies is of primary importance in this work. However, a different matter arises when we consider the path followed by a species in a determined reaction as we did in Chapter 4.2. In this case, we also need to evaluate the energy barriers involved in the single steps of the path, the so-called activation energies E_a.

The simplest approach to evaluate such quantities is given by the Arrhenius rate law,[85] which connects the rate constant of a reaction with the *apparent* activation energy E_{app}:

$$k = Ae^{-E_{app}/(RT)} \tag{2.19}$$

The energy differs from the actual activation energy E_a since its equation originates from empirical observations, ignoring any mechanistic considerations, *e.g.* if more than one intermediates are involved in the conversion to products. It is usually employed to have a first guess about a determined process.

In order to have a more precise approach is necessary to further develop the two parameters associated with Equation 2.19, the pre-exponential factor A and the activation energy itself. These issues are addressed by the Transition State Theory (TST), simultaneously developed by Eyring[86] and Evans and Polanyi.[87] Qualitatively, the reaction proceeds through an activated complex, the transition state (TS), located at the top of the energy barrier between reactants and products. The process is described by a single parameter, called the reaction coordinate, *e.g.* the stretching vibration between the two atoms in the dissociation of a diatomic molecule. The reaction can thus be visualized as a journey over a potential energy surface, where the transition state lies at the saddle point.

The application of the TST to complex system such as molecules adsorbate on surfaces is far from straightforward. Different methods have been developed; here we focus our attention on the Nudged Elastic Band (NEB). Once the initial and the final states are well defined, a series of "images" of the system are created along the reaction path. These images are then optimized to find the lowest energy possible, while maintaining equal spacing to neighboring images. This constrained optimization is achieved adding spring forces between images and projecting out the component of the force due to the potential perpendicular to the band. The method employed in this thesis

is a slight improvement of the NEB method, called Climbing-Image NEB (CI-NEB). Once a NEB is carried out, the image with the higher energy is driven up to the saddle point. This image does not feel the spring forces; instead, the true force at this image along the tangent is inverted. This way, the image tries to maximize its energy along the band, and minimize in all the other directions. To check if the retrieved structure is a true TS, its normal mode of vibration are calculated; all the frequency must be real value except for the one along the reaction coordinate which has to have an imaginary value, being a saddle point.

Chapter 3

Rutiles

Rutiles are a particular class of metal-oxides with common chemical formula MO_2 which has attracted a lot of attention in recent years.[88–92] Despite having the same structure shown in Figure 3.1 (TiO_2 also has two other polymorphs, anatase and brookite), they have quite different chemical properties (metallic and semiconductors), determined by the composing metal. Not only they have quite different properties and applications as isolated compounds, but also due to the structural similarity, they can easily combined to form new materials with tuned properties. Despite being largely employed in the industry and especially in heterogeneous catalysis, a systematic investigation of this class is still missing. To this end we have therefore chosen four of its compounds (Ir, Ru, Sn and Ti oxides) and studied them both as isolated nanoparticles and in combinations with each other. Some fundamental properties along with the most important applications of these four has been reported in Table 3.1

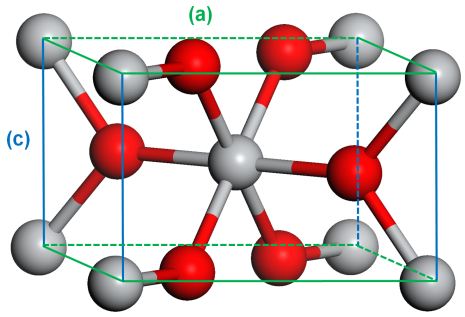

Figure 3.1: Bulk unit cell of rutile species. They are characterized by the same structure but different lattice parameters, reported in Table 3.1.

Table 3.1: Summary of information on four important Rutiles.

MO_2	**L. P.** (Å)	**Conductivity**	**Applications**
RuO_2	a = 4.490 c = 3.140	metal	Capacitor devices,[93,94] Cl_2 synthesis[95–107]
IrO_2	a = 4.510 c = 3.110	metal	Cl_2 synthesis[105,107]
SnO_2	a = 4.747 c = 3.186	semi-conductor	Redox gas sensors[17,18]
TiO_2	a = 4.594 c = 2.958	semi-conductor	Photocatalyst[1] Br_2 Synthesis,[108] Support[3–5]

3.1 Rutiles: isolated compounds

As stated in the introduction and shown in Figure 3.1, rutiles are characterized by the same unit cell. However, the crystal formed in thermodynamical equilibrium is different for each of the compounds and can easily be determined following the Wulff construction.[109] Basically, the lower the surface energy, the more extended will it be in the crystal. In this case, different lattice parameters and the chemistry of the element are fundamental factors: the difference between the surface energies will

vary, therefore quite different nanoparticles will be obtained, as shown in Figure 3.2. As an example, in the RuO_2 crystal, (110) and (101) facets have an equivalent surface, while in TiO_2 the (110) is far more extended up to 80 % of the total surface. The study of the different facets is of primary importance, since they possess different reactivity.

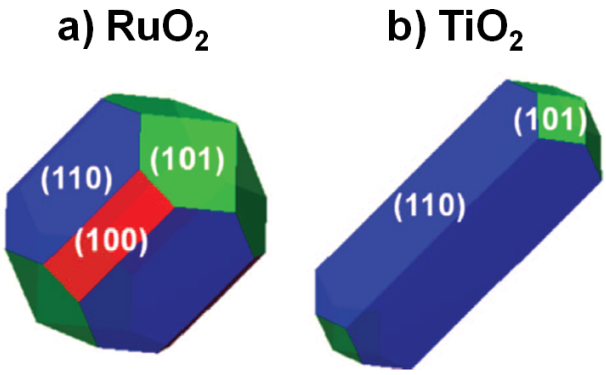

Figure 3.2: Wulff Structure for a) RuO_2 and b) TiO_2. Despite having the same unit cell, the rutiles end with quite different crystals.

3.2 Rutiles: alloys

Along with the use of the pure compounds, the employment of mixtures is a common practice and alloys can easily be formed for these rutiles possess the same stable structure. Secondary components can enhance the chemical and electrochemical properties, along with stability and selectivity.[110] The improved properties and the applications of some available combinations are reported in Table 3.2. For this reason, along with studying the rutiles as pure nanoparticles is very important to investigate the possible alloys. In the next sections, some

important properties related to the formation of alloys will be assessed.

Table 3.2: A summary of some important rutile alloys, with the applications and enhanced properties compared to the pure compounds.

primary component	**secondary component**	**enhanced properties**	**applications**
RuO_2	SnO_2	support (cheaper)	HCl oxidation[105, 107]
RuO_2, IrO_2		activity stability conductivity	Electrocatalysis[111] Dimensionally Stable Anodes (DSA)[102, 110, 112, 113]
TiO_2	IrO_2, RuO_2	stability	Cl_2 production anodes[114]
TiO_2	SnO_2	enhanced design	Dimensionally Stable Anodes (DSA)[115]

3.2.1 Solubility

First of all, we have to determine if one element is easily soluble into a host compound. As previously stated, despite having the same structure, these materials have different lattice parameters and different conductivity, as shown in Table 3.1. These two factors can hinder the formation of the alloy and this in turn will affect the maximum concentration of impurities allowed. From our analysis solubility is promoted only for the two metals, Ir and Ru oxides;[116] for all the other alloys the formation of mixture is unfavored but to a small extent. The conclusions drawn from these findings only refer to the thermodynamical aspect of this property. Also, the neglect of configurational entropy explains the difference with experimental results, where at least for low concentration, a solid solution is formed (see Table 3.3).

Table 3.3: Experimental maximum percentage of total solubility for different rutile pairs.

dopant	**host**	**percentage**
RuO_2, IrO_2		any[116]
IrO_2	TiO_2	5 %[117]
TiO_2	IrO_2	10 %[117]
SnO_2	IrO_2	1-2 %[117]
SnO_2	TiO_2	0.23 %[118]

3.2.2 Segregation

Once we have established the concentration of the dopant into an alloy, it is time to focus on the surface composition. It is not easily to evaluate nor to predict it, since the concentration of the impurity on the surface can greatly differ from the one in the bulk; this phenomena is known as segregation and it is illustrated in Figure 3.3

For metals, only one method exist to directly measure the segregation energy, called photoemission spectroscopy of surface core-level shifts.[119] It is limited to mixture with metal with close atomic numbers. Theoretically, different methods have been developed, such as the Langmuir-McLean relation:[120] it relates the segregation energy to the impurity concentration in the surface and the bulk. Other approaches have been proposed, based on Miedema theory[121] or tight-binding approximation. All these methods are only able to predict the sign of the segregation, or they are only applicable for late transition or noble metals.

As stated in the Introduction, metal oxides knowledge is limited compared to metals. In this case as well as in more complex metals,[122–124] we need to build an extensive database to find available trends and understand the general behavior. This has been done previously for some metal oxides,[125] but

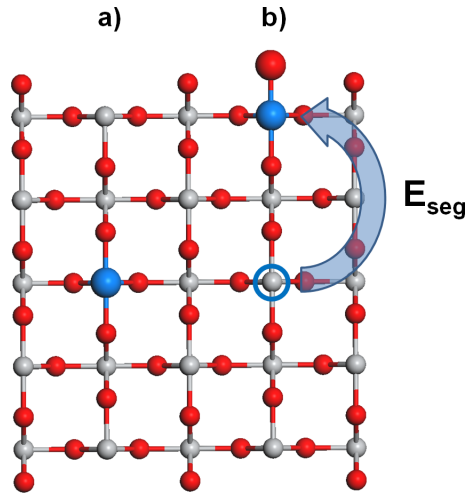

Figure 3.3: Scheme representing the segregation phenomena. In a) the impurity (blue sphere) is found in the bulk while in b) it migrates to the surface. The quantity E_{seg} gives an estimate of such process. This process can be greatly affected by the environment (in this case the oxygen, which forms a stronger bond with the substituent).

no studies have been made on rutiles. To this end, we have generated a database of E_{seg} of the four rutiles. An example is shown in Figure 3.4, where this quantity is reported for three different impurities (Ru, Sn, Ti) in IrO_2; a negative value means that the species tend to be on the surface.

The calculation has been extended to all the possible combinations, with the rutiles acting either as guest or host and to four low-index surfaces. To make the results more clear and to highlight possible trends, we have also employed a heat colour scale, where colder colours correspond to more likely processes.

From the analysis it turns out that for the metal hosts (Ru and Ir oxides), the semiconductors migrate strongly towards the surfaces (in the case of IrO_2, this also applies to Ru). With

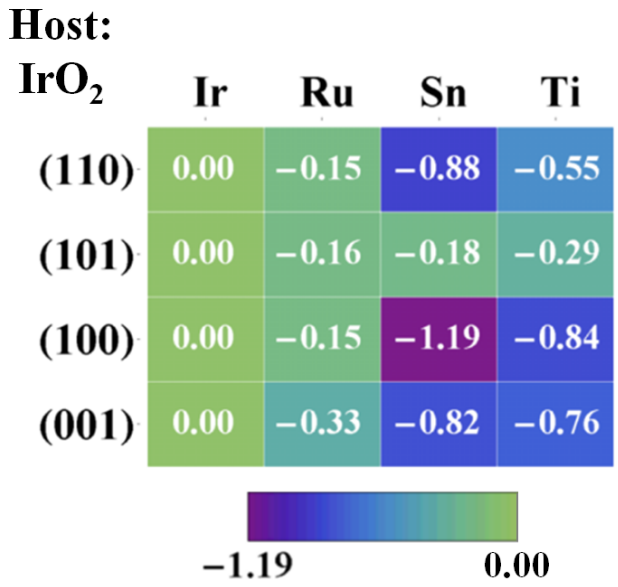

Figure 3.4: Segregation energy, E_{seg} in eV, of different guest (column) on different facets (row) for IrO_2. Colder colours correspond to more exothermic values (the element segregates more).

a few exception facet related, the semiconductor always acts as hosts, and they keep the other metals into the bulk; TiO_2 is also preferentially found on the surface within Sn oxide.

3.2.3 Adsorption induced segregation

The segregation phenomena can be greatly affected by the environment; in fact, molecules can adsorb and change the relative total energies. We refer to this process as *adsorption induced segregation*. This is due to the fact that impurities can bind preferentially with the adsorbates, therefore they will tend to stay on the surface. This phenomena is very important to assess the thermal stability of a particular alloy.

Quantitatively, we can describe the phenomena as following: Given an impurity A in a A_xB_{1-x} alloy, its condition to be at the surface can be expressed by the following:

$$E_{seg}(A) + E_{ads}(A) - E_{ads}(B) < 0 \tag{3.1}$$

where $E_{seg}(A)$ is the segregation energy of A and $E_{ads}(A)$ and $E_{ads}(B)$ are the adsorption energies of the adsorbate on element A and B respectively. This means that if the difference between the adsorption energies is too high, it will yields a reversed segregation. A scheme of the oxygen induced segregation was presented in Figure 3.3.

Again, a complete database is needed in order to understand the property. The most important adsorbate in the case of rutiles is oxygen, for these compounds are often used in oxygen rich environments and Ir and Ru oxides can easily adsorb it. Not surprisingly, the results are almost opposite of the ones obtained for the compounds in vacuum: the metal hosts (Ir and Ru oxides) tend greatly to be on the surface when acting as impurities, while as hosts they block the segregation of the semiconductors (Sn and Ti oxides), which stays into the bulk.

3.2.4 Overlayers

Finally, the epitaxial growth of a rutile on top of another is addressed; this phenomena is shown in Figure 3.5 for one and two layers. This property is very important, since these rutiles (especially Ti and Sn oxides) are extensively employed as supports.[3–5,105,107] This phenomena could be hinder by the mismatch between different lattice parameters, as reported in Table 3.1; an evaluation of its extent is needed. To do so, we have evaluated the Adhesion energy E_{adh}, which is related to the surface energies at the interface (γ) and of the native surface (γ_0):

$$\gamma/\gamma_0 = (\gamma_{int} - \gamma_h)/\gamma_0 = 1 + E_{adh}/(A \cdot \gamma_0) \qquad (3.2)$$

where γ_{int} us the interface energy and γ_h is the surface energy of the oxide support.

The Adhesion controls the possibility for bidimensional or tridimensional growth. A negative (exothermic) value of its energy means that a bond is formed between the layers, therefore a second layer can easily grow on top of another one. From our study it is clear that this is not the case, as the adhesion energy, is exothermic in all the cases. This means that there is always the formation of a bond between a host rutile and a layer of a guest from the series. The same applies to the formation of another layer on top, and we can extend this result to any amount of layers.

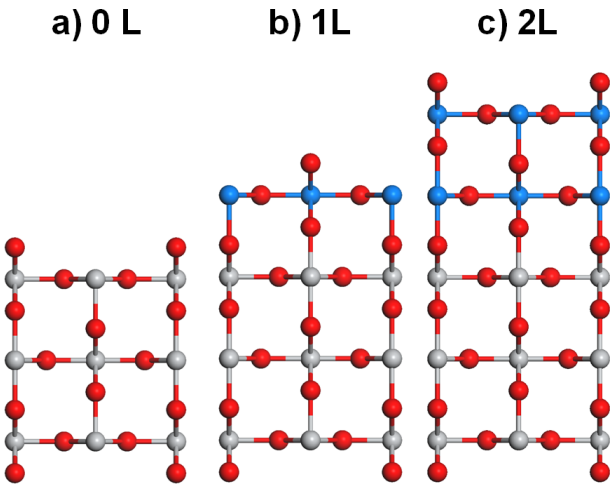

Figure 3.5: Epitaxial grow of a guest rutile on top of a host one. a) clean host rutile, b) one layer of guest on top and c) two layers.

3.2.5 Conclusions

Metal oxides are employed in a great range of applications but their understanding is quite limited compared to metals. This is due to more complex structure and chemical properties. Rutiles are a class within the metal oxides which are characterized by the same structure but different conductivity.

We have carried on a rigorous study on these compounds, especially focusing on the formation of alloys. In fact, this is easily achieved due to the structural similarity and yield to the design of brand new materials with fine tuned properties. The amount of impurities is somewhat limited by the different nature of the metals involved, therefore only for Ru and Ir oxide, a mixture is readily obtained with any composition.

Surface composition can be very different compared to the one in the bulk, due to a phenomena known as segregation. This is quite hard to evaluate experimentally and to model theoretically even for metals. However, a grasp on the thermodynamic properties can be obtained by DFT. To investigate this for metal oxides and rutiles it is therefore needed to build a full database with all the possible combinations. In the specific case, the semiconductor Ti and Sn oxides tend to stay on the surface and block the metals in the bulk.

This phenomena can be affected by the bond with adsorbates. For rutiles, oxygen greatly influence the segregation since it preferentially bind with Ir and Ru, pushing them on the surface. At the same time, when RuO_2 and IrO_2 act as hosts, they keep the semiconductor deep behind the surface.

Finally, it is possible to epitaxially grow any rutile on top of another despite the mismatch between the lattice parameters; this means that any of them can be used as a support for another one and this is very useful since some of the rutiles are quite expensive.

Chapter 4

Alcohols adsorption and reactions on titanium dioxide

Alcohols can be the precursor of a great variety of compounds, when reacting on Titanium Dioxide. In fact the hydroxyl can be converted to important functional groups,[126–128] as shown in Figure 4.1. Alcohols also possess applications ranging from probes of reactive sites,[129–133] to models for the investigation of photoxidation of organic contaminants.[134,135]

In this chapter, the interaction of small mono- and poly-alcohols on Titanium Dioxide is analyzed. In the first part, the phenomena of adsorption is deeply investigated for a series of alcohols with increasing chain length and number of hydroxyls. For a more complete analysis, both molecular and dissociative adsorption are assessed. Also, the study has been carried on stoichiometric as well defective surfaces. Next, the dehydration process is studied for Ethylene glycol and 1,3-Propanediol; a reaction profile is generated and a mechanism explaining the difference between the two compounds was proposed. The stoichiometric and defective (vacancy on the surface and the bulk)

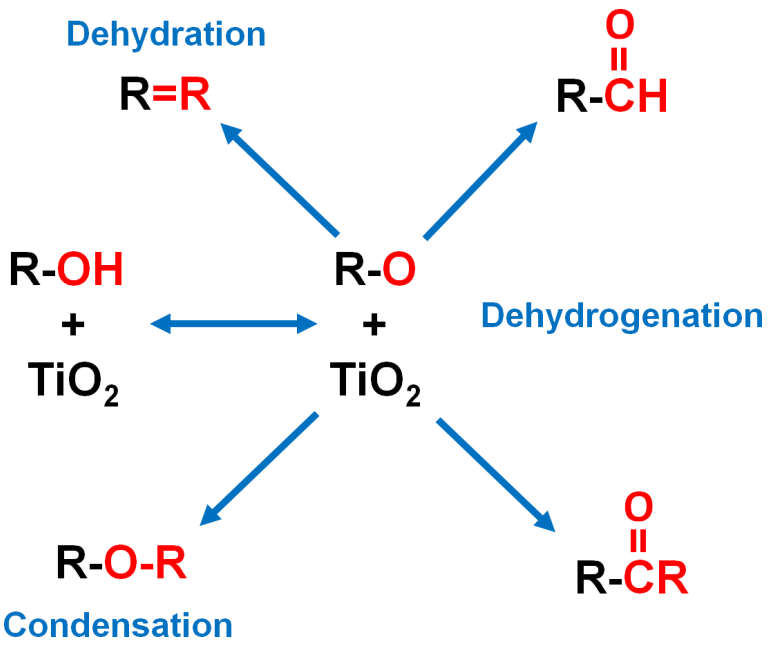

Figure 4.1: Possible reaction products of alcohols on TiO_2.

structures of TiO_2 are shown in Figure 4.2.

4.1 Adsorption

On titania, two sites are available for the adsorption, the Titanium in Coordinatively Unsaturated Site (Ti_{cus}) and the vacancy (V_O) formed when one oxygen in bridge position (O_b) is missing. This process has been deeply investigated and a large amount of experimental data is available, summarized in Table 4.1

Despite this abundance of information, to model the adsorption phenomena can be challenging. This is particularly evident for quite different values are found for the same alcohol. Among other properties, this is primary due to the dif-

Table 4.1: Experimental adsorption energies, E_{ads}, in eV, for different alcohols, ROH on TiO_2 (110). Additional information on the type of adsorption, $Type_{ads}$, Position of the substrate and the Coverage, in ML, are reported when available.

ROH	**Type**$_{ads}$	**E**$_{ads}$	**Coverage**	**Position**
MeOH	*M*	-0.96[136]	0.22	Ti_{cus}
		-0.95[137]	-	-
	D_1	-1.32[137]	-	-
EtOH	*M*	-0.68, -0.48[128]	0.75, 3.75	-
		-0.99[136]	0.20	Ti_{cus}
		-0.91[138]	-	V_O
		-0.81, -1.03[139]	0.80	Ti_{cus} , V_O
		-0.93, -0.80[131]	Saturation	Ti_{cus}, V_O
	D_1	-1.67, 1.64[131]	Saturation	Ti_{cus}, V_O
		-1.66[139]	0.80	V_O
		-1.10, -0.68[128]	0.75, 3.75	-
		-1.64[138]	-	V_O
1-PrOH	*M*	-1.08[136]	0.19	Ti_{cus}
		-0.93, -0.94[131]	Saturation	Ti_{cus} ,V_O
	D_1	-1.62, -1.57[131]	Saturation	Ti_{cus}, V_O
1-ButOH	*M*	-1.11[136]	0.17	Ti_{cus}
i-PrOH	*M*	-1.03[136]	0.23	Ti_{cus}
		-0.93, -0.86[140]	0.20	Ti_{cus}
		-0.92[141]	0.18	Ti_{cus}
		-1.03[139]	0.60	V_O
		-0.93, -0.94[131]	Saturation	Ti_{cus}, V_O
	D_1	-1.66[139]	0.60	V_O
		-1.47[131]	Saturation	-
		-1.33[141]	0.18	V_O
	-	-0.96, -1.53[142]	0.90	-
2-ButOH	*M*	-1.11[136]	0.17	Ti_{cus}
t-ButOH	*M*	-0.99[136]	0.27	Ti_{cus}
1,2-EtOH	*M*	-1.26[143]	0.25	Ti_{cus}
		-1.08[131]	Saturation	Ti_{cus}, V_O

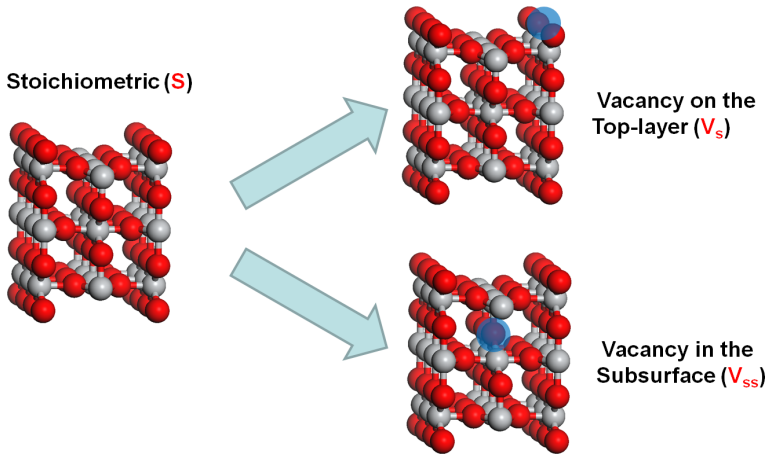

Figure 4.2: TiO_2 (110) facets: the stoichiometric surface (S, left side) can lose one oxygen and create a vacancy (right side, represented by blue shadowed spheres), either on the top layer (V_s) or in the second layer (V_{ss}).

ferent coverage and to the different adsorption site. The latter problem is a consequence of the formation of vacancies, which is very common in titanium dioxide and will be described in details in the next section. In this study, we investigated the adsorption phenomena of a series of mono-(linear and branched) and poly-alcohols on the (110) facet (the most stable) of TiO_2. In particular, we want to assess the possibility to employ the simplest members of the series like methanol, as surrogates for more complex molecules. This in turn allows the construction of scaling relationships, *i.e.* to express the adsorption energy as a function of the number of CH_2 and functional groups.[144]

4.1.1 Titanium dioxide (110)

As previously stated, the study of metal oxides can be particular challenging and their knowledge lays behind that of metals. In particular, the presence of different acid (the metal) and ba-

sic (the oxygen) centers is of primary concern; regarding TiO_2 (110) there are two other factors to consider: the corrugation of the surface and the formation of vacancies.

The corrugation refers to the particular termination of the (110) facet. The packing of Titanium ions in Coordinatively Unsaturated Site (Ti_{cus}) and in-plane oxygens is attenuated by rows of oxygens in bridge position (O_b). These rows can both sterically hinder the adsorption of reactants (which usually takes place on the Ti_{cus}) and reinforce the bonding (*e.g.* through hydrogen bonds). The formation of vacancy is very common in TiO_2; in fact, this compound can easily be reduced, with some Titanium becoming formally Ti^{3+}, but generating a delocalized charge. The reason behind this is rooted in the nature of Titanium which almost lose all the electrons at the d and s levels upon oxide formations. We can either have them on the surface, or in the bulk and in both cases there are two electrons left by the missing oxygen, affecting the electronic structure. If the leaving oxygen is a O_b, it also produces a new site which can compete for the adsorption of the substrate. The three surfaces, stoichiometric (S), with vacancy on top (V_s) and with the vacancy in the subsurface (V_{ss}) are shown in Figure 4.2 We have calculated the adsorption energies of a series of mono- (linear and branched) and poly-alcohols on TiO_2 (110), stoichiometric, and with both kinds of vacancies. Moreover, we have also considered the dissociation of the molecules on the surface upon adsorption, for this is an important step in the reaction paths of Figure 4.1. In the next section, the results of this analysis has been reported.

4.1.2 Results

Once the adsorption energies have been computed, the results have been analyzed following different parameters, such as the degree of dissociation, the length/encumbrance of the hydro-

carbon part and the number of hydroxyl groups. An example is represented in Figure 4.3: on top it has been reported the molecular adsorption, while on the bottom the dissociative. The data are also subdivided between linear, branched (both mono-alcohols) and poly-alcohols.

The obtained results warn against the use of surrogates *i.e.* small molecules as models for more complex systems. This is especially true in this case, since the surface corrugation is comparable with the length of the molecules. It is clear that primary and secondary alcohols are perfect to fill the vacancies, somehow further confine the active sites along the [001] channels. However, this is no longer true for tertiary ROH because steric hindrance greatly limits the accessibility to vacancy positions. Polyalcohols behave in a more complex way, thanks to internal hydrogen bonds which can stabilize some of the configurations. When the adsorption is molecular, all the alcohols prefer the Ti_{cus} sites, and need two of these for a proper interactions. Upon dissociation instead, the alcohols with two hydroxyls close to each other greatly prefer the vacancy sites, while the others can equally pick both sites. Finally, we want to stress that the energies are almost constant for the monoalcohols, independently on the chain length, again the tert-butil being less stable. Polyalcohols are less stable with the increasing number of hydroxyls or if these are not next to each other.

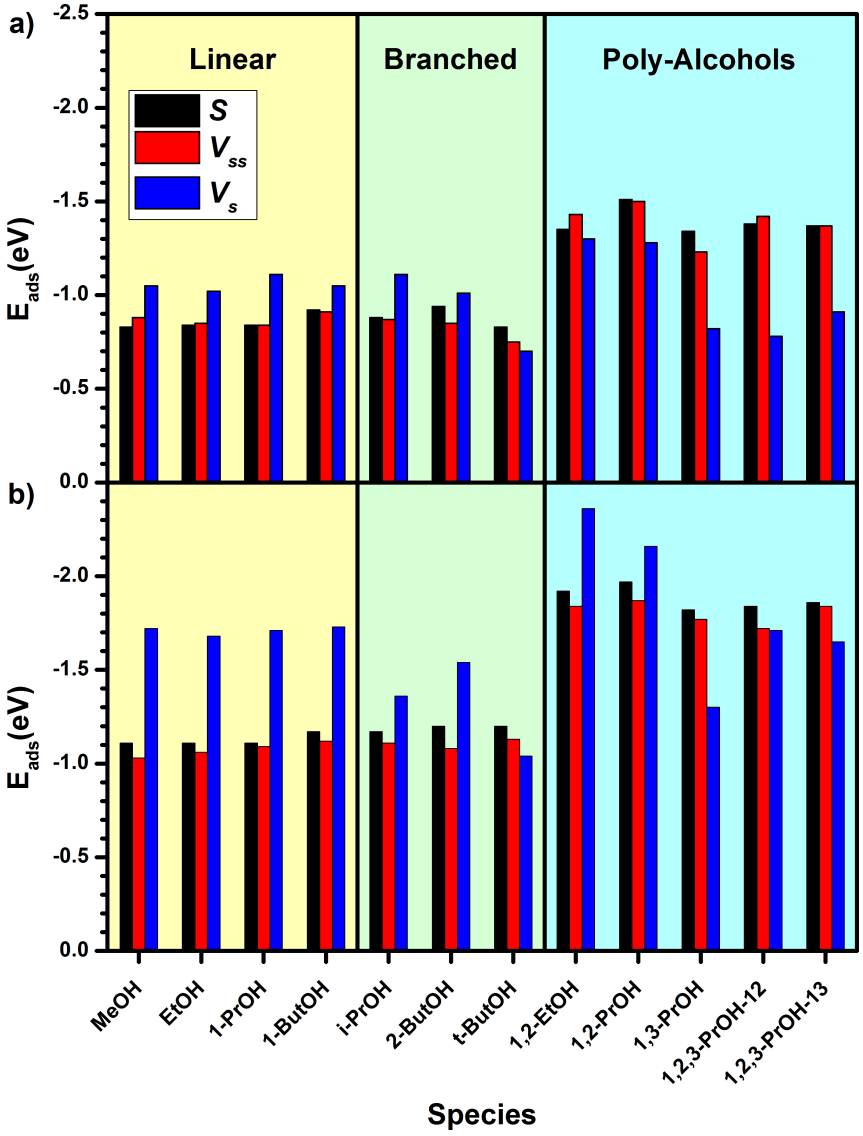

Figure 4.3: Results of the analysis of alcohols adsorption on TiO_2. a) molecular adsorption and b) dissociative. The data have also been subdivided between linear, branched (both these two are mono-alcohols) and poly-alcohols.

4.2 Dehydration of diols on titanium dioxide

Once adsorbed, small polyalcohols can take part to different reactions and a particularly useful process is the catalytic dehydration to alkene, with the formation of water

$$\text{R-CH}_2\text{-OH} \rightarrow \text{R=CH}_2 + \text{H}_2\text{O}$$

The group of Dohnálek proposed a mechanism based on Scanning Tunneling Microscope (STM) experiments coupled with DFT simulations. Small diols like ethylene Glycol and 1,3-propanediol (1,2-EtOH and 1,3-PrOH in this text) were used as surrogates for more complex system.[145] TPD experiments were also reported, see Figure 4.4.

The described pathway turns out to be very complex for it includes the migration of vacancies, for it need two vacancies to be next to each other. This situation is unlikely, since the total concentration of vacancy is 5-10% in the total surface.[146,147] The mechanism also comprehends the formation of radical species, which require very high energies (almost 3 eV for 1,3-PROH). In the light of these factors, we have investigated an alternative route for the process, by means of DFT simulations. As shown in the next sections, this mechanism includes only few simple steps and far lower energy barriers. In particular, only one vacancy is needed for a cycle.

4.2.1 Proposed Mechanism

We can divide the whole process in two parts. In the first, 1,2-EtOH and 1,3-PrOH adsorption on a vacancy V_O is readily followed by the hydroxyl dissociation; the freed hydrogen is subject to diffusion and ends bound to the bridge oxygen O_b next to the second hydroxyl. In the second part, the two diols take different paths which yield alkenes and water molecules

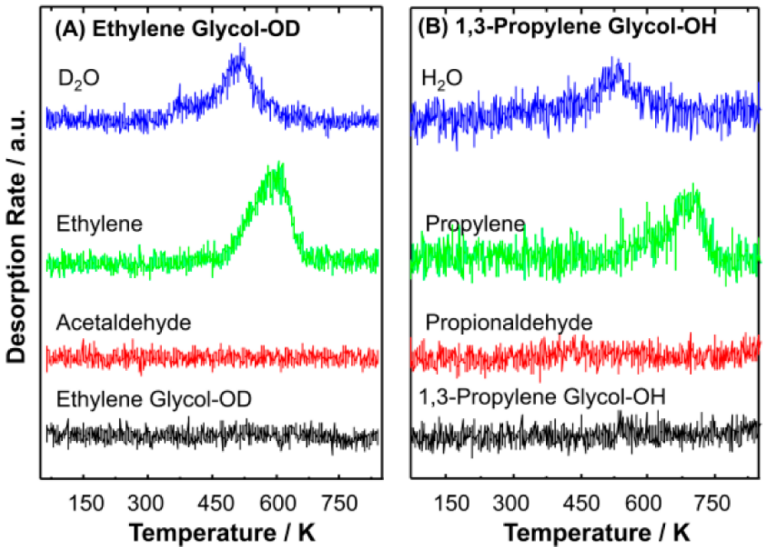

Figure 4.4: From Reference of Acharya *et al.*:[145] TPD spectra of the desorbing species observed following the 0.05 ML dose of (A) ethylene glycol and (B) propylene glycol OH at 90 K. The desorption of EG-OD was monitored at 32 amu, which is the most intense cracking fragment. Desorption of D_2O at 20 amu, ethylene (CH_2CH_2) at 27 amu, and acetaldehyde (CH_3CHO) at 29 amu. The desorption of 1,3-PG-OH was monitored at 31 amu, which is the most intense cracking fragment. Desorption of H_2O at 18 amu, propylene (CH_2CHCH_3) at 41 amu, and propionaldehyde (CH_3CH_2CHO) at 58 amu.

as final products. The whole reaction profile is represented in Figure 4.5.

Initial state: Adsorption at the vacancy

In the first step, the diols adsorb on the surface, with one of the hydroxyl filling a vacancy (OH-1) while the other (OH-2) is weakly bound to the closest Titanium in Coordinatively

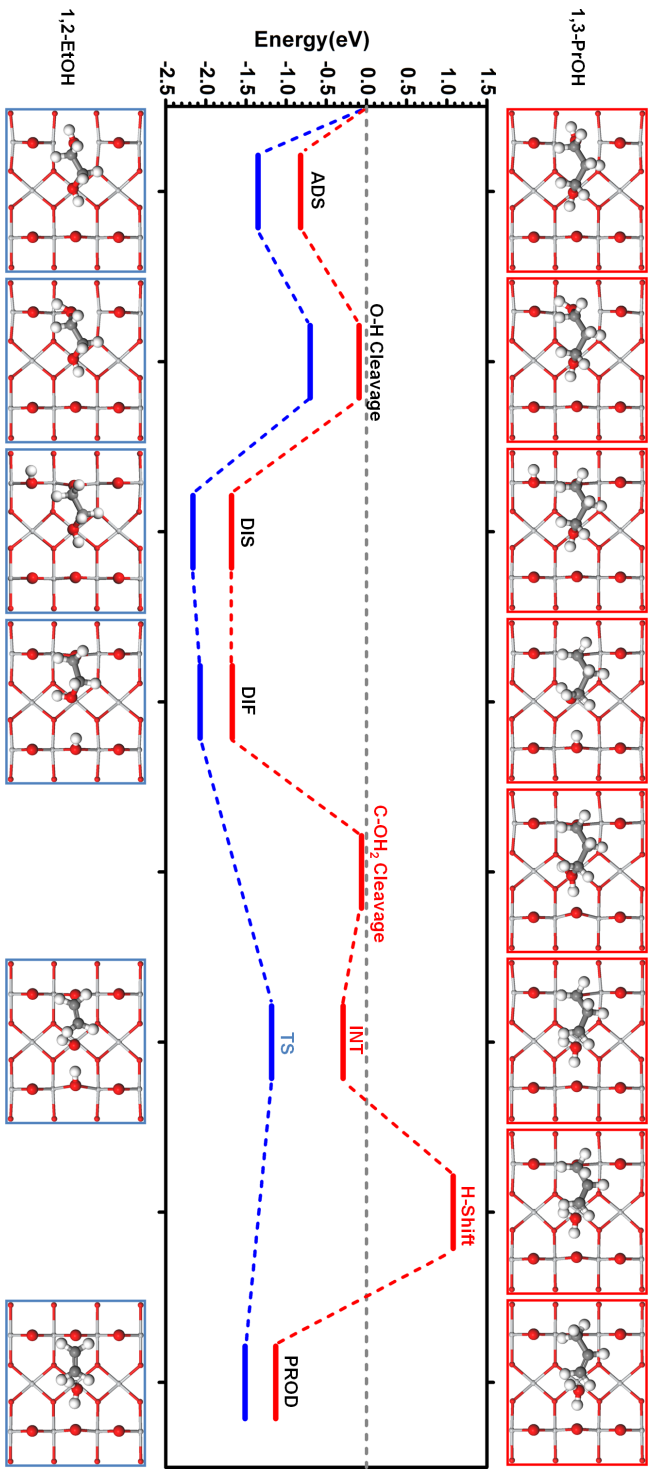

Figure 4.5: Reaction profile of Dehydration for the diols 1,2-EtOH and 1,3-PrOH.

Unsaturated Site (Ti_{cus}); this is shown for the 1,3-PrOH in Figure 4.6.

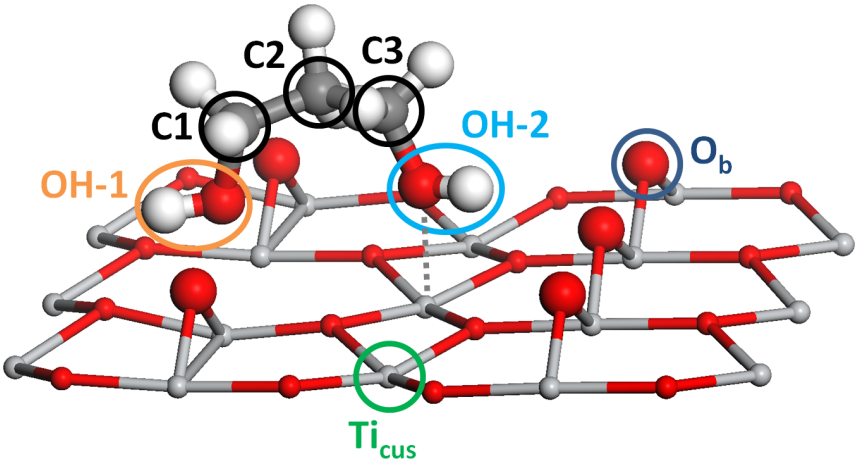

Figure 4.6: 1,3-PrOH adsorbed on TiO_2. One of the hydroxyl (OH-1) is filling the vacancy, while the other (OH-2) is slightly bound to one Ti_{cus}. The most important elements have been highlighted.

The adsorption process has been deeply investigated in Chapter 4.1. Here there are reported the adsorption energies (E_{ads}, in eV) for both the diols on stoichiometric and defective surfaces, see Table 4.2. Negative values represent exothermic processes.

From the results it is shown that the molecular adsorption is favored (slightly in the case of the glycol) on the stoichiometric surface, for both the species. However for the 1,2-EtOH the dissociation process favors the binding of the substrate to the vacancy, being more stable than on the stoichiometric. 1,3-PrOH on the other hand turns out to be favored on the latter (*i.e.* bound exclusively on the Ti_{cus}) in both its molecular and dissociative state. This difference can be explained among other factors with the different distance of the substrate from the

Table 4.2: Adsorption energy, E_{ads} in eV, of 1,2-EtOH and 1,3-PrOH on TiO_2 (110). The value for both stoichiometric (S) and defective (V_s) surfaces are reported. Molecular (M) and dissociative (D) type of adsorption have been considered.

Substrate	**Surface**	**Type**	$\boldsymbol{E_{ads}}$
1,2-EtOH	S	M	-1.35
		D	-1.61
	V_s	M	-1.30
		D	-2.13
1,3-PrOH	S	M	-1.34
		D	-1.65
	V_s	M	-0.82
		D	-1.26

surface. In the case of 1,2-EtOH, the distance Ti_{cus}-O increases with a molecular adsorption, from S to V_s. Upon dissociation, the molecule can accommodate better, and there is a decrease in the distance, hence lower energy. For 1,3-PrOH the distance is always larger when adsorbed in the vacancy; the system is less stable and E_{ads} is higher. Once the molecule is bound the surface the two compounds follow a common path for the first steps.

First Dissociation and Diffusion

The oxygen in the vacancy can lose the hydrogen to a close Oxygen in Bridge position (O_b). The freed hydrogen can easily migrate for diffusion, therefore we find it bound to the O_b close to OH-2. This first part is shown in the Figure 4.7

The energy profile between the two compounds is almost the same, separated by a constant energy value. A small difference in the diffusion state is retrieved since in 1,2-EtOH the rotation of OH-2 around the C-O bond is hindered and its arrangement

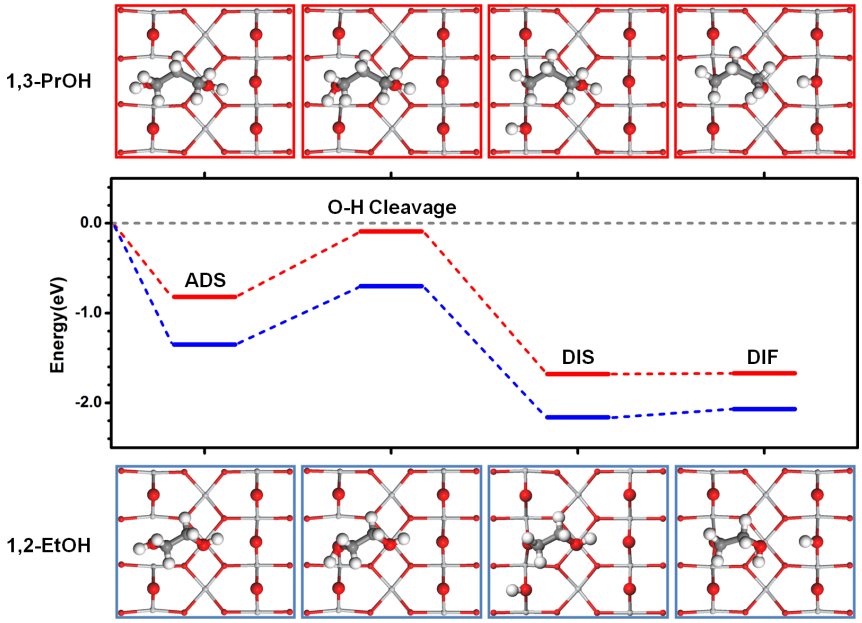

Figure 4.7: Common path of the reaction profile of Ethylene glycol (1,2-ETOH, in blue) and 1,3-propanediol (1,3-PrOH, in red) dehydration on TiO_2. The O-H bond of the hydroxyl OH-1 (see Figure 4.6) is broken and the released hydrogen migrates for diffusion to the O_b to the side of OH-2.

with the O_b-H is not perfect; on the other hand, for 1,3-PrOH such rotation is almost free.

After the hydrogen diffusion the two systems enter different pathways, as illustrated in the next sections.

Different paths to the products

In the last part the two compounds follow different reaction paths. In the case of 1,2-EtOH, a single step is needed to get to the products. The hydrogen found on the O_b next to the OH-2 binds to such hydroxyl. the oxygen is now connected to two hydrogens, therefore can easily leave as water. This determines

the rearrangement of the electrons to form the double C=C bond as well as the breaking of the second C-O bond. At the end of the step, ethylene and water are formed on the surface and the vacancy has been healed with the oxygen from the hydroxyl OH-1. The reaction step is shown in Figure 4.8.

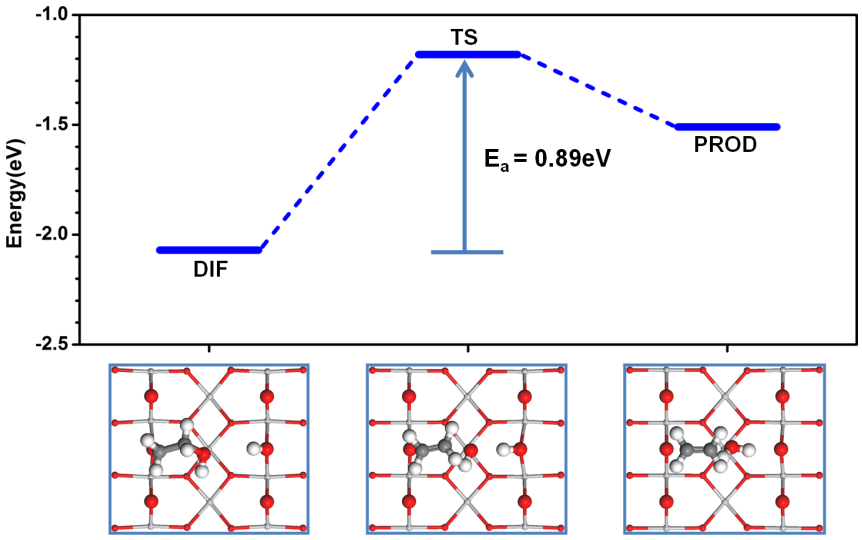

Figure 4.8: Second part of the dehydration for 1,2-EtOH. The system evolves to the products in a single step, with the simultaneous formation of water and breaking of both the C-O bonds.

For 1,3-PrOH the path is more complex. Like the smaller alcohol, there is the formation of water. However, in contrast with 1,2-EtOH, a high energy intermediate is obtained and a second step is needed to get to the products. Such process consists in the formation of the double bond C=C, which includes an H-shift between the central carbon and the terminal one connected to the OH-1. This finally results in the breaking of the second C-O bond and the formation of the alkene (see Figure 4.9).

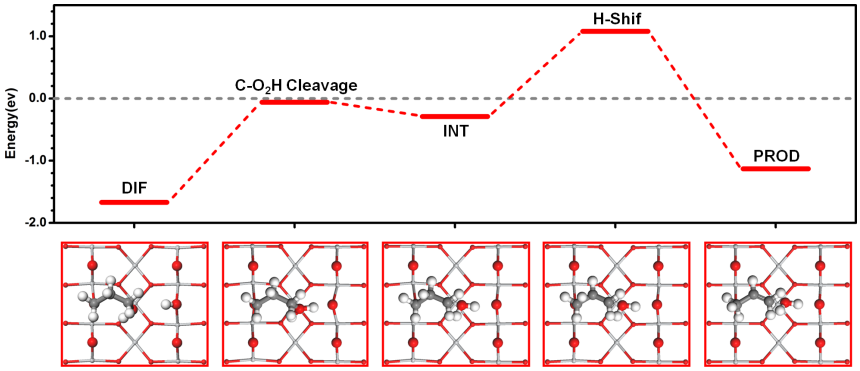

Figure 4.9: Second part of the dehydration for 1,3-PrOH. This is more complex than the path for 1,2-EtOH and includes an high energy intermediate with the water still bound to the molecule. This system evolves to the products with a second step, where the migration of the hydrogen is coupled with the breaking of both C-O bonds.

4.2.2 Discussion

The described mechanism shows that, although the two reactants are very similar, two different paths are followed. In fact, 1,3-PrOH dehydration comprehends three steps and passes for an high-energy intermediate, while 1,2-EtOH just evolves to the products in two steps. The highest barrier is retrieved for both the compounds after the hydrogen diffusion step, following the first dissociation. This corresponds to a value of 0.89 eV for 1,2-EtOH and 1.61 eV for 1,3-PrOH. The formation of the high-energy intermediate is the reason why 1,3-PrOH requires more energy compared to 1,2-EtOH (see Figure 4.4). This explanation, along with the analysis of the adsorption process (see Section 4.1), strongly advice against the use of smaller surrogates as models for more complex systems, especially when the corrugation of the surface is comparable with the lengths of the reactants.

Another important point is the oxidation state of the surface. At the beginning of the process one vacancy is present, but it gets restored at the end of the reaction. This means that the process is actually *non-catalytic* and also explains the high temperature, which is needed to form new vacancies. This explain the high temperature (> 600 K) found in the TPD experiment shown in Figure 4.4.

4.3 Conclusions

Alcohols on TiO_2 show a very rich chemistry, where the hydroxyl group can be converted to a variety of functional groups. The initial step is the adsorption of alcohols on the surface. To shed a light on this process, we have carried out a systematical investigation of a series of mono- and poly-alcohols. For a more complete analysis we have considered molecular and dissociative adsorption on both stoichiometric and defective surfaces. The results warn against the use of small molecules as surrogates for more complex systems, especially when the corrugation of the surface is comparable with the length of the molecules. Primary and secondary alcohols are perfect to fit the vacancies but this is not true anymore for sterical hindered molecules such as tert-butanol. Polyalcohols behave quite differently, the ones with two hydroxyls close to each other preferring the vacancy only upon dissociation. Instead, polyalcohols with distant or more than two hydroxyls are equally distributed. The energies are almost constant for the monoalcohols, again the only exception represented by the tert-butanol. In the second part of this chapter, we have proposed a mechanism for the conversion of ethylene glycol and 1,3-propanediol to ethylene and propene, respectively. After adsorption on a vacancy for both compounds, there follows the dissociation of the hydroxyl; the released hydrogen is subject to diffusion and ends bound to a O_b next to the second hydroxyl. Successively,

the two diols follow different paths: 1,2-EtOH evolves rapidly to the products in a single step, while 1,3-PrOH evolution includes a high energy intermediate, followed by the migration of hydrogen from C-2 to C-1 and the formation of the double bond. This description is in line with the experimental findings, which yield a higher energy needed to dehydrate 1,3-PrOH compared to the other. The different paths again strongly warn against the use of smaller surrogates to study more complex systems. Also the process turns out to be non-catalytic since the vacancy is restored at the end of the reaction.

Chapter 5

Wetting of hydrophobic rare-earth oxides

Many reactions involving metal oxides take place in aqueous environments. This is particularly true for biomass derived compounds. For this reason, the interaction with water is important in the analysis of the adsorption phenomena and we investigated such process in Rare-Earth Oxides (REOs). Since Rare-Earth metals react with oxygen vigorously to form oxides,[148] REOs turn out to be thermally very stable. They are also characterized by a strong hydrophobicity which allows them to be employed in harsh conditions.[149] As expected, this class of compounds has a variety of technical applications. As an example, lanthanides oxides could replace silica as dielectric in field effect transistors.[150,151] In particular CeO_2 is important in catalysis, as support that can have also a more active role.[152] It is also frequently doped with promoters to improve its properties like ionic conductivity (with Gd and Sm),[153] reducibility and oxygen storage (with Zr and Hf).[154–156] The effect of promoters on the electronic conductivity and the vacancy formation energy have been investigated by Farra *et al.*.[157] A comprehensive review on REOs has been published by Adachi and Imanaka,[158] while the electronic properties have been studied

by means of first principles by Jiang et al.[159]

As for the composition, most of the lanthanides are stable as sesquioxides with formula R_2O_3 and at ambient pressure, different structures are available. Light lanthanide oxides usually are found in an hexagonal arrangement, while heavier elements organize in a cubic one, called bixbyte. Both the structures are shown in Figure 5.1. An intermediate monoclinic form is also available; medium-weight oxides tend to adopt it but also one of the others, depending on the position in the row.

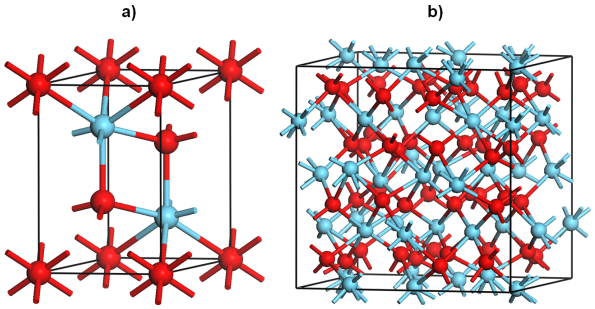

Figure 5.1: Two of the polymorphs of rare-earth sesquioxides of formula R_2O_3; a) hexagonal of $P\bar{3}m1$ symmetry and b) cubic bixbyte of $Ia\bar{3}$ symmetry.

Not all the rare-earth metal are trivalent when forming oxides. Some of them can be divalent or tetravalent. The latter is typical of Cerium, in fact its most stable oxide is CeO_2 and its structure is sketched in Figure 5.2

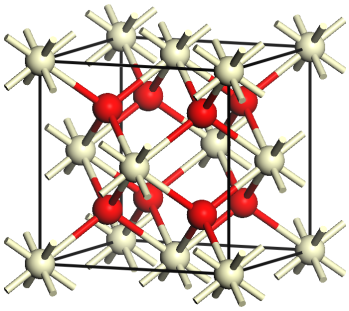

Figure 5.2: Cerium dioxide (CeO_2) bulk structure, a cubic of symmetry $\frac{4}{m}\bar{3}\frac{2}{m}$ (fluorite). This rare-earth metal adopt a tetravalent form.

5.1 Contact angle as a measure of hydrophobicity

The hydrophobicity of REOs was experimentally investigated by Azimi et al.[160] To evaluate this property, the contact angle (θ) formed by water and other liquid interacting with the surface was measured; hydrophobic materials have a value of $\theta > 100°$, while hydrophilic compounds have very small value ($\sim 10°$). This is sketched in Figure 5.3.

The results of the investigation have been reported in Figure 5.4.

An explanation for the phenomena has also been proposed, and the primary factor responsible was supposed to be the electronic structure of the surface. In fact, in hydrophilic materials (such as α-Al_2O_3), empty $3p$ orbitals can accommodate the oxygen lone pairs of the water molecules; the result is a strong interaction with the surface. In the REOs on the other hand, the empty $4f$ orbitals are surrounded by the $5s$ electrons and therefore they are inaccessible; a weaker adsorption between the surface and the water is determined. The process is summarized in Figure 5.5.

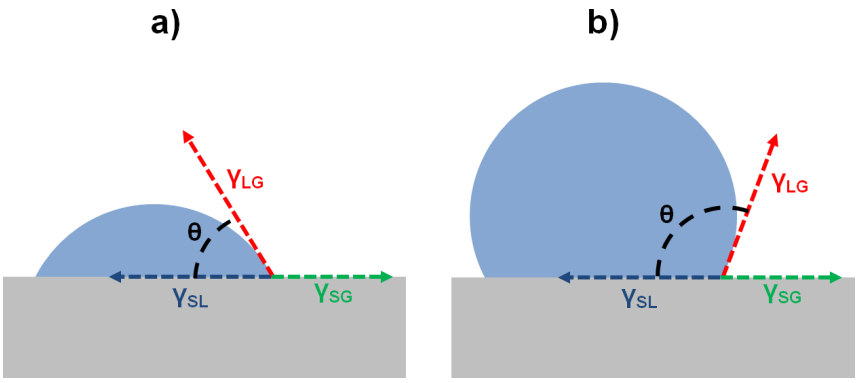

Figure 5.3: Sketch of the interaction of a liquid with a surface. The contact angle θ is usually small for hydrophilic materials (a) and large for hydrophobic ones (b).

In this chapter, we present an alternative interpretation, primary related on the geometrical features of the system. One of the most stable arrangement of water molecules in the ice structure consists of hexagons where the molecules are either parallel to the plane or perpendicular to it. The distance between two molecules in the same configuration is equal to 4.806 Å; the structure is not completely planar and two adjacent molecules are displaced of 0.2 Å along the z direction.

Since the water oxygens tend to be affected by the position of the metals, the closer the distance between these (d_{Me-Me}) is to the one in the ice, the better can this be accommodated, hence the stronger the adsorption. In the case of alumina, d_{Me-Me} has almost exactly the value of the water distance in ice, therefore an optimum interaction is obtained. On the other hand, this distance in the REOs is shorter and the ice turns out to be compressed, weakening the bond between it and the surface, resulting in a strong hydrophobicity. A similar effect is expected if d_{Me-Me} is larger than the ideal value; this would determine the stretching of the hexagonal structure, *i.e.* a poor

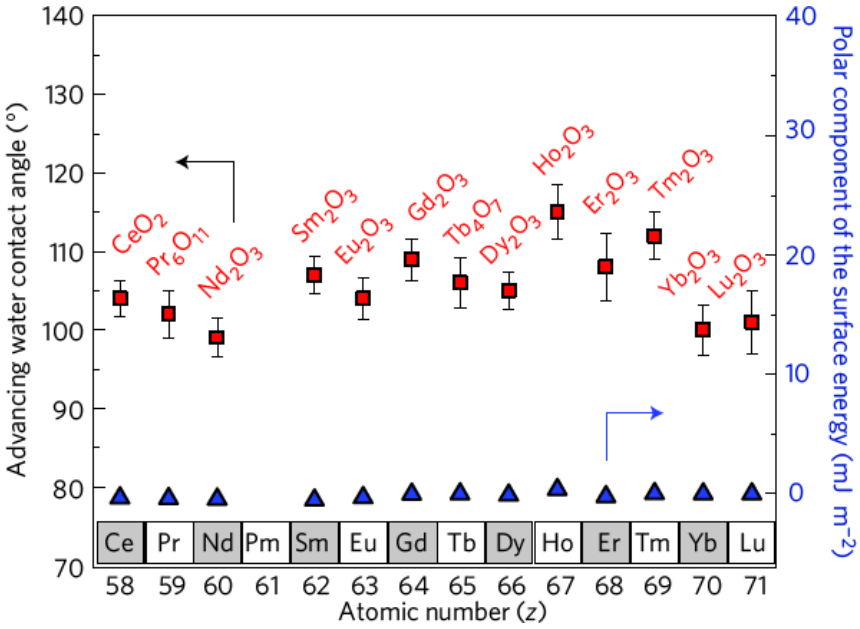

Figure 5.4: From Azimi *et al.*:[160] Measured advancing water contact angle (left axis) and the polar component of the surface free energy (right axis) of sintered REOs.

interaction. A representation is presented in Figure 5.6.

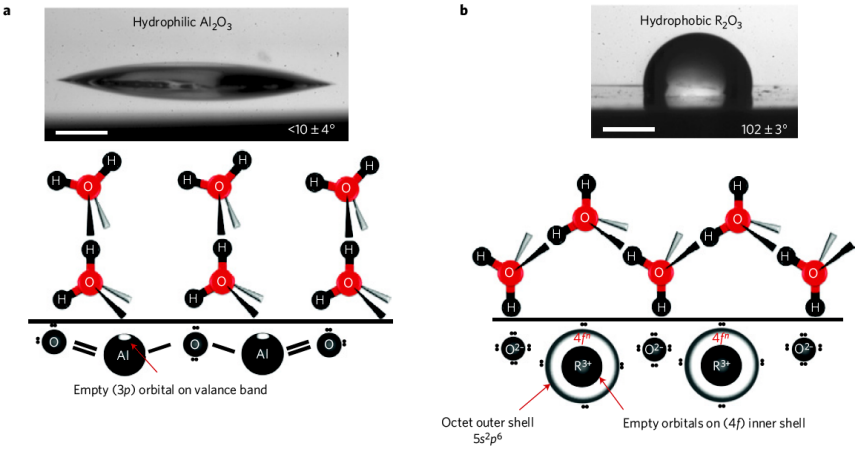

Figure 5.5: From Azimi *et al.*:[160] Schematic of the orientation of water molecules and the associated wetting properties of a surface. a) Hydrophilicity and schematic of the water molecules next to an alumina surface. b) Hydrophobicity and schematic of the water molecules next to a REO surface. As the $4f$ orbitals of rare-earth atoms are completely shielded, they have no tendency to interact with water molecules. Thus, water molecules next to the surface cannot maintain their hydrogen-bonding network and are expected to have a hydrophobic hydration structure. The photograph shows a water droplet beading up on a smooth neodymia surface. Scale bars, 1 mm.

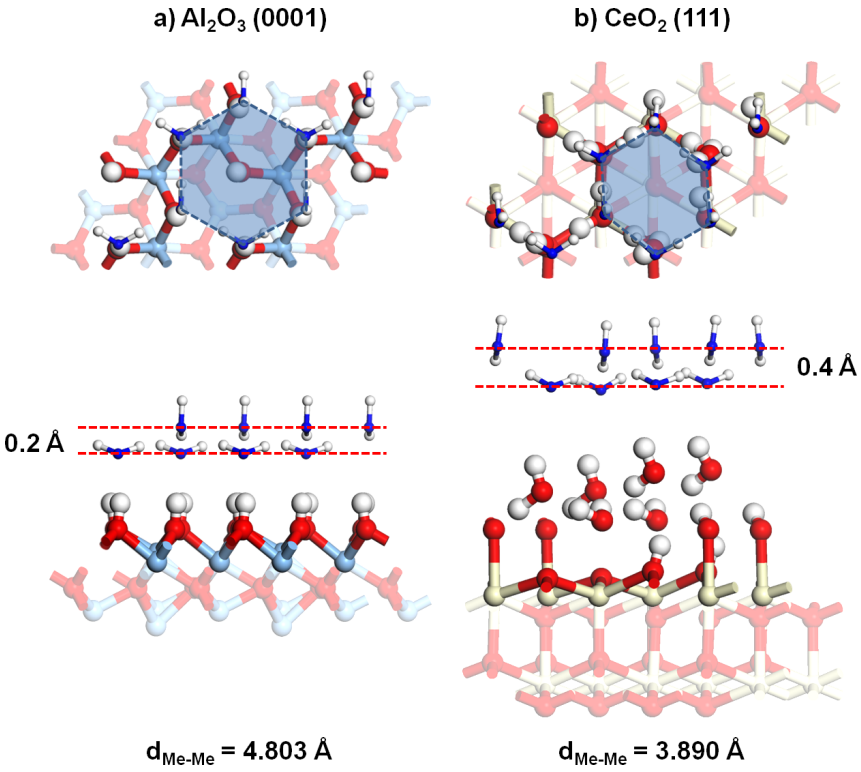

Figure 5.6: Ice layer adsorbed on top of a) α-Al_2O_3 and b) CeO_2. The distance metal metal in alumina is close to the ideal value in the water bulk, while such distance in Ceria is shorter. As a result, the water layer is perfectly disposed on the former while on the latter the structure is compressed and there is a tetragonal distortion.

5.2 Results and Discussion

In order to validate our model we first computed the contact angle for a small series of REOs, CeO_2 (111) and Nd_2O_3 (0001). As a comparison, it also has been computed the same angle for α-Al_2O_3, a well known hydrophilic material. On a second step we modified d_{Me-Me} by doping with external ions (La and Zr) in order to tune the hydrophobic property.

The Young formula expresses the contact angle θ of a liquid on an ideal solid surface as a function of the surface tensions present at the interface (see Figure 5.3)

$$\cos(\theta) = \frac{\gamma_{SG} - \gamma_{SL}}{\gamma_{LG}} \tag{5.1}$$

where γ_{XX} represent the surface energy of the different interfaces (with S, L and G stand for Solid, Liquid and Gas phases).

In fact an ideal solid surface has zero contact angle hysteresis, implying that the advancing and receding contact angles are equal. Therefore, there is only one thermodynamically stable contact angle. In theory, the direct evaluation of the mixed term γ_{SL} is quite complex; however, the liquid close to the surface adopts the typical ice configuration and its interaction is just the ice adsorption energy divided by the covered area

$$\gamma_{SL} = \gamma_{SG} + \frac{E_{ads}^{ice}}{Area} \tag{5.2}$$

Substituting this result in Equation 5.1 we finally obtain

$$\cos(\theta) = \frac{-E_{ads}^{ice}}{Area \cdot \gamma_{LG}} \tag{5.3}$$

where we only need to calculate is the adsorption energy, E_{ads}^{ice}, of the ice layer on top of the different surfaces. This quantity is defined negative for an exothermic process and its value is obtained from a series of DFT calculations

$$E_{ads}^{ice} = E_{sys} - E_{ice} - E_{surf} \tag{5.4}$$

where E_{sys}, E_{ice} and E_{surf} are the energy of the total system, of the ice layer and of the clean surface, respectively.

5.2.1 CeO_2 and Nd_2O_3

Special care need to be employed with the first water layer in contact with the surface. In fact, the water close to the facet will tend to dissociate to some degree, breaking the ice hexagon (see Figure 5.6 b). To simplify our problem, we consider the surface plus this dissociated layer as the basis on top of which we adsorb the successive layer. We will analyze the distance between water molecules in this second layer. In order to proceed, we therefore have to find the most stable configuration of the basis surface, *i.e.* the degree of dissociation of the first layer. To do so, we have calculated the adsorption energies E_{ads} of this first layer for an increasing number of dissociated water, from one to four. The results are shown in Table 5.1; for both the REOs the most stable configuration is obtained when half of the molecules are dissociated.

Table 5.1: Energies relative to the different degree of dissociation of CeO_2 and Nd_2O_3 (E_{ads} in eV). In bold are reported the most stable configurations; for Nd_2O_3, the dissociation of more than two water makes the system particularly unstable.

Dis. H_2O	$\boldsymbol{E_{ads}}$**(CeO_2)**	$\boldsymbol{E_{ads}}$**(Nd_2O_3)**
0	-0.20	-0.31
1	-0.39	-0.27
2	**-0.42**	**-0.55**
3	-0.37	-
4	-0.35	-

Once we have established the reference configuration, we added an ice layer on top of it and computed the adsorption energy. We employed this value to calculate the contact angle using Equation 5.3. The results are reported in Table 5.2 and are in perfect agreement with the experimental data.[160] As previously stated, we applied the described method to tune the hydrophobic character in Ceria by doping the surfaces with different ions, La and Zr. The results confirm our hypothesis. In fact, if a smaller ion like Zr is inserted into Ceria, the distance between the metals is reduced, therefore the ice structure will be further compressed, determining a wider contact angle. On the other hand, when inserting a larger ion as La, d_{Me-Me} is increased and closer to the optimal distance in the ice bulk; in this case, the water structure is less distorted and a smaller contact angle is retrieved.

Table 5.2: Summary of the results obtained for CeO_2 and Nd_2O_3. The contact angle versus the metal-metal distances are reported for the stoichiometric surfaces along with the doped ones. Experimental results calculated by Azimi et al.[160] are also present as comparison.

System	**Doping**	% **Stoich.**	$\mathbf{d}_{Me-Me}$	$\boldsymbol{\theta^{cal}}$	$\boldsymbol{\theta^{exp}}$
CeO_2	La (0.08 %)	1.02	3.927	98.9	-
	Stoich.	-	3.890	99.9	103 ± 2
	Zr (0.08 %)	0.97	3.772	112.9	-
Nd_2O_3	Stoich.	-	3.860	103.2	101 ± 3

5.2.2 α-Al_2O_3

Concerning α-Al_2O_3, the water is able to subtract an Al ion, therefore the surface ends hydroxilated, "gibbsite-like", see Figure 5.6 a. The mechanism behind this process has been investigated by Ranea *et al.*[161] As previously done for the REOs, once

we have established the basis, we added an ice layer on top of it and computed the adsorption energy. The results are reported in Table 5.3, again corroborated by the experimental data.[160] We also tried to make Alumina less hydrophilic substituting an Al ion with a larger one (La). In this case the large difference of radius between the two ions is sufficient to completely distort the water structure, even for a very small concentration. As a result, even if the mean distance Al-Al is almost the same of the clean surface, the evaluated contact angle is much larger, up to 77°.

Table 5.3: Summary of the results obtained for α-Al_2O_3. The contact angle versus the metal-metal distances are reported for the stoichiometric surface along with the doped one. Experimental results calculated by Azimi et al.[160] are also present as comparison.

System	**Doping**	% **Stoich.**	$\mathbf{d}_{Me-Me}$	$\boldsymbol{\theta^{cal}}$	$\boldsymbol{\theta^{exp}}$
α-Al_2O_3	Stoich.	-	4.803	0.0	$< 10 \pm 4$
	La (<0.01 %)	1.00	∼4.803	76.7	-

5.3 Conclusions

Biomass processing takes often place in harsh aqueous environment. Since metal oxides have an important role in its conversion, it is important to investigate their interaction with water. To this end we have investigated Rare-Earth Oxides (REOs), which show a strong hydrophobicity and would be particularly suitable for the scope. In this chapter, we have proposed a mechanism for such phenomena, based on the geometry of the system. Water in contact with a surface adopts a motif where each molecule is located at a vertex of a regular hexagon, in alternate configurations. The distance between two molecules

in the same configuration is related to the distance between two ions in the surface, d_{Me-Me}. The more this is close to the ideal value present in an ice bulk, the better the interaction between water and surface and the more hydrophilic the material. In order to assess the reliability of our model, we have first computed the contact angle (a measure of a material hydrophilic/hydrophobic character) for CeO_2, Nd_2O_3 and α-Al_2O_3. The computed contact angles are in good agreement with the experimental results. Afterwards, based on our assumption, we successfully tuned the hydrophobicity of Ceria substituting a certain amount of cations with La and Zr. In the first case, the mean d_{Me-Me} become larger releasing the tension in the hexagon and improving the interaction with the surface (smaller contact angle). In the latter the mean d_{Me-Me} gets smaller compressing the water structure and broadening the angle. Finally, we also tried to modify the hydrophilicity of α-Al_2O_3 with La impurities. In this case the large difference of radius between the ions greatly distort the hexagon even for very small quantity of impurity; the computed contact angle varies more than 70°.

Chapter 6

Costless derivation of C_6 parameters to reproduce van der Waals forces in metals

With a few exceptions, all the work carried out in the previous chapters is based on the evaluation of adsorption energies. Therefore, in order to be reliable, it is important that such energies are calculated with the necessary accuracy. Unfortunately, as we pointed out in Chapter 2, standard DFT formulations do not include non-local interactions such as the dispersion part of the vdW forces.[162] The available methods to recover this shortcoming have been presented and here we report a brief summary.

The Random Phase Approximation (RPA)[163] accurately describes the electron correlation and seamlessly includes the van der Waals interaction; its recent application to DFT[164–167] is usually limited to benchmarks, due to the high computational cost.

A cheaper alternative consists in a family of non-local func-

tionals such as the vdW-DF by Lundqvist *et al.*[55,78–81] The principal problem is the lack of consistency, for the accuracy is highly dependent on the combination between the exchange and the correlation parts.[82]

Finally, for a negligible computational cost, it is possible to describe the weak interaction in a pairwise motif, following the approach by London[72]

$$E_{vdW}(R_{AB}) = -\frac{C_6}{R_{AB}^6} - \frac{C_8}{R_{AB}^8} \dots \tag{6.1}$$

Different procedures are followed to define the set of parameters (C_6, C_8, ...) needed. The most famous are the Grimme vdW-D2[71] and vdW-D3[74] methods, where the coefficients are derived from atomic properties; unfortunately this leads to overbinding in metal systems.[73]

More recently, Tkatchenko and Scheffler have developed a series of related methods; in this case, the C_6 parameters are determined non-empirically from the electron density and the environment dependency is included employing the effective volume.[75] A screening corrected version is available for the accurate description of metals.[77] The drawback in this method is that it relies on Reflection Electron Energy-Loss Spectroscopy (REELS) data. Therefore it is not entirely first principles. A summary of all the methods is reported in Table 6.1, along with the relative computational cost and the primary limitations.

In this work we have employed the Grimme D2 correction, for it yields acceptable results for the specific systems investigated. This is not always the case and it is clear that the available methods are still far from satisfactory, especially concerning metal surfaces. In this chapter, In order to improve this situation, we have developed a new, cheap procedure to determine the C_6 parameters; its derivation is completely first principle and the results obtained show a correct description of metal systems.

Table 6.1: Scheme of the different methods to include vdW interactions in a DFT calculation.

Computational Cost	Method	Limitations
High	RPA	-
Medium	vdW-DF *et al.*	Lack of consistency
Low	DFT-vdW^{surf}	REELS dependency
Low	DFT-D2 *et al.*	Overbinding in metals

6.1 Theoretical Basis

If we consider two bodies A and B acting as isotropic oscillators, their long range interaction, E_{vdW} can be expressed as a series of dispersion coefficients C_m:

$$E_{vdW}(R_{AB}) = -\frac{C_6}{R_{AB}^6} - \frac{C_8}{R_{AB}^8} - \dots \tag{6.2}$$

if there is a fluctuating electromagnetic field in each of the two bodies, the coefficients can be expressed as a function of their polarizabilities, α_A and α_B:

$$C_6 = \frac{3h}{2\pi^2} \int_0^\infty d\omega \alpha_A(i\omega^I)\alpha_B(i\omega^I) \tag{6.3}$$

The polarizabilities are dynamic thus frequency dependent, and evaluated at imaginary frequency.

These can be further expanded in terms of the static frequency $\alpha_A(0)$ following the method by London[72]

$$\alpha_A(i\omega^I) = \frac{\alpha_A(0)}{1 + (\omega^I/\omega_1)^2} \tag{6.4}$$

where ω_1 is the characteristic frequency; therefore the coefficients turn out to be

$$C_6 = \frac{3h}{2}\alpha_A(0)\alpha_B(0)\frac{\omega_{1A}\omega_{1B}}{\omega_{1A}+\omega_{1B}} \tag{6.5}$$

and since the characteristic frequency multiplied by h is close to the ionization potential I

$$C_6 \simeq \frac{3}{2}\alpha_A(0)\alpha_B(0)\frac{I_A I_B}{I_A+I_B} \tag{6.6}$$

Finally, if we consider an ensemble of identical objects B (such as in a metal surface)

$$C_6 \simeq \frac{3}{4}\alpha_B(0)^2 I_B \tag{6.7}$$

To obtain the parameter we only have to evaluate the polarizability for a metal. This can be easily done applying an external electric field $\vec{E}$ and then evaluating the response of the dipole $\vec{\mu}$,[168] as shown in Figure 6.1. The latter can be computed from the charge density obtained from a DFT simulation, as described up ahead.

Therefore, we can write

$$\vec{\mu} = \alpha(0)\vec{E} \tag{6.8}$$

The electric field can be introduced as an effect of a dipole sheet present in the vacuum region of the system in exam.[169] Once we have the C_6 parameter we use half of the distance between two atoms in the relaxed bulk as the R_0 in the formula. The parameters for the molecule and the damping function were taken from those reported by Grimme.[71]

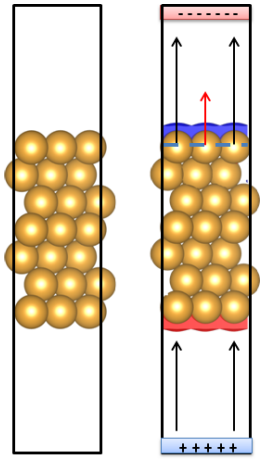

Figure 6.1: Schematic representation of the surface dipole generated by an applied electric field. The blue area represents electron density accumulation, while the red one depletion.

6.2 Application of the method

The electronic charge density ρ for different values of $\vec{E}$ is computed; the difference between this value and ρ without electric field is plotted against the distance from the bottom of the cell. An example of this is reported in Figure 6.2 (a); it is clear that only the the topmost atoms are affected by the field, for this cannot penetrate inside the slab.

The integration of the curve give us the differential charge q; we can use this value to compute the surface dipole $\vec{\mu_i}$ in the following:

$$\vec{\mu_i} = qd\hat{n} \tag{6.9}$$

where d is the distance from the bottom and $\hat{n}$ the surface vector. Once we have the dipole we can plot it versus the external electric field. The slope corresponds to the polarizability, in eÅ^2/V, as shown in Figure 6.2 (b)

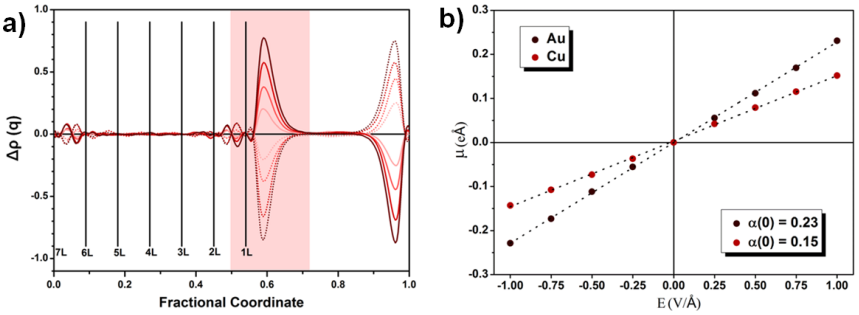

Figure 6.2: Plot of the charge density difference, $\Delta\rho(q)$ and the distance from the bottom of the cell, in reciprocal coordinate. Only the superficial atoms are affected by the field, for it cannot penetrate inside the metal

These polarizabilities $\alpha_i(0)$ can be used to calculate the coefficients, as described in the previous section. In case of the presence of steps, the coefficients need to be modified, since polarization of the surface atoms is not as effective due to the angle between the surface vector and the electric field. In this case the total surface dipole can be decomposed with each atom in a low-index plane keeping the polarizability obtained in the low-index surface model.

$$\vec{\mu} = \sum_{i}^{surface} \vec{\mu_i} = \sum_{i}^{surface} \alpha_i(0)\vec{E}\hat{n} \tag{6.10}$$

6.3 Benzene Adsorption

To evaluate the goodness of the coefficients found we have computed the binding energy, BE, of benzene (Bz) on a metal surface; This is defined positive for an exothermic process:

$$BE = -(E_{surf+Bz} - E_{surf} - E_{Bz}) \tag{6.11}$$

Benzene is optimal to test this kind of weak interactions, since it is a large close-shell molecule with aromatic electrons easily polarizable. For this reason, a wide variety of experimental data are available for comparison. the evaluated binding energies for a series of metals are reported in Figure 6.3 and Table 6.2, as well as the values calculated with other methods and experiments.

Table 6.2: Binding energies (in eV) for the adsorption of Benzene on different metal surfaces (M). The values obtained with the different theoretical methods are presented, along with experimental data retrieved from TPD and Microcalorimetry (in parenthesis) experiments.

M	**PBE**	**D2**	**D3**	**vdW^{surf}**	**This Work**	**Exp.**
M(4x4) + $2C_6H_6$						
Pd	0.84	2.58	1.91	-	1.88	1.64^{170} - 1.83^{171}
Pt	0.59	3.04	1.99	-	1.57	1.54^{172} - 1.60^{173} $(1.54)^{10}$
M(3x3) + C_6H_6						
Pd	1.22	2.82	2.22	2.14	2.17	-
Pt	0.97	3.23	2.27	1.96	1.92	$(1.94)^{10}$
Cu	0.14	0.91	1.02	0.86	0.47	0.70^{174} - 0.71^{175}
Ag	0.07	0.90	0.77	0.75	0.41	0.46^{176} - 0.45^{177}
Au	0.05	1.35	0.88	0.74	0.48	0.63^{178}

From the results, it is clear that this new methodology yields results in good agreement with the experimental results and a net improvement over the previous methods. In fact, for Cu, Ag and Au, benzene is weakly physisorbed to the point that PBE gives and endothermic adsorption; DFT-D2 leads to overbinding, as previously described, while our method and the DFT-vdW^{surf} give a similar value to the experimental, with a 0.15 eV maximum difference. Pd and Pt are characterized by a strong chemisorption, and the D2 and D3 methods yield qualitative wrong results. Our approach on the other hand just slightly overestimate the interaction. In a similar way, it is possible to apply the procedure to alloys: results indicate that

the coefficients can vary more than 60 %, the largest changes are obtained when smaller atoms are placed as overlayers while they are smaller of similar diameter. Nevertheless, benzene adsorption does not significantly change in most cases.

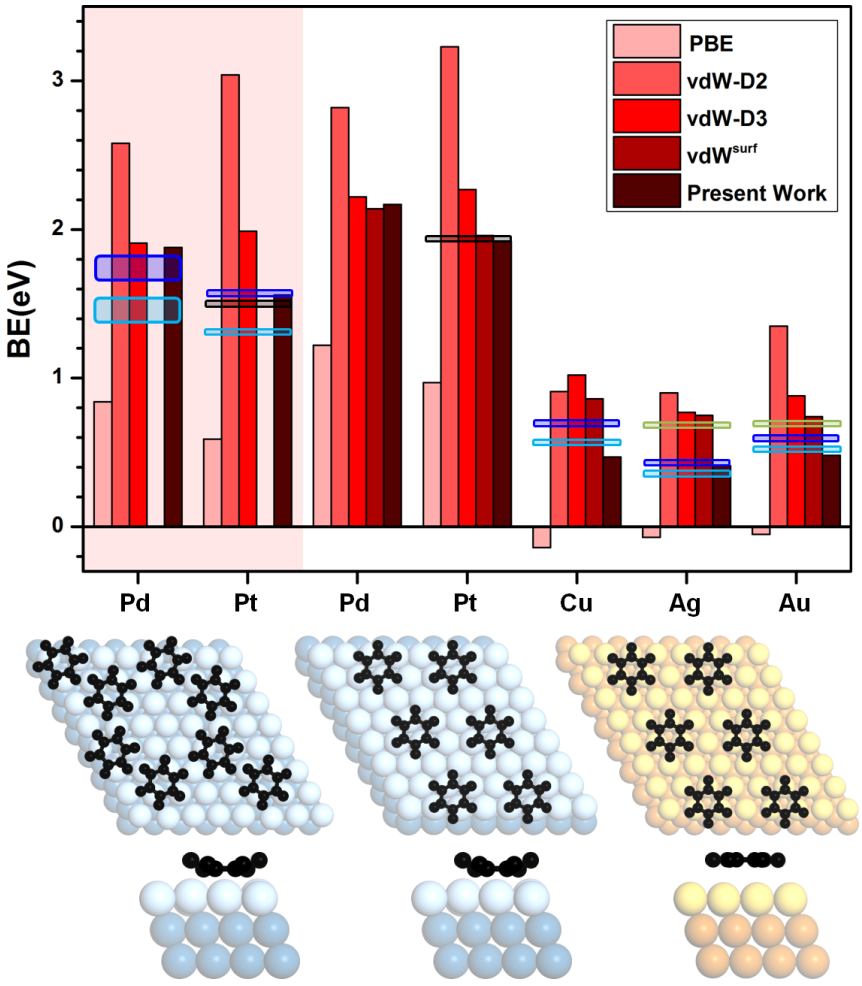

Figure 6.3: Binding energies of benzene for different metal surfaces. For comparison there have been reported the calculations with alternative methods along with experimental data; data from TPD experiments (evaluated with two different approximation) and microcalorimetry (Pt) are reported.

6.4 Conclusions

Many different methods have been developed to include non-local interaction, which are missing in standard DFT applications. All these approaches have some serious limitations, ranging from excessive cost (RPA), to inaccurate description in metals (DFT-D2 and D3) or lack of consistency (vdW-DF). In this chapter, a cheap procedure to obtain C_6 parameters for the pairwise interactions have been presented. This method is manly first principles, it has negligible cost and shows an accurate description of metal systems. In fact, the new parameters have been tested against the binding energy of benzene (an ideal model for the weak interactions) on metal surfaces, yielding results in good agreement with the experimental data and a clear improvement over other methods.

Chapter 7

Conclusions

Despite its importance in the chemical industry, many aspects of heterogeneous catalysis are still unclear. Among these, the description of the geometric and electronic structure of the system composed by the reactants and the catalyst is especially challenging. In this Thesis we have investigated such interface relative to some catalytic systems, by means of Density Functional Theory (DFT). It follows a detailed description of the conclusions drawn for the different topics.

- *Impurities and overlayers of the rutile class*

  Thanks to the structural similarity it should be possible to easily dope one of the rutile compounds with another one. However, the energies retrieved show endothermic values for the solubility, which means the formation of bimetallic alloys is hindered. The only exception is represented by Ru and Ir oxides, which can be mixed to any composition. Experimentally, a certain amount of impurities is always allowed; the small values retrieved and the neglect of configurational entropy explains our findings. Finally, the general trend is well reproduced.

  Surface composition can be very different compared to the one in the bulk, due to a phenomena known as segre-

gation. This is quite hard to evaluate experimentally and to model theoretically, even for metals. For this reason, to investigate this property we completed a database with all the possible combinations. As a result, the semiconductors Ti and Sn oxides tend to migrate to the surface while Ir and Ru tend to stay in the bulk. On the other hand, oxygen greatly influences the segregation, since it preferentially binds with Ir and Ru; when it is present, these cations are pushed on the surface when acting as guests, while as hosts they block the segregation of Ti and Sn.

Finally, it is possible to epitaxially grow any rutile on top of another, despite the mismatch between the lattice parameters; this facilitates the employment of a cheaper compound (TiO_2) as support for a more expensive material (IrO_2).

- *Alcohols adsorption and reactions on Titanium Dioxide*

  From the analysis of the adsorption of a series of alcohols on Titanium Dioxide (TiO_2), we have found that they always tend to dissociate when bound to the surface. The presence of a superficial vacancy yields a competitive site (V_O) to the Titanium in Coordinatively Unsaturated Site (Ti_{cus}), which is preferred by the adsorbates unless they turn out very bulky (like tert-butanol), or possess more the one OH group (except ethylene glycol). When it comes to the energies, they slightly oscillate around a constant value. These results strongly advice against the employment of methanol or other small alcohols as surrogates to model reactions for more complex substrates; in fact, the energies and geometries are hardly scalable with the chain length or number of hydroxils.

  We have also proposed a mechanism for the conversion of ethylene glycol (1,2-EtOH) and 1,3-propanediol (1,3-

PrOH) to the corresponding alkenes, which takes place on TiO_2. Initially, a common path is followed by both the compounds: the polyalcohol adsorbs on the surface with one hydroxyl (OH^1) filling one vacancy and the second (OH^2) bound to a Ti_{cus}. From the study of the adsorption, we already know that 1,2-EtOH prefers the vacancy to the Ti_{cus} but this is not the case of 1,3-PrOH. Higher temperature is therefore needed to promote the diffusion of the latter. The next steps involve the breaking of the O-H bond of OH^1 and after diffusion, the dissociated hydrogen is bound to the oxygen in bridge position (O_b) next to the OH^2. From this point, the two alcohols follow a different path. In the case of 1,2-EtOH, the hydrogen binds to OH^2; this transition state rapidly evolves to the final products, ethylene and water. For 1,3-PrOH, there is an high energy intermediate once the water is formed. From this state, an Hydrogen shift from the central carbon determine the cleavage of the last C-O bond and the formation of the products. It is worth noticing that the process is not pure catalytic, since at the end of the cycle the vacancy has been healed.

- *Hydrophobicity of Rare-Earth Oxides (REOs)*

  As many processes happen for polyalcohols with water, we have investigated the mechanism of the strong hydrophobicity shown by Rare-Earth Oxides (REOs). As a result, it turns out that this property is related to the geometry of the system; in fact, water close to the surface tends to form hexagons with molecules at its vertices arranged in two different alternating configurations. The position of the molecules is also connected to the metals in the surface. If the distance between the metals (d_{Me-Me}) changes, so it does the one between the water molecules. If d_{Me-Me} differs from the one in an ice

sample, the resulting structure turns out to be distorted both in the plane and along the z direction. This weakens the interaction between the surface and water, hence the system turns out to be hydrophobic. This property can be tuned since the doping of a material also modifies d_{Me-Me}. This mechanism has been tested with three oxides: α-Al_2O_3, CeO_2 and Nd_2O_3. In all cases, the results are in good agreement with the measured ones. We also have successfully tuned the hydrophobicity of CeO_2, doping the surface with La (larger d_{Me-Me}) and Zr (shorter d_{Me-Me}).

- *Accurate van der Waals (vdW) coefficients for metals*

  Accuracy is a must in study of adsorption. Apart from extremely demanding methods such as the Random Phase Approximation (RPA), the currently available methods to include van der Waals (vdW) forces in metals either rely heavily on experimental data or are not easily scalable. In the last chapter, we developed a new methodology which is easy, cheap and manly first principles; it also can be applied to pristine as well as defective surfaces. Based on the London formula, vdW forces are described by a sum of pair interactions of C_6 coefficients divided by R^6. The novelty is that such coefficients can be expressed as a function of surface polarizability; this quantity itself turns out to be a function of the dipole generated on the surface by an external electric field. The so-obtained parameters have successfully been tested in the study of the adsorption energy of benzene.

Bibliography

[1] Fujishima, A. and Honda, K., *Nature* 1972, **238**, 37–38.

[2] González-Navarrete, P., Gracia, L., Calatayud, M., Andrés, J., Gonza, P. and Andre, J., *J. Phys. Chem. C* 2010, **114**, 6039–6046.

[3] Remediakis, I. N., López, N. and Nørskov, J. K., *Angew. Chemie Int. Ed.* 2005, **44**, 1824–1826.

[4] Valden, M., Lai, X. and Goodman, D. W., *Science* 1998, **281**, 1647–1650.

[5] Haruta, M., *Catal. Today* 1997, **36**, 153–166.

[6] Somorjai, G. A. and Li, Y., *Introduction to Surface Chemistry and Catalysis*, John Wiley & Sons, New York, 2010.

[7] Crowe, M. C. and Campbell, C. T., *Annu. Rev. Anal. Chem.* 2011, **4**, 41–58.

[8] Gottfried, J. M., Vestergaard, E. K., Bera, P. and Campbell, C. T., *J. Phys. Chem. B* 2006, **110**, 17539–17545.

[9] Ajo, H. M., Ihm, H., Moilanen, D. E. and Campbell, C. T., *Rev. Sci. Instrum.* 2004, **75**, 4471.

[10] Ihm, H., Ajo, H. M., Gottfried, J. M., Bera, P. and Campbell, C. T., *J. Phys. Chem. B* 2004, **108**, 14627–14633.

[11] Xu, Y., Hofmann, O. T., Schlesinger, R., Winkler, S., Frisch, J., Niederhausen, J., Vollmer, A., Blumstengel, S., Henneberger, F., Koch, N., Rinke, P. and Scheffler, M., *Phys. Rev. Lett.* 2013, **111**, 226802.

[12] Morgenstern, K., *Prog. Surf. Sci.* 2011, **86**, 115–161.

[13] Koch, N., Gerlach, A., Duhm, S., Glowatzki, H., Heimel, G., Vollmer, A., Sakamoto, Y., Suzuki, T., Zegenhagen, J., Rabe, J. P. and Schreiber, F., *J. Am. Chem. Soc.* 2008, **130**, 7300–7304.

[14] Lu, W. and Lieber, C. M., *Nat. Mater.* 2007, **6**, 841–850.

[15] Tautz, F. S., *Prog. Surf. Sci.* 2007, **82**, 479–520.

[16] Waser, R. and Aono, M., *Nat. Mater.* 2007, **6**, 833–840.

[17] López, N., Prades, D. J., Hernández-Ramírez, F., Morante, J. R., Pan, J. and Mathur, S., *Phys. Chem. Chem. Phys.* 2010, **12**, 2401–2406.

[18] Barsan, N., Koziej, D. and Weimar, U., *Sensors Actuators B Chem.* 2007, **121**, 18–35.

[19] Poole, C. P. J., Datta, T. and Farach, H. A., *Copper Oxide Superconductors*, Wiley-Interscience, New York 1988.

[20] Wefers, K. and Misra, C., *Oxides and Hydroxides of Aluminum: Alcoa Technical Paper No. 19, Revised*, Alcoa Laboratories, Pittsburgh 1987.

[21] Hohenberg, P. and Kohn, W., *Phys. Rev.* 1964, **136**, B864–B871.

[22] Van Doren, V. E., Van Alsenoy, C. and Geerlings, P., *Density functional theory and its application to materials: Antwerp, Belgium, 8-10 June 2000*, American Institute of Physics, New York 2000.

[23] Kohn, W. and Sham, L. J., *Phys. Rev.* 1965, **140**, A1133–A1138.

[24] Ceperley, D. M. and Alder, B. J., *Phys. Rev. Lett.* 1980, **45**, 566–569.

[25] Gunnarsson, O. and Lundqvist, B. I., *Phys. Rev. B* 1976, **13**, 4274–4298.

[26] Haas, P., Tran, F. and Blaha, P., *Phys. Rev. B* 2009, **79**, 85104.

[27] Da Silva, J. L. F., Stampfl, C. and Scheffler, M., *Phys. Rev. Lett.* 2003, **90**, 66104.

[28] Darling, G. R. and Holloway, S., *Reports Prog. Phys.* 1995, **58**, 1595.

[29] Langreth, D. C. and Mehl, M. J., *Phys. Rev. Lett.* 1981, **47**, 446–450.

[30] Hammer, B., Hansen, L. B. and Nørskov, J. K., *Phys. Rev. B* 1999, **59**, 7413–7421.

[31] Honkala, K., Hellman, A., Remediakis, I. N., Logadottir, A., Carlsson, A., Dahl, S., Christensen, C. H. and Nørskov, J. K., *Science* 2005, **307**, 555–558.

[32] Perdew, J. P., Chevary, J. A., Vosko, S. H., Jackson, K. A., Pederson, M. R., Singh, D. J. and Fiolhais, C., *Phys. Rev. B* 1992, **46**, 6671–6687.

[33] Perdew, J. P., Burke, K. and Ernzerhof, M., *Phys. Rev. Lett.* 1996, **77**, 3865–3868.

[34] Hafner, J. and Hafner, R., *J. Comput. Chem.* 2008, **29**, 2044–2078.

[35] Godby, R. W., Schlüter, M. and Sham, L. J., *Phys. Rev. Lett.* 1986, **56**, 2415–2418.

[36] Rinke, P., Qteish, A., Neugebauer, J., Freysoldt, C. and Scheffler, M., *N. J. Phys.* 2005, **7**, 126.

[37] Kelkkanen, A. K., Lundqvist, B. I. and Nørskov, J. K., *J. Chem. Phys.* 2009, **131**, 46102.

[38] Da Silva, J. L. F., Ganduglia-Pirovano, M. V., Sauer, J., Bayer, V. and Kresse, G., *Phys. Rev. B* 2007, **75**, 45121.

[39] Anisimov, V. I., Aryasetiawan, F. and Lichtenstein A, I., *J. Phys. Condens. Matter* 1997, **9**, 767.

[40] Perdew, J. P., Kurth, S., Zupan, A. and Blaha, P., *Phys. Rev. Lett.* 1999, **82**, 2544–2547.

[41] Moroni, E. G., Kresse, G., Hafner, J. and Furthmüller, *Phys. Rev. B* 1997, **56**, 15629–15646.

[42] Becke, A. D., *J. Chem. Phys.* 1993, **98**, 5648–5652.

[43] Stephens, P. J., Devlin, F. J., Chabalowski, C. F. and Frisch, M. J., *J. Phys. Chem.* 1994, **98**, 11623–11627.

[44] Paier, J., Hirschl, R., Marsman, M. and Kresse, G., *J. Chem. Phys.* 2005, **122**, 234102.

[45] Paier, J., Marsman, M. and Kresse, G., *J. Chem. Phys.* 2007, **127**, 24103.

[46] Adamo, C. and Barone, V., *J. Chem. Phys.* 1999, **110**, 6158–6170.

[47] Heyd, J., Scuseria, G. E. and Ernzerhof, M., *J. Chem. Phys.* 2003, **118**, 8207–8215.

[48] Franchini, C., Bayer, V., Podloucky, R., Paier, J. and Kresse, G., *Phys. Rev. B* 2005, **72**, 45132.

[49] Franchini, C., Podloucky, R., Paier, J., Marsman, M. and Kresse, G., *Phys. Rev. B* 2007, **75**, 195128.

[50] Bohm, D. and Pines, D., *Phys. Rev.* 1951, **82**, 625–634.

[51] Pines, D. and Bohm, D., *Phys. Rev.* 1952, **85**, 338–353.

[52] Bohm, D. and Pines, D., *Phys. Rev.* 1953, **92**, 609–625.

[53] Langreth, D. C. and Perdew, J. P., *Solid State Commun.* 1975, **17**, 1425–1429.

[54] Langreth, D. C. and Perdew, J. P., *Phys. Rev. B* 1977, **15**, 2884–2901.

[55] Andersson, Y., Langreth, D. C. and Lundqvist, B. I., *Phys. Rev. Lett.* 1996, **76**, 102–105.

[56] Dobson, J. F. and Wang, J., *Phys. Rev. Lett.* 1999, **82**, 2123–2126.

[57] Dobson, J., *Time-Dependent Density Functional Theory*, volume 706, Springer US, Berlin 2006.

[58] Furche, F., *Phys. Rev. B* 2001, **64**, 195120.

[59] Aschroft, N. W. and Mermin, N. D., *Solid State Physics*, Saunders College Publishing, Harcourt 1976.

[60] Phillips, J. C., *Phys. Rev.* 1968, **166**, 832–838.

[61] Mercurio, G., McNellis, E. R., Martin, I., Hagen, S., Leyssner, F., Soubatch, S., Meyer, J., Wolf, M., Tegeder, P., Tautz, F. S. and Reuter, K., *Phys. Rev. Lett.* 2010, **104**, 36102.

[62] Von Lilienfeld, O. A., Tavernelli, I., Rothlisberger, U. and Sebastiani, D., *Phys. Rev. Lett.* 2004, **93**, 153004.

[63] Johnson, E. R. and Becke, A. D., *J. Chem. Phys.* 2005, **123**, 24101.

[64] Tkatchenko, A., Romaner, L., Hofmann, O. T., Zojer, E., Ambrosch-Draxl, C. and Scheffler, M., *MRS Bull.* 2010, **35**, 435–442.

[65] Steinmann, S. N. and Corminboeuf, C., *J. Chem. Phys.* 2011, **134**, 44117.

[66] Mackie, I. D. and DiLabio, G. A., *J. Phys. Chem. A* 2008, **112**, 10968–10976.

[67] Sato, T. and Nakai, H., *J. Chem. Phys.* 2009, **131**, 224104.

[68] Gräfenstein, J. and Cremer, D., *J. Chem. Phys.* 2009, **130**, 124105.

[69] Silvestrelli, P. L., Benyahia, K., Grubisiĉ, S., Ancilotto, F. and Toigo, F., *J. Chem. Phys.* 2009, **130**, 74702.

[70] Klimeš, J. and Michaelides, A., *J. Chem. Phys.* 2012, **137**, 120901.

[71] Grimme, S., *J. Comput. Chem.* 2006, **27**, 1787–1799.

[72] London, F., *Trans. Faraday Soc.* 1937, **33**, 8b–26.

[73] Tonigold, K. and Groß, A., *J. Comput. Chem.* 2012, **33**, 695–701.

[74] Grimme, S., Antony, J., Ehrlich, S. and Krieg, H., *J. Chem. Phys.* 2010, **132**, 154104.

[75] Tkatchenko, A. and Scheffler, M., *Phys. Rev. Lett.* 2009, **102**, 73005.

[76] Zaremba, E. and Kohn, W., *Phys. Rev. B* 1976, **13**, 2270–2285.

[77] Ruiz, V. G., Liu, W., Zojer, E., Scheffler, M. and Tkatchenko, A., *Phys. Rev. Lett.* 2012, **108**, 146103.

[78] Lee, K., Murray, E. D., Kong, L., Lundqvist, B. I. and Langreth, D. C., *Phys. Rev. B* 2010, **82**, 81101.

[79] Langreth, D. C., Lundqvist, B. I., Chakarova-Käck, S. D., Cooper, V. R., Dion, M., Hyldgaard, P., Kelkkanen, A., Kleis, J., Kong, L., Li, S., G., M. P., Murray, E., Puzder, A., Rydberg, H., Schröder, E. and Thonhauser, T., *J. Phys.-Condens. Mat.* 2009, **21**, 84203.

[80] Dion, M., Rydberg, H., Schröder, E., Langreth, D. C. and Lundqvist, B. I., *Phys. Rev. Lett.* 2005, **95**, 109902.

[81] Dion, M., Rydberg, H., Schröder, E., Langreth, D. C. and Lundqvist, B. I., *Phys. Rev. Lett.* 2004, **92**, 246401.

[82] Hamada, I. and Otani, M., *Phys. Rev. B* 2010, **82**, 153412.

[83] Redhead, P. A. and Division, E. E., *Vacuum* 1962, **12**, 203–211.

[84] Campbell, C. T. and Sellers, J. R. V., *J. Am. Chem. Soc.* 2012, **134**, 18109–18115.

[85] Arrhenius, S. A., *Z. Phys. Chem.* 1889, **4**, 96–116.

[86] Eyring, H., *J. Chem. Phys.* 1935, **3**, 107–115.

[87] Evans, M. G. and Polanyi, M., *Trans. Faraday Soc.* 1935, **31**, 875–894.

[88] Kahk, J. M., Poll, C. G., Oropeza, F. E., Ablett, J. M., Céolin, D., Rueff, J.-P., Agrestini, S., Utsumi, Y., Tsuei,

K. D., Liao, Y. F., Borgatti, F., Panaccione, G., Regoutz, A., Egdell, R. G., Morgan, B. J., Scanlon, D. O. and Payne, D. J., *Phys. Rev. Lett.* 2014, **112**, 117601.

[89] Kubacka, A., Fernandez-Garcia, M. and Colon, G., *Chem. Rev.* 2012, **112**, 1555–1614.

[90] Grätzel, M., *Nature* 2001, **414**, 338–344.

[91] Ryan, J. V., Berry, A. D., Anderson, M. L., Long, J. W., Stroud, R. M., Cepak, V. M., Browning, V. M., Rolison, D. R. and Merzbacher, C. I., *Nature* 2000, **406**, 169–172.

[92] Henrich, V. E. and Cox, P. A., *The Surface Science of Metal Oxides*, Cambridge University Press, Cambridge 1994.

[93] Hu, C.-C., Chang, K.-H., Lin, M.-C. and Wu, Y.-T., *Nano Lett.* 2006, **6**, 2690–2695.

[94] Over, H., *Chem. Rev.* 2012, **112**, 3356–3426.

[95] Hibi, T., Okuhara, T., Seki, K., Abekawa, H. and Hamamatsu, H., *WO200110550-A1* 2001.

[96] Hibi, T., Nishida, H. and Abekawa, H., *US Pat. 5871,707* 1999.

[97] Hibi, T., Abekawa, H., Seki, K., Suzuki, T., Suzuta, T., Iwanaga, K. and Oizumi, T., *EP936184* 1999.

[98] Iwanaga, K., Seki, K., Hibi, T., Issoh, K., Suzuta, T., Nakada, M., Mori, Y. and Abe, T., *Sumitomo Kagaku* 2004.

[99] Wolf, A., Mleczko, L., Schłuter, O. F., Schubert, S. and Schlüter, O. F., *EP2026905* 2006.

[100] Wolf, A., Kintrup, J., Schłuter, O. F., Mleczko, L. and Schlüter, O. F., *EP2027062* 2006.

[101] Wolf, A., Mleczko, L., Schubert, S. and Schłuter, O. F., *EP2027063* 2006.

[102] Trasatti, S., *Electrochim. Acta* 2000, **45**, 2377–2385.

[103] López, N., Gómez-Segura, J., Marín, R. P. and Pérez-Ramírez, J., *J. Catal.* 2008, **255**, 29–39.

[104] Seki, K., *Catal. Surv. Asia* 2010, **14**, 168.

[105] Teschner, D., Farra, R., Yao, L., Schloegl, R., Soerijanto, H., Schomaecker, R., Schmidt, T., Szentmiklosi, L., Amrute, A. P., Mondelli, C., Perez-Ramirez, J., Novell-Leruth, G. and López, N., *J. Catal.* 2012, **285**, 273–284.

[106] Teschner, D., Novell-Leruth, G., Farra, R., Knop-Gericke, A., Schloegl, R., Szentmiklosi, L., Gonzalez, M. H., Soerijanto, H., Schomaecker, R., Perez-Ramirez, J. and López, N., *Nat. Chem.* 2012, **4**, 739–745.

[107] Deacon, H., *Br. Pat. 1403* 1868.

[108] Moser, M., Czekaj, I., López, N. and Pérez-Ramírez, J., *Angew. Chemie Int. Ed.* 2014, **126**, 8772–8777.

[109] Wulff, G., *Z. Kryst. Min.* 1901, **34**, 449.

[110] Trasatti, S., *Electrochim. Acta* 1991, **36**, 225–241.

[111] Lee, Y., Shin, H.-Y., Chun, S. H., Lee, J., Park, W. J., Baik, J. M., Yoon, S. and Kim, M. H., *J. Phys. Chem. C* 2012, **116**, 16300–16304.

[112] Cheng, J., Zhang, H., Chen, G. and Zhang, Y., *Electrochim. Acta* 2009, **54**, 6250–6256.

[113] Rossmeisl, J., Qu, Z.-W., Zhu, H., Kroes, G.-J. and Nørskov, J. K., *J. Electroanal. Chem.* 2007, **607**, 83–89.

[114] Takasu, Y., Sugimoto, W., Nishiki, Y. and Nakamatsu, S., *J. Appl. Electrochem.* 2010, **40**, 1789–1795.

[115] Trotochaud, L. and Boettcher, S. W., *Chem. Mat.* 2011, **23**, 4920–4930.

[116] McDaniel, C. L. and Schneide, S. J., *J. Res. Natl. Bur. Stand. Sect. A - Phys. Chem.* 1969, **A 73**, 213–219.

[117] McDaniel, C. L. and Schneide, S. J., *J. Res. Natl. Bur. Stand. Sect. A - Phys. Chem.* 1967, **A 71**, 119–123.

[118] Mahanty, S., Roy, S. and Sen, S., *J. Cryst. Growth* 2004, **261**, 77–81.

[119] Johansson, B. and Mårtensson, N., *Phys. Rev. B* 1980, **21**, 4427–4457.

[120] Howe, J. M., *Interfaces in materials*, John Wiley & Sons, New York 1997.

[121] Chelikowsky, J. R., *Surf. Sci. Lett.* 1984, **139**, L197–L203.

[122] Ruban, A., Skriver, H. and Nørskov, J. K., *Phys. Rev. B* 1999, **59**, 15990–16000.

[123] Ruban, A. V. and Skriver, H. L., *Comput. Mat. Sci.* 1999, **15**, 119–143.

[124] Christensen, A., Ruban, A. V., Stoltze, P., Jacobsen, K. W., Skriver, H. L., Nørskov, J. K. and Besenbacher, F., *Phys. Rev. B* 1997, **56**, 5822–5834.

[125] Martínez, J. I., Hansen, H. A., Rossmeisl, J. and Nørskov, J. K., *Phys. Rev. B* 2009, **79**, 45120.

[126] Brinkley, D. and Engel, T., *Surf. Sci.* 1998, **415**, L1001 – L1006.

[127] Bahruji, H., Bowker, M., Brookes, C., Davies, P. R. and Wawata, I., *Appl. Catal. A Gen.* 2013, **454**, 66–73.

[128] Gamble, L., Jung, L. S. and Campbell, C. T., *Surf. Sci.* 1996, **348**, 1–16.

[129] Martinez, U., Hansen, J. Ø., Lira, E., Kristoffersen, H. H., Huo, P., Bechstein, R., Lægsgaard, E., Besenbacher, F., Hammer, B. and Wendt, S., *Phys. Rev. Lett.* 2012, **109**, 155501.

[130] Li, B., Zhao, J., Onda, K., Jordan, K. D., Yang, J. and Petek, H., *Science* 2006, **311**, 1436–1440.

[131] Farfan-Arribas, E. and Madix, R. J., *J. Phys. Chem. B* 2002, **106**, 10680–10692.

[132] Kim, K. S. and Barteau, M. A., *J. Mol. Catal.* 1990, **63**, 103–117.

[133] Kim, K. S. and Barteau, M. A., *Surf. Sci.* 1989, **223**, 13–32.

[134] Pirilä, M., Lenkkeri, R., Goldmann, W., Kordás, K., Huuhtanen, M. and Keiski, R., *Top. Catal.* 2013, **56**, 630–636.

[135] Panagiotopoulou, P., Karamerou, E. E. and Kondarides, D. I., *Catal. Today* 2013, **209**, 91–98.

[136] Li, Z., Smith, R. S., Kay, B. D., Dohnálek, Z. and Dohn, Z., *J. Phys. Chem. C* 2011, **115**, 22534–22539.

[137] Henderson, M. A., Otero-Tapia, S., Castro, M. E. and Henderson, M. A., *Faraday Discuss.* 1999, **114**, 313–329.

[138] Hansen, J. Ø., Huo, P., Martinez, U., Lira, E., Wei, Y. Y., Streber, R., Lægsgaard, E., Hammer, B., Wendt, S. and Besenbacher, F., *Phys. Rev. Lett.* 2011, **107**, 136102.

[139] Kershis, M. D. and White, M. G., *Phys. Chem. Chem. Phys.* 2013, **15**, 17976–17982.

[140] Bondarchuk, O., Kim, Y. K., White, J. M., Kim, J., Kay, B. D., Dohnálek, Z. and Dohnalek, Z., *J. Phys. Chem. C* 2007, **111**, 11059–11067.

[141] Brinkley, D. and Engel, T., *J. Phys. Chem. B* 1998, **102**, 7596–7605.

[142] Kim, Y. K., Kay, B. D., White, J. M. and Dohnálek, Z., *J. Phys. Chem. C* 2007, **111**, 18236–18242.

[143] Li, Z., Kay, B. D. and Dohnalek, Z., *Phys. Chem. Chem. Phys.* 2013, **15**, 12180–12186.

[144] García-Muelas, R. and López, N., *J. Phys. Chem. C* 2014, **118**, 17531–17537.

[145] Acharya, D. P., Yoon, Y., Li, Z., Zhang, Z., Lin, X., Mu, R., Chen, L., Kay, B. D., Rousseau, R. and Dohnálek, Z., *ACS Nano* 2013, **7**, 10414–10423.

[146] Walle, L. E., Borg, A., Uvdal, P. and Sandell, A., *Phys. Rev. B* 2009, **80**, 235436.

[147] Schaub, R., Thostrup, P., López, N., Lægsgaard, E., Stensgaard, I., Nørskov, J. K. and Besenbacher, F., *Phys. Rev. Lett.* 2001, **87**, 266104.

[148] Eyring, L., *Synthesis of Lanthanide and Actinide Compounds*, Kluwer Academic Publisher, Dordrecht 1991.

[149] Quéré, D., *Reports Prog. Phys.* 2005, **68**, 2495.

[150] Schlom, D. G., Guha, S. and Datta, S., *MRS Bull.* 2011, **33**, 1017–1025.

[151] Fanciulli, M. and Scarel, G., editors, *Rare Earth Oxide Thin Films - Growth, Characterization, and Applications*, Springer, Heidelberg 2007.

[152] Trovarelli, A., *Catalysis by Ceria and Related Materials*, Imperial College Press, London 2002.

[153] Mogensen, M., *Solid State Ionics* 2000, **129**, 63–94.

[154] Nolan, M., *J. Phys. Chem. C* 2009, **113**, 2425–2432.

[155] Fally, F., Perrichon, V., Vidal, H., Kaspar, J., Blanco, G., Pintado, J. M., Bernal, S., Colon, G., Daturi, M. and Lavalley, J. C., *Catal. Today* 2000, **59**, 373–386.

[156] Putna, E. S., Bunluesin, T., Fan, X. L., Gorte, R. J., Vohs, J. M., Lakis, R. E. and Egami, T., *Catal. Today* 1999, **50**, 343–352.

[157] Farra, R., García-Melchor, M., Eichelbaum, M., Hashagen, M., Frandsen, W., Allan, J., Girgsdies, F., Szentmiklósi, L., López, N. and Teschner, D., *ACS Catal.* 2013, **3**, 2256–2268.

[158] Adachi, G.-y. and Imanaka, N., *Chem. Rev.* 1998, **98**, 1479–1514.

[159] Jiang, H., Rinke, P. and Scheffler, M., *Phys. Rev. B* 2012, **86**, 125115.

[160] Azimi, G., Dhiman, R., Kwon, H.-M., Paxson, A. T. and Varanasi, K. K., *Nat. Mater.* 2013, **12**, 315–320.

[161] Ranea, V. A., Carmichael, I. and Schneider, W. F., *J. Phys. Chem. C* 2009, **113**, 2149–2158.

[162] Stone, A. J., *The Theory of Intermolecular Forces*, Clarendon Press, Oxford 1996.

[163] Nozières, P. and Pines, D., *Phys. Rev.* 1958, **1**.

[164] Harl, J., Schimka, L. and Kresse, G., *Phys. Rev. B* 2010, **81**, 115126.

[165] Lebègue, S., Harl, J., Gould, T., Ángyán, J. G., Kresse, G. and Dobson, J. F., *Phys. Rev. Lett.* 2010, **105**, 196401.

[166] Schimka, L., Harl, J., Stroppa, A., Grüneis, A., Marsman, M., Mittendorfer, F. and Kresse, G., *Nat. Mater.* 2010, **9**, 741–744.

[167] Harl, J. and Kresse, G., *Phys. Rev. Lett.* 2009, **103**, 56401.

[168] Deshlahra, P., Wolf, E. E. and Schneider, W. F., *J. Phys. Chem. A* 2009, **113**, 4125–4133.

[169] Neugebauer, J. and Scheffler, M., *Phys. Rev. B* 1992, **46**, 16067–16080.

[170] Tysoe, W. T., Ormerod, R. M., Lambert, R. M., Zgrablich, G. and Ramirez-Cuesta, A., *J. Phys. Chem.* 1993, **97**, 3365–3370.

[171] Waddill, G. D. and Kesmodel, L. L., *Phys. Rev. B* 1985, **31**, 4940–4946.

[172] Xu, C., Tsai, Y. L. and Koel, B. E., *J. Phys. Chem.* 1994, **98**, 585–593.

[173] Campbell, J. M., Seimanides, S. and Campbell, C. T., *J. Phys. Chem.* 1989, **93**, 815–826.

[174] Xi, M., Yang, M. X., JO, S. K., Bent, B. E. and Stevens, P., *J. Chem. Phys.* 1994, **101**, 9122–9131.

[175] Lukas, S., Vollmer, S., Witte, G. and Wöll, C., *J. Chem. Phys.* 2001, **114**, 10123–10130.

[176] Meserole, C. A., Vandeweert, E., Postawa, Z., Haynie, B. C. and Winograd, N., *J. Phys. Chem. B* 2002, **106**, 12929–12937.

[177] Rockey, T. J., Yang, M. and Dai, H.-L., *J. Phys. Chem. B* 2006, **110**, 19973–19978.

[178] Syomin, D., Kim, J., Koel, B. E. and Ellison, G. B., *J. Phys. Chem. B* 2001, **105**, 8387–8394.

List of Publications

1. **On the properties of binary rutile MO_2 compounds, M = Ir, Ru, Sn and Ti: A DFT study** Novell-Leruth, G., Carchini, G. and López, N., *J. Chem. Phys.* 2013, **138**, 194706.

2. **Adsorption of small mono- and poly-alcohols on rutile TiO_2: a density functional theory study** Carchini, G. and López, N., *Phys. Chem. Chem. Phys.* 2014, **16**, 14750-14760.

3. **Costless Derivation of Dispersion Coefficients for Metal Surfaces** Almora-Barrios, N., Carchini, G., Błoński, P. and López, N., *J. Chem. Theory Comput.* 2014, **10**, 5002-5009.

The author has performed all the calculations in publication 2 and the second part of publications 1 and 3, employing the density functional theory code VASP. He has written the first draft of publication 2 and part of publications 1 and 3. Moreover, the author as actively contributed to the following papers:

1. **How Theoretical Simulations Can Addresss the Structure and Activity of Nanoparticles** Carchini, G., Almora-Barrios, N., Revilla-López, G., Bellarosa, L., García-Muelas, R., García-Melchor, M., Pogodin, S., Błoński, P. and López, N., *Top. Catal.* 2013, **56**, 1262-1272.

2. **State-of-the-art and challenges in theoretical simulations of heterogeneous catalysis at the microscopic level** López, N., Almora-Barrios, N., Carchini, G., Błoński, P., Bellarosa, L., García-Muelas, R., Novell-Leruth, G. and Carcía-Mota, M., *Catal. Sci. Technol.* 2012, **2**, 2405-2417.

which are included at the end of this Thesis.

AIP | The Journal of Chemical Physics

On the properties of binary rutile MO2 compounds, M = Ir, Ru, Sn, and Ti: A DFT study

Gerard Novell-Leruth, Giuliano Carchini, and Núria López

Citation: The Journal of Chemical Physics **138**, 194706 (2013); doi: 10.1063/1.4803854
View online: http://dx.doi.org/10.1063/1.4803854
View Table of Contents: http://scitation.aip.org/content/aip/journal/jcp/138/19?ver=pdfcov
Published by the AIP Publishing

THE JOURNAL OF CHEMICAL PHYSICS **138**, 194706 (2013)

On the properties of binary rutile MO_2 compounds, M = Ir, Ru, Sn, and Ti: A DFT study

Gerard Novell-Leruth, Giuliano Carchini, and Núria López[a)]
Institute of Chemical Research of Catalonia (ICIQ), Avgda. Països Catalans 16, 43007 Tarragona, Catalonia, Spain

(Received 23 January 2013; accepted 15 April 2013; published online 20 May 2013)

We have studied the properties of bulk and different surfaces of rutile oxides, IrO_2, RuO_2, SnO_2, and TiO_2, and their binary compounds by means of density functional theory. As mixtures are employed in many applications, we have investigated the solubility, segregation, and overlayer formation of one of these oxides on a second metal from the series, as these aspects are critical for the chemical and electrochemical performances. Our results show that the bulk solubility is possible for several combinations. The electronic structure analysis indicates the activation of Ir states in $Ir_xTi_{1-x}O_2$ mixtures when compared to the parent IrO_2 compound or the reduction in the band gap of TiO_2 when Sn impurities are present. Segregation and oxygen-induced segregation of the second metal for the most common surfaces show a great extent of possibilities ranging from strong segregation to antisegregation, which depends on the oxygen ambient. The interaction of guest rutile overlayers on hosts is favourable and a wide range of growth properties (from multilayer formation to tridimensional particles) can be observed. Finally, a careful comparison with experimental information is presented, and for those cases where no data is available, the computed database can be used as a guideline by experimentalists. © *2013 AIP Publishing LLC*. [http://dx.doi.org/10.1063/1.4803854]

I. INTRODUCTION

Among all oxides, rutiles constitute a class that shows the most impressive technological applications which span several of the most challenging areas of physics and chemistry, including energy production and storage and catalysis.[1–7] For instance, RuO_2 has been proposed in capacitor devices,[7,8] as catalyst, and electrocatalyst in the production of Cl_2.[9–20] Regarding TiO_2, it has a huge number of uses: as support in oxidation reactions that might play an active role,[21–23] or in energy-related applications as a photocatalyst (its band gap fits the solar spectra well),[24] as support for dye-sensitized solar devices,[5,25–27] and in the oxygen evolution in electrocatalysis.[28] In turn, SnO_2 compounds are employed as redox gas sensors.[29,30] All these oxides share this common, very stable, rutile structure but they show very different chemical properties.[31] In fact, the degree of surface oxidation, reduction, and the basic electronic properties depend on the particular element: while RuO_2 and IrO_2 compounds are metallic in nature and adsorb oxygen easily, Ti and Sn oxides are semiconductors that can be doped by losing some of it. This is related to the nature of these metal atoms: while Ti (and Sn) almost lose all the electrons at the *d* and *s* levels (or *p* and *s* levels for Sn), some electrons are left in the *d* states of Ru and Ir upon oxide formation.

As both RuO_2 and IrO_2 are quite expensive, in practical applications (including the catalytic and electrocatalytic synthesis of HCl), mixed rutile compounds containing more than one of the Ru, Sn, Ti, and Ir metals are preferred.[19,32] Secondary components can improve the chemical and electrochemical properties (i.e., activity or selectivity) or act as stability promoters and selectivity enhancers.[4] Thus, the ability of the rutiles to form mixtures and their segregation under different environments are mandatory aspects to understand the properties of multicomponent materials. RuO_2 and IrO_2 are major components of Dimensionally Stable Anodes (DSA) in electrochemical environments.[4,16,33] For them, an improved electrocatalytic activity than that of the native IrO_2 and a better stability than for RuO_2 are obtained from the formation of solid solutions.[34] An example of the properties of mixed compounds can be found in the long-term stability of Cl_2 production anodes. For instance, in long term tests (more than 10 years), RuO_2-TiO_2/Ti lost a 43% of the Ru content while lower percentages were reported for the IrO_2-RuO_2-TiO_2/Ti, where only about 15% for Ir and Ru was lost.[35] New challenges and opportunities in the formulation of the binary compounds arise from the appearance of new synthetic techniques, based either on the use of wet organic-ligand mediated synthesis or by physical vapor transport process.[36,37] In the first case, enhanced design control, allowing core/shell nanoparticles with tunable lattice constants and morphologies, was presented for SnO_2-TiO_2.[36] In the second metastable, $Ir_xRu_{1-x}O_2$ structures were obtained in the full *x* range. In addition, the analysis of RuO_2 on TiO_2 and the atomic level redistribution have been analyzed as a function of the nanoparticle dimensions by HRTEM.[38] It was found that small RuO_2 nanoparticles (below 2 nm) can accommodate to the TiO_2 rutile surface in the form of epitaxial growth.

A systematic investigation on the properties of single metal oxides was presented by Nørskov and co-workers[39] recently. In that work, the cohesive energy of rutile compounds was obtained quite accurately, provided that the RPBE

a)E-mail: nlopez@iciq.es

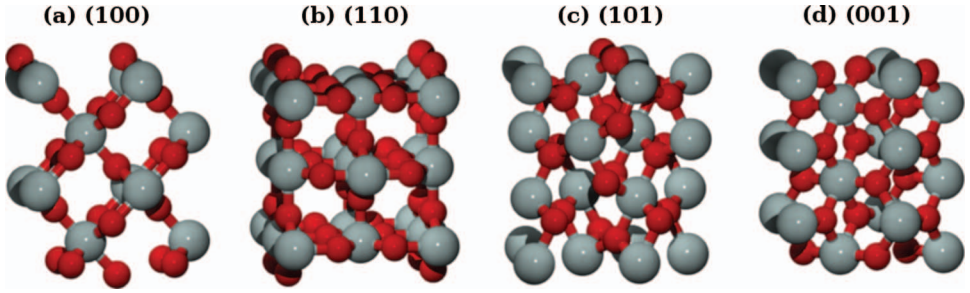

FIG. 1. Rutile surfaces in perspective views. Grey large spheres correspond to metal atoms, while red small ones correspond to oxygen anions.

(a revision of the Perdew-Burke-Ernzerhof functional),[40] was used and that water was employed as a reference for the oxygen state. This result indicated that, even if the main energy parameters regarding rutile oxides are reasonably well described with such functionals, more sophisticated schemes (a corrected version of the Generalized Gradient Approximation) are needed when impurities create areas of defects with different redox states.[41,42]

The aim of the present study is to employ Density Functional Theory (DFT) to bulk models and slabs to determine the most common surface for all the rutiles investigated (MO_2, M = Ir, Ru, Sn, and Ti), and to analyze the degree of mixing in the bulk and segregation of impurities towards the surfaces. Since all the ions considered show a similar charge state in the rutile form, RPBE can be used to obtain the relative energies for different configurations describing the phenomena. Similar studies on metal alloys have been proven to be very useful when assessing their chemical properties,[43–45] and a wonderful platform to guide experimental groups when investigating the surface composition.

II. COMPUTATIONAL DETAILS

We employed first principles density functional theory through the VASP code, version 5.2.[46,47] The functional of choice was RPBE[40] and the inner electrons were represented by Projector Augmented Wave (PAW) pseudopotentials[48] of [Kr] and [Ar] configurations for Ru and Ir, respectively. The *p* and *d* semi-core states were treated as valence states for Ti and Sn. The outermost electrons were expanded in plane waves with a maximum kinetic energy of 400 eV. It has to be noted that the energies obtained with the RPBE for rutiles without changes in the charge state of cations give good energy estimates.[39] Moreover, the metallic nature of both RuO_2 and IrO_2 is well reproduced in the calculations. For Ti and Sn oxides, as no change in redox properties occurs in any of the processes investigated, we have considered that the GGA approach employed here is sufficient to obtain the trends in segregation and adsorption. We would like to point out that other more sophisticated approaches such as GGA + U are not free of the arbitrarity when choosing the U parameter and this will add an extra degree of uncertainty. In the bulk, the k-point sampling was $11 \times 11 \times 12$.[49] A sequential optimization was carried out to determine the unit cell parameters: first, the volume was obtained and then, the individual parameters $a = b$, c and the internal u position were derived.

To analyze the solubility of the different metals, we performed a series of calculations with $(2 \times 2 \times 2)$ supercells $M_gM_hO_2$, using a k-point sampling of $6 \times 6 \times 7$. The total M_g concentration was 6.25%. Solubilities depend on the number of impurities and their relative positions,[50,51] but the present estimates can be employed to compare the relative strength of the substitutions. Although this model might seem rough, it constitutes an indication for the solubility of the secondary metal on the first and follows investigations for metal alloys. Entropic contributions would favor impurity dissolution, specially at low concentrations, and more sophisticated models imply small corrections to the values presented here.[52]

Surface calculations were performed for all the low index facets: (110), (101), (100), and (001), as shown in Figure 1. (110), (101), and (100) contain five-fold coordinated M atoms, M_{cus}, and either fully coordinated oxygens O_{3c} or bridge-like coordinated O_b ones. In contrast, the (001) termination exhibits four-fold coordinated cations, M_{cus}, and bridge O_b anions. We built slabs containing 10 metal atoms and 20 oxygens, and the k-point sampling has been set to $8 \times 4 \times 1$ (110), $5 \times 6 \times 1$ (101), $6 \times 8 \times 1$ (100), and $6 \times 6 \times 1$ for (001). The size of the models presented here is large enough to ensure the convergence of the main properties.[53] In these calculations the outermost two layers were allowed to relax while the others were frozen to their bulk positions. The asymmetric nature of the slabs presented here implies the use of a factor two in the definition of the surface energy that we employ in Sec. III A. The dipole correction was introduced to eliminate potential artificial electric fields induced by the asymmetry of our construction.[54]

Segregation phenomena both under vacuum and oxygen conditions were analyzed with five layers slabs in a $p(2 \times 1)$ reconstruction of (110), (101), and (001) surfaces, while for the (100) a $p(1 \times 2)$ supercell was used; finally a 10 Å vacuum was added to avoid interactions between the periodic images. Tests have identified that this vacuum space is sufficient to obtain adsorption energies with less than 0.001 eV error. The corresponding k-point samplings were $4 \times 4 \times 1$, $3 \times 6 \times 1$, $3 \times 6 \times 1$, and $6 \times 4 \times 1$, respectively. In these models, a substitutional oxide was studied with a single M_h atom replaced by M_g. Two positions, either in the center of the slab or at the M_{cus} on the surface, were investigated. The energy difference between these two configurations corresponds to the segregation energy, i.e., the tendency of the impurity to be on the surface. Since the materials in this study show a very different behavior with respect to oxygen adsorption, we have considered also the possibility of oxygen-induced M_g

TABLE I. Optimized cell parameters for the rutile structures: a = b, c in Å, and the internal parameter u, in internal coordinates. Cohesive and formation energies, E_{coh} and ΔE_f, and corresponding experimental data, E_{coh}^{exp} and $\Delta H_f^{\circ exp}$, all in eV/MO_2.

Oxide	a	c	u	a_{exp}	c_{exp}	E_{coh}	E_{coh}^{exp} (Ref. 55)	ΔE_f	$\Delta H_f^{\circ exp}$ (Ref. 56)
IrO_2	4.533	3.190	0.308	4.490	3.140	14.00	...	−1.89	−2.84
RuO_2	4.533	3.136	0.306	4.510	3.110	14.07	15.07	−2.48	−3.16
SnO_2	4.802	3.240	0.306	4.747	3.186	12.88	14.40	−4.51	−5.99
TiO_2	4.635	2.972	0.304	4.594	2.958	19.09	19.90	−8.53	−9.79

segregation towards the surface with the same calculation set-up. In segregation and induced-segregation models, the three uppermost layers and the atoms that are directly in contact with the impurities, or in the same layer, were allowed to relax, while the rest were kept fixed to the bulk positions.

Overlayer stability was analyzed by depositing one (two) M_gO_2 overlayer on a host slab containing four (three) M_hO_2, and calculating the corresponding adhesion energy, E_{adh} (in eV/Å^2). The guest cell parameters follow those of the host material, and relaxations along the z-direction were allowed for three upper layers in the complete slab.

III. RESULTS AND DISCUSSION

In the following, we first present the data corresponding to the bulk properties. In a second step, the surface energies are discussed for the low-index facets. Then mixed phases, such as impurities and overlayers, both in the bulk and on the surface, are addressed. At the end of each section a comparison to experimental results is presented.

A. Pure phases: Bulk and surface energies

Table I shows the cell parameters for all the pure phase oxides, MO_2 with M = Ir, Ru, Sn, and Ti. Our results are in agreement with previous data in the literature[56–58] and the total volume is found to increase along the series $TiO_2 < RuO_2 < IrO_2 < SnO_2$. The errors between the calculated structures and the experimental unit cell parameters are smaller than 0.07 Å, corresponding to about less than 1.5%. The cohesive energy is defined with respect to gas-phase oxygen and the gas-phase atomic metal reference, through the equation: $E_{coh} = -(E_{b-MO_2} - E_{O_2} - E_{a-M})$, where positive values imply exothermic processes. The obtained estimates are somehow smaller than those reported experimentally.[55] The differences, about 1 eV, are due to the wrong estimation of the O_2 binding energy. Ways to circumvent this problem have been developed, for instance employing a water reference instead of a molecular oxygen-based one.[39] However, the method above reproduces correctly the experimental trends: the highest cohesive energy corresponds to TiO_2, followed by RuO_2 and IrO_2, and the smallest value is obtained for SnO_2. Formation energies have also been calculated as follows: $E_f = E_{b-MO_2} - E_{O_2} - E_{b-M}$ with respect to the metal bulk state (Ti(hcp), Ru(hcp), Ir(fcc), Sn(tetragonal I41/*amd*)) and molecular oxygen in gas phase. Again, formation energies suffer from a systematic error of about the same size as the cohesive energies. The trend is as follows: $TiO_2 > SnO_2 > RuO_2 > IrO_2$, thus reproducing the experiments.[56] The differences in the ordering between cohesive and formation energies come from the fact that metallic Sn shows a lower cohesive energy than its counterparts. Since bulk metals constitute a better reference than metal atoms, we have employed formation energies in the comparison of different materials.

As for the surfaces represented in Figure 1, we have computed their corresponding surface energies, γ_X, which are obtained through

$$\gamma_X = \left[\left(E_X^{nr} - NE_b\right)/2 + \left(E_X^r - E_X^{nr}\right)\right]/A_X, \qquad (1)$$

where E_X^r and E_X^{nr} are the energies corresponding to the relaxed and non-relaxed slabs of the X surface; E_b is the bulk energy per formula unit; N is the number of formula units in the slab, and A_X the corresponding surface. As indicated in Sec. II, the "2" denominator in Eq. (1) comes from the fact that two surfaces are generated when constructing the slab. γ_X and the relaxations for the undercoordinated metal atom are shown in Table II.

The corresponding surface energies follow the trend $TiO_2 < RuO_2 \approx SnO_2 < IrO_2$. This ordering is due both to the formation energies and the unit cell size. From this data, in mixed overlayer systems the structure showing the lowest surface energy, TiO_2 would be on the surface, while IrO_2 would be preferentially at the core. In addition, the (110) facet presents the minimum surface energy for all these oxides. This can be understood since the number of total bonds lost per surface unit cell is the lowest for this particular face. In addition, relaxation of M_{cus} atoms correlates with the surface energy. Indeed, the smallest displacements are found for the (110) direction (about ∼0.05 Å). Instead, larger changes of about 0.1 Å are found for (001).

Under vacuum conditions, the equilibrium shape can be estimated by the Wulff structure:[59] the structures are depicted in Figure 2 and analyzed in Table II. In the particular case of the studied rutiles, (110) and (101) are the most common facets: for all the systems except for TiO_2, these surfaces are equally represented in the nanoparticles. In the case of TiO_2 a larger asymmetry is found and the (110) surface represent more than 80% exposed area, and results for TiO_2 agree qualitatively with those of Selloni and co-workers.[60]

It has to be noticed that for IrO_2, RuO_2, and SnO_2, the ratios between the different surfaces in the Wulff construction are almost independent of the material, and thus the presence of impurities would not imply severe modifications.

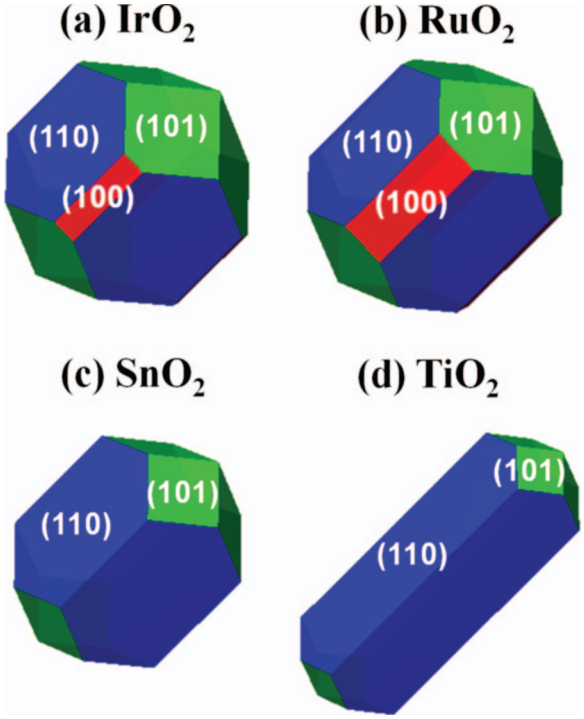

FIG. 2. Wulff structure for the different rutiles: the blue planes belong to the {110}, the green ones to the {101}, and red for the {100}.

B. Binary mixtures: Impurities in the bulk

In this section we discuss several aspects of the presence of impurities in the rutile lattices. First, we present the energy needed to introduce the secondary metal in the host rutile, the solubility E_{sol}. This parameter is reported in Figure 3 and has been calculated according to the following reaction:

$$M_gO_2 + M_hO_2 \rightarrow M_gM_hO_2 + M_hO_2. \quad (2)$$

The corresponding equation is

$$E_{sol} = E_{M_gM_hO_2} + M_hO_2(b \text{ per metal}) - E_{M_hO_2} - E_{M_gO_2}(b \text{ per metal}), \quad (3)$$

where $E_{M_gM_h}O_2$ and $E_{M_hO_2}$ are the energies of the $(2 \times 2 \times 2)$ bulk with and without the substitutional guest, $E_{M_hO_2}(b)$ and $E_{M_gO_2}(b)$ are the corresponding host and guest bulk energies per formula unit.

The solubility is endothermic in almost all cases but the values are relatively small, in particular if mixing entropies are taken into account. This agrees with the large experimental evidence gathered regarding metastable structures for which quite long lives can be found.[4] The difficulties to form

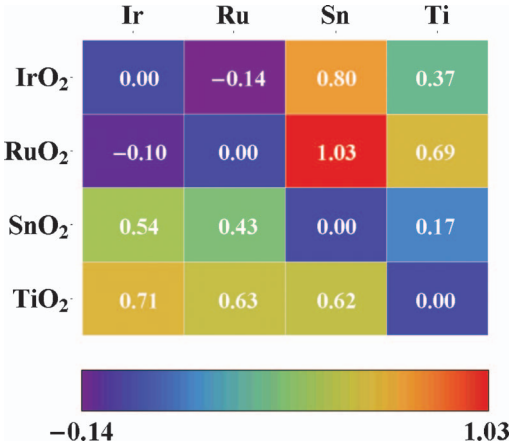

FIG. 3. Solubility energy, E_{sol}, in eV. The energy is obtained for the reaction $M_gO_2 + M_hO_2 \rightarrow M_gM_hO_2 + M_hO_2$ for all possible pairs. Columns represent the guest atoms M_g, while rows stand for the host M_h.

the bimetallic oxide are greater for Sn in RuO_2, and to a lesser extent for Sn in IrO_2, followed by Ti in RuO_2 and Ir, Ru, and Sn in TiO_2. A moderate endothermic value is found for Ti in SnO_2. In contrast, exothermic solubility is retrieved only for the combinations of Ir-Ru oxides. It shall be noted, though, that the present values correspond to upper (unfavoured) energy estimates, due to the presence of a larger configurational entropy for mixed phases[61] when compared to pure states.

Our results are in line with several experimental observations on the appearance of oxide solid solutions. As for Ir and Ru, they form a binary system that presents a high solubility with a unique rutile phase below 1000 °C for the whole composition and solid solution.[62] This was also observed in electrochemical experiments.[34] In turn, Ir-Ti and Ir-Sn phase diagrams with oxygen demonstrate that for the equilibrium TiO_2-IrO_2 there is a phase separation.[63] Only tiny amounts of Ir can be incorporated in the TiO_2 lattice (below 5%), while the solubility of Ti in IrO_2 can reach up to 10% at temperatures close to 1040 °C. When the mixture corresponds to Ir and Sn, the system is poorly soluble in IrO_2 (about 1%–2%), in agreement with the computed energy displayed in Figure 3. Only metastable RuO_2-SnO_2 mixed oxides in the form of solid solutions have been reported.[64] Also, SnO_2 and TiO_2 present complete solubility up to 0.23 at. % and Sn promotes the transformation of anatase to rutile.[65] Similarly, the thermodynamically stable phases of Ti and Sn, $Ti_xSn_{1-x}O_2$, are only formed for x = 0.1 and Sn-rich x = 0.9 ones.[66] Still, solid Ti-Sn solutions can be formed and their XRD patterns show diffraction peaks between TiO_2 and SnO_2 along the composition range with the corresponding lattice deformation.[67] For these structures, the abatement of the

TABLE II. Surface energy, γ_X, in eV/Å^2, for the low index X-surfaces together with the relaxation of the M_{cus} position towards the bulk and $d_{M_{cus}-O}$ in Å. The lowest surface energies are indicated in bold.

Oxide	γ_{100}	$d_{M_{cus}-O}$	S	γ_{110}	$d_{M_{cus}-O}$	S	γ_{101}	$d_{M_{cus}-O}$	S	γ_{001}	$d_{M_{cus}-O}$	S
IrO_2	0.084	0.046	6	**0.066**	−0.012	46	0.077	−0.001	48	0.121	−0.038	...
RuO_2	0.047	−0.036	15	**0.041**	−0.056	42	0.051	−0.041	43	0.075	−0.072	...
SnO_2	0.070	−0.005	...	**0.042**	−0.047	65	0.064	−0.021	35	0.132	−0.055	...
TiO_2	0.022	−0.164	...	**0.014**	−0.170	84	0.044	−0.124	16	0.057	−0.170	...

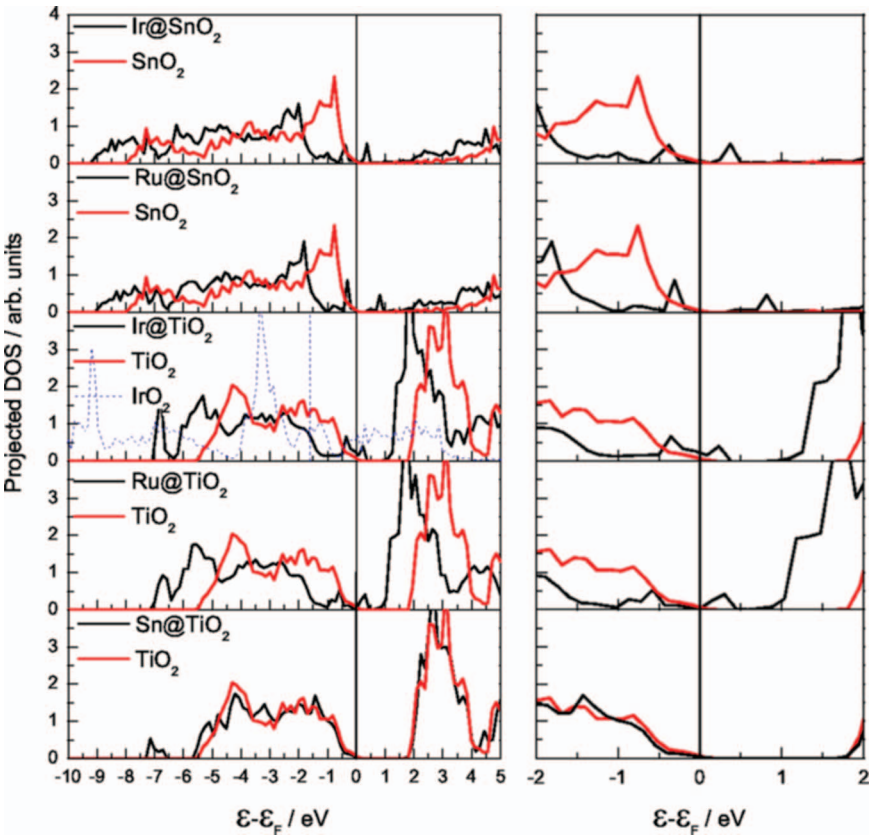

FIG. 4. Density of states for the TiO_2 and SnO_2 systems containing Ru and Ir impurities (black line), the bulk TiO_2 and SnO_2 references (red line), and Sn in TiO_2. For Ir in TiO_2, the native IrO_2 structure is presented in blue. The alignment of the DOS in this case has been done with respect to ϵ-$\epsilon_F(TiO_2)$ and its corresponding Fermi level is expressed in the dotted vertical line. In the right column an enlargement of the area around the Fermi level is presented.

anatase phase and the tunability of the lattice parameters were described experimentally.[36,68]

C. Electronic structure of impurity containing rutiles

We have also obtained the Density of States (DOS) corresponding to the bulk containing impurities as shown in Figure 4. For instance, both SnO_2 and TiO_2 are semiconductors and thus GGA functionals retrieve small band gaps,[69] as this is clearly seen in Figure 4 (red line). Still, this deviation does not affect any of the properties studied here and thus the GGA approach is enough to analyze the segregation processes. When impurities, like Ir or Ru, are present the gap is narrower and metal gap states appear. The main contribution to these states comes from the new metal impurity, although the surrounding oxygen atoms can also participate in the shoulder at the top of the valence band.

In addition, Sn substitution in the TiO_2 lattice ($Sn_xTi_{1-x}O_2$ with x = 0.25) has been found to improve the photocatalytic response of native TiO_2.[67,70] Indeed, in the XPS of the $Sn_xTi_{1-x}O_2$, it was found that there is a small shift in the main valence band toward the Fermi energy together with a small increase of intensity. The tail in the bandgap was attributed to surface states corresponding to Sn.[68] The calculated DOS shows that this is the case, as Sn substitution reduces the band gap for TiO_2, see Figure 4, where the states related to Sn are found to form the lower part of the conduction band.

Yet, another aspect concerns Ir-Ti mixtures. Electrochemical experiments show that the formation of the mixed bond and the compression induced by the TiO_2 cell would push the IrO_2 levels enhancing the "true" electrocatalytic activity per Ir site at low concentrations.[71] This can be again observed in Figure 4. The Ir states are higher in energy when sitting as an impurity in TiO_2, due to the fact that the Fermi level for this system is higher than that of clean IrO_2 (marked by a dotted line in Figure 4). Therefore, enhanced activity of these centers comes from the level alignment more than to the change of the chemical nature of the atoms in the surroundings.

D. Binary mixtures: Segregation of impurities

Once solubilities are known, the preferential segregation of vacancies towards the surface can be described through the segregation energy, E_{seg}, defined as

$$E_{seg} = E_{M_gM_hO_2}(M_g^s) - E_{M_gM_hO_2}(M_g^b), \quad (4)$$

where $E_{M_gM_hO_2}(M_g^s)$ corresponds to the surface with the impurity, Fig. 5(b), on the topmost layer and $E_{M_gM_hO_2}(M_g^b)$, Fig. 5(c), is that of the impurity in the bulk. A schematic illustration of the process for the reaction is shown in Figures 5(b) and 5(c) for the (110) surface.

We have performed these calculations for all the low-index surfaces considered in Table I. Negative values imply that the guests are more likely to be at the surface

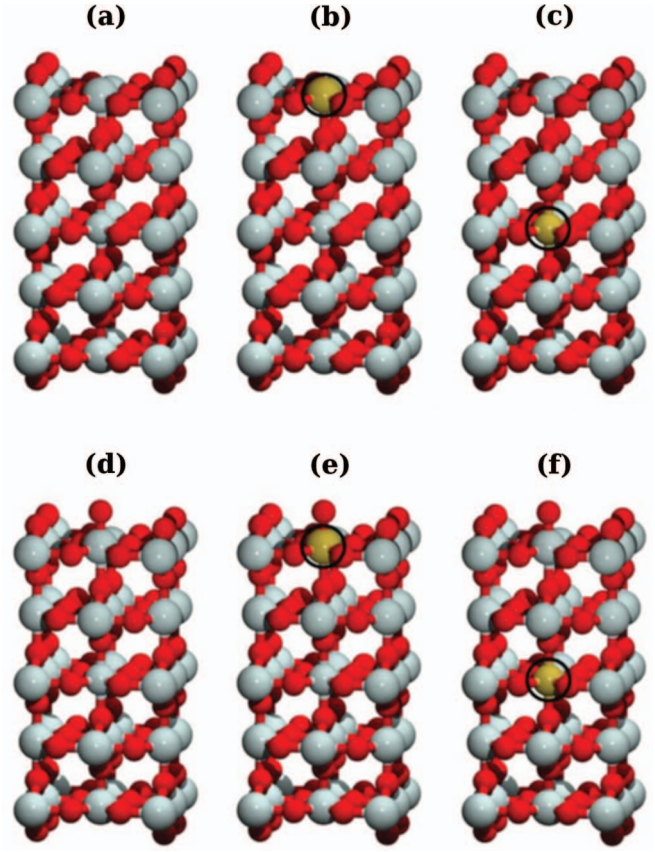

FIG. 5. Structures representing segregation and induced segregation of $M_gM_hO_2(110)$ surfaces. (a) Clean structure; (b) impurity on the surface; (c) impurity in the bulk; (d) oxygen on the surface; (e) oxygen bonded to the impurity on the surface; and (f) oxygen bonded to the surface with the impurity in the bulk. Grey colors stand for the metal atoms (M_h), gold for the impurities (M_g), and red ones correspond to oxygen anions (O).

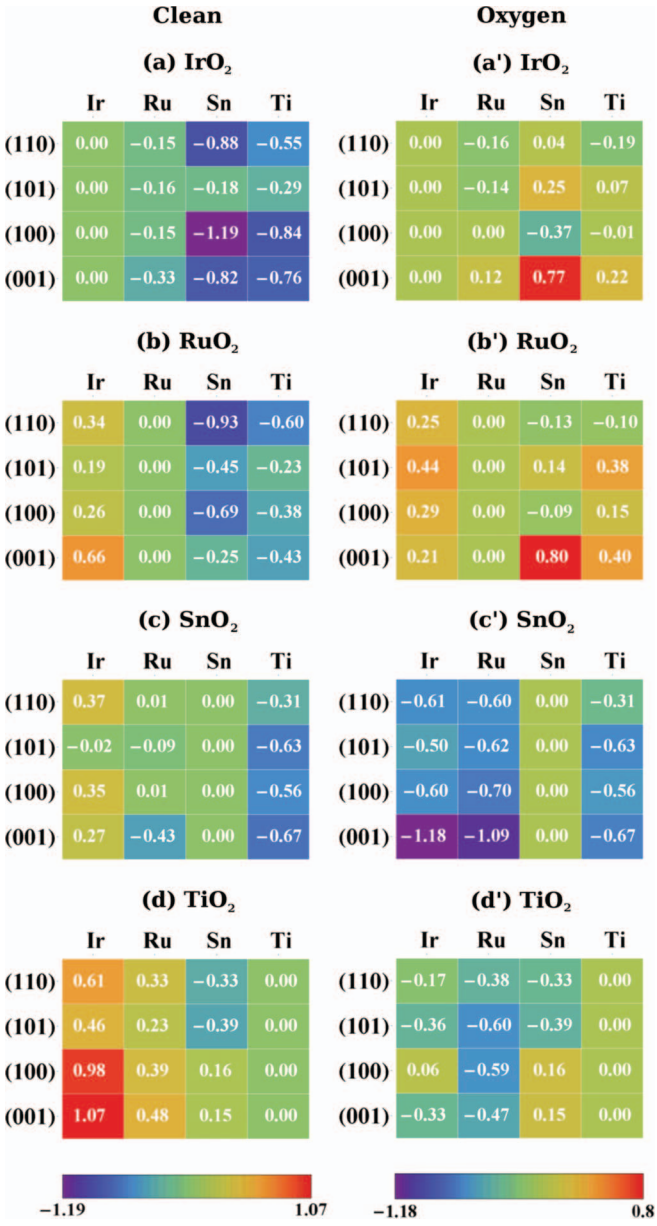

FIG. 6. Segregation energy (left column), E_{seg} in eV, and induced segregation energy (central column), $E_{seg}(O)$, both in eV, for the different metal oxide surfaces: (a) and (a′) IrO_2; (b) and (b′) RuO_2; (c) and (c′) SnO_2; and (d) and (d′) TiO_2, with all the guest metals (columns) and all the low index faces (in rows). In the right column, the oxygen adsorption energies are presented. Cold colors indicate exothermic processes, while warm ones stand for endothermic processes.

(segregation), while positive values indicate that they stay in the bulk (antisegregation). The results are shown in Figure 6. Notice that configurational entropy would tend to favour bulk positions.

We can describe the results according to the different materials. For IrO_2, Ru is slightly segregated towards all facets, while Ti is to a larger extent followed by Sn. As for RuO_2, Ir does not segregate, and Sn and Ti behave as in IrO_2. SnO_2 turns out to show the least contaminated surface as only Ti can be segregated, to a small extent. Finally, for TiO_2, Ir is antisegregated, while Sn can be mildly segregated.

In electrochemical environments, Sn added to IrO_2 is found to preferentially sit in the outermost layers.[72] Indeed, the computed value is about 0.8 eV. Ti segregates towards the surface in IrO_2 ($Ti_xIr_{1-x}O_2$) for solid solutions with compositions $0.2 < x < 1.0$ as found in Energy Dispersive X ray (EDX) analysis. Moreover, the oxide layer does not possess fully metallic properties in impedance measurements.[71,73] Preferential segregation is found in the calculations for Ti in all IrO_2 planes, see Figure 6(a), and antisegregation is retrieved for Ir in the TiO_2, Figure 6(d), in agreement with the experimental observations described above.

XPS data showed that the SnO_2-RuO_2 metastable solid solutions are complete in the whole volume and that the external layers were partially enriched on Sn, as also reflected in electrochemical measurements.[74] This agrees with the −0.93 to −0.24 eV values found for Sn E_{seg} on RuO_2. In turn, TiO_2 segregates in RuO_2 as found by XPS and backscattering spectrometry and the effect was claimed to be less pronounced for high Ru contents.[64] The estimates for E_{seg} in this case range from −0.60 to −0.23 eV. For Sn-doped rutile TiO_2 systems, preferential segregation of Sn was observed by XPS,[68] in agreement with the $E_{seg} = -0.3$ eV in Figure 6(d).

Still, a second interpretation can be obtained from the data above if the perspective is taken from the different facets. (110) planes of IrO_2 and RuO_2 show a much larger scatter of the segregation energies than the corresponding (101). In

contrast, the (110) and (101) planes of SnO_2 and TiO_2 show similar energy ranges but the values for the (101) SnO_2 are always more exothermic than their (110) counterparts.

E. Oxygen adsorption and oxygen induced segregation

Rutiles have been proposed as oxidation materials for a number of applications, including electrochemical generation of O_2 and HCl oxidations.[9–19] Adsorption on such surfaces takes place at the coordinatively unsaturated sites, M_{cus}; these are the fivefold M_{cus} positions in (110), (101), (100), and the four-fold coordinated metal position in (001). The stability of impurities in oxygen-rich environments might be of fundamental interest when trying to understand the long-term properties of mixed materials. Oxygen adsorption on clean and impurity containing (both on the topmost and deeper layers) surfaces is reported in Figure 7. As expected, metallic systems (RuO_2 and IrO_2) are avid to adsorb oxygen, while Sn and Ti are not prone to react with it. As O adsorption reduces the surface energy of very open surfaces, such as (001)-like, nanocrystal growth in oxygen-rich environments affects the equilibrium (Wulff) nanocrystal structure, and open surfaces are more likely to be present. In the presence of impurities, the oxygen adsorption characteristics are kept for systems where impurities are in the bulk, and reverted when they are on the surface.

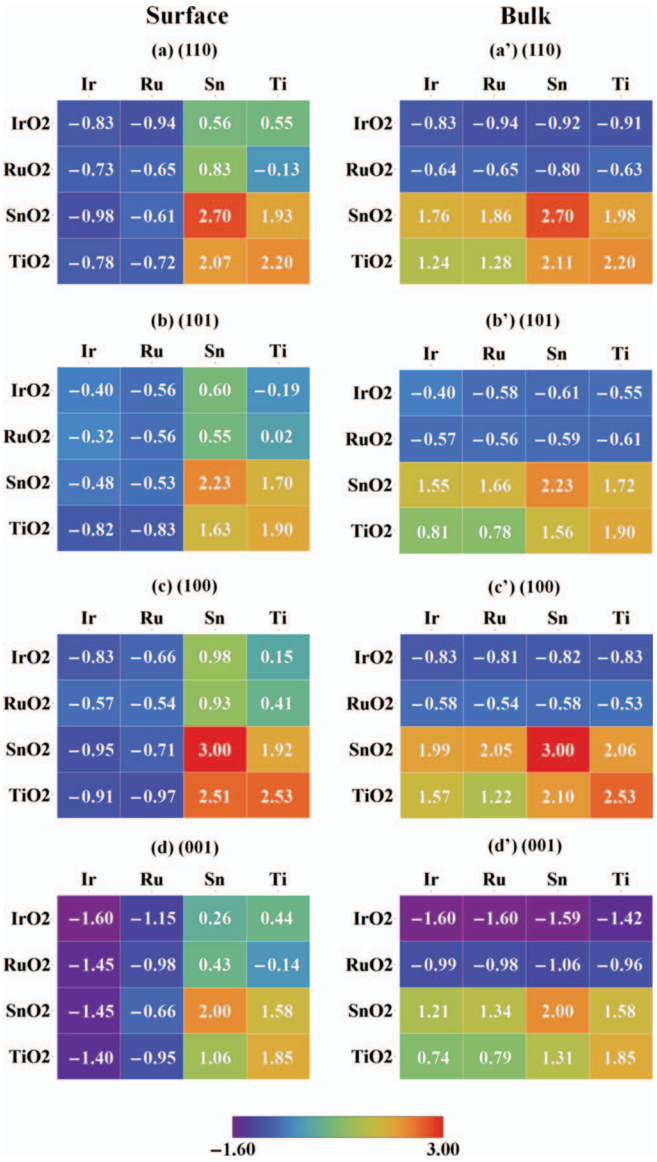

FIG. 7. Oxygen adsorption energy, $E_{seg}(O)$ in eV, for the systems with the impurities on the surface (left column) or in the bulk (right column). Cold colors indicate exothermic processes, while warm ones stand for endothermic processes.

Since these rutile materials are known to show very different properties if oxygen is present, we have calculated the corresponding segregation energies induced by the presence of atomic oxygen adsorbed on the lattice, $E_{seg}(O)$:

$$E_{seg}(O) = \min\left\{E_{O-M_gM_hO_2}(M_g^s),\, E_{M_gM_hO_2}(M_g^s) + \frac{1}{2}O_2\right\} - \min\left\{E_{O-M_gM_hO_2}(M_g^b),\, E_{M_gM_hO_2}(M_g^b) + \frac{1}{2}O_2\right\}.$$

Figure 6 shows the results for $E_{seg}(O)$. As expected, several segregation energies are a strong function of the amount of oxygen present (Sn, Ti), while others are less sensitive (Ru, Ir).

Again, we can describe our data for the different materials. For IrO_2, Ru and Ti do not show a marked preference, while Sn is definitely stable inside the bulk. This happens for all the facets considered and thus it is at odds with the results reported when no oxygen is available, see Figure 6. In the case of RuO_2, all the impurities tend significantly to stay in the bulk, Sn would be the most stable on the surfaces followed by Ti and Ir, in particular, for the (110) facet. However, the segregation values are much smaller compared to the non-oxygen covered surface. On the contrary, in both SnO_2 and TiO_2, Ru strongly moves to the top, followed by Ir and, to a lesser extent, Ti (for SnO_2), or Sn (in the case of TiO_2). In any case, the ability of Ru and Ir to reach higher oxidation states is behind the properties shown.

When comparing to available experiments, Ir is strongly segregated in SnO_2 in 30%–70% molar mixtures and 300 °C–500 °C both by cyclic voltammetry and Auger electron microscopy. Indeed with a 10% Ir in the bulk, the surface was found to be saturated with the precious metal.[75] The calculated values correspond to the large contribution of the interaction with water moieties, as then the oxygen-induced segregations range from −0.50 to −1.18 eV, while positive $E_{seg}(O)$ were obtained for the vacuum system.

In $Ir_xTi_{1-x}O_2$, cracks are found to be richer in Ir,[71] which agrees with the calculations for open surfaces that the Ir segregation is more energy favoured, see Figure 6.

As in the previous case, a second interpretation can be obtained from the data above if we focus on the different planes. Both for IrO_2 and RuO_2, oxygen-induced segregation is favored for the (110) plane, while the impurities are more stable in the bulk than on the (101) plane. This can be traced back to the structure of these two facets (see Figure 1), where it is clear that the density of M_{cus} positions is larger for the (101), and thus, both relaxation upon oxygen adsorption and oxygen-oxygen lateral interactions are more important. As for

SnO_2, both facets are characterized by segregation, (101) having larger values. Finally, the same behavior can be observed for TiO_2, but with smaller energy differences between the two terminations.

With respect to the effect of impurities in oxygen-rich environments on the structure of the nanocrystal, our results show that they would stabilize open surfaces with high concentrations of active impurities.

F. Binary mixtures: Overlayers

A final aspect regarding the interaction of different metal-oxides relies on the ability of these materials to form ordered overlayers, grown epitaxially on another rutile-like structure. Such systems are present in the commercial catalyst for HCl oxidation,[9–15,18,19] and have been investigated in other studies.[76] The schematic representation of the models employed to analyze the adhesion of one or two layers of the guest rutile on the host following the parameters of the host (epitaxial growth) are presented in Figure 8. The synthetic techniques based on the formation of core/shell particles also rely on adhesion properties.[36] Adhesion controls the possibility for bidimensional or tridimensional growth (wetting or dewetting) and relates the surface energy of the interface, γ, to that of the native surface, γ_0, as follows:

$$\gamma/\gamma_0 = (\gamma_{int} - \gamma_h)/\gamma_0 = 1 + E_{adh}/(A * \gamma_0), \qquad (5)$$

where γ_{int} is the interface energy, γ_h is the surface energy of the oxide support and E_{adh} is the total binding energy.

In Figure 9, the adhesion energy is shown, calculated as

$$E_{adh} = (E_{M_gM_hO_2}(L) - E_{M_gO_2}(N) - E_{M_hO_2}(L-N))/A, \qquad (6)$$

where $E_{M_gM_hO_2}(L)$ is the total energy of the composite structure containing N layers of M_hO_2 and $(L-N)$ layers of M_gO_2. The $E_{M_gO_2}(N)$ and $E_{M_hO_2}(L-N)$ are the corresponding energies of the guest and the host calculated independently, and A is the area of the exposed facet.

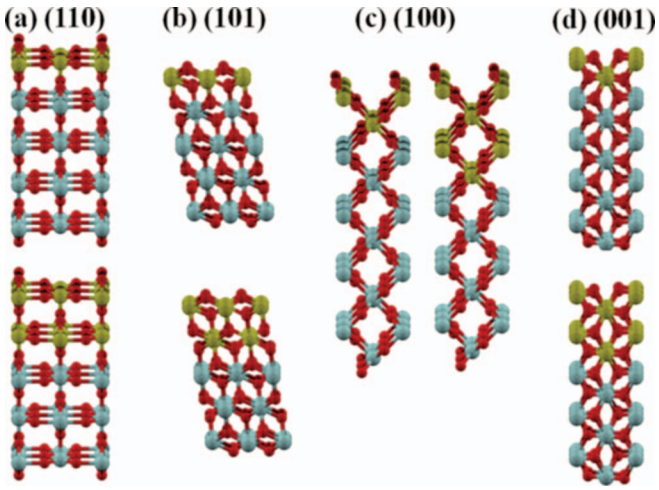

FIG. 8. Schematic representation of the models with one or two layers of the guest on the host rutile for all the facets investigated. Same color code as in Figure 5.

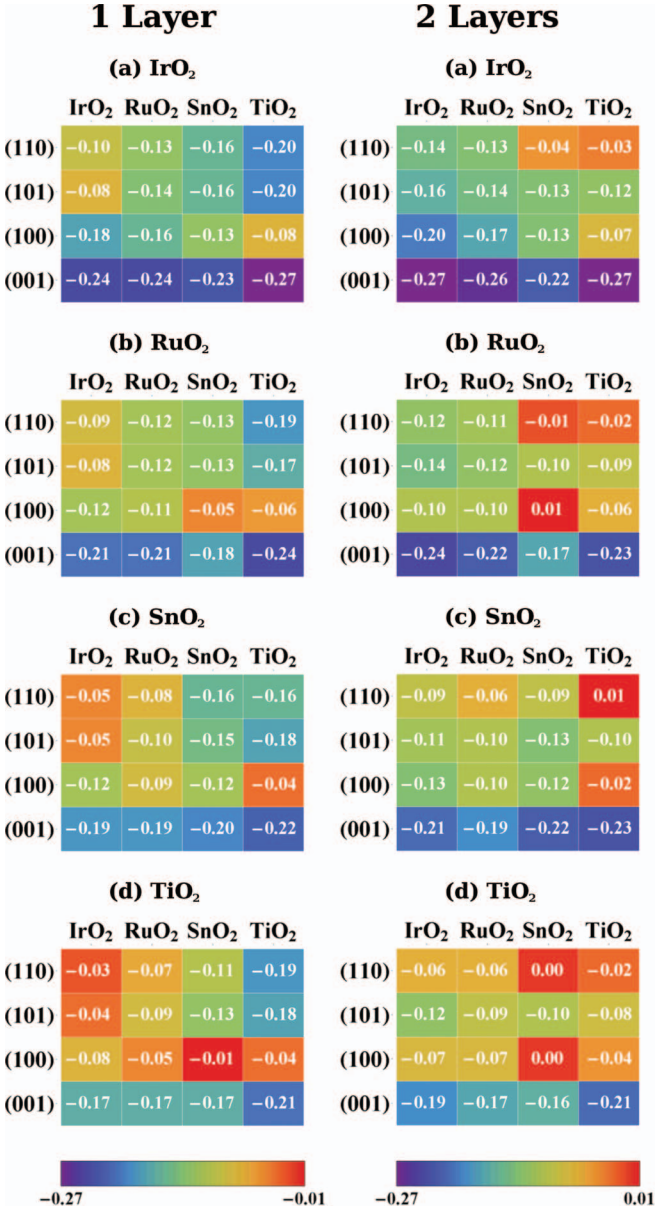

FIG. 9. Adhesion energy in eV/Å^2 for the rutile pairs, with either one (left) or two (right) layers of the guest rutile on the host. The models employed are those in Figure 8.

For one layer adhesion, the energies are exothermic in all cases, which is indicative of the formation of the bond at the interface in spite of the mismatch between guest and host structures. For IrO_2, epitaxy for all surfaces on RuO_2 and lesser wetting for SnO_2 and TiO_2 are expected. RuO_2 would easily form layers on IrO_2 and more stressed overlayers are expected again for SnO_2 and TiO_2. For RuO_2 on TiO_2, it has been found experimentally[38] that epitaxy is more likely for small structures. This agrees with the calculations which show a large reduction from -0.19 eV/Å^2 to -0.02 eV/Å^2 in the adhesion of 1 and 2 monolayers of the guest on the host. In contrast, SnO_2 coatings shall be more resistant on IrO_2 than for RuO_2, and less likely on TiO_2. This poses some stability issues to the core/shell structures described in Ref. 36. Finally, TiO_2 grows epitaxially on all the other surfaces with the exception of SnO_2. From the comparison in Figure 9, the results

described above seem to be rather independent of the number of layers.

IV. CONCLUSIONS

We have studied the properties of different rutile mixtures in order to describe the solubility, segregation, oxygen-induced segregation, and epitaxial growth for a set of metals oxides that form rutile structures: RuO_2, TiO_2, SnO_2, and IrO_2. We have provided a full database that can be useful in the analysis of the solubility of impurities of one of these materials in the rest of the investigated rutiles. As Wulff structures are quite similar, the presence of low-concentration impurities of any of the other metals would not affect the nanocrystals. The main deviation could take place for TiO_2 as the corresponding nanocrystal is the most different to the others. As for the segregation process, TiO_2 is shown to have the lowest surface energy and thus it would tend to stay on the surface forming shell structures. Solubility is best for the two transition metal atoms, Ru and Ir, that are closer neighbors in the periodic table. In addition, segregation can make surface stoichiometries possible, although the bulk solubility is not energetically favored.

Oxygen-induced segregation is enhanced for Ru and Ir oxides, as they show a much larger affinity for oxygen than either TiO_2 or SnO_2. When acting as hosts, both TiO_2 and SnO_2 behave as semiconductors, while the presence of Ru and Ir increases the number of states in the band. Epitaxial growth is relatively easy for these compounds as they share the same chemical structures and very little differences in the cell parameters. The detailed comparison with experimental data presented, shows the high degree of agreement and thus we are confident that the present database can serve as a guideline for experimentalists.

ACKNOWLEDGMENTS

We are thankful to Bayer Materials Science (BMS) and MCINN for support through project CTQ2012-33826/BQU. We thank BSC-RES for generously providing computational resources.

[1]V. E. Henrich and P. A. Cox, *The Surface Science of Metal Oxides* (Cambridge University Press, Cambridge, 1994).
[2]A. Fujishima and K. Honda, Nature (London) **238**, 37 (1972).
[3]J. Ryan, A. Berry, M. Anderson, J. Long, R. Stroud, V. Cepak, V. Browning, D. Rolison, and C. Merzbacher, Nature (London) **406**, 169 (2000).
[4]S. Trasatti, Electrochim. Acta **36**, 225 (1991).
[5]M. Grätzel, Nature (London) **414**, 338 (2001).
[6]A. Kubacka, M. Fernandez-Garcia, and G. Colon, Chem. Rev. **112**, 1555 (2012).
[7]H. Over, Chem. Rev. **112**, 3356 (2012).
[8]C.-C. Hu, K.-H. Chang, M.-C. Lin, and Y.-T. Wu, Nano Lett. **6**, 2690 (2006).
[9]T. Hibi, H. Nishida, and H. Abekawa, U.S. patent 5,871,707 (16 February 1999).
[10]T. Hibi, H. Abekawa, K. Seki, T. Suzuki, T. Suzuta, K. Iwanaga, and T. Oizumi, European patent EP936184 (1999).
[11]T. Hibi, T. Okuhara, K. Seki, H. Abekawa, and H. Hamamatsu, WO200110550-A1 (2001).
[12]K. Iwanaga, K. Seki, T. Hibi, K. Issoh, T. Suzuta, M. Nakada, Y. Mori, and T. Abe, Sumitomo Kagaku **2004**, 1.
[13]A. Wolf, L. Mleczko, O. F. Schlüter, and S. Schubert, European patent EP2026905 (25 February 2009).
[14]A. Wolf, J. Kintrup, O. F. Schlüter, and L. Mleczko, European patent EP2027062 (25 February 2009).
[15]A. Wolf, L. Mleczko, S. Schubert, and O. F. Schlüter, European patent EP2027063 (25 February 2009).
[16]S. Trasatti, Electrochim. Acta **45**, 2377 (2000).
[17]N. López, J. Gomez-Segura, R. P. Marin, and J. Perez-Ramirez, J. Catal. **255**, 29 (2008).
[18]K. Seki, Catal. Surv. Asia **14**, 168 (2010).
[19]D. Teschner, R. Farra, L. Yao, R. Schloegl, H. Soerijanto, R. Schomaecker, T. Schmidt, L. Szentmiklosi, A. P. Amrute, C. Mondelli, J. Perez-Ramirez, G. Novell-Leruth, and N. López, J. Catal. **285**, 273 (2012).
[20]D. Teschner, G. Novell-Leruth, R. Farra, A. Knop-Gericke, R. Schlogl, M. G.-H. L. Szentmiklosi, H. Soerijanto, R. Schomacker, J. Perez-Ramirez, and N. Lopez, Nat. Chem. **4**, 739 (2012).
[21]M. Haruta, Catal. Today **36**, 153 (1997).
[22]M. Valden, X. Lai, and D. Goodman, Science **281**, 1647 (1998).
[23]I. N. Remediakis, N. López, and J. K. Nørskov, Angew. Chem., Int. Ed. **44**, 1824 (2005).
[24]A. Fujishima and K. Honda, Kogyo Kagaku Zasshi **74**, 355 (1971).
[25]F. De Angelis, A. Tilocca, and A. Selloni, J. Am. Chem. Soc. **126**, 15024 (2004).
[26]M. Planells, L. Pelleja, J. N. Clifford, M. Pastore, F. De Angelis, N. López, S. R. Marder, and E. Palomares, Energy Environ. Sci. **4**, 1820 (2011).
[27]V. Makinen, K. Honkala, and H. Hakkinen, J. Phys. Chem. C **115**, 9250 (2011).
[28]M. García-Mota, A. Vojvodic, H. Metiu, I. C. Man, H. Su, J. Rossmeisl, and J. K. Nørskov, Chem. Cat. Chem. **3**, 1607 (2011).
[29]N. Barsan, D. Koziej, and U. Weimar, Sens. Actuators B **121**, 18 (2007).
[30]N. López, J. D. Prades, F. Hernandez-Ramirez, J. R. Morante, J. Pan, and S. Mathur, Phys. Chem. Chem. Phys. **12**, 2401 (2010).
[31]E. M. Fernandez, P. G. Moses, A. Toftelund, H. A. Hansen, J. I. Martinez, F. Abild-Pedersen, J. Kleis, B. Hinnemann, J. Rossmeisl, T. Bligaard, and J. K. Nørskov, Angew. Chem., Int. Ed. **47**, 4683 (2008).
[32]H. Deacon, UK patent 1403 (1868).
[33]J. Rossmeisl, Z. W. Wu, H. Zhu, G. J. Kroes, and J. K. Nørskov, J. Electroanal. Chem. **607**, 83 (2007).
[34]J. Cheng, H. Zhang, G. Chen, and Y. Zhang, Electrochim. Acta **54**, 6250 (2009).
[35]Y. Takasu, W. Sugimoto, Y. Nishiki, and S. Nakamatsu, J. Appl. Electrochem. **40**, 1789 (2010).
[36]L. Trotochaud and S. W. Boettcher, Chem. Mater. **23**, 4920 (2011).
[37]Y. Lee, H.-Y. Shin, S. H. Chun, J. Lee, W. J. Park, J. M. Baik, S. Yoon, and M. H. Kim, J. Phys. Chem. C **116**, 16300 (2012).
[38]G. Xiang, X. Shi, Y. Wu, J. Zhuang, and X. Wang, Sci. Rep. **2**, 801 (2012).
[39]J. I. Martinez, H. A. Hansen, J. Rossmeisl, and J. K. Nørskov, Phys. Rev. B **79**, 045120 (2009).
[40]B. Hammer, L. B. Hansen, and J. K. Nørskov, Phys. Rev. B **59**, 7413 (1999).
[41]C. Di Valentin, G. Pacchioni, and A. Selloni, J. Phys. Chem. C **113**, 20543 (2009).
[42]P. M. Kowalski, M. F. Camellone, N. N. Nair, B. Meyer, and D. Marx, Phys. Rev. Lett. **105**, 146405 (2010).
[43]A. V. Ruban, H. L. Skriver, and J. K. Nørskov, Phys. Rev. B **59**, 15990 (1999).
[44]A. U. Nilekar, A. V. Ruban, and M. Mavrikakis, Surf. Sci. **603**, 91 (2009).
[45]N. López and C. Vargas-Fuentes, Chem. Commun. (Cambridge) **48**, 1379 (2012).
[46]G. Kresse and J. Hafner, Phys. Rev. B **47**, 558 (1993).
[47]G. Kresse and J. M. Furthmüller, Phys. Rev. B **54**, 11169 (1996).
[48]G. Kresse and D. Joubert, Phys. Rev. B **59**, 1758 (1999).
[49]H. J. Monkhorst and J. D. Pack, Phys. Rev. B **13**, 5188 (1976).
[50]J. Carrasco, F. Illas, N. López, E. A. Kotomin, Y. F. Zhukovskii, R. A. Evarestov, Y. A. Mastrikov, S. Piskunov, and J. Maier, Phys. Rev. B **73**, 064106 (2006).
[51]K. R. Hahn, A. Tricoli, G. Santarossa, A. Vargas, and A. Baiker, Surf. Sci. **605**, 1476 (2011).
[52]N. Lopez, N. Almora-Barrios, G. Carchini, P. Blonski, L. Bellarosa, R. Garcia-Muelas, G. Novell-Leruth, and M. Garcia-Mota, Catal. Sci. Technol. **2**, 2405 (2012).
[53]H. Perron, C. Domain, J. Roques, R. Drot, E. Simoni, and H. Catalette, Theor. Chem. Acc. **117**, 565 (2007).

[54]G. Makov and M. C. Payne, Phys. Rev. B **51**, 4014 (1995).
[55]K. M. Glassford and J. R. Chelikowsky, Phys. Rev. B **46**, 1284 (1992).
[56]*CRC Handbook of Chemistry and Physics*, edited by D. R. Lide (CRC, New York, 2006).
[57]R. Wyckoff, *Crystal Structures* (Interscience, New York, 1964), Vol. 1.
[58]B. A. Hamad, Eur. Phys. J. B **70**, 163 (2009).
[59]G. Wulff, Z. Krystal. Min. **34**, 449 (1901).
[60]C. Sun, L. Liu, A. Selloni, G. Q. M. Lu, and S. C. Smith, J. Mater. Chem. **20**, 10319 (2010).
[61]P. Atkins and J. De Paula, *Physical Chemistry*, 8th ed. (Oxford University Press, Oxford, 2006).
[62]C. Mcdaniel and S. J. Schneider, J. Res. Natl. Bur. Stand., Sect. A **73A**, 213 (1969).
[63]C. Mcdaniel and S. J. Schneider, J. Res. Natl. Bur. Stand., Sect. A **71A**, 119 (1967).
[64]J. Gaudet, A. Tavares, S. Trasatti, and D. Guay, Chem. Mater. **17**, 1570 (2005).
[65]S. Mahanty, S. Roy, and S. Sen, J. Cryst. Growth **261**, 77 (2004).
[66]H. Naidu and A. Virkar, J. Am. Ceram. Soc. **81**, 2176 (1998).
[67]H. Uchiyama and H. Imai, Chem. Commun. (Cambridge) **2005**(48), 6014.
[68]F. Oropeza, B. Davies, R. Palgrave, and R. Egdell, Phys. Chem. Chem. Phys. **13**, 7882 (2011).
[69]J. P. Perdew and M. Levy, Phys. Rev. Lett. **51**, 1884 (1983).
[70]H. Tian, J. Ma, X. Huang, L. Xie, Z. Zhao, J. Zhou, P. Wu, J. Dai, Y. Hu, Z. Zhu, H. Wang, and H. Chen, Mater. Lett. **59**, 3059 (2005).
[71]L. da Silva, V. Alves, M. da Silva, S. Trasatti, and J. Boodts, Can. J. Chem. **75**, 1483 (1997).
[72]A. Marshall, B. Borresen, G. Hagen, M. Tsypkin, and R. Tunold, Electrochim. Acta **51**, 3161 (2006).
[73]K. Endo, Y. Katayama, T. Miura, and T. Kishi, J. Appl. Electrochem. **32**, 173 (2002).
[74]A. D. Battisti, G. Lodi, M. Cappadonia, G. Battaglin, and R. Kotz, J. Electrochem. Soc. **136**, 2596 (1989).
[75]C. D. Pauli and S. Trasatti, J. Electroanal. Chem. **396**, 161 (1995).
[76]A. Beltrán, J. Andrés, J. R. Sambrano, and E. Longo, J. Phys. Chem. A **112**, 8943 (2008).

PCCP

PAPER

View Article Online
View Journal | View Issue

Cite this: *Phys. Chem. Chem. Phys.*, 2014, **16**, 14750

Adsorption of small mono- and poly-alcohols on rutile TiO_2: a density functional theory study

Giuliano Carchini and Núria López*

Received 9th April 2014,
Accepted 23rd May 2014

DOI: 10.1039/c4cp01546k

www.rsc.org/pccp

We have studied by means of density functional theory including dispersion contributions, the interaction of small chain alcohols with up to four carbons and three hydroxyl groups on the TiO_2(110) rutile surface with different reduction degrees. Adsorption takes place through an acid–base interaction that can lead to both molecular and dissociated species. The latter are energetically preferred. Bulk reduction does not apport significant change neither in the structure nor in the adsorption energies, because the electrons are delocalized to a great extent. If vacancies are present at the surface these are the best adsorption sites for primary and secondary monoalcohols. Tertiary or poly-alcohols prefer the Ti_{cus} channels, but the reasons for the site preference are different. In the case of bulky alcohols, steric hindrance is the main adsorption-controlling factor, while templating effects of the basic (oxygen) sites on the surface are the key parameters to understand the adsorption of poly-alcohols. Vicinal polyalcohols behave even in a more complex way, for that they prefer the vacancy position only when dissociated, otherwise they stay in the Ti_{cus} channel. Our results warn about the use of small surrogates to investigate the chemistry of large alcohols as the adsorption patterns are not only quantitatively but also qualitatively wrong.

1. Introduction

Titanium dioxide (TiO_2) has been deeply investigated in recent years,[1–5] for its role as a support[6–9] but also as an active component[4,10–13] in photo(electro-)catalytic processes. Compared to adsorption on metals, the study of oxides is particularly challenging, because the surfaces possess different acid–base centers (metal and oxygens) and are characterized by different oxidation states.[14] In fact, oxygen atoms can be easily removed from rutile TiO_2, either by heating or by a reductive environment. Oxygen removal leaves two electrons behind which reduce two titanium ions, further affecting the chemical properties.[1,15] The degree of localization of such defect states has been subjected to a number of investigations, however it seems to be now clear that interconversion between different local configurations through polaron diffusion is averaging these structures.[16]

Alcohols are very important as probes of reactive sites on metal oxides[4,17–20] and models in the studies of photooxidation of organic contaminants.[21,22] More importantly, their chemical transformation is needed in the conversion of biomass derived chemicals. On rutile surfaces most of the alcohols adsorbs in a molecular form but a fraction dissociates *via* O–H bond cleavage. These so-formed alkoxy species can further dehydrate to alkenes, dehydrogenate to aldehydes or ketones,[23] condense to ethers, and/or rehydrogenate to alcohols.[24,25]

A large amount of experimental data has been gathered for the adsorption of alcohols on oxides,[4,18–20,25–30] and recently summarized by Campbell and Sellers.[31] Another important piece of work is represented by the review reported by Dohnálek *et al.*,[32] which focuses on the dynamical aspects of this system, such as the formation of the vacancies and intrinsic and extrinsic diffusion of the adsorbates on the surfaces, ranging from hydrogen and oxygen to alcohols and water. A deep experimental analysis on the reactivity related to water splitting and oxidation of organic contaminants, like phenols has also been reported. In general, small alcohols up to four C atoms are used to understand: the most likely adsorption site,[31] the molecular-dissociated equilibria,[29] the adsorption energies and reactivity[30] by means of Scanning Tunnelling Microscopy, STM, and Temperature Programmed Desorption, TPD.

Alcohols on titania have also been the target of an impressive number of theoretical studies.[33,34] In particular, there has been interest for the simplest alcohol available, methanol. Zhao *et al.*[35] have deeply analyzed a range of different configurations (up to eleven) of MeOH on titania, reporting the structure-dependent energies, the overlayer electronic structures, surface-adsorbate charge-transfer properties and surface dipole moments. Guo *et al.*[36] have investigated the whole dissociation reaction by experimental and theoretical means; they found the two states molecular and dissociated being almost isoenergetic (the latter slightly endothermic) and possessing a quite high reaction barrier.

Institute of Chemical Research of Catalonia (ICIQ), Av. Països Catalans 16, 43007 Tarragona, Spain. E-mail: nlopez@iciq.es; Tel: +34 977920237

Still, several questions remain open such as the degree of dissociation, the role of defects and the possibility to employ small alcohols as surrogates for large molecules and this could explain the apparent contradiction and discrepancies between the huge amount of information present nowadays in the literature.

To this end we have computed the adsorption of eleven alcohols and poly-alcohols up to four carbon atoms on the surface of rutile TiO_2. For a more realistic analysis, we also considered possible defects, *i.e.* oxygen vacancies which are common in oxides and might change the complete landscape for adsorption.

2. Computational details

We have employed first principles density functional theory through the VASP code, version 5.2.[37,38] We have chosen the RPBE[39] functional and we have represented the inner electrons by PAW pseudopotentials,[40] except the Ti *p* semi-core states which were treated explicitly. The energy cutoff for the plane-waves was set to 400 eV. TiO_2 presents a rutile structure for which the lowest energy surface corresponds to the (110) plane, indeed the crystallites contain *ca.* 84% of this facet.[41] We have built a seven trilayer slab, as in rutile systems this is the minimum $OTiO_2O$ packing unit along the [110] direction. We investigated different supercells (see below) but in all the cases each trilayer cointains 8 metals and 16 oxygen atoms and it is connected with the others in an AB motif. Finally a vacuum was added to the system to ensure that there was at least 13 Å between the adsorbate and the periodic image of the slab. To study adsorption, the two topmost layers were allowed to relax, while the others were kept fixed as representative of the bulk. To have a better description of these systems, we have also included the van der Waals interactions in our simulations. It is well known that standard DFT calculations cannot take into account these kinds of forces. Different strategies are possible to include this interaction; in this study we have applied the semiempirical correction vdW-D2 by Grimme.[42]

We have examined the stoichiometric (S) as well as the reduced surface for which two configurations were taken into account: (a) with the vacancy on the surface (V_s) *i.e.* created by removing one of the bridging oxygen atoms and (b) in the subsurface layers (V_{ss}) by removing a three-fold coordinated oxygen atom. Standard GGA calculations are usually able to reproduce many of the properties of the defect-free surface, as Ti is formerly charged 4+, so it presents empty d orbitals. Upon vacancy formation two Ti ions are reduced to Ti^{3+}, therefore a GGA + *U* approach is necessary to describe correctly the localized d orbitals. For the *U* parameter, a value of 4.2 eV gives accurate results.[43]

Finally, we have taken a sufficiently large simulation box which renders a coverage for the defects or adsorbates equivalent to 0.25 ML. For the S and V_{ss} this means a $p(4 \times 1)$ reconstruction; in fact, the configurations are the same for both cases. For V_s we have used a $p(2 \times 2)$ reconstruction, otherwise there would be two vacancies close to each other. Besides being an unrealistic model for this system, the charge excess would make it unstable. For the expansion of the planewaves we used *k*-point meshes of $3 \times 5 \times 1$ (S, V_{ss}) and $5 \times 3 \times 1$ (V_s).

3. Results and discussion

In order to discuss the adsorption we have taken into account only a TiO_2(110) surface, the most stable, interacting with a long series of alcohols with different numbers of hydroxyl groups and branching. We will first analyze the results for the stoichiometric surface and then increase the complexity by considering the role of vacancies. We have examined two kinds of adsorption: molecular and dissociative. For both S and V_{ss}, the adsorbate binds to the surface with the oxygen on one of the Ti_{cus} and the acid proton is directed towards one of the O_b (molecular – M) or bound to it (dissociative – D_1). In the poly-alcohols the two hydroxyls are practically equivalent, so only one of them is taken into account for D_1. Finally, we have studied a double dissociation where both of the OH bonds are broken and the hydrogens are connected to the closest O_b. As for the V_s, the most stable configuration is given by the alcohol's oxygen to fill the vacancy and for the poly-alcohols the second oxygen is bound on one of the Ti_{cus}. In this case, the two oxygens of the poly-alcohols are not equivalent, therefore we have considered four structures: molecular (M), dissociation of the OH bond with the

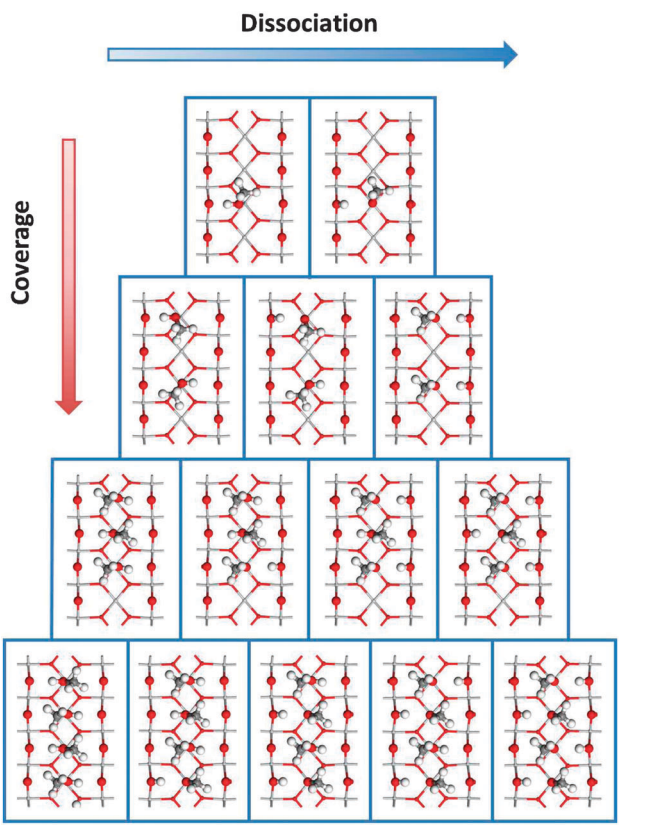

Fig. 1 Geometric configurations at different coverages of CH_3OH on the TiO_2(110).

O in the vacancy (D_1), dissociation of the other OH bond on the Ti_{cus} (D_2), and dissociation of both the hydroxyls (D_{12}).

3.1 Stoichiometric surface

3.1.1 Mono-alcohols. The adsorption of mono-alcohols occurs when the molecule interacts with the most basic site on the surface, the oxygen bridging atom O_b, and the most acid one, the undercoordinate cation Ti_{cus}. Experimentally, it is not clear if adsorbates on the surface are molecular or dissociated. While some STM evidence has been put forward for the molecular state, some claim that dissociative might be favored.[29,30,44,45] We have first considered the smallest possible alcohol to assess the problems related to dissociation. The calculated structures are presented in Fig. 1 and the computed energies are presented in Table 1.

At low coverage, $\theta = 0.25$ ML, methanol interacts through the acid–base ends with both the bridging oxygen and the acid Ti position. In doing so the methyl group lies along the [001] Ti_{cus} rows as less steric interaction is found along this direction. From this molecular state dissociation takes place exothermically by more than half an eV, with a low barrier, 0.10 eV. Therefore, at very low coverages on a clean surface the interaction is strong and leaves dissociated methoxy species with the organic fragment parallel to the Ti_{cus} rows. However, dissociation is much less effective at higher concentrations. Indeed the dissociation of two MeOH contributes only for 0.1 eV energy for each molecule, while when both adsorbates are dissociated, the system is isoenergetic with the full molecular state. This is due to the repulsive interaction between the different methyl groups, because methoxy species lays perpendicular to the Ti_{cus} rows [001]. Our results are in agreement with the energy difference obtained by Bates *et al.*[46,47] As many of the previous calculations in the literature deal with high coverages, either 0.5 ML or 1 ML, the structures in Fig. 1 for 0.5 ML are the ones predicted earlier. Increasing the coverage further does not significantly change the energy difference. However, the differential adsorption for the fourth molecule is far too weak to ensure that all sites are simultaneously occupied. Notice that the differential energy goes from −0.80 eV for the third molecule to only −0.22 eV, which can be easily surpassed by the gas-phase entropic contribution.

Table 1 Adsorption energy for different coverages of methanol and propanol and different dissociation degrees, E_{ads}/N_{mol}, in eV. When all the molecules are adsorbed in the same way (all M or D) we have also evaluated the differential energy, ΔE

Molecule	N_{tot}	N_M	N_D	E_{ads}/N_{mol}	ΔE
Methanol	1	1	0	−0.83	
		0	1	**−1.11**	
	2	2	0	−0.82	**−0.80**
		1	1	**−0.92**	
		0	2	−0.84	−0.56
	3	3	0	−0.62	−0.22
		2	1	−0.71	
		1	2	−0.70	
		0	3	−0.74	−0.55
	4	4	0	−0.50	**−0.15**
		3	1	−0.60	
		2	2	−0.60	
		1	3	**−0.63**	
		0	4	−0.57	−0.08
1-Propanol	1	1	0	−0.84	
		0	1	**−1.11**	
	2	2	0	−0.85	−0.86
		1	1	−0.98	
		0	2	**−1.02**	**−0.92**
	3	3	0	−0.67	**−0.31**
		2	1	−0.77	
		1	2	**−0.80**	
		0	3	−0.72	−0.14
	4	4	0	−0.21	1.17
		3	1	−0.34	
		2	2	−0.31	
		1	3	**−0.36**	
		0	4	−0.26	**1.13**

Table 2 Molecular, M, and dissociative, D_1, adsorption energies, E_{ads} in eV, for mono-alcohols on TiO_2 (S and V_{ss}), along with important averaged distances, in Å

ROH	Surf	Ads	E_{ads}	$d_{Ti_{cus}-O}$	d_{O-H}	d_{O_b-H}
MeOH	S	M	−0.83	2.280	0.992	1.887
	S	D_1	−1.11	2.206	2.642	0.971
EtOH	S	M	−0.84	2.176	1.016	1.672
	S	D_1	−1.11	1.796	2.261	0.973
1-PrOH	S	M	−0.84	2.174	1.019	1.645
	S	D_1	−1.11	1.793	2.279	0.973
1-ButOH	S	M	−0.92	2.181	1.016	1.659
	S	D_1	−1.17	1.802	2.262	0.974
i-PrOH	S	M	−0.88	2.163	1.004	1.712
	S	D_1	−1.17	1.774	2.386	0.972
2-ButOH	S	M	−0.94	2.128	0.984	2.044
	S	D_1	−1.20	1.807	2.107	0.979
t-ButOH	S	M	−0.83	2.165	1.007	1.675
	S	D_1	−1.20	1.774	2.289	0.974
MeOH	V_{ss}	M	−0.83	2.250	0.995	1.858
	V_{ss}	D_1	−1.04	1.811	2.533	0.975
EtOH	V_{ss}	M	−0.85	2.219	0.999	1.808
	V_{ss}	D_1	−1.06	1.805	2.349	0.975
1-PrOH	V_{ss}	M	−0.84	2.232	1.001	1.777
	V_{ss}	D_1	−1.09	1.809	2.387	0.974
1-ButOH	V_{ss}	M	−0.91	2.246	0.997	1.840
	V_{ss}	D_1	−1.12	1.809	2.361	0.975
i-PrOH	V_{ss}	M	−0.87	2.153	1.003	1.748
	V_{ss}	D_1	−1.11	1.781	2.472	0.973
2-ButOH	V_{ss}	M	−0.85	2.115	0.993	1.874
	V_{ss}	D_1	−1.08	1.795	2.095	0.985
t-ButOH	V_{ss}	M	−0.76	2.160	1.005	1.711
	V_{ss}	D_1	−1.13	1.778	2.357	0.974

Therefore, our calculations set a maximum coverage around 0.75 ML in excellent agreement with the experiments by Li *et al.*[28] who reported a value of 0.77 ML for primary alcohols and 0.44 ML for the secondary and the tertiary.

When we compare different monoalcohols we observe the following: all molecular states at low coverage show a relatively constant value for adsorption between −0.83 and −0.92 eV. The typical distances between the alcohol and the oxygen bridge position are between 1.6 and 1.9 Å, see Table 2. If we increase the complexity of the chain we have a −0.83 eV for *t*-ButOH followed by i-PrOH and 2-ButOH up to −0.94 eV.

Dissociation can then take place from the molecular state forming the structures shown in Fig. 2. The proton is stripped by the O_b forming a hydroxyl group with a typical O–H distance of 0.974 Å, while the alkoxy is sitting at the cationic site with average values of 1.850 Å. As for the adsorption, D_1 states are almost isoenergetic, around −1.15 eV, see Table 2. This means that the adsorption is no longer affected by the characteristics of the chain. This is due to the proton transfer, which allows the chain to move away from the surface, see Fig. 2. In fact, the

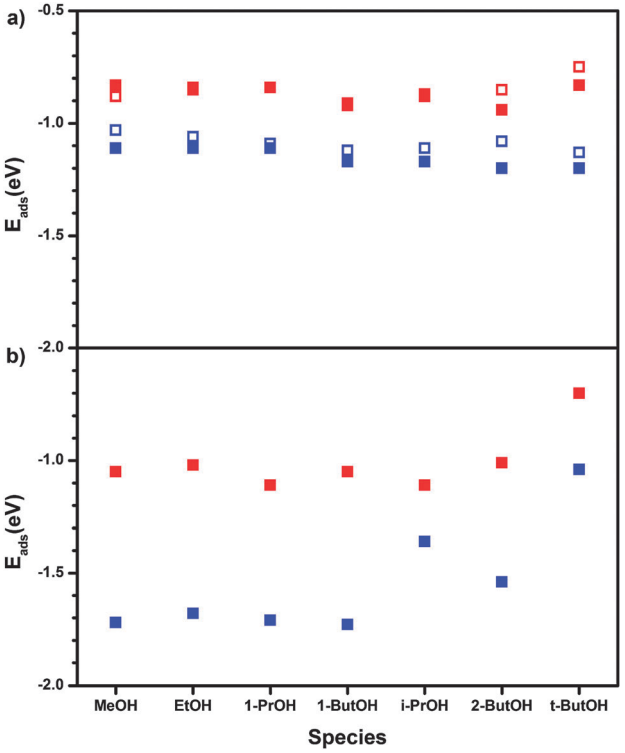

Fig. 3 Adsorption energies (in eV) of mono-alcohols adsorbed on TiO_2. (a) S (solid) and V_{ss} (empty) and (b) V_s. Red stands for M and blue for D_1.

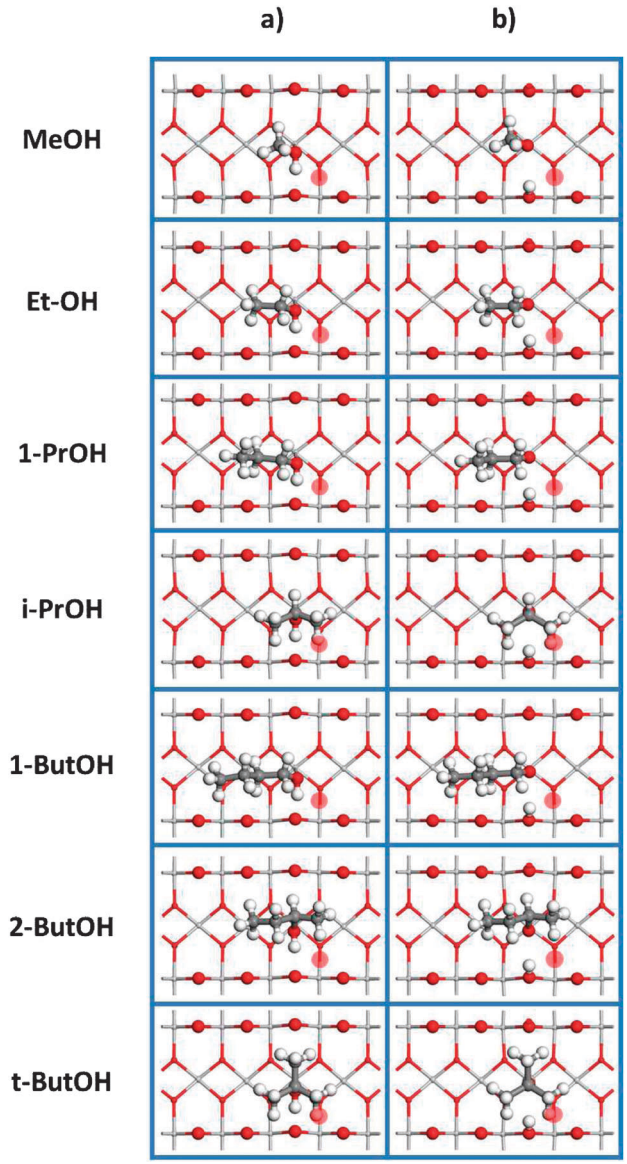

Fig. 2 Top view of the structures of the mono-alcohols adsorbed on TiO_2 S and V_{ss}, (a) M and (b) D_1. The faded red circle represents the position of the vacancy in the second layer in V_{ss}.

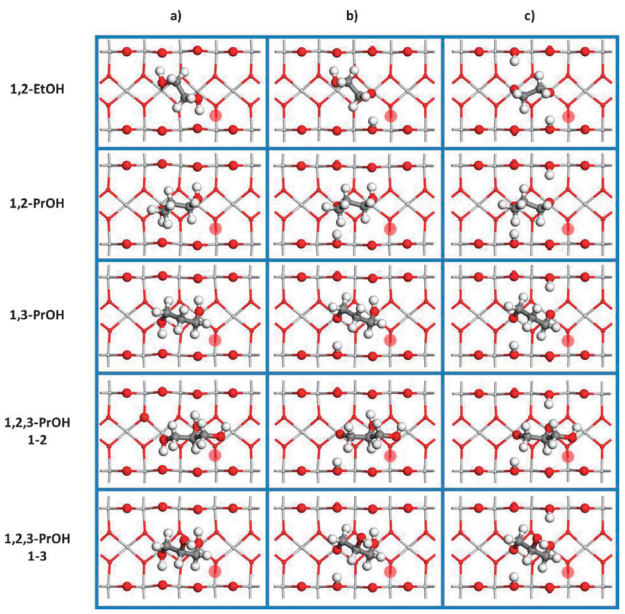

Fig. 4 Top view of the structures of the poly-alcohols adsorbed on TiO_2 S and V_{ss}, (a) M, (b) D_1 and (c) D_{12}. The faded red circle represents the position of the vacancy in the second layer in V_{ss}.

Table 3 Molecular, M, monodissociated, D_1, and didissociated D_{12} adsorption energies, E_{ads} in eV, for poly-alcohols on TiO_2 (S and V_{ss}), along with important averaged distances, d in Å

$R(OH)_2$	Surf	Ads	E_{ads}	$d_{Ti_{cus}-O}$	d_{O-H}	d_{O_b-H}
1,2-EtOH	S	M	−1.35	2.289	1.005	1.733
	S	D_1	−1.61	1.830, 2.341	2.311, 1.000	0.973, 1.744
	S	D_{12}	−1.92	1.835	2.319	0.977
1,2-PrOH	S	M	−1.51	2.241	0.996	1.890
	S	D_1	−1.80	1.824, 2.241	2.363, 0.996	0.976, 1.871
	S	D_{12}	−1.97	1.833	2.288	0.978
1,3-PrOH	S	M	−1.34	2.233	0.986	2.035
	S	D_1	−1.65	1.836, 2.231	2.306, 0.981	0.976, 2.127
	S	D_{12}	−1.82	1.834	2.284	0.977
1,2,3-PrOH-12	S	M	−1.38	2.294	0.993	1.919
	S	D_1	−1.68	1.831, 2.205	2.232, 0.989	0.976, 1.989
	S	D_{12}	−1.84	1.841	2.144	0.979
1,2,3-PrOH-13	S	M	−1.37	2.241	0.987	2.039
	S	D_1	−1.73	1.836, 2.257	2.302, 0.979	0.976, 2.264
	S	D_{12}	−1.86	1.836	2.297	0.977
1,2-EtOH	V_{ss}	M	−1.43	2.289	1.002	1.761
	V_{ss}	D_1	−1.61	1.835, 2.334	2.355, 0.998	0.974, 1.756
	V_{ss}	D_{12}	−1.84	1.835	2.332	0.978
1,2-PrOH	V_{ss}	M	−1.50	2.238	0.995	1.902
	V_{ss}	D_1	−1.76	1.836, 2.234	2.393, 0.994	0.975, 1.881
	V_{ss}	D_{12}	−1.87	1.837	2.287	0.977
1,3-PrOH	V_{ss}	M	−1.23	2.224	0.984	2.074
	V_{ss}	D_1	−1.53	1.837, 2.233	2.350, 0.980	0.976, 2.161
	V_{ss}	D_{12}	−1.77	1.835	2.291	0.977
1,2,3-PrOH-12	V_{ss}	M	−1.42	2.290	0.992	1.934
	V_{ss}	D_1	−1.62	1.845, 2.200	2.208, 0.988	0.977, 2.006
	V_{ss}	D_{12}	−1.77	1.844	2.109	0.981
1,2,3-PrOH-13	V_{ss}	M	−1.37	2.238	0.985	2.087
	V_{ss}	D_1	−1.71	1.840, 2.250	2.365, 0.978	0.976, 2.298
	V_{ss}	D_{12}	−1.84	1.837	2.308	0.977

Ti–O–C angle changes from an average value of 135° in the molecular state to 151° in the dissociated one. It is important to notice that out of the values found, the van der Waals contribution is about 0.4 eV and this demonstrates once again that this is fundamental to estimate adsorption energies correctly. The results are summarized in Fig. 3(a).

3.1.2 Poly-alcohols. The adsorption of poly-alcohols has been investigated through the analysis of ethanediol, propanediol (both 1,2 and 1,3), and 1,2,3-propanetriol (glycerol), see Fig. 4 for the structures. The adsorption of these molecules is a compromise between the acid–base interactions with the surface and the intramolecular hydrogen bonds present in the molecule. Moreover, the geometric disposition of the anions on the surface implies a templating effect that in some cases cannot be fitted simultaneously by the incoming alcohols, thus the number of variables and the topology of the surface make adsorption of poly-alcohols a structure-sensitive process.

The ethanediol molecule fits almost perfectly the channel of the TiO_2(110) surface and can interact simultaneously with two basic groups of the surface, see Fig. 4(a) with an O_b–H distance of around 1.733 Å. However, when doing so, the interaction with the surface Lewis acid sites is less effective and the mean distance is 2.289 Å, somehow elongated from that of ethanol, 2.176 Å. As a consequence, the adsorption energy for the molecular state of ethanediol is more exothermic than its ethanol counterpart but less than twice of methanol, see Tables 2 and 3. The 0.25 eV energy penalty (with respect to 2 MeOH) thus corresponds to both the lost intramolecular hydrogen bond and the constraints induced by the poly-alcohol backbone. The trends above are reproduced for any molecular adsorption of poly-alcohols on the surface. In any case, adsorption accounts for at most two hydrogen bonds on the surface even when the triol is considered.

As for dissociation, it can take place in two different steps. First, an O_bH group is left on the surface with the corresponding alkoxy bound to the acidic site, see Fig. 4(b). The typical distance for this hydroxyl group is 0.975 Å, while Ti–O is about 1.831 Å the second hydrogen of the alcohol which is left in the residual bonds to basic groups of the surface, d_{O_bH} = 1.999 Å. The dissociation adds an extra 0.3 eV to the energy and it is constant all along the series. This contribution can be understood as it relieves part of the stress induced by opposing forces of fitting the two hydrogen bonds, whilst keeping the backbone and

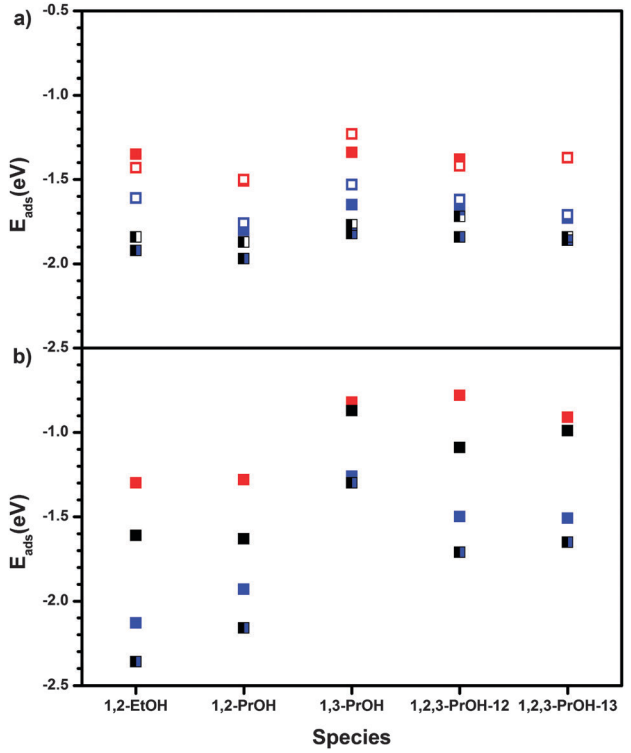

Fig. 5 Adsorption energies of poly-alcohols on TiO_2. (a) S (solid) and V_{ss} (empty) and (b) V_s. Red squares stand for M, blue for D_1 and blue-black (half black, half empty in V_{ss}) for D_{12}. Black squares in V_s represent the alternative mono-dissociation D_2.

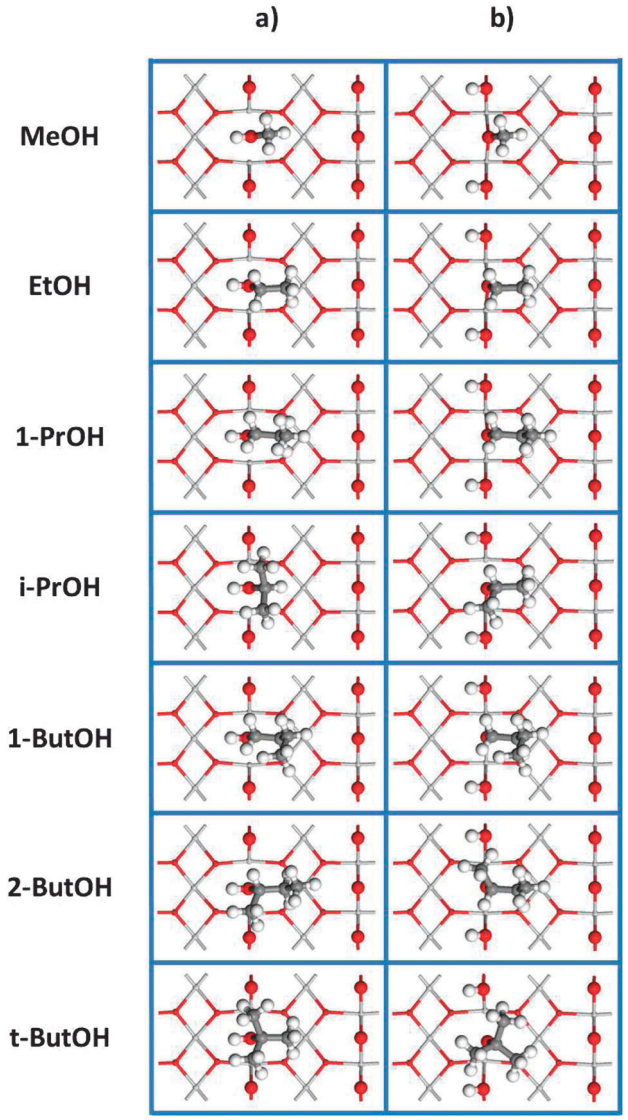

Fig. 6 Top view of the structures of the mono-alcohols adsorbed on TiO_2, (a) M and (b) D_1. One of the oxygens in bridge position is missing and replaced by the OH group.

intramolecular bonds. The second dissociation induces again an extra stabilization, only slightly smaller than the first. The final structure leads to two O_bH bonds on the surface of 0.978 Å, see Fig. 4. The distance between O–O groups fits well with the Ti-Ti pattern along the [001] direction, thus forming a hexagonal ring. In the 1,3-PrOH or for the triol, where the terminal groups are interacting with the surface, the backbone can be rotated to achieve the desired geometry. The O–Ti distance is around 1.836 Å as for the previous case.

1,2-Propanol is slightly more stable than its counterpart with three hydroxyls by 0.12. As a first hypothesis we thought the two hydroxyl to be independent, therefore we considered the D_1 energy as the plain sum of D_1 plus M mono-alcohol energies. We followed the same reasoning for D_{12} energy, seen as two times mono-alcohol D_1. It turns out that the two groups are affecting each other, and the resulting value is 0.15 to 0.25 eV lower per hydroxyl group than the hypothesized value. The main reason for this effect is that when the two groups bind on the surface at the same time, they have to arrange in an unfavorable *gauche* (and partially eclipsed) conformation. The energies are presented in Fig. 5(a) and listed in Table 3.

3.1.3 Effect of bulk reduction. TiO_2 is prone to contain a non-negligible amount of oxygen vacancies and this is particularly true for some of the experimental setups that require conductive samples. Reduction implies the formation of oxygen vacancies and/or Ti interstitials, only the first have been considered in the present study. Oxygen vacancies generate new states in the band gap and therefore can modify adsorption. We have represented this kind of defect by a subsurface vacancy, V_{ss}. In this model, the structures of the adsorbates are similar to those reported for the stoichiometric surface. The agreement is qualitatively so robust that the same schematic representation can be used in both cases, thus this vacancy is represented by a red faded dot in Fig. 2 and 4. The energies are reported in Table 2 for the mono-alcohols and in Table 3 for the poly-alcohols.

For the mono-alcohols, M energies range from −0.83 eV for MeOH to −0.91 eV for ButOH. Besides the the monodissociated D_1 show an almost constant value of −1.09 eV. This behavior can be completely extrapolated to poly-alcohols, *i.e.* all the M energies range about a constant value of 1.39 eV, while the adsorption patterns are maintained. It is clear that the V_{ss} systems are almost isoenergetic with the S ones. This is particularly evident from the graphic representations of the

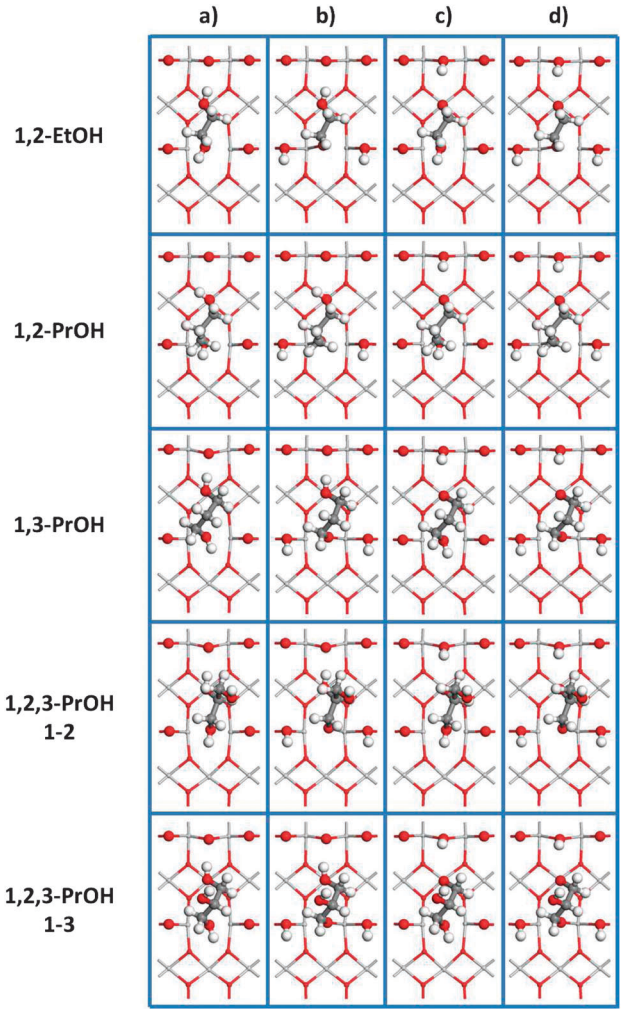

Fig. 7 Top view of the structures of the poly-alcohols adsorbed on TiO_2 V_s, (a) M, (b) D_1, (c) D_2 and (d) D_{12}. One of the oxygens in bridge position is missing and replaced by the OH group.

energy values in Fig. 3 and 5, where there is almost an overlapping between the different points. The reason behind this is the strong delocalization of the excess electrons, which in turn does not affect neither the structures, nor the energies.

3.2 Reduced surface: vacancies on the top layer

In this last section we discuss the reduced surface V_s. Typical surfaces exhibit bridge vacancies of about 5–10% of these sites, but recent results have demonstrated that vacancies can be extracted from subsurface positions by molecules like oxygen,[48,49] thus increasing the amount of these defects. The final structures can be found in Fig. 6 and 7, where again we have taken into consideration molecular and dissociated forms.

3.2.1 Mono-alcohols. We have examined the two configurations M and D_1, with the hydroxyl group filling the vacancy. The energies are presented in Fig. 3(b) and their values are listed in Table 4. In both cases, the alkylic chain is perpendicular to the line formed by the O_b. When compared to the regular surface, in M, the O group interacting with the Titanium atoms in the rows is placed at about 2.4 Å. In the latter,

Table 4 Molecular, M, and dissociative, D_1, adsorption energies, E_{ads} in eV, for mono-alcohols on TiO_2 V_s, along with important averaged distances, in Å

ROH	Ads	E_{ads}	$d_{Ti_{cus}-O}$	d_{O-H}	d_{O_b-H}
MeOH	M	−1.05	2.351	0.975	—
	D_1	−1.72	2.063	—	0.973
EtOH	M	−1.02	2.367	0.979	—
	D_1	−1.68	2.054	—	0.973
1-PrOH	M	−1.11	2.349	0.982	—
	D_1	−1.71	2.058	—	0.973
1-ButOH	M	−1.05	2.381	0.981	—
	D_1	−1.73	2.065	—	0.973
i-PrOH	M	−1.11	2.379	0.977	—
	D_1	−1.36	2.083	—	0.970
2-ButOH	M	−1.01	2.385	0.979	—
	D_1	−1.54	2.147	—	0.972
t-ButOH	M	−0.70	2.450	0.977	—
	D_1	−1.04	2.237	—	0.972

the OH bond is broken and the hydrogen is bound to one of the O_b. Due to sterical reasons, the formation of a hydrogen bond is not feasible. The overall energies of linear and branched alcohols are very close to the mean value of −1.06 eV. The noticeable exception is represented by *t*-ButOH which is very unstable compared to the others with its E_{ads} of −0.70 eV. D_1 behaves as the S case for the linear alcohols with an almost constant value of −1.71 eV. The bulky ones on the other hand are far less stable this time with E_{ads} ranging from −1.54 (2-ButOH) to −1.04 eV (*t*-ButOH). Clearly the oxygen filling the vacancy leaves the alkylic chain very close to the O_b and this causes a very strong sterical stress if branched.

3.2.2 Poly-alcohols. The two hydroxyls are not equivalent, thus we have to consider both separately. In fact, one of the OH is filling the vacancy, while the second is bound to one of the Ti_{cus}. The first is not participating in any hydrogen bond, even when it is dissociated. On the other hand, the hydrogen on the second OH is involved in a hydrogen bond with the closest O_b. As a result we end with four distinct configurations: M, D_1, D_{12} as the previous cases, plus dissociation of the other OH group (D_2).

We can divide the adsorption behaviour as follows. In the molecular case, 1,2-EtOH and 1,2-PrOH exhibit a similar adsorption energy and site pattern, while a different group is formed by 1,3-PrOH, 1,2,3-PrOH1,2 and 1,2,3-PrOH1,3. A similar splitting can be made for the dissociated, except for the 1,3-PrOH which turns out to be much less stable than its group members. Therefore, in the dissociated case, the number of OH groups remaining on the backbone controls the effectiveness of the bond. The results are reported in Table 5.

4. Discussion

The results above can clarify a group of indications in the literature that are summarized in Table 6. The energies are evaluated computing TPD data,[25,26,28] through the first order

Table 5 Molecular, M, monodissociated, D_1 and D_2, and didissociated D_{12} adsorption energies, E_{ads} in eV, for poly-alcohols on TiO_2 V_s, along with important averaged distances, d in Å

$R(OH)_2$	Ads	E_{ads}	$d_{Ti_{cus}-O}$	d_{O-H}	d_{O_b-H}
1,2-EtOH	M	−1.30	2.493	0.979	2.500
	D_1	−2.13	2.171	0.979	2.583, 0.973
	D_2	−1.61	1.886, 2.455	2.498, 0.977	0.975
	D_{12}	−2.36	1.851, 2.077	2.554	0.974
1,2-PrOH	M	−1.28	2.451	0.976	2.953
	D_1	−1.93	2.254	0.973	2.975, 0.973
	D_2	−1.63	1.884, 2.485	2.454, 0.977	0.975
	D_{12}	−2.16	1.850, 2.262	2.477	0.974
1,3-PrOH	M	−0.82	2.510	0.980	2.114
	D_1	−1.26	2.309	0.983	2.156, 0.972
	D_2	−0.87	1.866, 2.559	2.575, 0.974	0.973
	D_{12}	−1.30	1.843, 2.301	2.691	0.973
1,2,3-PrOH-12	M	−0.78	2.415	0.982	2.357
	D_1	−1.50	2.190	0.984	2.337, 0.973
	D_2	−1.09	1.893, 2.423	2.585, 0.977	0.973
	D_{12}	−1.71	1.857, 2.179	2.628	0.973
1,2,3-PrOH-13	M	−0.91	2.431	0.979	2.273
	D_1	−1.51	2.181	0.980	2.310, 0.973
	D_2	−0.99	1.872, 2.444	2.761, 0.978	0.973
	D_{12}	−1.65	1.857, 2.113	2.666	0.973

Redhead equation.† As the experiments are carried out with different quantities of the substrate, different temperature peaks are retrieved.

First of all, the dissociation degree of adsorbed alcohols has been a matter of discussion. TPD spectra indicate the presence of two main bands for the small linear alcohols.[31] However, the analysis of these spectra is difficult as TPD does not offer adsorption or configuration sites. In the interpretation of the TPD for MeOH, Li *et al.*[28] indicated three peaks: one at 500 K, another at 250–400 and multilayer adsorption below this range. Temptatively, these are described as recombinative desorption of alkoxy species with O_bH (500 K), and desorption from Ti^{4+} (400 K) and the molecular contribution (<200 K). In view of our calculations, the high energy peak corresponds to an alkoxy species bound at a vacancy site and thus it would be better represented by a O_bH + O_bMe, calculated adsorption energy of −1.11 eV. The medium temperature peak would correspond to molecular desorption from Ti_{cus} site, DFT estimation of −0.83 eV. In comparison, STM experiments[29] exposed at ethanol at 140 K at a coverage of 0.025 ML identified the molecules preferentially at the titanium sites with a little contribution from molecules in the bridge (vacancy positions, about 15%). However, they are mobile, and at higher temperatures they completely revert the population (the cus only contains 15%). Three kinds of species were identified: EtOH at the bridge positions, EtOH molecules and ethoxy fragments on Ti_{cus}. The authors conclude that there is no need for oxygen vacancies in order to dissociate the alcohols on the surface. In any case, we have shown that the most stable structures correspond to dissociated states and that different adsorption peaks do not differ in the degree of ionization but rather in the particular adsorption site. However, we have observed that the energy difference between the two states is a function of the degree of bulk reduction, and therefore the quality of the sample is crucial to control the degree of alcohol dehydrogenation. In another STM experiment, Leon *et al.*,[56] studied the adsorption of ethanol on titania. Upon annealing at room temperature, almost only methoxy groups remained attached to the surface preferentially on the Ti_{cus}, indicating the dissociated state to be more stable. Moreover, after further annealing, the oxidation state of the surface changes, generating a certain amount of vacancies. It has been found that under this condition the methoxy groups shift from the Ti_{cus} positions to fill them, lowering their energies.

In agreement with the experiments, we have also observed coverage limitations. Li *et al.*[28] have indicated that the maximum coverage for methanol is 0.77 ML. In our calculations, the differential adsorption energy for methanol changes from exothermic to endothermic when raising the coverage from 0.75 to 1 ML indicating that the amount of alcohol on the surface is in between. In addition, these authors set the maximum coverage for *t*-ButOH at 0.44 ML.[28] The configuration obtained in our calculations, Fig. 2, supports this limit as the *t*-But moiety partially blocks the neighboring sites upon adsorption.

A second important point regards the use of surrogates. In some cases, large molecules are not suited to the detailed information that can be obtained through some Surface Science techniques, or the reactivity is better understood when small molecules are taken as models. These kinds of generalizations

† We started from an initial guess evaluated with the well known Arrhenius formula, considering a typical exponential factor of 10^{-13} and employing T_{max} retrieved from the experiment. On a second step, we used this to calculate iteratively a more accurate value employing the first order Redhead equation,[50] until the energy difference between the two last iterations is smaller than 10^{-3} kJ mol^{-1}.

Table 6 Experimental adsorption energy, E_{ads}, in eV, for different alcohols, ROH. Additional information about the type of adsorption, $Type_{ads}$, position of the substrate and the Coverage, in ML, will be reported when available

ROH	$Type_{ads}$	E_{ads}	Coverage	Position
MeOH	M	−0.96[28]	0.22	Ti_{cus}
		−0.95[26]		
	D_1	−1.32[26]		
EtOH	M	−0.68, −0.48[25]	0.75, 3.75	
		−0.99[28]	0.20	Ti_{cus}
		−0.91[29]		V_s
		−0.81, −1.03[51]	0.80	Ti_{cus}, V_O
		−0.93, −0.80[18]	Saturation	Ti_{cus}, V_O
	D_1	−1.67, 1.64[18]	Saturation	Ti_{cus}, V_O
		−1.66[51]	0.80	V_O
		−1.10, −0.68[25]	0.75, 3.75	
		−1.64[29]		V_O
1-PrOH	M	−1.08[28]	0.19	Ti_{cus}
		−0.93, −0.94[18]	Saturation	Ti_{cus}, V_O
	D_1	−1.62, −1.57[18]	Saturation	Ti_{cus}, V_O
1-ButOH	M	−1.11[28]	0.17	Ti_{cus}
i-PrOH	M	−1.03[28]	0.23	Ti_{cus}
		−0.93, −0.86[52]	0.20	Ti_{cus}
		−0.92[53]	0.18	Ti_{cus}
		−1.03[51]	0.60	V_O
		−0.93, −0.94[18]	Saturation	Ti_{cus}, V_O
	D_1	−1.66[51]	0.60	V_O
		−1.47[18]	Saturation	
		−1.33[53]	0.18	V_O
		−0.96, −1.53[54]	0.90	
2-ButOH	M	−1.11[28]	0.17	Ti_{cus}
t-ButOH	M	−0.99[28]	0.27	Ti_{cus}
1,2-EtOH	M	−1.26[55]	0.25	Ti_{cus}
		−1.08[18]	Saturation	Ti_{cus}, V_O

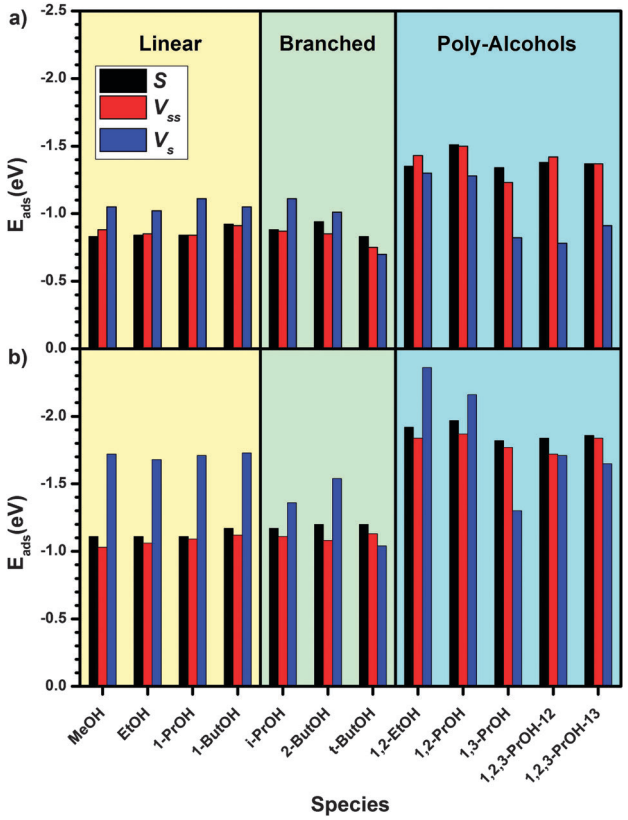

Fig. 8 Comparison between S, V_{ss} and V_s of (a) M and (b) D_1 (D_{12} for poly-alcohols) adsorption energies (E_{ads}) of every alcohol. The systems are displayed by increasing complexity.

are excessive when the molecules are large in comparison to the surface corrugation, then structure sensitivity patterns might occur thus limiting the applicability of surrogates. The particular topology of the TiO_2(110) surface shown here is one of the clearest examples. Our results indicate that primary and secondary alcohols are perfect to fill the surface vacancies healing vacancies and could somehow further confine the active sites along [001] channels. STM experiments for 2-ButOH have reported that although adsorption at vacancy positions seems to be dominant, occupancy of the Ti_{cus} occurs.[45] However, this is no longer true for tertiary ROH because steric hindrance greatly limits the accessibility to the vacancy positions.

Poly-alcohols behave in a more complex way. The gas-phase molecules present internal hydrogen bonds that stabilize some of the configurations. Upon adsorption these bonds compete with the most basic oxygens on the surface. TPD experiments for 1,2-ethanediol observe a main peak at 475 K with a saturation coverage of 0.43 ML.[55] This agrees with the desorption from a molecular state around −1.35 eV, see Fig. 3. This configuration corresponds to the sketch in Fig. 4(a) which clearly identifies that the molecule needs two Ti_{cus} positions, or equivalently the maximum coverage is 0.5 ML. STM experiments by Acharya *et al.*[30] have shown that 1,2-ethanediol and 1,2-propanediol adsorb on the Ti_{cus} positions. The authors propose a dynamic equilibrium between molecular and dissociated states on the surface. Upon diffusion the mobile diols can get anchored to oxygen vacancies and react. This agrees with our results, for these two compounds in the molecular state prefer adsorbing in the Ti_{cus} channel; on the other hand, in the dissociated state, the vacancy position becomes much more favourable compared to the former, see Fig. 8.

5. Conclusions

In this work we have studied the adsorption on rutile titania (110) facets of a series of alcohols of increasing complexity. For a complete analysis we have considered the substrates to adsorb molecularly and dissociatively, on models representing the stoichiometric material and diverse defective structures. Adsorption can occur in different positions on the surface.

Monoalcohols preferentially decorate oxygen vacancies, except for very bulky ones, *t*-ButOH; the same occurs for vicinal diols. Instead molecules with separated OH groups or with more functionalities (*i.e.* three OH groups) do no longer prefer surface defects. The present results warn against the use of molecular surrogates to analyze the chemistry of large, bulky, or poly-functionalized molecules. The estimated adsorption

energies and the degree of dissociation also clarify several issues in the literature. DFT shows that energy evaluations require the introduction of the van der Waals contributions in order to properly obtain results comparable to experiments. Although dissociated states seem to be more stable, the difference between molecular and dissociated adsorption is affected by the degree of bulk reduction.

Acknowledgements

This work has been supported through the "Biomass to Chemicals: Catalysis design for a sustainable chemical industry tendash Theoretical Simulations" (ERC–2010–StG–258406). The calculations were done in MareNostrum III at BSC-RES Barcelona Supercomputing Centre – Centro Nacional de Supercomputación (The Spanish National Supercomputing Center).

References

1 C. Sun, L.-M. Liu, A. Selloni, G. Q. M. Lu and S. C. Smith, *J. Mater. Chem.*, 2010, **20**, 10319–10334.
2 U. Diebold, *Surf. Sci. Rep.*, 2003, **48**, 53–229.
3 M. A. Barteau, *Chem. Rev.*, 1996, **96**, 1413–1430.
4 B. Li, J. Zhao, K. Onda, K. D. Jordan, J. Yang and H. Petek, *Science*, 2006, **311**, 1436–1440.
5 C. L. Pang, R. Lindsay and G. Thornton, *Chem. Rev.*, 2013, **113**, 3887–3948.
6 P. González-Navarrete, L. Gracia, M. Calatayud and J. Andrés, *J. Phys. Chem. C*, 2010, **114**, 6039–6046.
7 I. N. Remediakis, N. López and J. K. Nørskov, *Angew. Chem., Int. Ed.*, 2005, **44**, 1824–1826.
8 M. Valden, X. Lai and D. W. Goodman, *Science*, 1998, **281**, 1647–1650.
9 M. Haruta, *Catal. Today*, 1997, **36**, 153–166.
10 M. García-Mota, A. Vojvodic, H. Metiu, I. C. Man, H.-Y. Su, J. Rossmeisl and J. K. Nørskov, *ChemCatChem*, 2011, **3**, 1607–1611.
11 A. Fujishima and K. Honda, *Nature*, 1972, **238**, 37–38.
12 A. Fujishima and K. Honda, *Kogyo Kagaku Zasshi*, 1971, **74**, 355.
13 A. Migani, D. J. Mowbray, A. Iacomino, J. Zhao, H. Petek and A. Rubio, *J. Am. Chem. Soc.*, 2013, **135**, 11429–11432.
14 H. Metiu, S. Chrétien, Z. Hu, B. Li and X. Sun, *J. Phys. Chem. C*, 2012, **116**, 10439–10450.
15 E. Farfan-Arribas and R. J. Madix, *Surf. Sci.*, 2003, **544**, 241–260.
16 P. M. Kowalski, M. F. Camellone, N. N. Nair, B. Meyer and D. Marx, *Phys. Rev. Lett.*, 2010, **105**, 146405.
17 U. Martinez, J. O. Hansen, E. Lira, H. H. Kristoffersen, P. Huo, R. Bechstein, E. Lægsgaard, F. Besenbacher, B. Hammer and S. Wendt, *Phys. Rev. Lett.*, 2012, **109**, 155501.
18 E. Farfan-Arribas and R. J. Madix, *J. Phys. Chem. B*, 2002, **106**, 10680–10692.
19 K. Kim and M. Barteau, *J. Mol. Catal.*, 1990, **63**, 103–117.
20 K. Kim and M. Barteau, *Surf. Sci.*, 1989, **223**, 13–32.
21 M. Pirilä, R. Lenkkeri, W. Goldmann, K. Kordás, M. Huuhtanen and R. Keiski, *Top. Catal.*, 2013, **56**, 630–636.
22 P. Panagiotopoulou, E. E. Karamerou and D. I. Kondarides, *Catal. Today*, 2013, **209**, 91–98.
23 D. Brinkley and T. Engel, *Surf. Sci.*, 1998, **415**, L1001–L1006.
24 H. Bahruji, M. Bowker, C. Brookes, P. R. Davies and I. Wawata, *Appl. Catal., A*, 2013, **454**, 66–73.
25 L. Gamble, L. S. Jung and C. T. Campbell, *Surf. Sci.*, 1996, **348**, 1–16.
26 M. A. Henderson, S. Otero-Tapia and M. E. Castro, *Faraday Discuss.*, 1999, **114**, 313–329.
27 Z. Zhang, O. Bondarchuk, J. M. White, B. D. Kay and Z. Dohnálek, *J. Am. Chem. Soc.*, 2006, **128**, 4198–4199.
28 Z. Li, R. S. Smith, B. D. Kay and Z. Dohnálek, *J. Phys. Chem. C*, 2011, **115**, 22534–22539.
29 J. O. Hansen, P. Huo, U. Martinez, E. Lira, Y. Y. Wei, R. Streber, E. Lægsgaard, B. Hammer, S. Wendt and F. Besenbacher, *Phys. Rev. Lett.*, 2011, **107**, 136102.
30 D. P. Acharya, Y. Yoon, Z. Li, Z. Zhang, X. Lin, R. Mu, L. Chen, B. D. Kay, R. Rousseau and Z. Dohnálek, *ACS Nano*, 2013, **7**, 10414–10423.
31 C. T. Campbell and J. R. V. Sellers, *Chem. Rev.*, 2013, **113**, 4106–4135.
32 Z. Dohnálek, I. Lyubinetsky and R. Rousseau, *Prog. Surf. Sci.*, 2010, **85**, 161–205.
33 R. Sánchez de Armas, J. Oviedo, M. A. San Miguel and J. F. Sanz, *J. Phys. Chem. C*, 2007, **111**, 10023–10028.
34 J. Oviedo, R. Sánchez de Armas, M. n. San Miguel and J. F. Sanz, *J. Phys. Chem. C*, 2008, **112**, 17737–17740.
35 J. Zhao, J. Yang and H. Petek, *Phys. Rev. B: Condens. Matter Mater. Phys.*, 2009, **80**, 235416.
36 Q. Guo, C. Xu, Z. Ren, W. Yang, Z. Ma, D. Dai, H. Fan, T. K. Minton and X. Yang, *J. Am. Chem. Soc.*, 2012, **134**, 13366–13373.
37 G. Kresse and J. Furthmüller, *Phys. Rev. B: Condens. Matter Mater. Phys.*, 1996, **54**, 11169–11186.
38 G. Kresse and J. Hafner, *Phys. Rev. B: Condens. Matter Mater. Phys.*, 1993, **47**, 558–561.
39 B. Hammer, L. B. Hansen and J. K. Nørskov, *Phys. Rev. B: Condens. Matter Mater. Phys.*, 1999, **59**, 7413–7421.
40 G. Kresse and D. Joubert, *Phys. Rev. B: Condens. Matter Mater. Phys.*, 1999, **59**, 1758–1775.
41 G. Novell-Leruth, G. Carchini and N. López, *J. Chem. Phys.*, 2013, **138**, 194706.
42 S. Grimme, *J. Comput. Chem.*, 2006, **27**, 1787–1799.
43 B. J. Morgan and G. W. Watson, *Surf. Sci.*, 2007, **601**, 5034–5041.
44 C. Zhou, Z. Ren, S. Tan, Z. Ma, X. Mao, D. Dai, H. Fan, X. Yang, J. LaRue, R. Cooper, A. M. Wodtke, Z. Wang, Z. Li, B. Wang, J. Yang and J. Hou, *Chem. Sci.*, 2010, **1**, 575–580.
45 Z. Zhang, O. Bondarchuk, B. D. Kay, J. M. White and Z. Dohnálek, *J. Phys. Chem. C*, 2007, **111**, 3021–3027.
46 S. P. Bates, G. Kresse and M. Gillan, *Surf. Sci.*, 1998, **409**, 336–349.
47 S. P. Bates, M. J. Gillan and G. Kresse, *J. Phys. Chem. B*, 1998, **102**, 2017–2026.
48 M. Setvín, U. Aschauer, P. Scheiber, Y.-F. Li, W. Hou, M. Schmid, A. Selloni and U. Diebold, *Science*, 2013, **341**, 988–991.

49 N. López, J. D. Prades, F. Hernández-Ramírez, J. R. Morante, J. Pan and S. Mathur, *Phys. Chem. Chem. Phys.*, 2010, **12**, 2401–2406.
50 P. Redhead, *Vacuum*, 1962, **12**, 203–211.
51 M. D. Kershis and M. G. White, *Phys. Chem. Chem. Phys.*, 2013, **15**, 17976–17982.
52 O. Bondarchuk, Y. K. Kim, J. M. White, J. Kim, B. D. Kay and Z. Dohnálek, *J. Phys. Chem. C*, 2007, **111**, 11059–11067.
53 D. Brinkley and T. Engel, *J. Phys. Chem. B*, 1998, **102**, 7596–7605.
54 Y. K. Kim, B. D. Kay, J. M. White and Z. Dohnálek, *J. Phys. Chem. C*, 2007, **111**, 18236–18242.
55 Z. Li, B. D. Kay and Z. Dohnálek, *Phys. Chem. Chem. Phys.*, 2013, **15**, 12180–12186.
56 C. P. Leon, K. Sagisaka, D. Fujita and L. Han, *RSC Adv.*, 2014, **4**, 8550–8557.

JCTC Journal of Chemical Theory and Computation
Article
pubs.acs.org/JCTC

Costless Derivation of Dispersion Coefficients for Metal Surfaces

Neyvis Almora-Barrios,[†] Giuliano Carchini,[†] Piotr Błoński,[†,‡] and Núria López*,[†]

[†]Institute of Chemical Research of Catalonia, ICIQ, Av. Països Catalans 16, E-43007 Tarragona, Spain
[‡]Institute of Nuclear Physics, Polish Academy of Sciences, ul. Radzikowskiego 152, PL-31-342 Krakow, Poland

Supporting Information

ABSTRACT: Many common density functional theory methods used in the study of adsorption on metals lack dispersion contributions. Formulations like the random phase approximations would mitigate this error, but they are computationally too expensive. Therefore, semiempiric treatments based on dispersion coefficients turn out to be a practical solution. However, the parameters derived for atoms and molecules are not easily transferable to solids. In the case of metals, they cause severe overbinding as screening is not properly taken into consideration. Alternative ways to determine these parameters for metal surfaces have been put forward, but they are complex and not very flexible when employed to address low-coordinated atoms or alloys. In this work, we present a self-consistent, fast, and costless tool to obtain the dispersion coefficients for metals and alloys for pristine and defective surfaces. Binding energies computed with these parameters are compared to both the experimental and theoretical values in the literature thus demonstrating the validity of our approach.

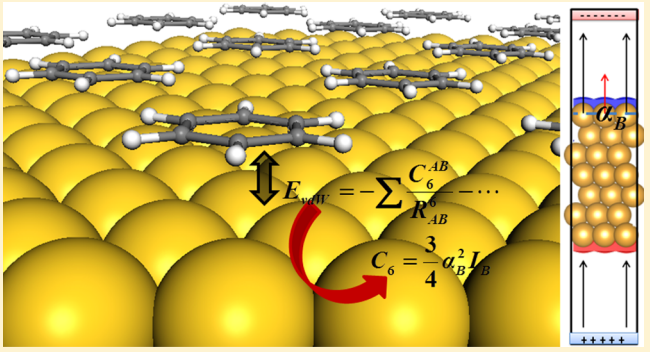

1. INTRODUCTION

Density functional theory (DFT) predicts many phenomena occurring on solid surfaces very successfully.[1] However, a serious shortcoming of the standard DFT based methods is that they do not account for van der Waals, vdW, interactions resulting from dynamical correlations between fluctuating charge distributions.[2] Thus, these calculations fail to reproduce the binding energies of the weakly interacting systems, e.g. organic molecules on metal surfaces.[3] In recent years, there has been a need to extend the applicability of the DFT-based methods to these new problems. We will discuss some of the main approaches that have been developed, but for more detailed discussion, we recommend refs 4−12.

The vdW interaction between an atom and a metal surface was understood to have a leading contribution of the type C_3/z^3 where z is the distance between the molecule and the surface.[13] The C_3 coefficients were then estimated from the polarizability of the molecule and the dielectric function of the surface derived from the Lifshitz formula.[14] This kind of approximation was used to estimate the contribution of these forces in the activation of methane on Ir(111).[15] However, the pair (molecule and surface) information contained in the C_3 parameter made it unpractical.

Alternatively, different functionals that include dispersion have been put forward. Lundqvist et al.[16−20] proposed a nonlocal correlation functional (vdW-DF) that accounts for dispersion interactions approximately. The results were found to depend on the particular combination between the exchange and the nonlocal correlation functionals (see, e.g., ref 21.). A formal rigorous alternative which includes the vdW energy seamlessly and accurately is offered by the random phase approximation (RPA),[22] combined with the adiabatic connection and fluctuation dissipation theorem (ACFDT)[23,24] as proposed by Kresse and Harl.[25−28] Unfortunately, it implies a heavy computational burden; hence it is more suitable for benchmarking than for extensive use, especially when studying reactivity of large molecules on metal surfaces.

On the other hand, the simplest correction is offered by the semiempirical contributions introduced by Grimme et al.[29] (DFT-D2). In this approach, the dispersion is calculated by pairwise interactions from the London formula[30] leading to a sum over C_6/R^6 terms. The C_6 parameters were tabulated for isolated atoms. Significantly, for the heavy atoms the same values were reported for a whole row of the periodic table. However, the DFT-D2 method with the coefficients derived from atomic properties leads to a substantial overbinding when applied to metals.[31] The natural evolution of the DFT-D2 method includes the next terms (C_8−C_{10}) in the expansion, DFT-D3.[32] In this approach there is a range of precalculated coefficients for various elements in different reference states. For instance, the C_6 coefficients are assigned to each pair of atoms taking into account the number of neighbors. Despite these improvements, the water−metal interaction is still largely overestimated.[33]

An alternative formulation, known as DFT-vdW[34] has been developed since by Tkatchenko−Scheffler (henceforth referred to as TS). In the TS method, the C_6 coefficients and radii are

Received: July 21, 2014
Published: September 29, 2014

   dx.doi.org/10.1021/ct5006467 | J. Chem. Theory Comput. 2014, 10, 5002−5009

determined nonempirically from the electron density, and effective atomic volumes are used to obtain environment dependency. However, it was not clear if the scaling of the coefficients with the volume would yield accurate results for more complex systems, such as metal surfaces.[35] A possible remedy, as Ruiz et al.[35] have pointed out recently, is to determine a metal surface C_6 coefficient that accounts for the collective response (screening) of the substrate electrons, by employing the Lifshitz–Zaremba–Kohn (LZK) theory[13,14] (DFT-vdW^{surf}). In this way the C_3- and C_6-based formulations can be mapped.[36] The method implies the use of frequency-dependent dielectric functions for transition metals from reflection electron energy-loss spectroscopy.[37] Therefore, the DFT-vdW^{surf} method to evaluate polarizabilities is not purely first principles.

The aim of this work is to elaborate an alternative for evaluating polarizabilities for atoms in both regular and defective metal surfaces and for unraveling the contribution from heterometallic bond formation in alloys only based on calculated data. From these data, we have derived the corresponding van der Waals coefficients. To test this approach, we present the results of benzene adsorption on a variety of metal surfaces, specifically on Pd, Pt, Cu, Ag, Au, and on bimetallic alloys and near-surface alloys (NSAs) containing Au. We have compared the experimental data to the results obtained with existing theoretical approaches by Grimme (DFT-D2 and DFT-D3), Tkatchenko and Scheffler (DFT-vdW^{surf}), and ours.

2. THEORETICAL BACKGROUND

In general, the interaction between two bodies A and B acting like isotropic oscillators is expressed in terms of dispersion coefficients, C_m:

$$E_{vdW}(R_{AB}) = -\frac{C_6}{R_{AB}^{\ 6}} - \frac{C_8}{R_{AB}^{\ 8}} - \dots \tag{1}$$

Since the interaction may be considered as taking place through a fluctuating electromagnetic field in each of the two bodies, the C_6 coefficient can be expressed as[38]

$$C_6 = \frac{3\hbar}{2\pi^2}\int_0^\infty d\omega \alpha_A(i\omega^I)\alpha_B(i\omega^I) \tag{2}$$

where $\alpha_A(i\omega^I)$ and $\alpha_B(i\omega^I)$ are the dynamic (frequency-dependent (ω), evaluated at imaginary frequencies) polarizabilities of the two subsystems. We follow the original procedure by London[30,37] who calculated the attraction between two atoms within second-order perturbation theory. London used the Unsöld approximation[39] to the second-order energy in which all the energy denominators can be replaced by some average value (the average excitation energies further approximated by the first ionization energies of the interacting subsystems). When acting on an alternating field of the effective frequency, these terms are described as follows:[30]

$$\alpha_A(i\omega^I) = \frac{\alpha_A(0)}{1 + (\omega^I/\omega_1)^2} \tag{3}$$

where ω_1 is the characteristic frequency and $\alpha_A(0)$ is the static polarizability. Having introduced this approximation in eq 2, the evaluation of the integral can be rewritten as

$$C_6 = \frac{3\hbar}{2}\alpha_A(0)\alpha_B(0)\frac{\omega_{1A}\omega_{1B}}{\omega_{1A} + \omega_{1B}} \tag{4}$$

Since the characteristic frequency multiplied by $\hbar$ is in all these cases near equal to the ionization energy I,[30] C_6 can be simplified to

$$C_6 = \frac{3}{2}\alpha_A(0)\alpha_B(0)\frac{I_A I_B}{I_A + I_B} \tag{5}$$

In the case of an ensemble of identical objects "B" eq 5 can be expressed as

$$C_6 = \frac{3}{4}\alpha_B(0)^2 I_B \tag{6}$$

and, thus the coefficient only depends on the static polarizability. For metals the surface static polarizability can be retrieved from the response of the dipole to the presence of an electric field as shown by Schneider and co.[40] The corresponding equation can be written:

$$\vec{\mu} = \sum_i^{surface} \vec{\mu}_i = \sum_i^{surface} \alpha_i(0)\vec{E} \tag{7}$$

where $\vec{\mu}$ is the total surface dipole moment that can be assigned to the individual atoms, $\vec{\mu}_i$. Further decomposition indicates that the individual dipoles (atom-in-surface model) depend on the atomic polarizabilities when applying an electric field $\vec{E}$, in our case in the direction perpendicular to the surface, see Figure 1. Note that the free electrons in the bulk of the metal

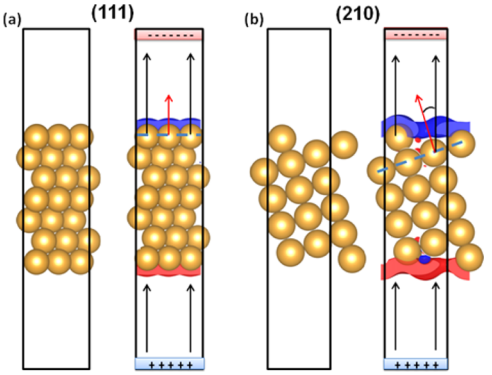

Figure 1. Side views of the surfaces of fcc metals and schematic representation of the method of imposing an electric field in surfaces where the electron spill is seen as electron density accumulation (blue) and depletion (red) on the surface: (111) the most densely packed surface (a) and (210) stepped surface (b).

show a zero frequency, i.e. do not contribute.[41] We consider that the main contribution to the bond to the surface would be due to the surface atoms, as dispersion forces show a $1/r^6$ dependence. The electric field can be introduced as a dipole sheet in the middle of the vacuum region, as proposed by Neugebauer and Scheffler[42] and the corresponding dipole can be obtained from the output of the DFT once the field is applied. The only limitation is that it should not be too strong to prevent spontaneous electron leakage from the surface and the metal-atoms rearrangement; its maximum values depend on the height of the supercell, as described below. The supercell dimensions used in this work allowed the use of electric fields up to (1 V Å^{-1}). Notice that only static polarizabilities and C_6 values corresponding to surface atoms can be obtained in this manner. The so-computed C_6 values are completely compatible

dx.doi.org/10.1021/ct5006467 | J. Chem. Theory Comput. 2014, 10, 5002−5009

with those derived from Grimme, as radii are very similar (see below) and the same damping function is employed.

The same methodology can be applied to different surface configurations like those presenting steps; see Figure 1b. In the particular case of a stepped surface, polarization of surface atoms is not as effective since the volume where electrons can polarize is not where the electric field drives them to. Thus, the angle formed between the electric field and surface normal needs to be taken into account. The total surface dipole can be decomposed considering that the atoms in low-index planes keep the polarizabilities obtained from the low-index surface calculations. Therefore, we have

$$\vec{\mu} = \sum_{i}^{\text{surface}} \vec{\mu}_i = \sum_{i}^{\text{surface}} \alpha_i(0)\vec{E}\hat{n} \tag{8}$$

where now $\hat{n}$ is the vector normal to the surface.

3. COMPUTATIONAL DETAILS

All calculations were based on density functional theory with periodic boundary conditions, using VASP code.[43−45] A basis set of plane waves, the generalized gradient approximation (GGA) and the Perdew−Burke−Ernzerhof (PBE) functional[46] were included. The interaction between valence and core electrons was described by the Projected Augmented Wave (PAW) method.[43] The number of plane waves was controlled by setting the cutoff energy to 400 eV. The metal surfaces were represented by different slab thickness, separated by 12 Å vacuum. In all cases, optimizations were performed for the two topmost layers where the rest were kept fixed to mimic the bulk. The corresponding k-point samplings were denser than 0.3 Å^{-1}.

An external electric field perpendicular to the slab was imposed using the method proposed by Neugebauer and Scheffler[42] as implemented in VASP.[47] The electric fields used were 0 to ±1 V Å^{-1} in four different steps of 0.25 V Å^{-1} size. The dipole moments were calculated by numerically integrating the charge density difference between a neutral slab and a slab with an applied electric field multiplied by the integration distance, following the procedure described by Schneider and co-workers.[40] The surface dipole can be written as

$$\vec{\mu} = qd\hat{n} \tag{9}$$

where q is the differential charge between the slab with and without electric field and d is the distance in angstroms. q is obtained by integration of the charge density assigned to the surface metal atom, from the midpoint between the surface, z_{1L}, and subsurface layer, z_{2L}, thus $(z_{1L} - z_{2L})/2$ to the point where the density difference is zero $z_{\Delta\rho=0}$:

$$q = \int_{z_{1L}-z_{2L}/2}^{z_{\Delta\rho=0}} \Delta\rho(z)\, \mathrm{d}z \tag{10}$$

and

$$d = z_{\text{total}}\left(z_{q=0} - \frac{z_{1L} - z_{2L}}{2}\right) \tag{11}$$

Tests of the convergence of the dipole moments with respect to the slab thickness were done (see in Supporting Information Table-S1). For the simplest surfaces, the variation of the dipole moment was then plotted against an applied electric field and the slope divided by the number of surface atoms corresponds to the polarizability, $\alpha(0)$. Then the C_6 coefficient was obtained by using the atomic ionization potentials I from the Handbook.[48] In each case, the radius, R_0, corresponds to half of the distance between two neighboring atoms in the relaxed bulk (see Table S-2). The obtained values are in line with those reported earlier in the literature.[35] The parameters for the molecules and the damping function were taken from those early reported by Grimme.[29]

4. RESULTS AND DISCUSSION

4.1. Polarizabilities and Dispersion Coefficients. The difference in electronic charge density between a neutral slab and one with the electric field imposed is showed in Figure 2.

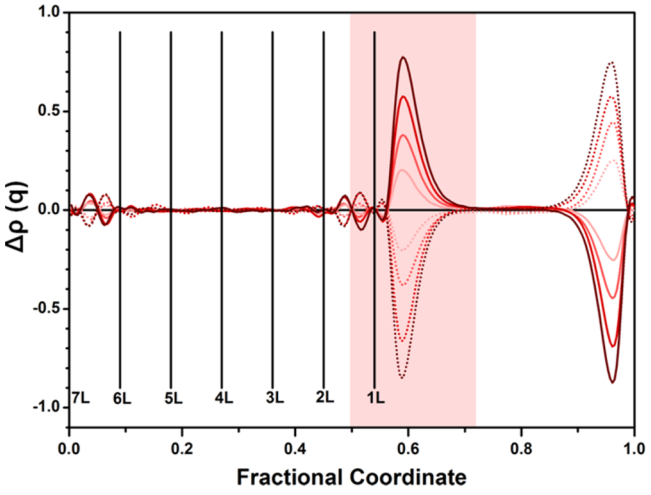

Figure 2. Plane-averaged electronic charge difference between a bare seven layer Au(111) slab calculated with and without external field. Vertical lines stand for the positions of the Au layers and the area of integration is in pink background.

The surface atoms are the only ones affected by the excess of the charge as it would be expected for a metal. They polarize in opposite sign on either side of the slab. We have then calculated the dipole using eq 9 for fcc (111) metal surfaces.

The dipole moment as a function of the electric field is plotted in Figure 3. A linear relation between the dipole and the imposed field is found and the slope directly represents the

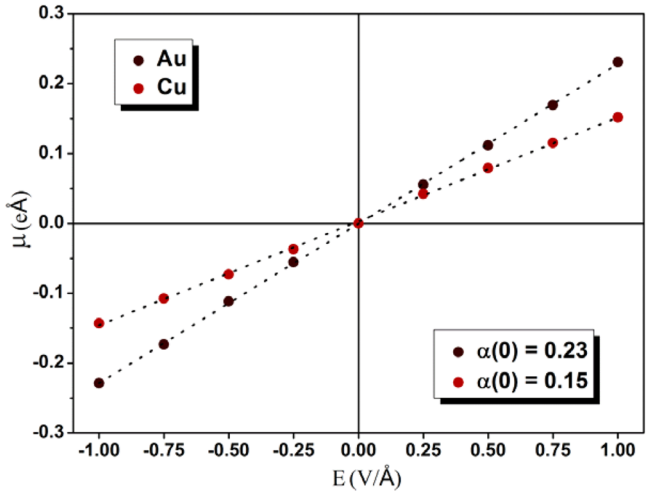

Figure 3. Au(111) and Cu(111) dipole moments as a function of the external electric field. The slope corresponds to the polarizabity in eÅ^2/V.

Table 1. Polarizabilities (α, bohr^3) for the Atom[a]

M (111)	α_{atom}[48]	α_{cal}	α_{LZK}[35]	C_6^{atom}	C_6^{cal}	$C_6^{DFT\text{-}vdW^{surf}}$[35]	$C_6^{DFT\text{-}D2}$[29]	$C_6^{DFT\text{-}D3}$[32]
Ni	45.9	14.7		447	46		189	129
Pd	32.4	19.5	13.9	243	88	102	432	266
Pt	43.9	19.5	14.5	478	94	120	1409	337
Cu	41.2	14.9	10.9	363	48	59	189	175
Ag	48.6	21.4	15.4	497	96	122	432	269
Au	39.1	22.4	15.6	392	128	134	1409	317

[a]From the Handbook for the isolated atom, α_{atom} our values for surface atom α_{cal}; and LZK from Tkatchenko–Scheffler α_{LZK}. Dispersion coefficients (C_6, hartree bohr^6) for the atom C_6^{atom}; our values C_6^{cal}; those from TS $C_6^{DFT\text{-}vdW^{surf}}$; and Grimme $C_6^{DFT\text{-}D2}$ and $C_6^{DFT\text{-}D3}$; parameters are also shown for comparison.

static polarizability $\alpha(0)$, according to eq 7. These atomic polarizabilities are significantly smaller than those obtain for the isolated metal atoms; see Table 1. The embedding environment thus acts by reducing the effect of the field in the surface atoms as most of the atomic density is compromised in forming bonds to the rest of the metal atoms. In general, we have found that the polarizability is around a 30% of the free atom value for Cu and Ni and around 60% for the rest. The metal $\alpha(0)$ increases with the Z number (for instance Ni vs Pd or Pt), but they are similar within the same period (compare Ni vs Cu values) as suggested by Grimme in his first tabulated data.[29] When compared to the LZK-derived α the values are slightly larger, about 25%, but the values from LZK correspond to bulk atoms.[35]

Using eq 6 the C_6 parameters for all the metals were obtained. Our results are presented in Table 1 and compared to other data in the literature. The present C_6 parameters are smaller than those of the free atoms or the DFT-D2 or DFT-D3 formulations, in some cases by even an order of magnitude. In contrast, the values are rather close to the values derived by TS.

4.2. Benchmark: Adsorption of Benzene. To evaluate the quality of these new coefficients, we proceeded to calculate the binding energy, BE, of benzene on the (111).[49] This energy is defined in such a way that an exothermic process yields a positive value:

$$BE = -(E_{Surf+Bz} - E_{Surf} - E_{Bz}) \quad (12)$$

Benzene is particularly suitable for testing weak interactions, as it is a large closed-shell molecule with aromatic electrons likely to be polarized. For this reason a large amount of data regarding benzene adsorption on a wide variety of surfaces is available for comparison. For the sake of comparison we employed the supercell reconstruction (3 × 3) for the (111) metal facet and the configuration for benzene from previous computational investigations; for Ag, Au, and Cu, this corresponds to hcp30°, while for Pd and Pt, it is bri30°, see inset Figure 4.[35,37] For the active metals Pd and Pt a dense phase with a p(4 × 4) supercell and two benzene rings was proposed,[31] and this better represents the experimental high coverage regime for which temperature-programmed desorption, TPD, values exist.[38,50−55] The results obtained have been represented in Figure 4 and summarized in Table 2, along with a PBE calculation, the Grimme approaches DFT-D2,[29] DFT-D3,[32] and DFT-vdW^{surf},[35,37] and experimental values. The binding energies were recalculated through the Redhead equation from TPD data,[39] employing both a default prefactor of 10^{13} or a entropy-corrected one (υ_{CS}), following the procedure of Campbell and Sellers.[56]

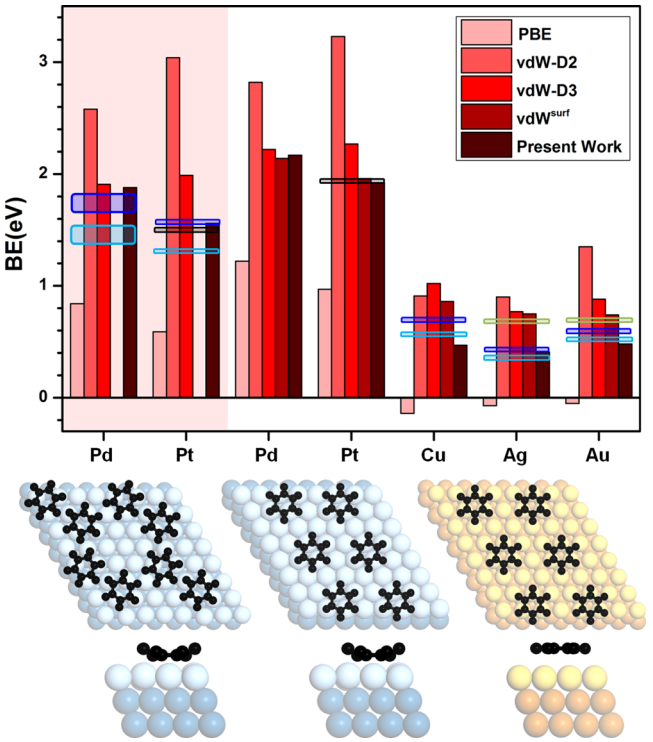

Figure 4. Binding energy (BE, in eV) for benzene on the (111) of different metals. The figure shows the comparison between different methodologies: PBE, Grimme DFT-D2 and DFT-D3 methods, DFT-vdW^{surf}, and the one developed in this work. The shaded area corresponds to high coverage models. The experimental values estimated from TPD data are shown by light (υ = 10^{13}) and dark (υ_{CS} = corrected prefactor)[56] blue areas. The estimates from experiments derived in ref 37 are marked by green shaded areas. For C_6H_6/Pt(111), we report microcalorimetric measurements in black.

For Cu, Ag, and Au, benzene is weakly physisorbed. PBE leads to endothermic adsorption and DFT-D2 leads to severe overbinding that is not mitigated with DFT-D3, which results in adsorption energies larger for Cu than for Au, at odds with the experimental ordering. DFT-vdW^{surf} yields values close to the experimental ones, with slight overestimation. In turn, our method provides slightly lower estimates than the experiments. The energy differences between experiments and our data are largest for Cu and in excellent agreement for Au and Ag.

In turn, Pt and Pd are characterized by a strong chemisorptions, thus in the TPD experiments a rather large coverage appears about 0.095 ML.[31] Again PBE underestimates the values while DFT-D2 and DFT-D3 overestimate adsorption. Even in this case, the calculated adsorption energy

Table 2. Binding Energies (BE, eV) for the Adsorption of Benzene on Different Metal Surfaces[a]

metal	PBE	DFT-D2	DFT-D3	DFT-vdW^{surf} [37]	this work	exp
			$M(4 \times 4) + 2C_6H_6$			
Pd	0.84	2.58	1.91		1.88	1.64[31]−1.83[50]
Pt	0.59	3.04	1.99		1.57	1.54[52]−1.60[51] (1.54)[57]
			$M(3 \times 3) + C_6H_6$			
Pd	1.22	2.82	2.22	2.14	2.17	
Pt	0.97	3.23	2.27	1.96	1.92	(1.94)[57]
Cu	0.14	0.91	1.02	0.86	0.47	0.70[53]−0.71[38]
Ag	0.07	0.90	0.77	0.75	0.41	0.46[58]−0.45[54]
Au	0.05	1.35	0.88	0.74	0.48	0.63[55]

[a]The experimental values estimated from TPD data are reported via an entropy-corrected prefactor.[56] For C_6H_6/Pt(111) we report microcalorimetric measurements in parentheses. The Ag data[54,58] corresponds to the shoulder that appears at the same coverage as our calculations were performed, 140 K. There is another higher temperature peak at lower coverages 205 K. The TPD data from Au[55] shows a high energy peak that continuously shifts from 239 to 175 K, thus the assignment is unclear.

is reversed from experiments thus leading to qualitative inaccuracies. In comparison, our method slightly overestimates the interaction respect to the experimental value. In the isolated regime represented by the $p(3 \times 3)$ supercell our results are very close to those of DFT-vdW^{surf}. Experimentally, more accurate data have been reported by Campbell and Sellers[56] for benzene adsorption on Pt(111) at low and high coverage (marked in black in Figure 4). Our estimates are within 0.1 eV error when compared the microcalorimetric values.

4.3. Structural Defects: Steps and Other Low-Coordinated Sites. Open surfaces containing atoms with low coordination numbers and/or structural defects might be responsible for the adsorption and activation of molecules. We have studied how polarizabilities and coefficients vary as a function of the facet exposed.[59−61]

The total dipole moment is generated by the contributions from the dipoles assigned to the individual atoms on the surface. Geometric considerations describe the total dipole moments considering that terrace atoms form an angle with the field; see Figure 5. We have determined the dipole moment for the (100), (110), and (210) surfaces from the DFT calculations. We have then investigated if the polarizability of the atoms only depends on the coordination number and thus the results from the low-index facets can be used to simplify the equations and to obtain the values for each atom on the surface. Table 3 shows the variation of both the static polarizability and the vdW coefficient with the coordination number of surface atoms.

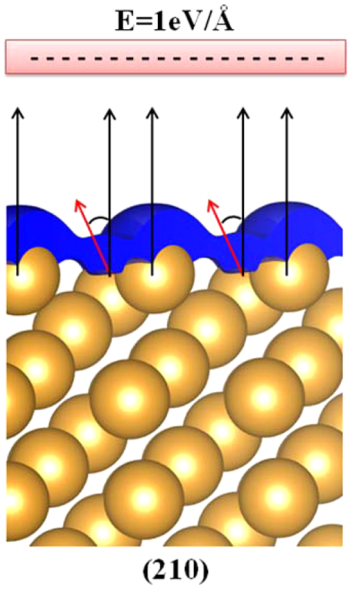

Figure 5. Schematic representation of the electron spill toward the vacuum by the electric field perpendicular to the edge of the step. The different orientation with the natural dipoles of the individual atoms is shown for clarity.

Table 3. Polarizabilities and Dispersion Coefficients as a Function of Coordination Number

	α (bohr^3)				C_6 (hartree bohr^6)			
	(111)	(100)	(110)	(210)	(111)	(100)	(110)	(210)
M	$N_c = 9$	$N_c = 8$	$N_c = 7$	$N_c = 6$	$N_c = 9$	$N_c = 8$	$N_c = 7$	$N_c = 6$
Ni	14.7	15.3	25.3	37.3	46	50	136	296
Pd	19.5	20.4	25.3	42.1	88	97	148	410
Pt	19.5	20.1	27.2	43.8	94	101	184	476
Cu	14.9	16.1	22.6	34.5	48	56	110	254
Ag	21.4	23.3	35.9	50.6	96	115	273	538
Au	22.4	23.3	35.0	48.6	128	140	314	606

The values found indicate that the polarization is larger when reducing the coordination number and it keeps the low values for 3d metals and higher ones for the rest. This variation has a second effect on the vdW coefficient which increases quite dramatically (almost 50 times) from the (111) facet to the coordination 6 of atoms at the steps of the (210) surface.

These variations with the Z number and the coordination can be summarized in a clearer way that allows us to understand the origin of the modulation of the C_6 parameter. Tkatchenko et al. suggested in ref 35 that the void volume surrounding an atom at the surface would imply a change in its polarizability as the electrons would be able to spill to a larger volume. This is clearly shown from our reported polarizabilities and C_6 parameters in Figure 6. To analyze the dependence we have defined the void volume, V, as follows:

$$V = (12 - N_c)V_{at}$$

where N_c is the coordination number of the atom and 12 represents its number of first neighbors in an fcc metal and V_{at} is the atomic volume. The calculated coordination-dependent polarizabilities are found to depend linearly on the void volume as shown in Figure 6−top. Correspondingly, the C_6 value follows quadratic dependence with the volume as it was put

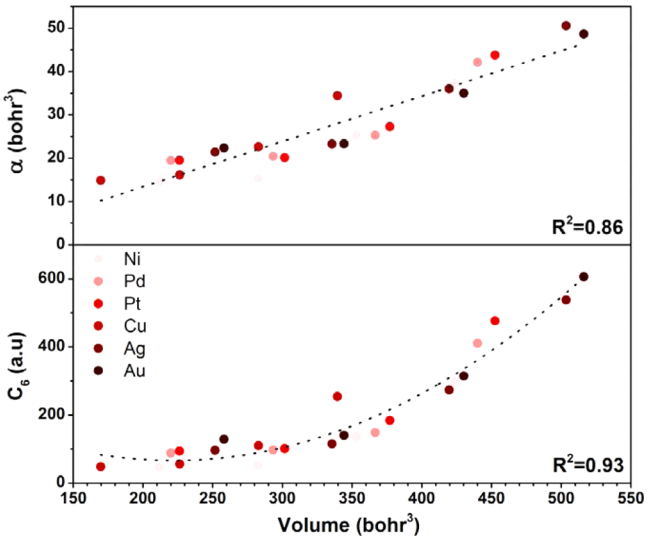

Figure 6. Polarizability as a function of volume of the exposed atoms $\alpha(0) = (0.105 \pm 0.009)V - 8 \pm 3$ and C_6 coefficient as a function of the exposed volume $C_6 = (0.0060 \pm 0.0009)V^2 + (-2.8 \pm 0.7)V + (372 \pm 108)$.

forward[35] initially but, more importantly, this dependence is found to be metal-independent.

4.4. Alloys. Our approach also allows the study of complexity in the form of alloys. In particular, we have derived C_6 parameters for overlayers and NSA; see Figure 7 for the

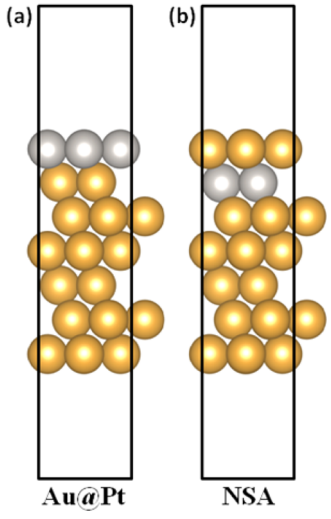

Figure 7. Schematic representation of the surfaces alloys Au@Pt (a) and NSA (b).

schematic representation. All these materials have proven their potential in catalysis and electrocatalysis.[1,62] In Figure 8, the results for different configurations of the Pd, Pt, Cu, Ag as overlayers, or NSA, are shown and compared to the pure metal values. Results indicate that the coefficients can vary more than 60%, the largest changes are obtained when smaller atoms are placed as overlayers on the surface. Au (Cu) can be taken as an example. This is again due to the change in the void volume. The correction is smaller for similar diameter atoms as overlayers (Pt). In turn, the changes do not affect the Au layer in the NSA models, again no modifications in volume are

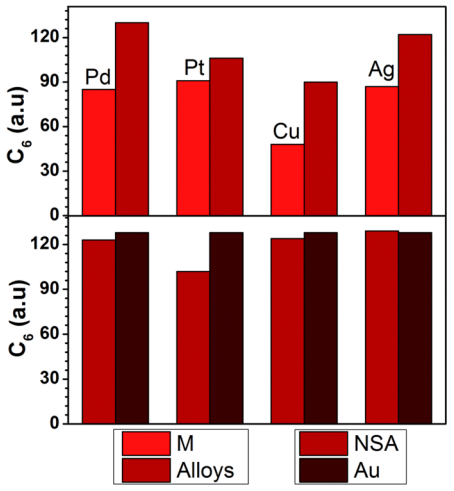

Figure 8. Dispersion coefficients (C_6, hartree bohr^6) for alloys and NSA. Metal pure parameters are also shown for comparison.

seen. The largest variation corresponds to Pt and correlates with the change in the position of the Fermi level for the NSA.

The contributions from the formation of the alloy indicate that adsorption does not significantly vary for many of the overlayers or alloys. Table 4 presents the test on benzene

Table 4. Binding Energies (BE, eV) for the Adsorption of Benzene (Bz) on Different Alloys and NSA Surfaces in the Isolated Molecule Configurations

metal	$BE^{C_6^M}$	$BE^{C_6^{alloy}}$	$BE^{C_6^{NSA}}$	$BE^{C_6^{Au}}$
Pd	2.23	2.37	0.50	0.48
Pt	2.26	2.29	0.49	0.48
Cu	0.50	0.67	0.33	0.48
Ag	0.44	0.51	0.48	0.48

adsorption. The largest variations observed are about 0.1−0.2 eV and correspond to the large increase in the value of C_6 for Cu on the overlayer and the concomitant reduction for the NSA. The enhancement is also found for Pd and Ag overlayers on Au.

5. CONCLUSIONS

van der Waals contributions are fundamental to obtain accurate estimates of the adsorption energies of large molecules on metals. Although robust ways of obtaining these energies are being developed, many of them are very computationally demanding and practical implementations would benefit from semiempirical approaches that can reduce the computational burden. For the interaction with metals, we have developed a method based on the determination of static polarizabilities that together with the ionization potentials provide reliable values for the C_6 coeffients for surface atoms. This simple model based on the response to an electric field can be applied to low-coordinated centers and alloys. In order to test the so-derived coefficients benzene adsorption energies have been taken as benchmark. Our results indicate that the method is robust and provides accurate results. In addition, a general dependence for the C_6 coeffients with the void volume, i.e. the volume where the electronic cloud can spill, has been found and can be employed as a fast estimate of coefficients for other metals. Finally, our values are compatible with already well-established contributions from atoms and molecules from Grimme's

dx.doi.org/10.1021/ct5006467 | J. Chem. Theory Comput. 2014, 10, 5002−5009

approach as it shares with this method the damping functions and follows radius definition. In addition, our results show excellent agreement with experimental determinations, in particular with the microcalorimetric measurements by Campbell and co. Finally, we consider that our costless, simple yet efficient tool can be a guide to extend the use of van der Waals contributions to different surface−adsorbate problems.

■ ASSOCIATED CONTENT

Supporting Information

Slab thickness convergence tests, atom radii, detailed TPD−computational adsorption energy comparisons. This material is available free of charge via the Internet at http://pubs.acs.org/.

■ AUTHOR INFORMATION

Corresponding Author

*E-mail: nlopez@iciq.es.

Notes

The authors declare no competing financial interest.

■ ACKNOWLEDGMENTS

This research has been supported by the ERC Starting Grant (ERC-2010-StG-258406), and we thank BSC-RES for providing us with generous computational resource. We are grateful to Dr. R. Valero (Ulsan National Institute of Science and Technology, Korea) for useful discussions.

■ REFERENCES

(1) Nørskov, J. K.; Bligaard, T.; Rossmeisl, J.; Christensen, C. H. Towards the computational design of solid catalysts. *Nat. Chem.* **2009**, *1*, 37−46.

(2) Hafner, J. Ab-initio simulations of materials using VASP: Density-functional theory and beyond. *J. Comput. Chem.* **2008**, *29*, 2044−2078.

(3) Mercurio, G.; McNellis, E. R.; Martin, I.; Hagen, S.; Leyssner, F.; Soubatch, S.; Meyer, J.; Wolf, M.; Tegeder, P.; Tautz, F. S.; Reuter, K. Structure and Energetics of Azobenzene on Ag(111): Benchmarking Semiempirical Dispersion Correction Approaches. *Phys. Rev. Lett.* **2010**, *104*, 036102.

(4) von Lilienfeld, O. A.; Tavernelli, I.; Rothlisberger, U.; Sebastiani, D. Optimization of Effective Atom Centered Potentials for London Dispersion Forces in Density Functional Theory. *Phys. Rev. Lett.* **2004**, *93*, 153004.

(5) Johnson, E. R.; Becke, A. D. A post-Hartree−Fock model of intermolecular interactions. *J. Chem. Phys.* **2005**, *123*, 024101.

(6) Tkatchenko, A.; Romaner, L.; Hofmann, O. T.; Zojer, E.; Ambrosch-Draxl, C.; Scheffler, M. Van der Waals interactions between organic adsorbates and at organic/inorganic interfaces. *MRS bull.* **2010**, *35*, 435−442.

(7) Steinmann, S. N.; Corminboeuf, C. A generalized-gradient approximation exchange hole model for dispersion coefficients. *J. Chem. Phys.* **2011**, *134*, 044117.

(8) Mackie, I. D.; DiLabio, G. A. Interactions in Large, Polyaromatic Hydrocarbon Dimers: Application of Density Functional Theory with Dispersion Corrections. *J. Phys. Chem. A* **2008**, *112*, 10968−10976.

(9) Sato, T.; Nakai, H. Density functional method including weak interactions: Dispersion coefficients based on the local response approximation. *J. Chem. Phys.* **2009**, *131*, 224104.

(10) Gräfenstein, J.; Cremer, D. An efficient algorithm for the density-functional theory treatment of dispersion interactions. *J. Chem. Phys.* **2009**, *130*, 124105.

(11) Silvestrelli, P. L.; Benyahia, K.; Grubisiĉ, S.; Ancilotto, F.; Toigo, F. Van der Waals interactions at surfaces by density functional theory using Wannier functions. *J. Chem. Phys.* **2009**, *130*, 074702.

(12) Klimeš, J.; Michaelides, A. Perspective: Advances and challenges in treating van der Waals dispersion forces in density functional theory. *J. Chem. Phys.* **2012**, *137*, 120901.

(13) Zaremba, E.; Kohn, W. Van der Waals interaction between an atom and a Solid-Surface. *Phys. Rev. B* **1976**, *13*, 2270−2285.

(14) Lifshitz, E. M. The theory of molecular attractive forces between solids. *Sov. Phys.−JETP* **1956**, *2*, 73−83.

(15) Henkelman, G.; Jónsson, H. Theoretical Calculations of Dissociative Adsorption of CH_4 on an Ir(111) Surface. *Phys. Rev. Lett.* **2001**, *86*, 664−667.

(16) Lee, K.; Murray, E. D.; Kong, L.; Lundqvist, B. I.; Langreth, D. C. Higher-accuracy van der Waals density functional. *Phys. Rev. B* **2010**, *82*, 081101.

(17) Dion, M.; Rydberg, H.; Schroder, E.; Langreth, D. C.; Lundqvist, B. I. Van der Waals density functional for general geometries. *Phys. Rev. Lett.* **2004**, *92*, 246401.

(18) Dion, M.; Rydberg, H.; Schroder, E.; Langreth, D. C.; Lundqvist, B. I. Erratum: Van der Waals Density Functional for General Geometries [Phys. Rev. Lett. 92, 246401 (2004)]. *Phys. Rev. Lett.* **2005**, *95*, 109902.

(19) Andersson, Y.; Langreth, D. C.; Lundqvist, B. I. van der Waals Interactions in Density-Functional Theory. *Phys. Rev. Lett.* **1996**, *76*, 102−105.

(20) Langreth, D. C.; Lundqvist, B. I.; Chakarova-Käck, S. D.; Cooper, V. R.; Dion, M.; Hyldgaard, P.; Kelkkanen, A.; Kleis, J.; Lingzhu, K.; Shen, L.; Moses, P. G.; Murray, E.; Puzder, A.; Rydberg, H.; Schröder, E.; Thonhauser, T. A density functional for sparse matter. *J. Phys.−Condens. Mater.* **2009**, *21*, 084203.

(21) Hamada, I.; Otani, M. Comparative van der Waals density-functional study of graphene on metal surfaces. *Phys. Rev. B* **2010**, *82*, 153412−153412−4.

(22) Nozières, P.; Pines, D. Correlation Energy of a Free Electron Gas. *Phys. Rev.* **1958**, *111*, 442−454.

(23) Dobson, J. F.; Dinte, B. P. Constraint Satisfaction in Local and Gradient Susceptibility Approximations: Application to a van der Waals Density Functional. *Phys. Rev. Lett.* **1996**, *76*, 1780−1783.

(24) Furche, F.; Van Voorhis, T. Fluctuation-dissipation theorem density-functional theory. *J. Chem. Phys.* **2005**, *122*, 164106.

(25) Harl, J.; Kresse, G. Accurate Bulk Properties from Approximate Many-Body Techniques. *Phys. Rev. Lett.* **2009**, *103*, 056401.

(26) Harl, J.; Schimka, L.; Kresse, G. Assessing the quality of the random phase approximation for lattice constants and atomization energies of solids. *Phys. Rev. B* **2010**, *81*, 115126.

(27) Lebègue, S.; Harl, J.; Gould, T.; Ángyán, J. G.; Kresse, G.; Dobson, J. F. Cohesive Properties and Asymptotics of the Dispersion Interaction in Graphite by the Random Phase Approximation. *Phys. Rev. Lett.* **2010**, *105*, 196401.

(28) Schimka, L.; Harl, J.; Stroppa, A.; Grüneis, A.; Marsman, M.; Mittendorfer, F.; Kresse, G. Accurate surface and adsorption energies from many-body perturbation theory. *Nat. Mater.* **2010**, *9*, 741−744.

(29) Grimme, S. Semiempirical GGA-type density functional constructed with a long-range dispersion correction. *J. Comput. Chem.* **2006**, *27*, 1787−1799.

(30) London, F. The general theory of molecular forces. *Trans. Faraday Soc.* **1937**, *33*, 8b−26.

(31) Tysoe, W. T.; Ormerod, R. M.; Lambert, R. M.; Zgrablich, G.; Ramirez-Cuesta, A. Overlayer structure and kinetic behavior of benzene on palladium(111). *J. Phys. Chem.* **1993**, *97*, 3365−3370.

(32) Grimme, S.; Antony, J.; Ehrlich, S.; Krieg, H. A consistent and accurate ab initio parametrization of density functional dispersion correction (DFT-D) for the 94 elements H-Pu. *J. Chem. Phys.* **2010**, *132*, 154104.

(33) Tonigold, K.; Groß, A. Dispersive interactions in water bilayers at metallic surfaces: A comparison of the PBE and RPBE functional including semiempirical dispersion corrections. *J. Comput. Chem.* **2012**, *33*, 695−701.

(34) Tkatchenko, A.; Scheffler, M. Accurate Molecular Van Der Waals Interactions from Ground-State Electron Density and Free-Atom Reference Data. *Phys. Rev. Lett.* **2009**, *102*, 073005.

(35) Ruiz, V. G.; Liu, W.; Zojer, E.; Scheffler, M.; Tkatchenko, A. Density-Functional Theory with Screened van der Waals Interactions

for the Modeling of Hybrid Inorganic-Organic Systems. *Phys. Rev. Lett.* **2012**, *108*, 146103.
(36) Liu, W.; Tkatchenko, A.; Scheffler, M. Modeling Adsorption and Reactions of Organic Molecules at Metal Surfaces. *Acc. Chem. Res.* **2014**, Article ASAP.
(37) Wei, L.; Victor, G. R.; Guo-Xu, Z.; Biswajit, S.; Xinguo, R.; Matthias, S.; Alexandre, T. Structure and energetics of benzene adsorbed on transition-metal surfaces: density-functional theory with van der Waals interactions including collective substrate response. *New J. Phys.* **2013**, *15*, 053046.
(38) Lukas, S.; Vollmer, S.; Witte, G.; Wöll, C. Adsorption of acenes on flat and vicinal Cu(111) surfaces: Step induced formation of lateral order. *J. Chem. Phys.* **2001**, *114*, 10123−10130.
(39) Redhead, P. A. Thermal desorption of gases. *Vacuum* **1962**, *12*, 203−211.
(40) Deshlahra, P.; Wolf, E. E.; Schneider, W. F. A Periodic Density Functional Theory Analysis of CO Chemisorption on Pt(111) in the Presence of Uniform Electric Fields. *J. Phys. Chem. A* **2009**, *113*, 4125−4133.
(41) Feynman, R. P.; Leighton, R. B.; Sands, M. L. Refractive Index of Dense Materials. In *The Feynman Lectures on Physics: Mainly electromagnetism and matter*; Gottlieb, M. A., Pfeiffer, P., Eds.; Addison-Wesley: California, 1965; Vol. *II*.
(42) Neugebauer, J.; Scheffler, M. Adsorbate-substrate and adsorbate-adsorbate interactions of Na and K adlayers on Al(111). *Phys. Rev. B* **1992**, *46*, 16067−16080.
(43) Kresse, G.; Joubert, D. From ultrasoft pseudopotentials to the projector augmented-wave method. *Phys. Rev. B* **1999**, *59*, 1758−1775.
(44) Kresse, G.; Furthmuller, J. Efficiency of ab-initio total energy calculations for metals and semiconductors using a plane-wave basis set. *Comput. Mater. Sci.* **1996**, *6*, 15−50.
(45) Kresse, G.; Furthmuller, J. Efficient iterative schemes for ab initio total-energy calculations using a plane-wave basis set. *Phys. Rev. B* **1996**, *54*, 11169−11186.
(46) Perdew, J. P.; Burke, K.; Ernzerhof, M. Generalized gradient approximation made simple. *Phys. Rev. Lett.* **1996**, *77*, 3865−3868.
(47) Feibelman, P. J. Surface-diffusion mechanism versus electric field: Pt/Pt(001). *Phys. Rev. B* **2001**, *64*, 125403.
(48) *CRC Handbook of Chemistry and Physics*, 84 ed.; Lide, D. R., Ed.; CRC Press: 2003; p 2616.
(49) Liu, W.; Carrasco, J.; Santra, B.; Michaelides, A.; Scheffler, M.; Tkatchenko, A. Benzene adsorbed on metals: Concerted effect of covalency and van der Waals bonding. *Phys. Rev. B* **2012**, *86*, 245405.
(50) Waddill, G. D.; Kesmodel, L. L. Benzene chemisorption on palladium surfaces. I. High-resolution electron-energy-loss vibrational spectra and structural models. *Phys. Rev. B* **1985**, *31*, 4940−4946.
(51) Campbell, J. M.; Seimanides, S.; Campbell, C. T. Probing ensemble effects in surface reactions. 2. Benzene adsorption on clean and bismuth-covered platinum(111). *J. Phys. Chem.* **1989**, *93*, 815−826.
(52) Xu, C.; Tsai, Y. L.; Koel, B. E. Adsorption of cyclohexane and benzene on ordered tin/platinum (111) surface alloys. *J. Phys. Chem.* **1994**, *98*, 585−593.
(53) Xi, M.; Yang, M. X.; Jo, S. K.; Bent, B. E.; Stevens, P. Benzene adsorption on Cu(111): Formation of a stable bilayer. *J. Chem. Phys.* **1994**, *101*, 9122−9131.
(54) Rockey, T. J.; Yang, M.; Dai, H.-L. Adsorption Energies, Inter-adsorbate Interactions, and the Two Binding Sites within Monolayer Benzene on Ag(111). *J. Phys. Chem. B* **2006**, *110*, 19973−19978.
(55) Syomin, D.; Kim, J.; Koel, B. E.; Ellison, G. B. Identification of Adsorbed Phenyl (C_6H_5) Groups on Metal Surfaces: Electron-Induced Dissociation of Benzene on Au(111). *J. Phys. Chem. B* **2001**, *105*, 8387−8394.
(56) Campbell, C. T.; Sellers, J. R. V. The Entropies of Adsorbed Molecules. *J. Am. Chem. Soc.* **2012**, *134*, 18109−18115.
(57) Ihm, H.; Ajo, H. M.; Gottfried, J. M.; Bera, P.; Campbell, C. T. Calorimetric Measurement of the Heat of Adsorption of Benzene on Pt(111). *J. Phys. Chem. B* **2004**, *108*, 14627−14633.
(58) Meserole, C. A.; Vandeweert, E.; Postawa, Z.; Haynie, B. C.; Winograd, N. Energetic Ion-Stimulated Desorption of Physisorbed Molecules. *J. Phys. Chem. B* **2002**, *106*, 12929−12937.
(59) Vilé, G.; Baudouin, D.; Remediakis, I. N.; Copéret, C.; Lõpez, N.; Pérez-Ramírez, J. Silver nanoparticles for olefin production: New insights into the mechanistic description of propyne hydrogenation. *ChemCatChem.* **2013**, *5*, 3750−3759.
(60) Almora-Barrios, N.; Novell-Leruth, G.; Whiting, P.; Liz-Marzán, L. M.; López, N. Theoretical Description of the Role of Halides, Silver, and Surfactants on the Structure of Gold Nanorods. *Nano Lett.* **2014**, *14*, 871−875.
(61) Vilé, G.; Almora-Barrios, N.; Mitchell, S.; López, N.; Pérez-Ramírez, J. From the Lindlar Catalyst to Supported Ligand-Modified Palladium Nanoparticles: Selectivity Patterns and Accessibility Constraints in the Continuous-Flow Three-Phase Hydrogenation of Acetylenic Compounds. *Chem.—Eur. J.* **2014**, *20*, 5926−5937.
(62) Greeley, J.; Mavrikakis, M. Alloy catalysts designed from first principles. *Nat. Mater.* **2004**, *3*, 810−815.

Top Catal (2013) 56:1262–1272
DOI 10.1007/s11244-013-0093-3

ORIGINAL PAPER

How Theoretical Simulations Can Address the Structure and Activity of Nanoparticles

Giuliano Carchini · Neyvis Almora-Barrios · Guillem Revilla-López · Luca Bellarosa · Rodrigo García-Muelas · Max García-Melchor · Sergey Pogodin · Piotr Błoński · Núria López

Published online: 25 June 2013

Abstract Theoretical simulations in the field of heterogeneous catalysis started about two decades ago when the main goal was to understand the activation of small molecules on infinite surfaces. The improvements in the accuracy and the large availability of computers with increasing power have raised the quality of the calculations, the reliability of the results and prompted the interest in their predictions. Such changes have also allowed the study of nanoparticles by the combined investigation of different facets or by taking into account the complete structures. As for the reactivity, theoretical simulations allow the comparison of different synthetic conditions within the same approximation. Consequently, large systematic studies with the same theoretical models can provide databases for properties, structures, prove and disprove hypothetical reaction paths, identify intermediates, and complete the understanding of reaction mechanisms. In some cases, simulations support and give explanations to experiments but new emerging aspects such as the prediction of new properties or the analysis of complex systems are possible. Several challenges are ahead the simulations of reactions on nanoparticles: (i) how to drive the synthesis to achieve the desired architectures and (ii) how to stabilize the active phase under reaction conditions.

Keywords DFT · Nanoparticles · Multiscale modelling · Simulations · Equilibrium shape

G. Carchini · N. Almora-Barrios · G. Revilla-López · L. Bellarosa · R. García-Muelas · M. García-Melchor · S. Pogodin · P. Błoński · N. López (✉)
Institute of Chemical Research of Catalonia, ICIQ, Avgda. Països Catalans, 16, 43007 Tarragona, Spain
e-mail: nlopez@iciq.es

1 Introduction

Nanoparticles have a wide range of application from plasmonics to heterogeneous catalyst. Reactions that can be catalysed by nanoparticles have been known and employed industrially since more than a hundred years [1]. As the reactions take place between a gas or liquid phase reactant and a solid surface it is usually described as heterogeneous process. Due to the interaction of molecules with the solid surface, reactants get activated and reduce the energetic requirement for the reaction. Therefore, the number of active sites available is crucial and this number of sites depends on the surface to volume ratio. As a consequence, the use of nanoparticles is crucial to enhance the catalytic activity. This fact was very early established as one of the fathers of Catalysis, Humphry Davy, reported that Pt was more active when finely divided [2]. As catalyst are made of expensive or rare metals there is a need to reduce the amount of material used and thus oxide supports or other carriers with high surface areas are routinely employed. In the case of active industrial catalysts, there are a few more components including binders, secondary metals and molecular modifiers which finely tune the electronic structure, and improve the activity, selectivity and stability under reaction conditions.

Nanoparticles have been employed with different catalytic purposes [3] but still it is a main challenge how to achieve a given dispersion, shape and size distribution that is optimum to catalytic performance. The last synthetic and characterization techniques have proven to enhance the degree of architecture control. For instance, different synthetic methods have been devised to achieve narrow distributions for sizes and shapes, but their effectiveness depends on the application. In heterogeneous catalysis maintain finely distributed nanoparticles might be difficult under typical harsh conditions. The main reason for the

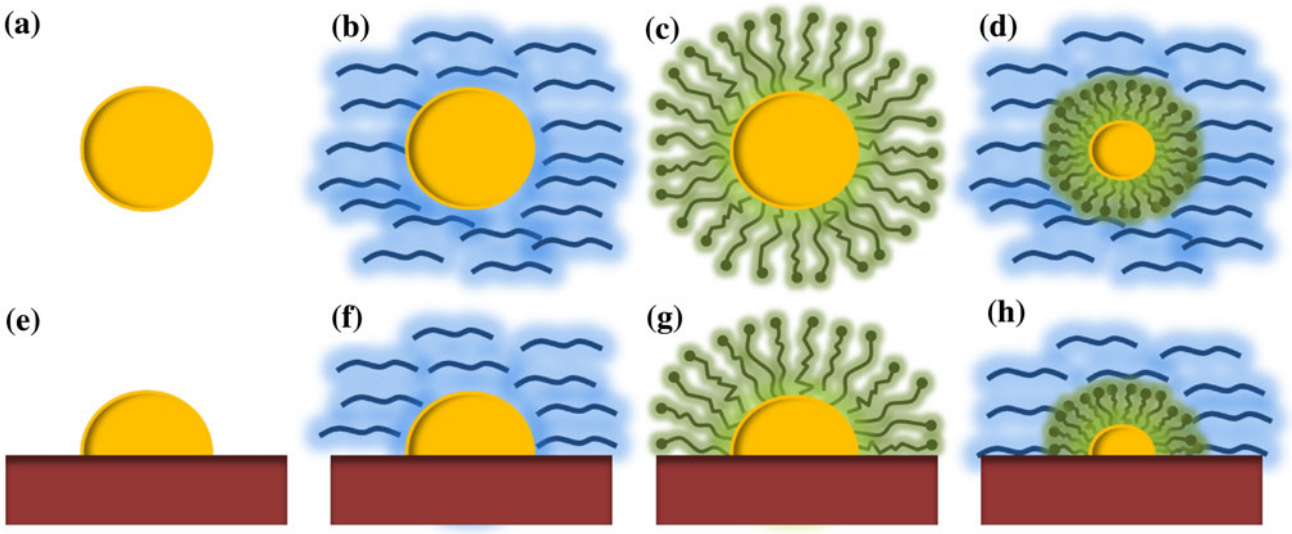

Fig. 1 Sketch of the different models for nanoparticles: **a** gas-phase, **b** solvated, **c** surfactant covered, **d** in solution, surfactant-covered, **e** supported, **f** supported, in solution, **g** supported, surfactant-covered, and **h** supported surfactant-covered nanoparticle in solution

stability issue is based on the large interaction between the reactants (intermediates or products) and the nanoparticles or the oxides serving as supports. From a theoretical point of view nanoparticles supported on oxides can be studied through the direct comparison to physical methods. Those are well-suited to detailed analysis, as atomistic modelling and benchmarking can be directly performed [4–6]. Care shall be taken though because the stable or metastable structures prepared in such manner are extremely sensitive to changes in temperature and partial pressures. Many of the so-prepared structures are dynamic and thus the representativity of these systems is compromised.

There are different ways to create nanoparticles for the chemical wet preparations. In particular the use of soft-templates and surfactants have been found as flexible, very versatile platforms that can adjust the size distribution and shape control [7]. However, attempting to remove the surfactants by increasing the temperature may induce metal coalescence and reduction of the surface area, and therefore reduces the benefits of wet synthesis. Such complex multicomponent and multiphase systems are difficult to represent from a computational perspective, so we are going summarize the major points that need to be taken into account to model the structure and reactivity of such nanoparticles.

In Fig. 1 we schematically show different representations of nanoparticles that can be studied through theoretical means and that will be described in the following.

2 Theoretical Simulations

Theoretical simulations are usually based on the solution of the time-independent version of the Schrödinger equation. The analytical solution for the wavefunction can only be obtained for monoelectronic atoms, therefore approximations need to be used with polyelectronic systems. In the traditional view of chemists this was achieved through a hierarchy of Quantum Chemistry methods. This list of methods starts with the Hartree–Fock (HF) approach, i.e. a mean field approximation, and then higher accuracy is achieved by including more terms in the expression of the wavefunction. Thus, in traditional molecular studies, expansions to the Møller–Plesset perturbation methods or more sophisticated formulations based on Configuration Interaction expansion were used to analyse particular properties, but they were excessively expensive in terms of computational resources. Besides, a localized basis set depicting the atomic and molecular orbitals that provided a relatively easy interpretation of the chemical bond has been employed for molecules and extended to small clusters. This approach is however not viable for systems containing more than 10 metal atoms as they strongly depend on the number of basis set functions which can rise from N^4 (HF) to N^{6-7} in Configuration Interaction approaches.

The alternative comes from the use of Density Functional Theory, DFT, which employs the electronic density as a function that only depends on the Cartesian coordinates and spin. The ultimate quality of the density is that it is a fundamental observable that can be directly compared to results from X-ray or neutron diffraction. The drawback of this simplification is the addition of an unknown exchange–correlation term to the energy. DFT energies are usually taken as the reference for more sophisticated approaches, such as medium field theories, or schemes that describe larger time and length scales suitable to be compared to experiments in both Materials Science and Catalysis [8].

The accuracy and efficiency of DFT-based methods depend on several technical choices [9], including the particular exchange–correlation functional, the basis set for the expansion of the Kohn–Sham (KS) orbitals and the algorithms employed to solve the KS equations. The choice of exchange–correlation functionals and the completeness of the basis set account for the accuracy, whereas the numerical algorithms are responsible for the efficiency. The hierarchy of exchange–correlation functionals was described by John Perdew in "the Jacob's ladder of DFT" with the computational demands and the accuracy as shown in Fig. 2 [10].

The lowest part of the ladder is the local density approximation (LDA) [12], where the exchange–correlation energy (E_{xc}) is expressed as that of a homogeneous electron gas of the same density, $n(r)$. The E_{xc} is parameterized from quantum Monte-Carlo simulations [13]. LDA solves many bulk [14] and surface systems but it usually leads to over-binding [15]. The second rung in the ladder is formed by a family of methods termed as generalised gradient approximation (GGA) [16, 17]. There E_{xc} depends not only on the electron density but on its local gradient, $\nabla n(r)$. The GGAs solves the over-binding of the LDA, with a tendency to over-correct it [18] but the attained accuracy is enough for many chemical reactions [19]. PW91 [20], PBE [21], revised PBE [18], PBEsol [22], MA05 [23], and WC [24] belong to this family of methods. PW91 and PBE have been the standard in reactivity during the last decade. However, GGAs have two serious drawbacks. First, they do not account for van der Waals (vdW) interactions resulting from dynamical correlations between fluctuating charge distributions [9]. The second weak point is related to the non-zero interaction of a single electron with its own density, known as self-interaction error (SIE). SIE is the cause of many of the failures of approximate functionals, such as excessively narrow band gaps [25, 26], wrong dissociation energies for molecules [27], and incorrect description of systems with localised f electrons [28]. Therefore a proper SIE correction is required for the nanostructures of oxides. Fixes to strong-correlated systems based on the Hubbard model have been applied to address issues such as the incorrect description of band gaps, and are known as DFT + U [29]. Normally the DFT employed is of the GGA level. The main concern is that the U, a parameter to describe interelectronic repulsion in d or f strongly correlated levels, depends on the particular observable to be calculated; this enters in contradiction with the universality claimed for the functional.

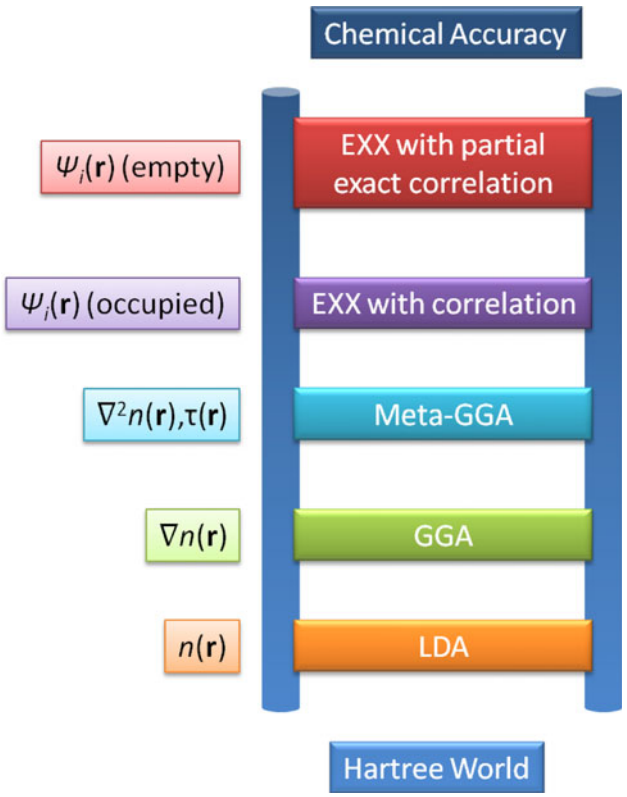

Fig. 2 Jacob's ladder of Density Functional Theory with the different approximations linking the Hartree World of Independent Electrons and the Heaven of Chemical Accuracy [11]. E_{XX} stands for the exact exchange, n for the density, τ for the kinetic terms and Ψ for the orbitals. Notice that no comparison to computational Chemical methods is presented and only from rung 4 upwards exact exchange (i.e. Hartree–Fock form) is taken into account

Meta-GGA includes higher-order terms of the gradient of the local kinetic energy density, $\nabla^2 n(r)$, and constitutes the third rung on the DFT ladder [30]. Unfortunately such methods do not systematically improve the properties from those obtained with GGA. Examples of this lack of consistency have been reported, such as the adsorption of small molecules on transition- and noble-metal surfaces [9] and the hydrogenation of benzene to cyclohexene on Ni(111) [31].

The next step in the ladder corresponds to hybrid functional, that mix exact E_{XX}, i.e. HF and DFT exchange, and describe correlation at the standard DFT level. The most popular hybrid in chemistry has been for more than one decade the B3LYP functional [32, 33], providing high accuracy for almost all properties of molecules, but failing when applied to metals and semiconductor solids, because the correlation part of the functional is incorrect in the homogeneous electron gas limit [34, 35]. Other hybrid approaches typically employed for solids are PBE0 [36] and HSE03 [37], which show better estimates for lattice parameters and bulk moduli of solids, and for the band gaps in semiconductors and insulators [34, 35]. In general, these hybrid functionals properly describe both insulating antiferromagnetic rare-earth and transition metal oxides which are not correct with GGAs [38, 39]. Atomisation energies and magnetic properties of metals are more accurate

through standard PBE. A difficulty in the use of hybrid functional is their great computational cost than standard DFT.

Dispersion interactions (vdW) are lacking in standard DFT calculations. Methods based on the random-phase approximation, combined with the adiabatic connection and fluctuation dissipation theorem [40] can account for these terms but they are extremely computationally demanding. As a consequence they can mostly be employed as benchmark for simplified models. To account for vdW effects, cheaper alternatives with modified functionals have been put forward. However there is a lack of robustness in some of the approaches that makes difficult to assess their long-term viability [41, 42]. The simplest way to introduce dispersive terms was given by semi-empirical force fields of Grimme [43] (DFT-D2). They are calculated through the London formula [44] leading to the $\Sigma C_6/R^6$ term and thus the choice of the C_6 parameter becomes crucial. Still, it has been applied to water layers on metals (one of the most complex systems to model) and holds promise for the modelling of complex solid/liquid interfaces, layered compounds, and weakly interacting systems [45].

3 Clusters, Nanoclusters and Their Simulations

Two types of approximations can be employed to the study of clusters in the nanometric regime. On one side nanoparticles are finite-size structures. Therefore, they can be modelled as large molecules, where the total amount of atoms is truly represented (i.e. through the use force fields, or first-principles approaches). However, if we are interested in complex electronic structures, the use of large molecules may not possible. Clusters with large sizes imply the treatment of 1,000 or more atoms which cannot be handled with traditional molecular codes, like Gaussian [46]. Newer algorithms implemented are more suited to address such large structures. For instance, the real space implementation of DFT in GPAW [47] can take into account large metal nanoparticles and oxide clusters and large metal oxide polyanions like -polyoxometallates.

In the description of nanoparticles two different regions can be identified. At small diameters non-scalable regimes appear: this means that the properties of a system with N constituents cannot be directly extrapolated to those of $N + 1$. From a technological point of view this is a dangerous path as the degree of control in the synthesis and long-term stability cannot ensure that the "active" species can be maintained for sufficiently large time scales. Scalability appears at larger diameters, and thus there is a systematic way to understand the properties of an $N + 1$ system provided that the N is known. The normal behaviour or activity as a function of the diameter of the particles is shown in Fig. 3.

3.1 Non-scalable Regime

3.1.1 Structure

The chemical properties of systems in the non-scalable regimes have been described for several examples. In the limit, the formation of benzene from ethylene on isolated Pd atoms on defects in MgO were described to show that one atom is enough for some interesting chemistry [48]. Larger cluster agglomerates, containing from a few to tenths of atoms, show some of the properties of molecules like (i) the fluxionality, the flexibility of the structure and (ii) a relatively large the number of low-lying configurations where different spin-states, separated by a finite energy, easily surmounted. In many cases, the study of such nanostructures is limited to the electronic and geometric ground state. This simplification can only be employed for applications where the temperatures considered are low and the systems are chemically insulated (such as memory storage) then the individual properties of ground state structures might be enough to represent these systems [49].

In chemical environments or where several relevant configurations might play a role, complex algorithms, usually based on basin hopping and minimization techniques, could serve as a first indication of the number of low-lying states within a small energy difference [50]. The role of these alternative structures implies that the proper description of the chemical phenomena taking place on these scales would require considering at least low-lying

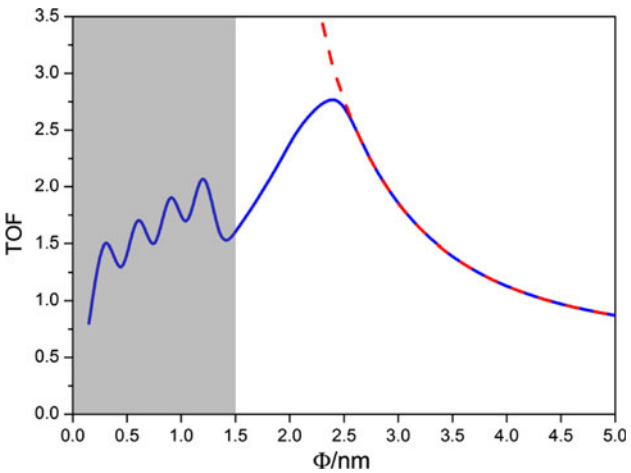

Fig. 3 Turn-over frequency (activity) as a function of the particle diameter. Scalable versus non-scalable (*shadowed*) regimes are shown. In the non-scalable regime, below 1.5 nm in diameter, the properties depend on the explicit number of atoms, but at higher diameters the properties are continuous. The *dashed red line* corresponds to the density of corners atoms in nanoparticles that scales as $1/r^3$

structures and weighting the properties by a distribution (i.e. Boltzmann for the equilibrium). Obviously this limits the availability of the atomistic theoretical simulations as they imply a large number of structures and wide sampling. The representativity of low-lying states and their corresponding properties, in particular those related to the chemistry, might be completely irrelevant.

For discrete clusters the energy levels are well separated. This has been exemplified in the comparison of the Density of States for the bulk of gold and two nanoparticles presented in Fig. 4. The HOMO–LUMO gaps are shown so that the convergence with the metal character represented by the bulk is clearly seen and this would account for the scalability at medium to large sizes. For small clusters, there is a group of structures that might behave as noble (or inert) as the parent compounds. These correspond to the appearance of magic numbers, which show the following properties: (i) a large energy difference of the ground state from the lowest to the next configuration, (ii) a close-shell structure with a large gap in the electronic structure and thus a HOMO–LUMO gap. In the case of monoelectronic metals it is very easy to identify which structures will behave as magic clusters. This can be extended to pseudo-monoelectronic metals such as Cu, Ag, and Au. The concept is more complex for metals in which the electronic configuration is less straightforward. Magic numbers can be understood in chemical terms as a kind of aromaticity that has been reported for clusters of carbon (the well-known fullerenes) [51], boron and other compounds.

Magic clusters might also appear for other chemical structures as they are potential energy wells and their appearance depends on (i) the nature of the system (i.e. type of material: metals, oxides, salts); (ii) the redox state of the metals and (iii) the environment (i.e. oxidative, reductive, solvent, surfactants…). Environmental factors might modify not only the surface structure with partial oxides but also generate new stoichiometries for which no models are known, therefore altering the composition and structure of magic clusters. As a consequence, synthetic processes carried out under mild conditions are more prone to show complexity compared to other preparations for which usual "cleaning" procedures, i.e. reduction at high temperatures, simplify the stoichiometry and composition.

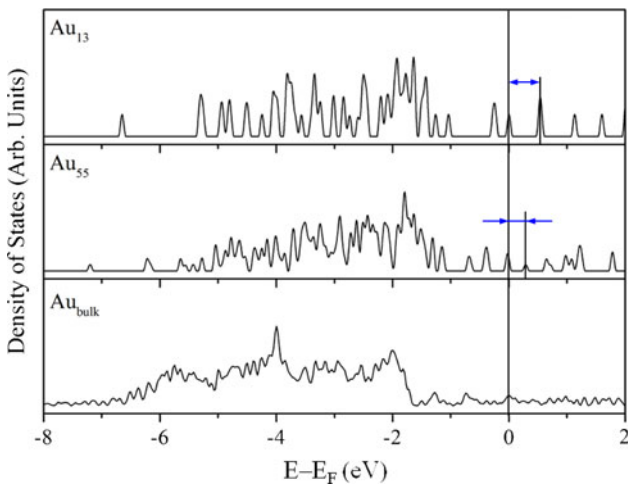

Fig. 4 Projected Density of States for two clusters of gold Au_{13}, Au_{55} compared to the Au_{bulk}. For the nanoparticles, the HOMO–LUMO gap opens indicated by the *blue arrows*

3.1.2 Activity

Examples of potential activity in the non-scalable regime have been presented for a number of reactions including the trimerization of ethylene [48], oxidation of CO by Au_8 [52] and the selective epoxidation of propyne [53]. For the first case it is clear that the well-anchored structure with a charge-promoted Pd atom sitting on a vacancy site could be enough for the reaction, as it is still active and sufficiently electronic rich to perform the transformation. Moreover, Pd would tend to sit on steps and oxygen vacancies on MgO, if those are present in significant amounts [48]. The concept above is a proof of site isolation presented by several groups in different context. If the isolation of the active centre (and even its promotion) is possible, then the catalyst would have the optimum activity, selectivity and stability. Obviously, the ensemble control would be easier for reactions taking place on isolated atoms than for other requiring more complex configurations. For the second case [52], the CO oxidation on Au_8 particles, it was clearly shown that the activity in the reaction has a lateral path, i.e. an O atom remains on the nanocatalyst. This can be detrimental to the overall stability as the O can fill the vacancy healing the anchoring site. So, after one or a few reaction cycles, the active centre is no longer present. The final example, even more interesting from a technological point of view, is the catalyst for epoxidation of ethylene, Ag, cannot be used for propylene due to the high basicity of the oxygen atoms carrying out the reaction [54]. Experiments and computational models have shown that for small clusters, i.e. containing less than ten atoms, the amount of oxygen on the surface might be reduced, leading to a sharp selectivity for the desired compound [53]. Again, the issue for the long-term stability of these silver-based epoxidation nanocatalysts is compromised if enough oxygen is around as agglomeration of the silver catalyst and thus its death is likely.

3.2 Scalable Regime

3.2.1 Structure

Scalable regimes corresponds to sizes larger than 1.5 nm diameter, where the properties of a system tend to converge

and do not explicitly depend on the number of atoms. The main problem of representing such structures is that at least 10^3 atoms need to be considered. These are not suited to traditional physic models that exploit plane waves and periodic boundary conditions as they do not benefit for further contractions of the reciprocal space once the direct lattice has a side of about 3 nm. To check for the convergence of cluster properties to the scalable regime, calculations with real space codes have been presented in the literature. For instance, they have shown how the extension and shape of the Au molecular orbitals converge with a diameter of nanoparticles of around 2.7 nm, or 561 atoms [55]. Also the algorithms at the core of the SIESTA package, which employs localized basis sets [56] with a cutoff for the interaction, allows the linear scalability for large enough systems.

Instead of this brute force approach that contains 10^3 atoms in the calculations of nanoparticles, the traditional view was to separate and study the contribution from different facets of the crystal and then add them up. This approach has been widely employed to understand the activity of nanoparticles and can be summarized as follows. First, the calculations are performed on different facets of the crystal. Thus, the surface energy (i.e. the energy needed to cut a particular facet) for each of the j cuts, γ_j, is obtained. Finally, the Wulff construction [57] is applied. The Wulff theorem, developed in 1901, states that the lower the surface energy of a facet, the largest contribution it has in the equilibrium structure of a given material. The Gibbs function of the equilibrium nanoparticle, ΔG_i, thus minimizes the summation for all the surface energies, times the area O_j of this particular facet:

$$\Delta G_i = \sum_j \gamma_j O_j.$$

The Wulff construction allows a smart evaluation of the exposed facets of a material with just few cheap calculations, and has been proven exceedingly successful predicting nanoparticle structures. Examples of these structures can be found in Fig. 5 for a prototypical fcc metal and two rutile compounds relevant in industrial processes. Still the Wulff model is oversimplified because it does not consider the energy required to form steps and edges [58]. Obviously, this approximation is less valid when considering small nanoparticles as the number of low-coordinated sites on them is larger. Also, relatively large structures, i.e. >1.5 nm, need to be included for the model to be relevant. Other approximations can be added on top of the simplified Wulff model. One of them relates to the effect of the environment. Clearly when growing under different conditions, e.g. the oxygen pressure, the surface energies change and this might control the facets exposed. This can be transferred to the Wulff's model and

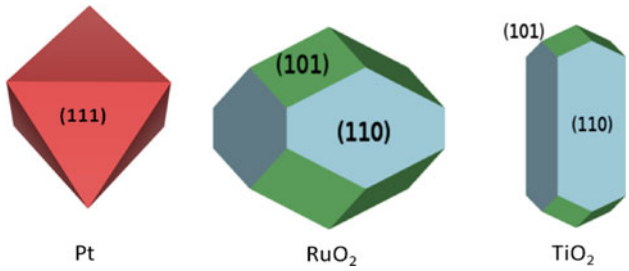

Fig. 5 Wulff construction for typical nanoparticles of fcc metals and two oxides with rutile structure

then the surface energy, under oxygen-rich or -lean conditions or with other compounds like CO [58], can be investigated instead of the raw value. The estimation of the surface free energy at a given temperature and pressure can be addressed through first-principles thermodynamics [59], thus adding extra degree of freedoms (and another source of error linked to the ideal gas models employed to account for temperature and pressure effects). This methodology includes the effect of the surroundings through the computation of the corresponding surface Gibbs free energies, by introducing the reaction temperature and the pressures or concentrations of the environment. These constructions are more approximated than the static calculations described before, but provide an insight on the real state of the catalyst that otherwise would be very difficult to determine under experimental conditions; when a sufficiently large pool of configurations is taken into account, a good description of the surface state is obtained. Recent examples on the nature of the self-poisoned Deacon catalyst have pointed out the full coverage of RuO_2 surfaces, which might in turn be important for the further development of the reaction. In the Deacon process, coverage effects make surface reoxidation the rate-determining step [60]. This implies that, when growing under different conditions, the nature of the exposed metals is changed. Therefore, instead of the surface energy for the clean surface, γ, that of the environment acting on it N_k, $\gamma_j(N_k)$, shall be used. The modified equations look then as follows:

$$\Delta G_i = \sum_j \gamma_j(N_k) O_j.$$

Finally, when considering real systems, the role of the interface between different parts (e.g. metal–oxide junctions or oxide–oxide interactions) should also be included within the Wulff construction. As one of the surfaces will be affected by the interaction with the support, symmetric structures will no longer exist, leading to differently wetting types of particles. The wetting equation derived by Young can be written in terms of the new surface energy at the interface between the cluster and

the carrier, γ and the clean reference, γ_0. Taking into account the interaction energy per surface, $\frac{\Delta E}{O}$, the equation reads as follows [61]:

$$\frac{\gamma}{\gamma_0} = \frac{(\gamma_{\text{int}} - \gamma_0)}{\gamma_0} = 1 + \frac{\Delta E}{O\gamma_0}.$$

In turn, the state of the carrier can be affected by the presence of reducing or oxidising environments that modify the quality of the surface (i.e. number of oxygen vacancies) such as for Cu/ZnO [62], or by the presence of water [63]. Furthermore, on some of the carrier surfaces, special active places for nucleation might exist due to the preparation methods [64].

Once the electronic structure is obtained, the different contributions to the activity and selectivity of a given reaction can be calculated in an isolated manner, employing the tools from first principles applied to slabs, and weighting the contributions corresponding to different facets [60]. In principle, the surface amount can be identified in the Wulff construction and then the reaction evaluated and added up. It might result that one of these high energy facets is more active or more selective and thus would be more interesting to show to a larger extent. While this result is important by itself, sometimes this design parameter cannot be employed as the Wulff construction is a thermodynamic sink and the nanoparticle structure will end up being of this kind.

Although the Wulff construction constitutes the simplest model to describe the structure of a nanoparticle, it has several drawbacks related to the lack of information of defects or low-coordinated sites, together with the fact that only nanoparticles that share the same crystal lattice than the bulk can be retrieved. More detailed thermodynamic investigations in the literature have accounted for unusual metal coordinations. Those models can provide a wide description of the morphologies and even phase diagrams, which can then be compared to tomographic experiments [65–68]. Still, they are being developed and do not consider environment effects, which in heterogeneous catalysis turn out to be more important.

In some cases, as a consequence of adopting different preparation methods controlled by kinetics, new crystal structures that would be metastable under other conditions might be the ground state. A beautiful example is Co nanocrystals, for which a different packing configuration, known as the ε crystal, has been shown. Formation of ε-Co is only possible by solution-phase chemistry, namely organometallic route, and generally using a combination of tight binding ligands or surfactants [69]. As this liquid route is not thermodynamically controlled, the surfactants might change the energetics by binding tightly around the growing crystal and the dissolved Co atoms. This is paradigmatic but in the small range confinement might allow magnetization, availability of different spin orderings, or other particular properties. On this issue, calculations are difficult as they need to assess varied structures in order to understand the nucleation and this task is cumbersome [70].

A good example of the complexity that can affect the theoretical study of nanoparticles, is given by Co and Fe containing clusters. Experiments have shown that such Fe- or Co-based nanoparticles form mixed oxides with rather undefined stoichiometries [71, 72]. Even if they keep an important magnetic moment useful during the separation process, the variable oxygen content adds an extra difficulty to the simulations. Actually, DFT-based calculations for Fe oxides have shown the large complexity in assessing properly even only the electronic structure of such strong-correlated systems. Special care shall be taken in correcting the SIE through DFT + U methods. The coupling between spin and orbital moments leads to intricate electronic structures that depend on the U value. Thus, the present theoretical models cannot yet be employed as black-boxes for this type of calculations [73, 74]. In summary, for some nanoparticles in the form of mixed oxides, to address the issue of the nature, stoichiometry, surface termination, dispersion and stability is still a challenge.

3.2.2 *Activity*

In many cases, when employing nanoparticles, a strong dependence of the activity on the number of atoms is found. The paradigmatic clear example for this corresponds to the activity of gold nanoparticles. While gold is known to be completely inert, when prepared as small particles usually between 2 and 3 nm in diameter, it presents an enhanced activity for oxidation and hydrogenation reactions [75, 76]. In the scalable regime, catalytic properties are closely linked to the large number of low-coordinated sites on these compounds compared to the total number of atoms. Obviously adsorption energies and vacancy formation energies (i.e. either molecule or site activation) do depend on the coordination number and accordingly, the larger the relative number of sites, the better the reactivity.

The case of sponges and membranes is particularly interesting because, under certain conditions, some metals can change their structure by incorporating a large amount of a second compound and obviously these properties might change when nanoparticles are considered. This is the case of Pd for which hydrides are easy to obtain [77]. The contribution of the hydride phase depends on the environment [78]. The hydrogenation capacity acts as a buffer if solvents are present, like in the hydrogenation of alkynes in the presence of alkenes through the Lindlar catalyst; in fact it

reduces the amount of hydrogen that is in contact with the metal surface, thus allowing the use of selectivity modifiers as quinoline, that would not be stable otherwise [79]. This kind of cooperative chemistry which relies on multiple elements to achieve a single property is very common in liquid-phase chemistry, but the implications at high pressure conditions or even electrochemical conditions have been less explored. Interestingly enough, some experiments have indicated that there is a difference in the storage ability when reaching the nanosize that enhance the activity in the hydrogenation of large olefins [80].

3.3 The Role of Surfactants

Wet synthesis methods usually employ soft-templates to control the shape of nanoparticles. These procedures are highly flexible and can generate a large number of morphologies. Due to their nature, only few examples have been reported in the heterogeneous catalysis literature. In most cases this can be attributed to structural properties. An example was presented by Häkkinen and co-workers [81], showing the structure of a capped nanoparticle as a function of a sulphide-based surfactant. However, the model did not include solvent effects. The final geometry of the nanocluster is thus given by a delicate balance between the metal–metal, surfactant–metal and surfactant–surfactant interactions. In a way, the effect of the surfactant might be seen as the modification of the surface energies, as described in the Wulff model in the previous section [58].

Yet another example on the electronic structure modifications induced by surfactants was presented for the materials that can be employed in quantum dots. Calculations on CdSe nanoparticles show that it is possible to fine tune the HOMO–LUMO gap by adsorbing different types of surfactants without changing the structure (i.e. the local coordination number of the surface atoms). The dipolar moment of the head adsorbed on the surface can slightly modify the position of the states, already different from the bulk values due to the final nature of the structure, resulting in more suitable light adsorption [82].

In the case of wet synthesis, the reactions take place in a liquid phase, where a number of solutes are presented. The system contains at least the metal salt out of which the nanoparticles are generated, the reductive agent, and the surfactant. In many cases morphology modifiers are also added. Such kind of synthesis exhibits a large degree of control for particles with interesting properties in sensing. The enhanced plasmons are then based on the asymmetry that can be induced by controlling the growth. Calculations with charged fragments present some difficulties but in principle a Born cycle can be prepared with different contributions. An example is shown in the cleaning of gold ores which is the inverse of the process [83].

In understanding the activity when surfactants have not been removed, the issue of diffusion to the active site (for reactants) and out to the liquid phase (for products) might be fundamental and compromise the activity of the catalyst. Transport problems of this kind are usually overlooked but they need to be addressed properly if the chemical properties are to be studied [84].

4 Understanding Activity

Heterogeneous catalysis as performed by nanoparticles usually follows the well-known Langmuir–Hinshelwood reaction scheme. This mechanism states that reactants are bonded to the surface, either to competitive sites or to different positions. Adsorption weakens the internal bonds reducing their strength and thus favouring either dissociative or associative paths. Then the activated reactants can interchange some of their fragments and generate the products that can leave the surface. There are several implications to the mechanism described above. First, coordination to the surface will depend on the properties of the nanoparticles, which in principle are different for the extended metals. As nanoparticles exhibit a larger number of low-coordinated sites, they are more prone to adsorb reactants, therefore they are believed to be more active than the rest of the surface. However it also implies the ability to break unwanted bonds, form impurities on the surface, get preferentially decorated, generate cokes or carbides and ultimately ruin the activity by poisoning.

The ability of different heterogeneous catalyst for a given reaction has been proven to follow the Sabatier principle, which states that the maximum activity for a given reaction is obtained by a balance at which relevant species are not coordinated too weakly (as then none would be adsorbed) or too strongly (as the surface would be poisoned). Therefore for large interaction energies, the catalyst surface is permanently blocked by one of the species of the catalytic cycle (either reactants, products or intermediates), while in the opposite case, when the binding energy is too small, the activation does not occur as the catalyst is empty for long time, rendering it inactive. For instance, this can be transferred to the activity of gold. When prepared as a surface, the binding energies of many atoms or molecules (particularly O_2) is far too low, therefore no oxidations can occur on those surfaces. On the contrary, if nanoparticles are prepared, the binding energy of oxygen lays on the highest activity point of the volcano curve representing the Sabatier principle, and thus maximum activity is retrieved in oxidation processes even at low temperatures. Alternatively, if a molecule or a fragment is easily adsorbed to the surface, it will adsorb even stronger to the defects. This can be explained by the d-band

		Nanoparticle	Supported Nanoparticle	Surfactant covered nanoparticle
Electronic effects	Low-coordinated sites	Yes	Yes	Likely blocked
	Charge effects	No	Yes (confined)	Yes
Geometric effects	Fluxionality	Yes	Yes	Yes
	Exposed facet	Yes	Yes	Yes
	Ensemble	Yes	Yes	Yes
Properties	Storage	Yes	Yes	Yes
	Transport	No	Yes	Yes

Fig. 6 List of potential modifications induced by the individual nanoparticles, adsorbed and surfactant-covered ones

model [85]. Therefore, small nanoparticles would be likely completely poisoned by these strongly interacting fragments rendering them inactive. As a general rule the binding energies of fragments to the isolated atoms (or even when present as complexes) are higher than for the metal nanoparticles followed by regular surfaces, resulting in a way to improve activity (for inactive metals) or poison them (for already active metal surfaces).

Figure 6 presents the link between the different systems summarized in Fig. 1, ranging from individual nanoparticles, supported or surfactant-covered ones. Theoretical simulations hold the key to answer the role of different phases, as simplified hierarchical models can be constructed adding complexity in steps. For instance, modifications in the structure of clusters with respect to bulk can be summarized mainly in two terms: electronic and geometric. The final state of the cluster either as a free nanoparticle, or supported or surfactant covered, might affect the number of low-coordinated sites (likely blocked in the surfactant preparations). Other electronic effects can be charge modifications likely induced by the presence of a support (although these are smoothed out for medium size nanoparticles) or by the presence of the surfactant. With respect to geometric effects, the fluxionality, exposed facets and ensembles, depend on the formation on nanoparticles, carriers and/or surfactants. Such electronic and geometric modifications affect the storage and transport properties to a large extent especially when interfaces are present.

An example of the transferability of the theoretical procedures to both organometallic homogeneous and heterogeneous catalysts has been recently presented. Selective activation of alkynes in the presence of alkenes on gold systems constitutes a paradigm. Experiments for nanoparticles have shown the exquisite selectivity for the hydrogenation of alkyne groups in the presence of alkenes. Alkynophilicity has also been termed in the field of homogeneous catalysis, indicating the preference in the activation of these C≡C bonds in multifunctionalized molecules. Theoretical modelling has found that on the nanoparticles there is a preferential adsorption of triple C–C bonds. This is due to the presence of two π-states that are able to interact with the high energy states of low-coordinated sites on the metal nanoparticles. For the homogeneous catalysts, states of the correct symmetry are not available for both π states resulting in lower energy interactions. This explains why the adsorption energy is more favourable for the alkene and how the activity cannot be expressed directly in the same manner for the homogeneous and heterogeneous cases [86]. Our results are not conclusive at this stage, while a wide set of experiments performed in the groups of Toste and co-workers [87], found some type of correlation between tridimensional surfaces and surfactant-covered clusters.

As for oxides the reaction can even be more complex. Our investigations have found that the tridimensional nature of the catalysts and its curvature can have a role in the activity of oxygen species on polyoxometallates. Activation of species that require two sites depends on spatial 3D configuration. Clearly, the structure for the atoms in the nanoparticles can have curvatures different from those on planar surfaces, leading to different activities and selectivities [88].

5 Conclusions

Theoretical simulations based on the extensive application of DFT coupled to models like first-principles thermodynamics and the Wulff construction, can give a good description of several aspects of the nature, structure, shape and surface stoichiometry of these nanoparticles under

different environments. Although these methods are very powerful in the sense that a hierarchical knowledge can be retrieved for the role of the different contributions, many challenges remain ahead of us. On one side non-equilibrium structures, or with many configurations and those with strong coupling between composition and electronic structure, are difficult to address in part due to the deficiencies associated to DFT and in part due to the large number of structures that need to be to be surveyed. On the other hand, the study of the reactivity of these particles can be strongly modified by adding diverse degrees of freedom, such as including supports, solvent, surfactants or a combination of all these issues. Even for those extremely complex cases, theoretical models represent a consistent way to identify leading contributions and fundamental property descriptors, which can be employed to address the synthesis of new, more industrially appealing compounds.

Acknowledgments We thank the MICINN for projects CTQ2009-07753/BQU, CSD2006-0003, ERC-Starting Grant Bio2chem-d 2010-StG-258406, and BSC-RES for providing generous computational resources.

References

1. Chorkendorff I, Niemantsverdriet JW (2003) Concepts of modern catalysis and kinetics. Wiley-VCH, Weinheim
2. McDonald D, Hunt LB (1982) A history of platinum and its allied metals. Johnson Matthey, London. Distributed by Europa Publications
3. Astruc D (2008) Nanoparticles and catalysis. Wiley-VCH, Weinheim
4. Heiz U, Sanchez A, Abbet S, Schneider WD (1999) J Am Chem Soc 121:3214
5. Tong X, Benz L, Kemper P, Metiu H, Bowers MT, Buratto SK (2005) J Am Chem Soc 127:13516
6. Sterrer M, Risse T, Giordano L, Heyde M, Nilius N, Rust H-P, Pacchioni G, Freund H-J (2007) Angew Chem Int Ed 46:8703
7. Pérez-Juste MJ, Mulvaney P, Liz-Marzán LM (2008) Chem Soc Rev 37:1783
8. López N, Almora-Barrios N, Carchini G, Błoński P, Bellarosa L, García-Muelas R, Novell-Leruth G, García-Mota M (2012) Catal Sci Technol 2:2405–2417
9. Hafner J (2008) J Comput Chem 29:2044
10. Van Doren VE, Van Alsenoy C, Geerlings P (2001) Density functional theory and its application to materials: Antwerp, Belgium, 8–10 June 2000. American Institute of Physics, Melville
11. Perdew JP, Ruzsinszky A, Tao J, Staroverov VN, Scuseria GE, Csonka GI (2005) J Chem Phys 123:062201
12. Kohn W, Sham LJ (1965) Phys Rev 140:1133–1135
13. Ceperley DM, Alder BJ (1980) Phys Rev Lett 45:566–569
14. Haas P, Tran F, Blaha P (2009) Phys Rev B 79:085104
15. Da Silva JLF, Stampfl C, Scheffler M (2003) Phys Rev Lett 90:066104
16. Darling GR, Holloway S (1995) Rep Prog Phys 58:1595–1672
17. Langreth DC, Mehl MJ (1981) Phys Rev Lett 47:446–450
18. Hammer B, Hansen LB, Nørskov JK (1999) Phys Rev B 59:7413–7421
19. Honkala K, Hellman A, Remediakis IN, Logadottir A, Carlsson A, Dahl S, Christensen CH, Nørskov JK (2005) Science 307:555–558
20. Perdew JP, Chevary JA, Vosko SH, Jackson KA, Pederson MR, Singh DJ, Fiolhais C (1992) Phys Rev B 46:6671–6687
21. Perdew JP, Burke K, Ernzerhof M (1996) Phys Rev Lett 77:3865–3868
22. Perdew JP, Ruzsinszky A, Csonka GI, Vydrov OA, Scuseria GE, Constantin LA, Zhou XL, Burke K (2008) Phys Rev Lett 100:136406
23. Armiento R, Mattsson AE (2005) Phys Rev B 72:085108
24. Wu ZG, Cohen RE (2006) Phys Rev B 73:235116
25. Godby RW, Schluter M, Sham LJ (1986) Phys Rev Lett 56:2415–2418
26. Rinke P, Qteish A, Neugebauer J, Freysoldt C, Scheffler M (2005) N J Phys 7:126
27. Kelkkanen AK, Lundqvist BI, Nørskov JK (2009) J Chem Phys 131:046102
28. Da Silva JLF, Ganduglia-Pirovano MV, Sauer J, Bayer V, Kresse G (2007) Phys Rev B 75:045121
29. Anisimov VI, Aryasetiawan F, Lichtenstein AI (1997) J Phys Condens Matter 9:767
30. Perdew JP, Kurth S, Zupan A, Blaha P (1999) Phys Rev Lett 82:2544–2547
31. Moroni EG, Kresse G, Hafner J, Furthmüller J (1997) Phys Rev B 56:15629–15646
32. Becke AD (1993) J Chem Phys 98:5648–5652
33. Stephens PJ, Devlin FJ, Chabalowski CF, Frisch MJ (1994) J Phys Chem 98:11623–11627
34. Paier J, Hirschl R, Marsman M, Kresse G (2005) J Chem Phys 122:234102
35. Paier J, Marsman M, Kresse G (2007) J Chem Phys 127:024103
36. Adamo C, Barone V (1999) J Chem Phys 110:6158–6170
37. Heyd J, Scuseria GE, Ernzerhof M (2003) J Chem Phys 118:8207–8215
38. Franchini C, Bayer V, Podloucky R, Paier J, Kresse G (2005) Phys Rev B 72:045132
39. Franchini C, Podloucky R, Paier J, Marsman M, Kresse G (2007) Phys Rev B 75:195128
40. Harl J, Kresse G (2009) Phys Rev Lett 103:056401
41. Dion M, Rydberg H, Schroder E, Langreth DC, Lundqvist BI (2004) Phys Rev Lett 92:246401
42. Lee K, Murray ED, Kong LZ, Lundqvist BI, Langreth DC (2010) Phys Rev B 82:081101
43. Grimme S (2006) J Comput Chem 27:1787–1799
44. London F (1937) Trans Faraday Soc 33:826
45. Błoński P, López N (2012) J Phys Chem C 116:15484–15492
46. Gaussian. www.gaussian.com. Accessed 4 Nov 2012
47. GPAW. https://wiki.fysik.dtu.dk/gpaw/. Accessed 4 Nov 2012
48. Abbet S, Sanchez A, Heiz U, Schneider WD, Ferrari AM, Pacchioni G, Rösch N (2000) J Am Chem Soc 122:3453–3457
49. Błoński P, Hafner J (2012) J Chem Phys 137:044710
50. Wales DJ, Scheraga HA (1999) Science 285:1368–1372
51. Hirsch A, Chen ZF, Jiao HJ (2000) Angew Chem Int Ed 39:3915
52. Yoon B, Hakkinen H, Landman U, Worz AS, Antonietti JM, Abbet S, Judai K, Heiz U (2005) Science 307:403–407
53. Lei Y, Mehmood F, Lee S, Greeley J, Lee B, Seifert S, Winans RE, Elam JW, Meyer RJ, Redfern PC, Teschner D, Schlogl R, Pellin MJ, Curtiss LA, Vajda S (2010) Science 328:224–228

54. Torres D, López N, Illas F, Lambert RM (2007) Angew Chem Int Ed 46:2055–2058
55. Kleis J, Greeley J, Romero NA, Morozov VA, Falsig H, Larsen AH, Lu J, Mortensen JJ, Dulak M, Thygesen KS, Nørskov JK, Jacobsen KW (2011) Catal Lett 141:1067–1071
56. Soler JM, Artacho E, Gale JD, García A, Junquera J, Ordejón P, Sánchez-Portal D (2002) J Phys Condens Matter 14:2745–2779
57. Wulff WG (1901) Z Kryst Miner 34:449–530
58. Barmparis GD, Remediakis IN (2012) Phys Rev B 86:085457
59. Wang XG, Chaka A, Scheffler M (2000) Phys Rev Lett 84:3650–3653
60. Teschner D, Farra R, Yao LD, Schlogl R, Soerijanto H, Schomacker R, Schmidt T, Szentmiklosi L, Amrute AP, Mondelli C, Pérez-Ramírez J, Novell-Leruth G, López N (2012) J Catal 285:273–284
61. López N, Nørskov JK, Janssens TVW, Carlsson A, Puig-Molina A, Clausen BS, Grunwaldt JD (2004) J Catal 225:86–94
62. Helveg S, Lopez-Cartes C, Sehested J, Hansen PL, Clausen BS, Rostrup-Nielsen JR, Abild-Pedersen F, Nørskov JK (2004) Nature 427:426–429
63. Lodziana Z, Topsoe NY, Nørskov JK (2004) Nat Mater 3:289–293
64. Wischert R, Laurent P, Coperet C, Delbecq F, Sautet P (2012) J Am Chem Soc 134:14430–14449
65. Barnard AS (2006) J Phys Chem B 110:24498–24504
66. Barnard AS, Curtiss LA (2007) J Mater Chem 17:3315–3323
67. Barnard AS, Young NP, Kirkland AI, van Huis MA, Xu H (2009) ACS Nano 3:1431–1436
68. Li ZY, Young NP, Di Vece M, Palomba S, Palmer RE, Bieloch AL, Curley BC, Johnston RL, Jiang J, Yuan J (2008) Nature 451:46–48
69. Dinega DP, Bawendi MG (1999) Angew Chem Int Ed 38: 1788–1791
70. Fjermestad T (personal communication)
71. Lagunas A, Payeras AMI, Jimeno C, Pericàs MA (2006) Chem Commun 12:1307–1309
72. Glaria A, Kahn ML, Lecante P, Barbara B, Chaudret B (2008) ChemPhysChem 9:776–780
73. Spiris N, Barbasz J, Lodziana Z (2006) Phys Rev B 74:155423
74. Lodziana Z (2007) Phys Rev Lett 99:206402
75. Haruta M (2005) Nature 437:1098–1099
76. Hashmi A, Stephen K, Hutchings GJ (2006) Angew Chem Int Ed 45:7896–7936
77. Manchester FD, San-Martin A, Pitre JM (1994) J Phase Equilib 15:62
78. García-Mota M, Bridier B, Pérez-Ramírez J, López N (2010) J Catal 273:92–102
79. García-Mota M, Gomez-Diaz J, Novell-Leruth G, Vargas-Fuentes C, Bellarosa L, Bridier B, Pérez-Ramírez J, López N (2011) Theor Chem Acc 128:663–673
80. Doyle AM, Shaikhutdinov SK, Jackson SD, Freund HJ (2003) Angew Chem Int Ed 42:5240–5243
81. Lopez-Acevedo O, Kacprzak KA, Akola J, Häkkinen H (2010) Nat Chem 2:329–334
82. Yang S, Prendergast D, Neaton JB (2012) Nano Lett 12:383–388
83. Gómez-Díaz J, Honkala K, López N (2010) Surf Sci 604: 1552–1557
84. Herves P, Perez-Lorenzo M, Liz-Marzán LM, Dzubiella J, Lu Y, Ballauff M (2012) Chem Soc Rev 41:5577–5587
85. Hammer B, Morikawa Y, Nørskov JK (1996) Phys Rev Lett 76:2141–2144
86. García-Mota M, Cabello N, Maseras F, Echavarren AM, Pérez-Ramírez J, López N (2008) ChemPhysChem 9:1624–1629
87. Witham CA, Huang WY, Tsung CK, Kuhn JN, Somorjai GA, Toste FD (2010) Nat Chem 2:36–41
88. López N, Novell-Leruth G (2010) Phys Chem Chem Phys 12: 12217–12222

Catalysis Science & Technology

Cite this: *Catal. Sci. Technol.*, 2012, **2**, 2405–2417

www.rsc.org/catalysis

PERSPECTIVE

State-of-the-art and challenges in theoretical simulations of heterogeneous catalysis at the microscopic level†

Núria López,*[a] Neyvis Almora-Barrios,[a] Giuliano Carchini,[a] Piotr Błoński,[a] Luca Bellarosa,[a] Rodrigo García-Muelas,[a] Gerard Novell-Leruth[b] and Mónica García-Mota[c]

Received 6th June 2012, Accepted 13th July 2012
DOI: 10.1039/c2cy20384g

Theoretical simulations of systems that represent heterogeneous catalysts constitute one of the main tools in the research for new catalytic materials. Theory plays a role in the three stages of the development ladder: characterisation, understanding and prediction. Due to the complexity of the computational methods, there is a strong need to integrate different models and cover the relevant scales in heterogeneous catalysis. This requirement constitutes an important drawback as scientists need training in several aspects of the problem including chemical, physical and engineering views of the modelling while keeping the experimental and industrial interests and needs in perspective. Here we present some of the latest developments in the field of theoretical simulations at the microscopic level while illustrating suitable examples that show how theory can shed light on several aspects of characterisation, activity, selectivity and long-term stability.

1 Introduction

The Holy Grail of theoretical simulations is the determination of a suitable stoichiometry and corresponding structures for a particular performance in a chemical process and the route to synthesise the active phase. The main goal of theory is to provide a deeper insight into the relation between structure and any of the three key parameters: activity, selectivity, and stability. The use of a black box set of programs containing all the theoretical models would be very practical, as that could shorten the time to commercialise new catalytic applications by designing suitable compounds and it would provide valuable suggestions for synthesis. At present, computational materials science and heterogeneous catalysis still have to overcome a large number of hurdles to reach this goal. Although the computational power accessible to theoretical simulations in heterogeneous catalysis has increased exponentially since mid-nineties and new tools and algorithms are being developed continuously, many important parts are still lacking in the present simulations. Moreover, not everything can or should be computed. Sometimes, the information stored in our detailed reaction networks may end up with a large number of elementary steps that are meaningless, or configurations with little, if any, role in the total reaction process and thus that do not contribute significantly to our overall knowledge. In this case, we need strategies to reduce the number of calculations and the computational effort required. Furthermore, the use of a single theoretical approach is not always enough and the coupling between different models is required. Particular effort needs to be devoted to the integration between different time and length scales. Therefore, the electronic structure obtained through Density Functional Theory (DFT) constitutes the keystone on which many of the longer space or time scale phenomena are built. The crucial role of DFT can be seen in Fig. 1 as adapted from the work of Vlachos.[1,2] It shows how

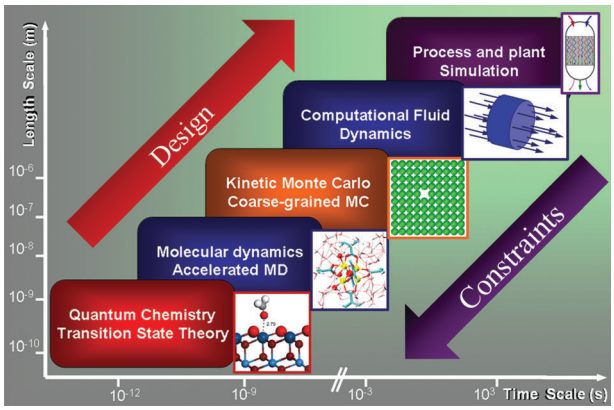

Fig. 1 The time and length scales for different simulation tools. Adapted from Vlachos.[1,2]

[a] *Institute of Chemical Research of Catalonia (ICIQ), Av. Països Catalans 16 – 43007 Tarragona, Spain. E-mail: nlopez@iciq.es; Fax: +34 977920231; Tel: +34 977920200 (Ext. 307)*
[b] *Department of Chemistry, CICECO, University of Aveiro, P-3810-193 Aveiro, Portugal*
[c] *Department of Chemical Engineering, Stanford University, Stanford, CA 94305, EEUU, USA*

† This article is dedicated to the memory of Dr Jaime Gómez-Díaz who did his PhD in our group (2007–2011).

the hierarchical structure of simulations in material science can easily be transferred to the theory in heterogeneous catalysis. The complexity of the catalytic phenomena requires the description of multiple time and length scales and thus, an intelligent way of adapting the relevant information from lower, more complete steps is crucial. In any case the detailed electronic structures need to be summarised and packed in a useful way for more qualitative approaches that, on the other hand, can reach larger time and space scales relevant in process and plant simulations.

Recently, several reviews have been presented in the field of simulations in the lowest space and time scales. Special effort has been dedicated to describe all the properties of materials,[3] to use linear-scaling relationships and screening[4,5] and lately to reach larger scales.[2,6] In the early days, the study of adsorption and the reaction energy profiles were determined for direct reaction that could convert reactants into products on a single surface. Nowadays, computational techniques can address not only the activity of different materials, but also the selectivity and the stability against reaction conditions. Desirable future goals would be (i) the implementation of filters based on descriptors to discard some of the targeted materials so that they fulfil industrial or laboratory requirements, and (ii) the ability to gather this information into usable databases for future data-mining.[5]

In the present perspective we aim at reviewing critically the latest achievements in the field, giving experimentalists a proper guide to assess the minimum requirements for the theoretical models and techniques that can be considered as reliable. In a second step, we will address the challenges theoretical simulations face.

2 State-of-the-art

Density functional theory

Density Functional Theory has achieved great success in computational catalysis. However, bridging gaps in the temperature, pressure, time and length scales accessible to DFT-calculations and those characteristic for real-world experiments still remains a challenge, even when using the most sophisticated codes. Moreover, the accuracy and efficiency of these methods depend on several technical choices,[7] for example an exchange-correlation functional, the basis-set for the expansion of the Kohn–Sham orbitals and algorithms to solve the corresponding equations. The choice of exchange-correlation functionals and the completeness of the basis-set determine the accuracy, whereas the numerical algorithms determine the efficiency of the calculations. The minimum functional requirements for different systems and properties are summarised in Fig. 2. The hierarchy of exchange-correlation functionals that allows us to achieve an increasing accuracy of DFT results has been dubbed by John Perdew as "the Jacob's ladder of DFT".[8]

The lowest rung of this ladder is the so-called Local Density Approximation (LDA),[9] where the exchange-correlation energy (E_{xc}) for a homogeneous electron gas of the same density, as obtained from quantum Monte-Carlo simulations,[10] is also applied to non-homogeneous situations. LDA has succeeded in solving many bulk[11] and surface problems. However, for chemical reactions occurring at surfaces, LDA usually leads to adsorbate over-binding.[12] Also, the potential-energy profiles for dissociations of diatomic molecules on metallic surfaces are badly characterised by LDA.[13]

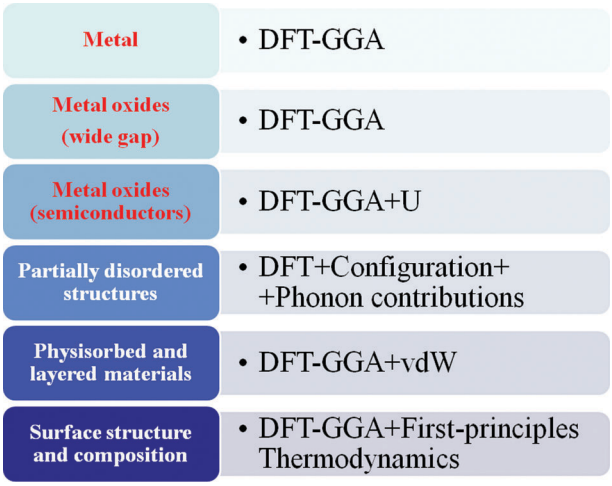

Fig. 2 Minimum density functional theory approximations for a set of catalytic materials and their characteristic properties.

The description is improved in the Generalised Gradient Approximation (GGA),[14,15] the second rung of the Perdew's ladder, which includes a dependence of E_{xc} on the local gradient of the electron density. The GGA heals the over-binding tendency of the LDA (although, with an inclination to over-correct).[16] Moreover, for many chemical reactions, the GGA allows us to achieve sufficient accuracy.[17] Indeed, this functional constitutes the proper description level for most of the reactions on metals, see Fig. 2. Several forms of the GGA have been proposed in the literature: PW91,[18] PBE,[19] revised PBE,[16] PBEsol,[20] MA05,[21] and WC.[22] PW91 and PBE are by far the most commonly used functionals. However GGA's have two serious shortcomings. The first one is that they do not account for van der Waals (vdW) interactions that result from dynamical correlations between fluctuating charge distributions.[7] The second problem, which arises from the approximate form of the exchange-correlation term, is the non-zero interaction of a single electron with its own density, which is known as self-interaction error (SIE). SIE is the cause of many of the failures of approximate functionals, such as too small band gaps,[23,24] wrong dissociation energies for molecules,[25] and a bad description of systems with localised f electrons. One approach to reduce SIE is the DFT + U method, in which Hubbard-type terms are added to account for the on-site Coulomb interactions in the localised d or f orbitals. The Hubbard parameter (U) can be fitted so that it reproduces experimental band-gaps, geometries or other properties. Unfortunately, U is not free from some arbitrariness, as fitting the parameter for one of the experimental terms does not ensure that the rest will be adequately reproduced. Some examples of oxide compounds that require this level of theoretical approximation are NiO and Ce_2O_3.[26] Therefore this is the minimum relevant description for reducible oxides, Fig. 2.

Meta-GGA including higher-order terms of the gradient of the local kinetic energy density is the third rung on the DFT ladder.[27]

Nevertheless, meta-GGA does not lead to a systematic improvement over the GGA, as shown by the ambiguous results for the adsorption of small molecules on transition- and noble-metal surfaces[7] and for the stepwise hydrogenation of benzene to cyclohexene on a Ni(111) surface.[28]

The next rung is represented by hybrid functionals that mix exactly, *i.e.* Hartree–Fock (HF) and DFT exchange, and describe correlation at the standard DFT level. The most popular hybrid in molecular chemistry is the B3LYP functional,[29,30] which combines LDA with HF exchange. The B3LYP functional achieves a very high accuracy for almost all properties of small molecules, but it fails when applied to metals and semiconductor solids, because the correlation part of the functional is incorrect in the homogeneous electron gas limit.[31,32] Extended systems are better represented by other hybrids such as the PBE0[33] and HSE03 functionals.[34] The results obtained for solids are unclear. PBE0 and HSE03 overall improve predictions for lattice parameters and bulk moduli of most solids, as well as for the band gaps in semiconductors and insulators,[31,32] moreover these hybrids offer an excellent description of insulating antiferromagnetic rare-earth and transition-metal oxides where the GGA failed to reproduce them correctly.[35,36] Atomisation energies, as well as magnetic metals, are described with a higher degree of accuracy through standard PBE.[31,32] In the latter case, hybrid functionals overestimate the exchange splitting and the magnetic moments, and broaden the *d*-bands,[37] therefore the overall description of the adsorbate–substrate complexes is not improved.[38] Another drawback of the hybrid-functionals is their very high computational cost.[31] Thus, climbing up to the highest rung of DFT ladder does not guarantee a solution to all problems but hybrids reduce the SIE of pure DFT due to the mixture of a certain amount of exact exchange.[16]

As it has already been mentioned, dispersion (van der Waals) interactions are missing in standard DFT calculations. At present, a method that accounts for the vdW energy seamlessly and accurately is the random-phase approximation (RPA), combined with the adiabatic connection and fluctuation dissipation theorem (ACFDT).[39] Since this method is computationally demanding, it is mostly restricted to small systems and can serve as a benchmark for assessing the reliability of less sophisticated approaches. Lundqvist *et al.*[40,41] proposed a non-local correlation functional that accounts approximately for dispersion interactions. Results achieved with a nonlocal vdW-DFT correlation functional depend on the judicious combination of the local and non-local contributions to the functionals. A simpler dispersion correction is offered by the semi-empirical force fields of Grimme *et al.* (DFT-D2).[42,43] In this method, the dispersion contributions are calculated by pair-wise interactions from the London formula[44] leading to the $\Sigma C_6/R^6$ term. Recently, Bučko *et al.*[45] applied Grimme's method to a large number of solids showing a wide range of chemical bonds such as molecular, ionic and covalent. This illustrates that Grimme's approach can be used for arbitrary systems irrespectively of the nature of dominant interactions. Moreover, a careful choice of the substrate interaction coefficient C_6[46,47] provides a good starting point to study the adsorption of molecules and films on conducting metal surfaces[48] and, potentially, on ionic or semiconducting solids.[47] Thus the Grimme or similar approaches constitute the minimum meaningful theory level when van der Waals interactions are important, *i.e.* in layered compounds (as PtO_2), or in physisorption, see Fig. 2.

As it was mentioned at the beginning of this section, standard calculations refer to systems under vacuum conditions. However, recent progress allows researchers to overcome these restrictions.[48] DFT combined with statistical mechanics in the grand canonical ensemble describes an adsorbate–substrate complex in equilibrium with a reactive atmosphere. Temperature effects are treated as corrections to static total-energy calculations by adding the vibrational free energy to the total energy from DFT calculations or using first principles canonical molecular dynamics simulations.[49]

Models for the materials

The materials involved in heterogeneous catalysis present a wide range of properties. Metals, semiconductors and insulators are employed in many cases in mixed configurations, thus adding an extra degree of complexity; hence not in all cases the same electronic structure approximation is optimum for the different constituents, see Fig. 2. Moreover, materials can be amorphous or crystalline, or have grain boundaries or porous structures that render the systematic assessment of their properties difficult. In general, different types of materials are studied by several approaches: while the chemistry of amorphous systems relies on the very local configurations that can be achievable, the description of crystalline materials is mostly based on their periodicity. The study of such materials has advanced very significantly and as a first approximation some of the properties of amorphous structures can be simplified to the periodic ones. For this reason we will focus on them.

A problem of DFT with periodic boundary conditions is caused by the complex lattices with several potential structures and/or structural disorder due to finite temperatures. In the first case, the as-calculated energies do not contain thermal contributions to the free energy that are needed for some delicate cases when multiple minima lie close in energy. A good example of this is the re-evaluation of the structure of dawsonite ($MAlCO_3(OH)_2$ M = Na, K, NH_4^+) compounds.[50] In this particular case, the experimental determination of the crystal structure is performed at finite temperatures at which the ammonium cations might rotate. The introduction of this thermal contribution is usually done by accounting for two different terms the zero-point vibrational energy and the contribution to the energy through the phonon distribution in the form of a summation.[50] This approach is also listed in Fig. 2, and constitutes the minimum description when trying to assess structures and reactivity of complex materials with close-lying structures and important phonon effects. Other catalytic solids exhibit some degree of disorder in the crystal site occupancies (this is different from amorphous disorder!). The models employed to deal with this kind of inhomogeneity can be classified into three broad groups:[51] (i) methods in which a sort of average atom is defined. They allow recovering the perfect periodicity as implemented in the virtual crystal approximation (VCA), where the potential felt by electrons is generated by average atoms. (ii) Methods involving a large supercell with a more or less random distribution of ions in the sites. A useful variation of this model is the special quasi-random structure,

where the ion positions in the supercell are chosen to mimic as closely as possible the most relevant near-neighbour pair and multisite correlation functions of the random substitutional alloy.[52] (iii) Multi-configurational supercell approaches, where the site-disordered solids are described as a set of configurations in a supercell representing a piece of the solid (*e.g.* as in ref. 53). This kind of approaches is useful to identify favourable ordering patterns,[54,55] to evaluate the evolution of ion disorder with the temperature,[56] or to examine the segregation of impurities at solid surfaces beyond the dilute limit.[57]

Once bulk structures are determined, selected cuts along the lower Miller index directions are performed and then the surface energy for the faces with different orientations is calculated. The Wulff construction,[58] a simple continuous model, determines that the lowest surface energy will be the most represented in the equilibrium structure of the metal nanoparticles in the catalysts. Extensions to materials covered by surfactant or molecular modifiers have been put forward.[59] However, the Wulff construction presents several approximations: (i) only surface energies are taken into account, *i.e.* the contribution from edges and other defects is overlooked and thus the representation is more accurate for medium size particles; (ii) only equilibrium structures are retrieved. Non-equilibrium structures are much more difficult to assess but, on the other hand, they are also difficult to characterise experimentally, thus this area remains somehow obscure to both experimental and theoretical worlds.

The reactivity of solid materials is usually first studied theoretically on the low Miller index facets that usually show lowest surface energies. This is at odds with the corresponding reactivity as the ability to adsorb new molecules does depend on the number of bonds of the substrate. Still several reasons justify this choice: first of all, these low energy surfaces are the most represented by the Wulff construction; moreover, the unit cells of low-index surfaces tend to be smaller than open surfaces or vicinal ones (so the number of different configurations for adsorbates is smaller and thus the number of possibilities to be investigated are lower) thus it reduces the calculation burden. This is the minimum calculation setup for a simple active phase (Case I) shown in Fig. 3.

In some cases, the adsorption or the activation of reactants on these surfaces is not strong enough, Case II in Fig. 3. This is for instance the case of the dissociative adsorption of nitrogen on Ru surfaces that is the key step in the synthesis of ammonia in the Haber–Bosch process.[17] Early in the investigation of this process, discrepancies between ultra-high vacuum measurements of adsorption and the barriers calculated by DFT were found, but after employing theoretical models containing steps the experimental value was retrieved. The reason for the highest dissociation activity of the open surface was correlated to the presence of B_5 sites that provided a transition state structure where no atoms were shared.[60] Since then, the suitable procedure when investigating a new reaction begins determining molecular and dissociative adsorption on low index surfaces. Then, if the reactivity of the surfaces seems exceedingly poor, the presence of defects is included in the study, usually starting with geometric perturbations, such as low-coordinated sites,[61] atomic vacancies and/or considering the presence of impurities from a secondary metal,[62] or fragments from some of the interacting molecules.[63]

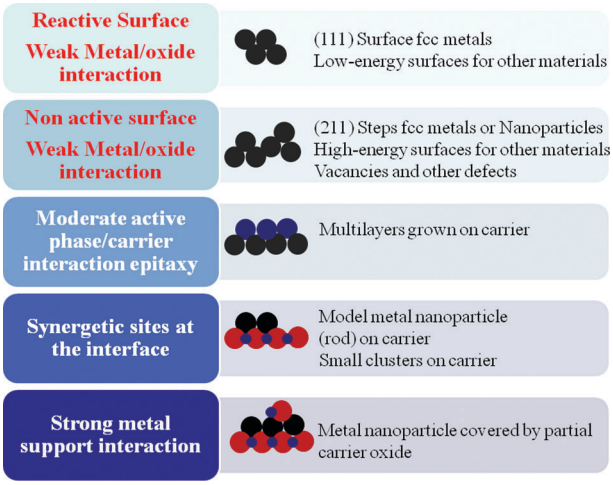

Fig. 3 Computational models for the interaction of metals and oxides (or other supports) as a function of the type of interaction.

With the approaches presented in the previous paragraph the representation of the middle size particles is reasonable, but still two questions remain open. First of all, when modelling finite size nanoparticles, the number of atoms that can be included in the simulations is rather small, few hundred atoms at most. Secondly, the shape of the particles also has a contribution and this is somehow even more difficult to assess. Recently the convergence of the properties with the size has been analysed.[64] Even if the convergence of the metal properties is found at relatively small number of atoms in the cluster, the mobility of the surface atoms generates more dynamic properties as the cohesive energy of the surface atoms is reduced when compared to the bulk. This problem is more acute for metals like Au, for which the melting temperature is quite low.

Although we employ the cluster as a particle of 2–5 nm in diameter, the representation is far from complete. In the preparation of catalysts, there is special interest in obtaining monodisperse samples, at least in research and for characterisation. The aim would be to obtain only particles with a given diameter but this is impossible when employing chemical methods. The alternative, use of physical methods (chemical vapour deposition with charge mass selection)[65] with very detailed separation, is scientifically relevant but not viable. The reasons for that are the high cost and the low surface areas of these model catalysts. Developments are still being made in this regard, and for instance, spray deposition controls particle size much better with smaller deviations.[66] There is a hidden issue that concerns the analysis of the size and shape of the nanoparticles, in general, Transmission Electron Microscopy even in high resolution experiments cannot adequately determine the particles below 1 nm in diameter. The fact that experiments are not accurate enough poses two different problems. In principle, the activity of the catalyst, when linked to the presence of low-coordinated sites, increases when decreasing the particle size as the number of exposed atoms with respect to the total metal content is larger.[67] This is a reason for the preference of low-diameter particles. But for very small nanoparticles, activity is not a continuous function as the electronic structure of small aggregates has a discrete spectrum and their fluxionality (conformational flexibility)

plays a crucial role. This is known as the non-scalable regime where each atom counts. Experiments have shown that for instance CO oxidation is possible for Au_8[68] and Au_{20}, whereas Au_{55} is inert.[69] The analysis of the reactivity of such small clusters does then depend on their electronic structure and, as a consequence, requires a tedious examination and the results from one cannot be extrapolated to the ability of the next.[65] From a theoretical point of view this opens up millions of possibilities, but at the same time it is a never-ending story as it is almost impossible to tailor the properties for all systems.

Another of the major questions when dealing with theoretical simulations in heterogeneous catalysis is the role of the support. Few model systems have been employed and presented in the literature. The problems with these materials are related to the additional demands required by electronic structure calculations. One of them is the need to use an extremely large unit cell to account at the same time for the active nanoparticles and the substrate.[70] Also, as the metal nanoparticles are small their transferability is more compromised. Moreover, the most common carriers are significantly difficult to model. Aluminas,[71] like the γ phase,[72] present unsolved issues; silica also poses problems due to its amorphous nature that cannot be obtained from typical DFT and periodic boundary conditions or in terms of the degree of hydroxylation.

The way the substrate affects the properties of the active phase can be separated from lower to higher interaction, see Fig. 3.[73] For instance, even weakly interacting substrates influence the dispersion and shape of nanoparticles. In this case, not only the stoichiometry of the support surface but also mesoscopic parameters such the Brunauer–Emmett–Teller (BET) area or porosity are crucial to influence the size and shape of the metallic nanoparticles. This control is quite indirect as the dispersion of the metals on the substrate is determined by the ability of the atoms to be anchored to the surface by particularly active carrier positions. Therefore, in weak interaction to the substrate Case I and II models are the first order approximation, see Fig. 3. If the interaction is stronger, dispersion of the active phase occurs. In the case of very small particles, even charge transfer can take place although screening for these materials is very effective and thus charge contributions are accommodated for medium-size particles. As the stoichiometry induces the shape and the dispersion, there is a reasonable parameter that needs to be eliminated when comparing different catalysts. In this case, the inclusion of the carrier in the DFT model is not required as its effect can be introduced indirectly. A particular case of moderate interaction between the active-phase and the carrier takes place for some catalysts as that employed in the Deacon reaction (HCl oxidation to Cl_2 that usually is carried out by RuO_2-based materials), where such strong interactions occur and the active layer grows epitaxially on the carrier. This corresponds to Case III in Fig. 3. A single monolayer has such a large interaction with the support that becomes inactive and thus a few layers are required to eliminate the electronic perturbation induced by the support.[74]

Another type of metal–support interaction can induce the formation of special sites at the interface between the active phase and the carrier, see Case IV in Fig. 3. Possible active sites that can benefit from the synergetic interaction have been put forward. CO oxidation on gold nanoparticles is a good example: CO adsorbs on the metal, and, simultaneously, oxygen can be activated by the partially reduced sample.[70] Some issues arise as the modelling of such bifunctional mechanisms requires adequate description of both the active phase and the support. In the submonolayer regime oxide growth on oxides has been observed for vanadia compounds on reducible oxides such as TiO_2 and CeO_2.[75,76] In both cases synergies between the small vanadia clusters and the oxide supports have been identified in experiments and described theoretically.

A final scenario can be envisaged where part of the reaction takes place in the carrier and spill-over to the (in principle) active phase takes place, see Case V in Fig. 3. In this case, simulations can be performed individually and the results can be combined to model the complex system. Similarly, the stability of the products shall be investigated against the acidity and basicity of the support, which can have an effect at this stage.

For very reducible oxides and/or high temperatures, a dynamical behaviour of the systems has been reported. For instance, some carriers are oxides and can lose oxygen during the reaction. Then, the active phase can change shape during the reaction and thus the number of active sites, their nature and the ability to generate mixed sites at the interface, significantly affecting the activity of the material. This is the particular case of Cu/ZnO,[77] the catalysts developed for the synthesis of methanol from CO and H_2. Still other dynamic behaviours, in particular related to the appearance of the strong-metal–support interaction,[78] can severely affect the catalytic properties and hinder the generation of a simple model for the catalyst. Obviously, these cases are the most complex model due to the long-time and long-length scale changes under true reaction conditions.

State of the catalyst

Preparation methods and pretreatments might affect the state of the catalyst. In the synthetic process a typical cleaning of the precursors is the reduction of the material. In particular, hydrogen atmospheres can change the relative stability of different surfaces. The history of the sample thus influences the ability to catalyse a given reaction. The study of the stability is usually addressed through first-principles thermodynamics which include not only the calculated energies but also the contributions of the pressure and the temperature and this constitutes the minimum computational set to address these properties, see Fig. 2. An illustrative example is given by the activity of Pd-based catalysts in the hydrogenation of alkyne–alkene mixtures in the treatment of feeds coming from oil reforming. The key issue in this case is that Pd behaves as a sponge and, in particular, when hydrogen or hydrocarbon atmospheres are present, it can generate hydrides or carbides.[79] The presence of hydrocarbons favours the formation of carbon and hydrocarbon surface deposits (coking).[81,82] Examples exist also in oxidations, like the epoxidation of olefins carried out with the help of a silver-based catalyst, Ag might convert at high oxygen conditions into the substoichiometric oxide.[80]

The formation of these competitive phases and subproducts has been investigated with theoretical methods using DFT on a list of structures that include a small set of configurations containing both the main active phase and the atoms from the gas-phase, (reactants or products). Upon characterisation of such configurations by DFT, first principles thermodynamics shall be employed to account for the temperatures and the pressures of the components.[83] The equations that aim at obtaining the Gibbs or Helmholtz free energies are related to the chemical potentials of the gas-phase compounds and thus the corresponding surface free energies for all configurations are obtained.

A few simplifications are employed to determine the free energies. For instance, the contributions from the phonons are neglected. This approach helps to evaluate the order of the introduced error. In addition, the gas-phase energies are taken from the ideal gas approximation, and either the experimental entropies or the ideal-gas statistical mechanics approximations are introduced. Configurational entropies are completely neglected or only introduced as an added fix in an approximate manner.[56] Even if first principles thermodynamics provide a way to derive the equilibrium structure it is not free of error sources. The problem is that configurations usually are generated by hand, and therefore some of them that do not seem obvious *a priori* might not be introduced in the calculation pool, thus missing representativity. Genetic algorithms can be employed to avoid this issue but unfortunately their introduction in the field is not straightforward, since the codes are usually fitted to the particular problem to be investigated and require a greater deal of effort.[84]

As first principles thermodynamics usually neglects a part of entropic contributions and rely on adsorption and desorption processes, the errors associated with the determination of pressures and temperatures are somehow larger than taking into account the whole reaction mechanism. Therefore, this technique is powerful and in particular qualitative when oxygen is one of the active gases and PW91 or PBE are employed to obtain the energies.

A similar situation might occur under operation conditions. Several catalysts are known to present an induction time where the as-prepared phase turns into the active phase. Moreover, some other materials that are active for a period might be inactive after being under reaction conditions for a sufficiently long time. This might occur by a change in the size and shape of the active phase, its formation or collapse, its volatilisation or the formation of carrier layers on the active part, just to name a few possibilities. The experimental detection of the changes taking place during this activation or deactivation is in general quite difficult as in several cases *in situ* experiments are required under reaction conditions. In some of these cases, first principles thermodynamics turns out to be a good tool to assess the state of the catalyst with respect to the reservoirs of the active gases that will be present in the reaction mixture.[85] Such approach can help filtering the structures that stay in the active phase under reaction conditions and also assessing the real surface termination. From our experience, we have seen that stability against harsh conditions might be the most important parameter for real applications. Whereas industry can cope with not so effective activities (as engineering solutions may reduce the low-activity impact), there is usually a much smaller toolbox to improve stability of the catalyst under reaction conditions.

Typical catalytic formulations under real synthetic conditions are somehow modular and, besides, from the base metal a secondary metal and/or one or more dopants and/or molecular (selectivity) modifiers are added. When dealing with complex materials with more than one component, the stability of the alloy both by itself and also under reaction conditions is mandatory. These parameters related to stability can be obtained by theoretical considerations and for instance a group of descriptors including, solubility, segregation and induced segregation energies, island formation, decoration of low coordinated sites and substitution at step sites among others can be identified. Examples of these have been put forward by several groups including ours and they can be extended to oxides and other materials.[62,86] Additives can be electron donors or acceptors that affect the charge at the surface,[87,88] or alternatively they can help to stabilise particular stoichiometries or geometries. Finally, molecular modifiers might affect adsorption energies for thermodynamic selectivity purposes, or reduce the size of the ensembles that might lead to selectivity, as in the Lindlar catalyst preparation.[89] In all these cases, theoretical simulations can provide an understanding on the individual role of the different components to the activity–selectivity–stability of the catalysts under reaction conditions.

Reaction mechanisms and kinetic parameters

The study of the reaction networks relies on linking the various potential configurations of reactants, intermediates and products on the surface and with respect to the gas-phase. In this way different mechanisms including these sets are investigated. The most robust algorithms to obtain the transitions state structures that link reactants and products belong to the family of the Nudged Elastic Band (NEB) methods.[90] In general, once both the initial and final states are known, a series of images are placed between these positions and then the optimisation of the full band takes place. We need to consider, firstly, that the computational requirements for these calculations correspond to those of a static calculation multiplied by the number of images in the band. Thus, these are the heaviest calculations when modelling reactions on surfaces. Secondly, that the use of the traditional NEB does not ensure that the highest point along the reaction path is the true transition state (TS). A vibrational analysis of the structure is needed in order to assess correctly that the point fulfils the mathematical definition of a TS (*i. e.* that it is a minimum along all possible directions except for that of the reaction coordinate, for which it is a maximum). This issue was solved with the advent of the Climbing Image version of the NEB algorithm (CI-NEB),[90] a much more robust way to obtain the TS structure and energy. However, as it has been mentioned before, calculations are still very demanding and thus algorithms aiming at shortening calculation times and computational requirements have been proposed. Examples of those are the Adaptative Nudged Elastic Band Approach (ANEBA),[91] where instead of choosing a large number of images to bracket the saddle point with high accuracy, the resolution in the neighborhood of the saddle point is increased. Other appealing methods are based on the dimer method,[92]

which is designed to search for saddle points corresponding to unknown elementary steps, where no final state is required and the TS structure is proposed; then upon calculation of the Hessian, the movement along the Potential Energy Surface and towards the TS structure is done by following this particular reaction coordinate. In any case, the search for TSs constitutes the bottleneck in the description of catalytic phenomena on surfaces, therefore further research into the algorithms will be required to make the calculations faster. As the number of databases and calculated points increase every day the inheritance of parent structures for the search of transition states in new more complex molecules shall be a way to reduce computational costs.

In many cases the reaction networks are constituted by a short list of reactions. This is the case of CO oxidation, for which two paths have been put forward and either the dissociative O_2 path or the associative one can take place, depending on the material.[93] This mechanism is relatively simple as only four elementary reactions need to be taken into account. When dealing with larger molecules or more complex mixtures, the situation becomes increasingly complex. For instance, in the selective hydrogenation of alkyne–alkene mixtures, the minimum set of reactions needs to take into account the following paths: (i) hydrogenation,[94] (ii) isomerisation of the intermediates on the surface,[95] (iii) carbide formation by decomposition of the hydrocarbon at low-coordinated sites,[96] and (iv) oligomerisation[82] and/or carbon deposits formation. Several of these steps, in particular, those that reduce the activity, selectivity, and stability (as (iii) and (iv)) are likely to be common to different transformation and thus they could, in principle, be retrieved from databases (*vide infra*).

In other cases, the reactivity needs to be calculated for a series of potential surface structures including the corresponding carbides, hydrides and selectivity modifier molecules. This is also the case of the hydrogenations on Pd. Then the determination of the TS paths needs to be considered for each potential structure in order to derive the structure–activity (selectivity) relationships.[82]

Still another scenario unfolds when considering sets of reactions that can be performed under different conditions. This is the case of HCN synthesis from ammonia and methane on PtRh catalysts, see Fig. 4.[97] The reaction can take place in aerobic (the one implemented in industry) and anaerobic conditions. The presence of oxygen atoms on the surface systematically reduces the energy demand of the H-dissociation steps but the price to be paid is that in the Andrussow oxidation the final C–N bond formation takes place from very strongly adsorbed atoms on the surface. Thus the main benefit found for the reaction thermodynamics when O_2 is present does not result in a large reduction in the kinetics or reaction temperatures (only 300 K lower), as there is a mechanistic switch for the C–N bond formation from partially hydrogenated molecules (in the non-oxidative case) to more bound atomic species (oxidative conditions), see Fig. 4.[98]

As shown above, the list of potential reaction paths and parallel elemental reactions is quite large even for simple reactions. In order to predict activities and selectivities, the amount of information stored in such calculations needs to be reduced to the most relevant parameters (descriptors) that can

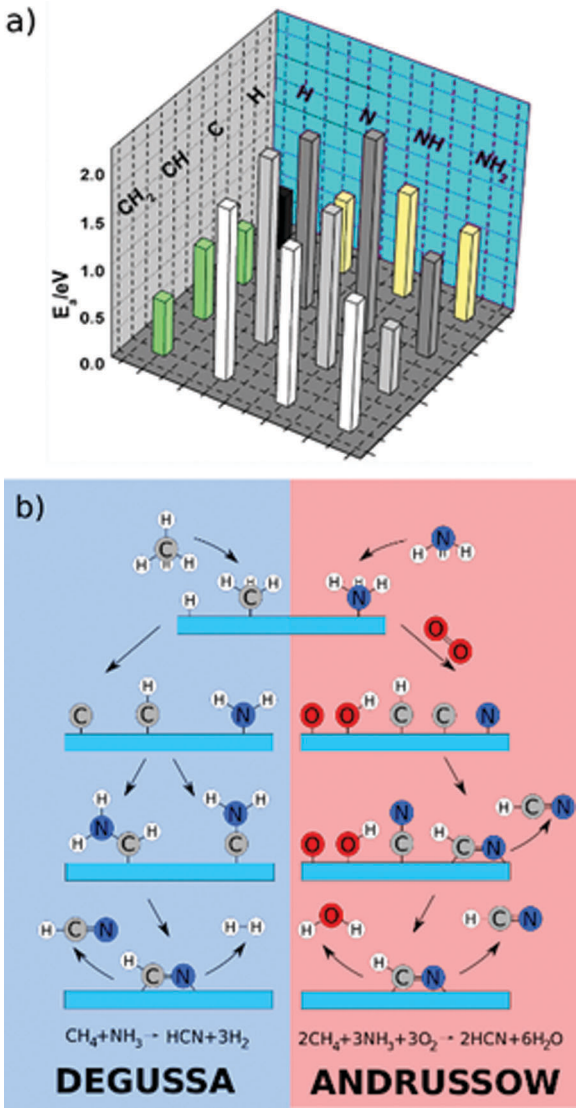

Fig. 4 (a) Reaction barriers for the coupling of different C and N-containing fragments. (b) Schematic representation of the two different possibilities for the HCN formation under O-lean and rich conditions.

affect the reactivity (activity or selectivity) by modification. Early descriptors, based on the activity of oxides, were already devised by Sabatier who confronted the reactivity of different transition metals towards the decomposition of formic acid against a thermodynamic parameter, the formation energy of the oxide.[99]

Over the last years, in particular in the group of Prof. Nørskov in Stanford, two different ways to describe relationships between energy parameters have been developed. The first one corresponds to the linear-scaling relationships.[100,101] In these, the binding energy of a fragment to a metal (also for oxides, nitrides, sulphides, carbides) correlates with the binding energy of the central atom to the surface. Moreover, the proportionality factor depends on the valence. Therefore, a simple explanation in terms of the density available to form different bonds and the valence of the heteroatom can be traced back in a simple yet effective manner. A second scaling relationship corresponds to the Brønsted–Evans–Polanyi rules, BEP.[102,103]

BEP states that the activation barrier depends on the reaction energy for this particular elementary step. Dissociation reactions are in many cases responsible for the activity found, as they constitute the rate-determining steps.[104,105] In such situations, BEP can be further simplified to the adsorption energy of the central heteroatom. BEP relationships are an extension of the linear scaling relationships described above. With these two approaches, many mechanisms can be simplified to just one or two significant descriptors.[93]

Microkinetic modelling

In many cases, dealing with the description of the complete reaction energy profile leaves open questions such as which are the rate-determinant or selectivity-determinant steps. This answer requires the modelling of the kinetic equations with the correct boundary conditions in order to be fully meaningful.

In general, the data obtained from Density Functional Theory with the appropriate approaches (*vide supra*) can be taken as starting point for the microkinetic (MK) simulations. The rate coefficients are normally obtained through the use of standard statistical thermodynamics and by using the harmonic transition state theory.[106,107] The list of kinetic elementary reactions, the site balance, and the boundary conditions introduced describe a system of Differential and Algebraic Equations that can be solved by different mathematical packages. In any case, the activity of the system can be described, the reaction orders retrieved, and the apparent activation energies and coverages of different species unravelled.[79] This completes the knowledge on the reacting conditions and, once the true path has been obtained and the relevant surface is taken into account and different reaction conditions can be easily plugged in. In some cases accuracy problems and unstable solutions might arise and thus this type of approach is not as straightforward as standard DFT packages.

Moreover, the reaction mechanism (understood as the list of reactions) does not change for the same process on a large number of catalysts. Therefore, taking into account the considerations made in the previous section, it is sometimes useful to simplify the problem by transferring all the relevant kinetic terms to the descriptors. Successful examples of such approach have been presented by the group of Prof. Nørskov for a number of processes including CO oxidation on metals and nanoparticles.[93] In particular, the Sabatier analysis with more than one descriptor has produced multidimensional volcano plots where the maximum of activity can be inferred. Another important point of microkinetic approaches is that it allows determining the weight of each step that composes the mechanism and the analysis of the role of the different elementary reactions.[6,108] Finally, MK modelling can assess important aspects such as the adequate analysis of the population of different species on the active substrates directly comparable to experiments. With such an approach it has been possible to determine why compensation effects occur in heterogeneous catalysis.[109]

In some cases, the classical MK has some deficiencies. Those are related to the lack of geometric information in the equations which limits the applicability of this technique, in particular when confined systems are considered.[108] Kinetic Monte-Carlo methods are better suited to deal with these in homogenous lattices, as the geometric information is already available. The reader is addressed to the Perspective by Reuter and co.[6] on the subject for a more detailed description.

3 Main challenges

Problems when addressing large/flexible molecules

Until recently, only the interaction of small molecules on metal systems was considered in theoretical simulations. Many heterogeneous catalysts deal with the activation of small molecules and their incorporation to other larger fragments (*i.e.* partial oxidations and hydrogenations) or the reshuffling of the internal bonds, like in the case of ammonia synthesis. Indeed, CO oxidation has been the favourite reaction for theoreticians so far.

The search for catalysts that can facilitate the implementation of new industrial processes faces here an important challenge. In the past, many of the interesting active molecules were obtained from oil. These active molecules were small and had a functional group at most. Examples are methanation, hydrogenation of alkynes in alkene mixtures, and even the Fischer–Tropsch reaction. Unfortunately, as these natural sources are being depleted fast, we will need to change gears and start employing larger molecules that present several functional groups. This poses many challenges to the modelling of the reactions that occur, the most important of which are: (i) the presence of multiple adsorption configurations due to the functionalities, (ii) the inordinate amount of potential parallel paths that need to be described with similar accuracy in order to properly obtain the selectivity, and (iii) the liquid nature of some of these compounds due to their high oxygen content. Therefore, even the investigation of the adsorption for all relevant configurations can become a challenge.[110] Moreover, when attempting microkinetic modelling a better assessment of the number of positions occupied (*i.e.* improved definition of the adsorption site) would be required just to account properly for the larger size of the molecules.[111] Two examples of how to address this particular problem have been put forward by the groups of Greeley and Vlachos.[112,113] In the first case, the study of glycerol decomposition on Pt(111) was estimated by an empirical correlation scheme later redefined by DFT calculations coupled to BEP analysis for the dehydrogenation and C–C bond scission. Salciccioli and Vlachos proposed a parametrisation of the thermochemical properties of $C_2H_xO_2$ intermediates and transition states for different bond breaking patters C–C, C–O, and O–H in the form of a functional group approach.

Flexibility poses also an important problem when looking at large molecules adsorbed on surfaces. In homogeneous catalysis, extensive searches for the most stable conformation of the catalysts, reactants, intermediates and products are performed routinely. This is not the case of the simulation of large molecules on surfaces. Just to give a small example, the rotation of a methyl group can increase the Pauli repulsion by 0.3 eV with respect to the same methyl adsorbed on the surface but with no direct H-interaction on Ag.[114]

Solvent effects

Solvent effects can have a strong influence on the study of catalysis[115] due to a non-homogenous electric field that perturbs

the electronic clouds of the solute and therefore its geometry, changing its properties when compared to the gas-phase species.[116] Solvent effects have been mainly characterised in homogeneous catalysis. Two main general approaches are commonly used: classical ensemble treatments and quantum mechanical continuum models.

The former include classical molecular dynamics simulations,[117–119] Monte-Carlo techniques,[120] free energy perturbation,[121–123] and Langevin dipole moments.[124] In many cases, solvent is treated explicitly as a rigid system with vdW ε/σ parameters and partial charges,[125–127] and the interaction between molecules is handled by pair-wise interactions between atoms.[128] These models give useful information about solute–solvent interactions, and describe conformational changes carefully. Their main drawback is the need for an appropriate potential function, extrapolated from other data, as well as the lack of a proper relaxation of the geometry and the dipole moment during the simulation.

The latter approach has its roots in the Onsager reaction field model.[129] According to this, the solute is placed in a cavity[130] that can be for the whole molecule or a summation of overlapping spheres centred on each atom (PCM)[116] immersed in a continuous medium with a dielectric constant ε. A dipole in the molecule will induce a reflection dipole in the solvent, and this, in turn, (reaction) will interact with the molecular dipole, leading to a net stabilisation. Given the structureless nature of the solvent, this approach is best suited to describe apolar systems or solvents where a specific interaction with solute (such as H bonds) is missing. Unlike classical field methods, no additional information concerning potential functions and related parameters is needed. In PCM, the surface potential is calculated by numerical differentiation, and its interaction with the solvent can then be computed self-consistently. This is equivalent to carrying out the dipole expansion to infinite order, strongly improving the Onsager model. Further developments are DPCM (dielectric),[131] CPCM[132] and IEFPCM.[133–135]

In heterogeneous catalysis, the focus has been on gas-phase processes and thus the introduction of solvent effects is much more recent. For instance in porous materials, like Metal–Organic Frameworks, (mixed organic inorganic compounds proposed to have tantalising properties, MOF) it has been possible to employ Born–Oppenheimer Molecular Dynamics to assess explicitly the role of water[136,137] or even Car–Parrinello calculations on the formation of the first aggregates for zeolite formation[138] (*vide infra*). In such cases, the solvation energies of atoms are taken properly into account for electrochemical purposes.[139] Water dynamics in the Car–Parrinello approaches has also been employed to study the relative stability of surfaces in semiconductors.[140] On metals, the situation is far more complex as first principle dynamics cannot be performed efficiently. In general, explicit water structures in the submonolayer regimes have been studied,[141] and in some cases tridimensional ice layers have been employed.[142,143]

Theoretical simulations have faced problems even in the description of such layers as many minima with similar energies exist and the proper evaluation of the dispersion contributions is needed.[48,141,144,145] Still, models based on systems with different ice configurations filling the space between two metal slabs can be employed and although the model is naïve and quite rigid, some important results have been obtained.[146] Following the reasoning in homogeneous catalysis, it would be worth attempting a similar approach in heterogeneous systems through the definition of cavities and continuous medium. So far, few initiatives with very few results have been presented in the literature in this direction.[147]

On the transformation of theoretical chemistry into an information technology

As computational approaches can systematically investigate different materials with a similar degree of accuracy it is possible to generate structured information in the form of databases. Over the last years the amount of information gathered has been increasing exponentially and a development is required to transform this Chemistry knowledge into a true information technology. As a consequence, several groups have started to consider the possibility of generating databases that could be mined when a new particular problem arises. Of course, several questions are open about how to structure the information to make it useful and relevant. The main challenges are: determining the main tags to be included and, for open repositories, how to assess the quality of calculations coming from different groups or subjects. However, the latter problem is also common to other collaborative information systems, and therefore it should be easier to solve.

As for the already existing databases, we would like to make special mention of those created by the group of Prof. Ceder in MIT which is devoted to the study of batteries,[148] and that of Prof. Nørskov's dedicated to heterogeneous catalysis.[149] A more general discussion on the role of these databases is presented by Prof. Lüthi and co. in ETH-Zürich.[150] Finally, the computational groups at ICIQ (Professors Bo's, Maseras', and Lopez') are currently developing a similar tool: SCIPIO.[151] A snapshot of our web platform, which is compatible with different kinds of software (VASP,[152] ADF,[153] and Gaussian,[154]) is shown in Fig. 5.

From synthesis to structure

The hardest goal in the field is to actually evaluate preparation methods that could eventually lead to the desired molecular architectures known to be particularly active, selective, or stable. Obviously, this is a multiscale problem where the complexity in the number of different steps in the preparation of a catalyst is a long-term challenge. For instance, surfactant chemistry has generated a new route for the monodispersion of gold-based catalysts. Still elimination of these surfactants while keeping the chemical functionalities is still a challenge.[155,156] The investigation of the role of surfactants in the final structures, *i.e.* how they can introduce modifications in the typical Wulff structures, is still in its infancy.

Other examples of potential contributions in the field regard the synthesis of zeolites and the mesopore formation by water or by hydroxides. Experimentally, lots of evidences have been gathered concerning the position of different atoms in the ordered lattices or how the overall porosity can be increased.[157] However, important points still remain unclear. The remarkable study of Van Santen and co. on the initial mechanisms in the

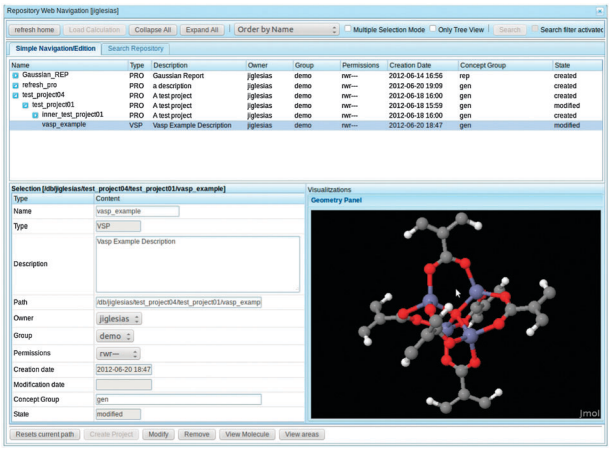

Fig. 5 Snapshot of the SCIPIO storage and database tool developed at ICIQ (www.scipio.iciq.es) showing MOF-5 results.

polymerisation of siloxane groups to configure zeolites, represents a true landmark in the way complex problems need to be addressed.[138] In this study, DFT calculations performed with solvent are accompanied by a Kinetic Monte-Carlo approach that extends the length- and time-scales of the study. Similar studies on the thermal stability of MOF also require at least the combination of Monte-Carlo simulations to assess the configurational contributions, and first principle molecular dynamics to obtain the true relevant parameters in the water induced lattice disruption.[136,137] The approaches above constitute a new direction where simulations can be powerful, this is the synthesis to structure challenge.

Towards a general theory of catalysis

The search for a new complete theory of catalysis has been under discussion for decades/years. In 2006, Nature[158] presented a list of what chemists wanted to know and, taking the sentence by Berthelot "Chemistry creates its object", it discussed the main issues to be developed in the field. Indeed the first question regarded the design of molecules/materials with specific properties and, therefore, chemistry was identified as "a science of particulars" including that "it would be ludicrous to look for a general theory of catalysis that applies to all enzymes, materials surfaces and so on". The methods employed by theoreticians to study all the potential materials are very similar in all cases and thus the formulation of parallelisms is possible. The main questions are still related to the ability to understand the typical jargon used by scientists with different backgrounds: such as engineering, physics, chemistry or organic chemistry.

Despite these critical assessments there have been several attempts to prove that the answer is not so straightforward. For instance, during the gold rush that started in 2000,[159] several processes that were proved to take place on gold nanoparticles were transferred to organometallic compounds and conversely. In turn, ruthenium is known to generate epoxides when prepared as organometallic and nanoclusters (known as polyoxometalates, POM) but these properties are not retrieved for ruthenium oxide. Experimental comparison between the activity of organometallic and Ru surfaces for polymerisation has also been put forward.[160] Last but not least, some sulphides that recall the structures present in the enzymes turn to be active in the electrochemical conversion of protons to hydrogen.[161] Thus, the number of proofs is important, but the degree of transferability of the chemical properties from isolated to tridimensional structures is not straightforward.

Analysing the similarities and differences in these materials is possible by employing an equivalent level of theory to enzymes, organometallic systems and surfaces. We have studied a couple of these systems. For instance, the nature of gold catalysis is based on different properties.[162] The differential adsorption of alkynes leads to selectivity, but organometallic alkenes are more likely to be coordinated to gold cations. Thus the similar chemistry, *i.e.* alkyne activation, has two different origins either a thermodynamic (heterogeneous) or a kinetic (homogeneous) one. As for the epoxidation of alkenes it occurs selectively on many Ru based homogeneous catalysts[163] and in nanoclusters[164] but the reaction is completely unselective for the surface oxide.[165] The reason for the selectivity is linked to the tridimensional structure and the curvature. One of the early stages of this reaction is given by the coordination of oxygen. On RuO_2, oxygen adsorbs dissociatively and the chemical potential of oxygen is high enough to prevent the formation of the intermediate. Curved surfaces as in POM compounds result in site isolation as in the organometallic compounds, thus also keeping the inability to split oxygen which improves the selectivity.

4 Conclusions

In the present perspective we have reviewed in a critical way the strengths and drawbacks of state-of-the-art theoretical methods when used to describe heterogeneous catalysis. The increasing capacity of computers and algorithms has opened a new field with great opportunities but several bottlenecks for the spread use of such integrated methods are still present. We also consider that training of both experimentally- and theoretically-oriented scientists in the abilities and limits of the present techniques will improve the synergies between both, enhancing the progress in the near future. The increased value that industries are giving to theoretical simulations is a clear demonstration of the future role of these techniques.

As for the challenges that the theoretical simulations of catalytic systems face, the integration of different computational methods and the ability to introduce larger molecules, solvent effects and transfer the practical results coming from several methods is a must. Finally, the creation of common databases that condense the results gathered by several groups and the identification of synthesis to structure rules would certainly help to generate a more general theory of catalysis get closer to application.

Acknowledgements

We thank the MICINN for projects CTQ2009-07753/BQU, CSD2006-0003, ERC-Starting Grant Bio2chem-d 2010-StG-258406, and BSC-RES for providing generous computational resources. We would like to thank Prof. J. Pérez-Ramírez, Dr Grau-Crespo and O. A. Salawu for useful discussions.

Notes and references

1 D. G. Vlachos, *AIChE J.*, 2012, **58**, 1314–1325.
2 M. Salciccioli, M. Stamatakis, S. Caratzoulas and D. G. Vlachos, *Chem. Eng. Sci.*, 2011, **66**, 4319–4355.
3 E. A. Carter, *Science*, 2008, **321**, 800–803.
4 J. K. Nørskov, T. Bligaard, B. Hvolbaek, F. Abild-Pedersen, I. Chorkendorff and C. H. Christensen, *Chem. Soc. Rev.*, 2008, **37**, 2163–2171.
5 J. K. Nørskov, T. Bligaard, J. Rossmeisl and C. H. Christensen, *Nat. Chem.*, 2009, **1**, 37–46.
6 M. K. Sabbe, M.-F. Reyniers and K. Reuter, *Catal. Sci. Technol.*, 2012, DOI: 10.1039/c2cy20261a.
7 J. Hafner, *J. Comput. Chem.*, 2008, **29**, 2044–2078.
8 V. E. Van Doren, C. Van Alsenoy and P. Geerlings, *Density functional theory and its application to materials : Antwerp, Belgium, 8–10 June 2000*, American Institute of Physics, Melville, N.Y., 2001.
9 W. Kohn and L. J. Sham, *Phys. Rev.*, 1965, **140**, 1133–1135.
10 D. M. Ceperley and B. J. Alder, *Phys. Rev. Lett.*, 1980, **45**, 566–569.
11 P. Haas, F. Tran and P. Blaha, *Phys. Rev. B: Condens. Matter Mater. Phys.*, 2009, **79**, 085104.
12 J. L. F. Da Silva, C. Stampfl and M. Scheffler, *Phys. Rev. Lett.*, 2003, **90**, 066104.
13 G. R. Darling and S. Holloway, *Rep. Prog. Phys.*, 1995, **58**, 1595–1672.
14 D. C. Langreth and M. J. Mehl, *Phys. Rev. Lett.*, 1981, **47**, 446–450.
15 D. C. Langreth and M. J. Mehl, *Phys. Rev. B: Condens. Matter Mater. Phys.*, 1983, **28**, 1809–1834.
16 B. Hammer, L. B. Hansen and J. K. Nørskov, *Phys. Rev. B: Condens. Matter Mater. Phys.*, 1999, **59**, 7413–7421.
17 K. Honkala, A. Hellman, I. N. Remediakis, A. Logadottir, A. Carlsson, S. Dahl, C. H. Christensen and J. K. Nørskov, *Science*, 2005, **307**, 555–558.
18 J. P. Perdew, J. A. Chevary, S. H. Vosko, K. A. Jackson, M. R. Pederson, D. J. Singh and C. Fiolhais, *Phys. Rev. B: Condens. Matter Mater. Phys.*, 1992, **46**, 6671–6687.
19 J. P. Perdew, K. Burke and M. Ernzerhof, *Phys. Rev. Lett.*, 1996, **77**, 3865–3868.
20 J. P. Perdew, A. Ruzsinszky, G. I. Csonka, O. A. Vydrov, G. E. Scuseria, L. A. Constantin, X. L. Zhou and K. Burke, *Phys. Rev. Lett.*, 2008, **100**, 136406.
21 R. Armiento and A. E. Mattsson, *Phys. Rev. B: Condens. Matter Mater. Phys.*, 2005, **72**, 085108.
22 Z. G. Wu and R. E. Cohen, *Phys. Rev. B: Condens. Matter Mater. Phys.*, 2006, **73**, 235116.
23 R. W. Godby, M. Schluter and L. J. Sham, *Phys. Rev. Lett.*, 1986, **56**, 2415–2418.
24 P. Rinke, A. Qteish, J. Neugebauer, C. Freysoldt and M. Scheffler, *New J. Phys.*, 2005, **7**, 126.
25 A. K. Kelkkanen, B. I. Lundqvist and J. K. Nørskov, *J. Chem. Phys.*, 2009, **131**, 046102.
26 J. L. F. Da Silva, M. V. Ganduglia-Pirovano, J. Sauer, V. Bayer and G. Kresse, *Phys. Rev. B: Condens. Matter Mater. Phys.*, 2007, **75**, 045121.
27 J. P. Perdew, S. Kurth, A. Zupan and P. Blaha, *Phys. Rev. Lett.*, 1999, **82**, 2544–2547.
28 E. G. Moroni, G. Kresse, J. Hafner and J. Furthmuller, *Phys. Rev. B: Condens. Matter Mater. Phys.*, 1997, **56**, 15629–15646.
29 A. D. Becke, *J. Chem. Phys.*, 1993, **98**, 5648–5652.
30 P. J. Stephens, F. J. Devlin, C. F. Chabalowski and M. J. Frisch, *J. Phys. Chem.*, 1994, **98**, 11623–11627.
31 J. Paier, R. Hirschl, M. Marsman and G. Kresse, *J. Chem. Phys.*, 2005, **122**, 234102.
32 J. Paier, M. Marsman and G. Kresse, *J. Chem. Phys.*, 2007, **127**, 024103.
33 C. Adamo and V. Barone, *J. Chem. Phys.*, 1999, **110**, 6158–6170.
34 J. Heyd, G. E. Scuseria and M. Ernzerhof, *J. Chem. Phys.*, 2003, **118**, 8207–8215.
35 C. Franchini, V. Bayer, R. Podloucky, J. Paier and G. Kresse, *Phys. Rev. B: Condens. Matter Mater. Phys.*, 2005, **72**, 045132.
36 C. Franchini, R. Podloucky, J. Paier, M. Marsman and G. Kresse, *Phys. Rev. B: Condens. Matter Mater. Phys.*, 2007, **75**, 195128.
37 A. Kiejna, G. Kresse, J. Rogal, A. De Sarkar, K. Reuter and M. Scheffler, *Phys. Rev. B: Condens. Matter Mater. Phys.*, 2006, **73**, 035404.
38 A. Stroppa and G. Kresse, *New J. Phys.*, 2008, **10**, 063020.
39 J. Harl and G. Kresse, *Phys. Rev. Lett.*, 2009, **103**, 056401.
40 M. Dion, H. Rydberg, E. Schroder, D. C. Langreth and B. I. Lundqvist, *Phys. Rev. Lett.*, 2004, **92**, 246401.
41 K. Lee, E. D. Murray, L. Z. Kong, B. I. Lundqvist and D. C. Langreth, *Phys. Rev. B: Condens. Matter Mater. Phys.*, 2010, **82**, 081101.
42 S. Grimme, *J. Comput. Chem.*, 2006, **27**, 1787–1799.
43 S. Grimme, J. Antony, S. Ehrlich and H. Krieg, *J. Chem. Phys.*, 2010, **132**, 154104.
44 F. London, *Trans. Faraday Soc.*, 1937, **33**, 8b–26.
45 T. Bučko, J. Hafner, S. Lebegue and J. G. Angyan, *J. Phys. Chem. A*, 2010, **114**, 11814–11824.
46 V. G. Ruiz, W. Liu, E. Zojer, M. Scheffler and A. Tkatchenko, *Phys. Rev. Lett.*, 2012, **108**, 146103.
47 G. X. Zhang, A. Tkatchenko, J. Paier, H. Appel and M. Scheffler, *Phys. Rev. Lett.*, 2011, **107**, 245501.
48 P. Błoński and N. Lopez, *J. Phys. Chem. C*, 2012, **116**, 15484–15492.
49 J. Hafner, *J. Phys.: Condens. Matter*, 2010, **22**, 384205.
50 Z. Łodziana, G. Stoica and J. Pérez-Ramírez, *Inorg. Chem.*, 2011, **50**, 2590–2598.
51 R. Grau-Crespo and U. V. Waghmare, *MolecularModeling for the Design of Novel Performance Chemicals and Materials*, CRC Press, 2012.
52 A. Zunger, S. H. Wei, L. G. Ferreira and J. E. Bernard, *Phys. Rev. Lett.*, 1990, **65**, 353.
53 R. Grau-Crespo, S. Hamad, C. R. A. Catlow and N. H. de Leeuw, *J. Phys.: Condens. Matter*, 2007, **19**, 256201.
54 R. Grau-Crespo, N. H. de Leeuw and C. R. A. Catlow, *Chem. Mater.*, 2004, **16**, 1954–1960.
55 J. Carrasco, N. Lopez and F. Illas, *Phys. Rev. Lett.*, 2004, **93**, 225502.
56 R. Grau-Crespo, A. Y. Al-Baitai, I. Saadoune and N. H. De Leeuw, *J. Phys.: Condens. Matter*, 2010, **22**, 255401.
57 R. Grau-Crespo, N. H. De Leeuw, S. Hamad and U. V. Waghmare, *Proc. R. Soc. A*, 2011, **467**, 1925–1938.
58 W. G. Wulff, *Z. Kryst. Miner.*, 1901, **34**, 449–530.
59 I. N. Remediakis and *et. al.*, personal communication.
60 S. Dahl, A. Logadottir, R. C. Egeberg, J. H. Larsen, I. Chorkendorff, E. Tornqvist and J. K. Nørskov, *Phys. Rev. Lett.*, 1999, **83**, 1814–1817.
61 N. Lopez, T. V. W. Janssens, B. S. Clausen, Y. Xu, M. Mavrikakis, T. Bligaard and J. K. Nørskov, *J. Catal.*, 2004, **223**, 232–235.
62 N. Lopez and C. Vargas-Fuentes, *Chem. Commun.*, 2012, **48**, 1379–1391.
63 R. T. Vang, K. Honkala, S. Dahl, E. K. Vestergaard, J. Schnadt, E. Laegsgaard, B. S. Clausen, J. K. Nørskov and F. Besenbacher, *Nat. Mater.*, 2005, **4**, 160–162.
64 J. Kleis, J. Greeley, N. A. Romero, V. A. Morozov, H. Falsig, A. H. Larsen, J. Lu, J. J. Mortensen, M. Dulak, K. S. Thygesen, J. K. Nørskov and K. W. Jacobsen, *Catal. Lett.*, 2011, **141**, 1067–1071.
65 U. Heiz, A. Sanchez, S. Abbet and W. D. Schneider, *J. Am. Chem. Soc.*, 1999, **121**, 3214–3217.
66 W. J. Stark, S. E. Pratsinis and A. Baiker, *Chimia*, 2002, **56**, 485–489.
67 M. Mavrikakis, P. Stoltze and J. K. Nørskov, *Catal. Lett.*, 2000, **64**, 101–106.
68 B. Yoon, H. Hakkinen, U. Landman, A. S. Worz, J. M. Antonietti, S. Abbet, K. Judai and U. Heiz, *Science*, 2005, **307**, 403–407.
69 H.-G. Boyen, G. Kastle, F. Weigl, B. Koslowski, C. Dietrich, P. Ziemann, J. P. Spatz, S. Riethmüller, C. Hartmann, M. Moller, G. Schmid, M. G. Garnier and P. Oelhafen, *Science*, 2002, **297**, 1533–1536.
70 I. N. Remediakis, N. Lopez and J. K. Nørskov, *Angew. Chem., Int. Ed.*, 2005, **44**, 1824–1826.
71 Z. Łodziana, N. Y. Topsoe and J. K. Nørskov, *Nat. Mater.*, 2004, **3**, 289–293.
72 M. Digne, P. Sautet, P. Raybaud, P. Euzen and H. Toulhoat, *J. Catal.*, 2002, **211**, 1–5.
73 J. Venables, *Introduction to Surface and Thin Film Processes*, Cambridge University Press, Cambridge, 2000.

74 D. Teschner, R. Farra, L. D. Yao, R. Schlogl, H. Soerijanto, R. Schomacker, T. Schmidt, L. Szentmiklosi, A. P. Amrute, C. Mondelli, J. Pérez-Ramírez, G. Novell-Leruth and N. Lopez, *J. Catal.*, 2012, **285**, 273–284.
75 M. Calatayud and C. Minot, *J. Phys. Chem. B*, 2004, **108**, 15679–15685.
76 M. V. Ganduglia-Pirovano, C. Popa, J. Sauer, H. Abbott, A. Uhl, M. Baron, D. Stacchiola, O. Bondarchuk, S. Shaikhutdinov and H.-J. Freund, *J. Am. Chem. Soc.*, 2010, **132**, 2345–2349.
77 P. L. Hansen, J. B. Wagner, S. Helveg, J. R. Rostrup-Nielsen, B. S. Clausen and H. Topsoe, *Science*, 2002, **295**, 2053–2055.
78 S. J. Tauster, S. C. Fung, R. T. K. Baker and J. A. Horsley, *Science*, 1981, **211**, 1121–1125.
79 D. Teschner, J. Borsodi, A. Wootsch, Z. Revay, M. Havecker, A. Knop-Gericke, S. D. Jackson and R. Schlogl, *Science*, 2008, **320**, 86–89.
80 M. Schmid, A. Reicho, A. Stierle, I. Costina, J. Klikovits, P. Kostelnik, O. Dubay, G. Kresse, J. Gustafson, E. Lundgren, J. N. Andersen, H. Dosch and P. Varga, *Phys. Rev. Lett.*, 2006, **96**, 146102.
81 S. Helveg, C. Lopez-Cartes, J. Sehested, P. L. Hansen, B. S. Clausen, J. R. Rostrup-Nielsen, F. Abild-Pedersen and J. K. Nørskov, *Nature*, 2004, **427**, 426–429.
82 M. Garcia-Mota, B. Bridier, J. Pérez-Ramírez and N. Lopez, *J. Catal.*, 2010, **273**, 92–102.
83 X. G. Wang, A. Chaka and M. Scheffler, *Phys. Rev. Lett.*, 2000, **84**, 3650–3653.
84 U. Martinez, L. B. Vilhelmsen, H. H. Kristoffersen, J. Stausholm-Moller and B. Hammer, *Phys. Rev. B: Condens. Matter Mater. Phys.*, 2011, **84**, 205434.
85 N. Lopez, J. Gomez-Segura, R. P. Marin and J. Pérez-Ramírez, *J. Catal.*, 2008, **255**, 29–39.
86 G. Novell-Leruth, G. Carchini and N. Lopez, submitted.
87 J. J. Mortensen, B. Hammer and J. K. Nørskov, *Phys. Rev. Lett.*, 1998, **80**, 4333–4336.
88 J. Gomez-Diaz, K. Honkala and N. Lopez, *Surf. Sci.*, 2010, **604**, 1552–1557.
89 M. Garcia-Mota, J. Gomez-Diaz, G. Novell-Leruth, C. Vargas-Fuentes, L. Bellarosa, B. Bridier, J. Pérez-Ramírez and N. Lopez, *Theor. Chem. Acc.*, 2011, **128**, 663–673.
90 G. Henkelman and H. Jonsson, *J. Chem. Phys.*, 2000, **113**, 9978–9985.
91 P. Maragakis, S. A. Andreev, Y. Brumer, D. R. Reichman and E. Kaxiras, *J. Chem. Phys.*, 2002, **117**, 4651–4658.
92 G. Henkelman and H. Jonsson, *J. Chem. Phys.*, 1999, **111**, 7010–7022.
93 H. Falsig, B. Hvolbaek, I. S. Kristensen, T. Jiang, T. Bligaard, C. H. Christensen and J. K. Nørskov, *Angew. Chem., Int. Ed.*, 2008, **47**, 4835–4839.
94 D. Mei, P. A. Sheth, M. Neurock and C. M. Smith, *J. Catal.*, 2006, **242**, 1–15.
95 J. Andersin, N. Lopez and K. Honkala, *J. Phys. Chem. C*, 2009, **113**, 8278–8286.
96 L. Nykanen, J. Andersin and K. Honkala, *Phys. Rev. B: Condens. Matter Mater. Phys.*, 2010, **81**, 075417.
97 L. Andrussow, *Angew. Chem.*, 1935, **48**, 593–595.
98 J. Gomez-Diaz and N. Lopez, *J. Phys. Chem. C*, 2011, **115**, 5667–5674.
99 I. Chorkendorff and J. W. Niemantsverdriet, *Concepts of modern catalysis and kinetics*, Wiley-VCH, Weinheim, 2003.
100 F. Abild-Pedersen, J. Greeley, F. Studt, J. Rossmeisl, T. R. Munter, P. G. Moses, E. Skulason, T. Bligaard and J. K. Nørskov, *Phys. Rev. Lett.*, 2007, **99**, 016105.
101 A. Vojvodic, F. Calle-Vallejo, W. Guo, S. Wang, A. Toftelund, F. Studt, J. I. Martinez, J. Shen, I. C. Man, J. Rossmeisl, T. Bligaard, J. K. Nørskov and F. Abild-Pedersen, *J. Chem. Phys.*, 2011, **134**, 244509.
102 J. N. Brønsted, *Chem. Rev.*, 1928, **5**, 231–338.
103 M. G. Evans and M. Polanyi, *Trans. Faraday Soc.*, 1938, **34**, 11–24.
104 T. Bligaard, J. K. Nørskov, S. Dahl, J. Matthiesen, C. H. Christensen and J. Sehested, *J. Catal.*, 2004, **224**, 206–217.
105 J. K. Nørskov, T. Bligaard, A. Logadottir, S. Bahn, L. B. Hansen, M. Bollinger, H. Bengaard, B. Hammer, Z. Sljivancanin, M. Mavrikakis, Y. Xu, S. Dahl and C. J. H. Jacobsen, *J. Catal.*, 2002, **209**, 275–278.
106 P. W. Atkins and J. de Paula, *Atkins' Physical Chemistry*, Oxford University Press, London, 8th edn, 2006.
107 K. J. Laidler, *Chemical kinetics*, Pearson Education, 2004.
108 K. Reuter and M. Scheffler, *Phys. Rev. B: Condens. Matter Mater. Phys.*, 2006, **73**, 045433.
109 D. Teschner, G. Novell-Leruth, R. Farra, A. Knop-Gericke, R. Schlögl, L. Szentmiklósi, M. González Hevia, H. Soerijanto, R. Schomäcker, J. Pérez-Ramírez and N. López, *Nat. Chem.*, 2012, DOI: 10.1038/nchem.1411.
110 B. Bridier, D. Karhanek, J. Pérez-Ramírez and N. Lopez, *ChemCatChem*, 2012, DOI: 10.1002/cctc.201200021.
111 A. Toftelund, *PhD Thesis*, DTU, 2012.
112 B. Liu and J. Greeley, *J. Phys. Chem. C*, 2011, **115**, 19702–19709.
113 M. Salciccioli and D. G. Vlachos, *J. Phys. Chem. A*, 2012, **116**, 4621–4628.
114 D. Torres, N. Lopez, F. Illas and R. M. Lambert, *Angew. Chem., Int. Ed.*, 2007, **46**, 2055–2058.
115 W. M. C. Sameera and F. Maseras, *Comput. Mol. Sci.*, 2012, **2**, 375–385.
116 J. Tomasi, B. Mennucci and R. Cammi, *Chem. Rev.*, 2005, **105**, 2999–3093.
117 J. A. McCammon and M. Karplus, *Annu. Rev. Phys. Chem.*, 1980, **31**, 29–45.
118 A. Warshel, S. T. Russell and A. K. Churg, *Proc. Natl. Acad. Sci. U. S. A.*, 1984, **81**, 4785–4789.
119 C. F. Wong and J. A. McCammon, *J. Am. Chem. Soc.*, 1986, **108**, 3830–3832.
120 W. L. Jorgensen and C. Ravimohan, *J. Chem. Phys.*, 1985, **83**, 3050–3054.
121 W. L. Jorgensen and J. K. Buckner, *J. Phys. Chem.*, 1987, **91**, 6083–6085.
122 D. L. Beveridge and F. M. Dicapua, *Annu. Rev. Biophys. Biophys. Chem.*, 1989, **18**, 431–492.
123 P. A. Bash, U. C. Singh, F. K. Brown, R. Langridge and P. A. Kollman, *Science*, 1987, **235**, 574–576.
124 A. Warshel and M. Levitt, *J. Mol. Biol.*, 1976, **103**, 227–249.
125 M. V. Bobetic and J. A. Barker, *Phys. Rev. B: Condens. Matter Mater. Phys.*, 1970, **2**, 4169–4175.
126 J. A. Barker, R. A. Fisher and R. O. Watts, *Mol. Phys.*, 1971, **21**, 657–673.
127 G. C. Maitland and E. B. Smith, *Mol. Phys.*, 1971, **22**, 861–868.
128 O. Tapia, *J. Math. Chem.*, 1992, **10**, 139–181.
129 L. Onsager, *J. Am. Chem. Soc.*, 1936, **58**, 1486–1493.
130 J. G. Kirkwood, *J. Chem. Phys.*, 1934, **2**, 351–361.
131 M. Cossi and V. Barone, *J. Chem. Phys.*, 1998, **109**, 6246–6254.
132 A. Klamt and G. Schuurmann, *J. Chem. Soc., Perkin Trans.*, 1993, **2**, 799–805.
133 E. Cances, B. Mennucci and J. Tomasi, *J. Chem. Phys.*, 1997, **107**, 3032–3041.
134 B. Mennucci, E. Cances and J. Tomasi, *J. Phys. Chem. B*, 1997, **101**, 10506–10517.
135 E. Cances and B. Mennucci, *J. Math. Chem.*, 1998, **23**, 309–326.
136 L. Bellarosa, S. Calero and N. Lopez, *Phys. Chem. Chem. Phys.*, 2012, **14**, 7240–7245.
137 L. Bellarosa, J. M. Castillo-Sánchez, T. J. H. Vlugt, S. Calero and N. Lopez, *Chem.–Eur. J.*, 2012, in press.
138 X.-Q. Zhang, T. T. Trinh, R. A. van Santen and A. P. J. Jansen, *J. Am. Chem. Soc.*, 2011, **133**, 6613–6625.
139 J. K. Nørskov, J. Rossmeisl, A. Logadottir, L. Lindqvist, J. R. Kitchin, T. Bligaard and H. Jonsson, *J. Phys. Chem. B*, 2004, **108**, 17886–17892.
140 X.-Q. Gong, A. Selloni, M. Batzill and U. Diebold, *Nat. Mater.*, 2006, **5**, 665–670.
141 J. Carrasco, A. Michaelides, M. Forster, S. Haq, R. Raval and A. Hodgson, *Nat. Mater.*, 2009, **8**, 427–431.
142 J. Andersin, P. Parkkinen and K. Honkala, *J. Catal.*, 2012, **290**, 118–125.
143 B. N. Zope, D. D. Hibbitts, M. Neurock and R. J. Davis, *Science*, 2010, **330**, 74–78.
144 P. J. Feibelman, *Science*, 2002, **295**, 99–102.
145 J. Carrasco, B. Santra, J. Klimes and A. Michaelides, *Phys. Rev. Lett.*, 2011, **106**, 026101.
146 K. Tonigold and A. Gross, *J. Comput. Chem.*, 2012, **33**, 695–701.

147 J. S. Hummelshoj, F. Abild-Pedersen, F. Studt, T. Bligaard and J. K. Nørskov, *Angew. Chem., Int. Ed.*, 2012, **51**, 272–274.
148 http://ceder.mit.edu/.
149 D. Landis, J. Hummelshoj, S. Nestorov, J. Greeley, M. Dulak, T. Bligaard, J. K. Nørskov and K. Jacobsen, *Comput. Sci. Eng.*, 2012, 1.
150 A. Elsener, C. C. M. Samson, M. P. Braendle, P. Buehlmann and H. P. Luethi, *Chimia*, 2007, **61**, 165–168.
151 J. J. Iglesias, C. Bo, F. Maseras and N. Lopez, www.scipio.iciq.es.
152 VASP, www.vasp.at.
153 ADF, www.scm.com.
154 Gaussian, www.gaussian.com.
155 O. Lopez-Acevedo, K. A. Kacprzak, J. Akola and H. Hakkinen, *Nat. Chem.*, 2010, **2**, 329–334.
156 J. A. Lopez-Sanchez, N. Dimitratos, C. Hammond, G. L. Brett, L. Kesavan, S. White, P. Miedziak, R. Tiruvalam, R. L. Jenkins, A. F. Carley, D. Knight, C. J. Kiely and G. J. Hutchings, *Nat. Chem.*, 2011, **3**, 551–556.
157 J. Pérez-Ramírez, *Nat. Chem.*, 2012, **4**, 250–251.
158 P. Ball, *Nature*, 2006, **442**, 500–502.
159 M. Haruta, *Nature*, 2005, **437**, 1098–1099.
160 N. M. Esfandiari and S. A. Blum, *J. Am. Chem. Soc.*, 2011, **133**, 18145–18147.
161 Y. Hou, B. L. Abrams, P. C. K. Vesborg, M. E. Björketun, K. Herbst, L. Bech, A. M. Setti, C. D. Damsgaard, T. Pedersen, O. Hansen, J. Rossmeisl, S. Dahl, J. K. Nørskov and I. Chorkendorff, *Nat. Mater.*, 2011, **10**, 434–438.
162 M. Garcia-Mota, N. Cabello, F. Maseras, A. M. Echavarren, J. Pérez-Ramírez and N. Lopez, *ChemPhysChem*, 2008, **9**, 1624–1629.
163 I. Serrano, M. I. Lopez, I. Ferrer, A. Poater, T. Parella, X. Fontrodona, M. Sola, A. Llobet, M. Rodriguez and I. Romero, *Inorg. Chem.*, 2011, **50**, 6044–6054.
164 R. Neumann and M. Dahan, *Nature*, 1997, **388**, 353–355.
165 N. Lopez and G. Novell-Leruth, *Phys. Chem. Chem. Phys.*, 2010, **12**, 12217–12222.